# THE CHARACTERISTICS OF COOL HYDROGEN DEFICIENT CARBON STARS

Warrick A. Lawson

A thesis submitted
for the degree of
Doctor of Philosophy
in
Astronomy

University of Canterbury
February 1990

Much of the work reported in this thesis has benefitted from having resident observers at Mount John University Observatory to obtain the necessary observations. I am indebted to Pam Kilmartin and Alan Gilmore for obtaining most of the photometric observations and Mike Clark for obtaining many of the échelle/LDA spectra.

The Mount Stromlo Observatory spectra of the 1988 decline of R CrB were obtained by Dr Peter Cottrell and Markus Buchhorn. The reduction and initial analysis of these spectra was done by them.

Photographic spectra covering the shock event in RY Sgr were discussed for my MSc thesis (University of Canterbury 1985). The analysis of spectra of RY Sgr reported in this thesis takes advantage of the digital format of LDA spectra.

Warrick Lawson

# Contents

Chapter Page

**Chapter** **Page**

# List of Figures

**Figure** **Page**

Figure Page

**Figure** **Page**

# List of Tables

**Table** **Page**

# Abstract

Observations of many R Coronae Borealis (RCB) stars and Hydrogen deficient Carbon (HdC) stars have been obtained to more fully understand the characteristics of these types of objects.

A long term photometric programme has been undertaken to observe most of the known RCB and HdC stars, including those in the Large Magellanic Cloud. Photometry has been obtained over durations of 700–1100 d for many of these stars, permitting a more accurate analysis of the light and colour curves of these objects than has been possible with previously published data. Properties of the low amplitude variations, observed in all these stars, are described and analysed using Fourier techniques. By combining the observed periods and estimated temperatures, the latter obtained from spectra, a period–temperature relationship is produced for these stars. Most stars have a period that can be identified with a radial pulsation mode from models of hydrogen deficient carbon stars.

Theoretical period decrease rates for these types of stars indicate that cooler ($T_{eff} \approx$ 5000 K) stars should dominate the temperature distribution. This is not observed. The reasons for this apparent lack of cooler stars are discussed. If the evolutionary models are correct, there should be many more cool hydrogen deficient carbon stars still to be discovered.

Observations obtained during declines of several RCB stars are discussed. The observations of the 1988 decline of R CrB represent the first occasion where both photometric and spectroscopic observations were obtained during the onset of the decline. For those declines for which extensive photometry is available, a major division in photometric properties is observed during the early stages of the decline. This division, where the colours of the star become either bluer, or redder, may be due to a range of dust formation angles, which alters the relative flux contributions of the photosphere and chromosphere of the star.

Additional aspects of two RCB stars, NSV 6708 and RY Sgr, are described in greater detail. For NSV 6708, the low radial velocity amplitude of NSV 6708 ($< 4$ kms$^{-1}$) causes some difficulty for the standard decline model for these stars, which assumes that the dust formation is linked to radial pulsations. For RY Sgr, observed changes in the pulsation period in the star are interpreted with an O–C analysis to the times of maxima. Only a series of linear solutions, which have lifetimes of $\sim$ 10 yrs, satisfy the O–C residuals to within the observational uncertainty. In addition, spectra have been obtained during the shock wave event of RY Sgr, which is seen as a splitting of the absorption lines near $V_{max}$. Low excitation lines have a greater shock amplitude, which is consistent with their formation in the upper regions of the photosphere of the highly extended atmospheres of these stars.

Finally, areas where additional progress could be made on the study of these stars are discussed.

# Chapter 1

# The cool hydrogen deficient carbon stars – an introduction

*'In a Universe in which hydrogen is so supremely abundant, the few stars with atmospheres deficient in hydrogen deserve careful study.'*

*D.L. Lambert, in Proceedings IAU Colloquium 87.*

## 1.1 HISTORICAL BACKGROUND AND PREAMBLE

In a Universe where the great majority of stars have a composition consisting of about 90 per cent hydrogen and 9 percent helium (by number), leaving around 1 per cent for all other elements, it must have come as something of a revelation when it was realised, in the first quarter of this century, that some stars were highly deficient in hydrogen.

One of the first stars where this situation was suspected of prevailing was R Coronae Borealis (R CrB), which was also the prototype of the enigmatic class of variables named after the star. (The class have been collectively called, during the past few decades, 'RCB stars' to minimise confusion with R CrB, the star.) Bidelman (1986) notes the non–detection of the H$\gamma$ line in R CrB by Ludendorf (1906) and, later, that of H$\beta$ and H$\delta$ by Frost. Alternative explanations to that of hydrogen deficiency were postulated, e.g. the filling–in of these lines by partial emission (Joy & Humason 1923). However, it was the pioneering analysis of R CrB by Berman (1935) which removed all doubt about the reality of the hydrogen question. Berman also noted the high abundance of carbon in R CrB. More recently, Cottrell & Lambert (1982a), found for R CrB and the RCB–type star XX Cam (of which more will be said below) log (H/Fe) ratios of 0.2 and $< -2.6$ respectively [compared to log (H/Fe) = 4.5 for the Sun], and log ($^{12}$C/Fe) ratios of 2.7 and 2.4 respectively [compared to log ($^{12}$C/Fe) = 1.2 for the Sun.]

The existence of RCB stars has been known for nearly two centuries. R CrB was discovered in 1795 by Piggott (1797) and is the tenth star of Argelander's list of variables, which were tabulated in their order of discovery (see Hoffmeister, Richter & Wenzel 1985). The type of variability is a rapid fade, or decline, in light over a timescale of one to two months and a gradual return to maximum light over several months to several years. The nature of these declines was deduced by Loreta (1934) and O'Keefe (1939) as being due to the obscuration of the star after the condensation of clouds of carbon particles around the star. This model was modified to the line of sight formation of material when infrared observations became available. These observations gave no indication of an increase in

flux at infrared wavelengths, in compensation for the reduction in visual flux, as would have been expected from a circumstellar cloud during the decline (see Feast 1986). Such infrared observations also discovered the presence of an infrared flux excess due to emission by material at typically 600–900 K. This material is generally associated with the material formed, and presumably expelled, during declines.

The second RCB star to be discovered was RY Sgr, which was noted to be a variable by Colonel E.E. Markwick, from Gibraltar (Pickering 1896). Jacchia (1933) found a $\sim$ 39 d period with an amplitude of $\sim$ 0.5 mag in his own observations of RY Sgr, covering 1920–1932, and concluded that the star was pulsating. [Such variations are also apparent in photographic observations of RY Sgr obtained at the Cape between 1897 and 1901 (Innes 1903) but, despite their clarity, they were not recognised.] A photometric and spectroscopic study of RY Sgr by Alexander *et al.* (1972) confirmed that RY Sgr was pulsating with a radial velocity amplitude of 30–40 $kms^{-1}$. A series of high resolution spectra, obtained by Cottrell & Lambert (1982b), showed line splitting in some spectra, which were later found to occur near maximum visual light (Lawson 1986).

It will become apparent throughout this thesis that RY Sgr has become a cornerstone of our understanding of these stars, but such attention is not without its disadvantages. In Chapter 2, where the photometric variations of a large sample of RCB stars, and related objects, are discussed, RY Sgr has the largest amplitude, and probably the most regular, photometric variations of known stars of this type. Much attention has been devoted to the $\sim$ 39 d pulsation period of this star, the variation of this period with time and the evolutionary considerations for this star (and by default other RCB stars). The pulsation period rate of change has been found to be consistent with models of hydrogen deficient carbon stars evolving towards higher temperatures (Section 5.1), but the period rate of change has not been determined reliably for any other such star.

Most other RCB stars were discovered on Harvard Observatory survey plates during the 1920s, as a consequence of the declines of these stars. After the removal of many mis-classifications e.g., V504 Cen (Kilkenny & Lloyd Evans 1989); AE Cir (Kilkenny 1989); SY Hyi (Feast 1979; Lawson *et al.* 1989), and some later additions (in particular NSV 6708; see Chapter 4), the class numbers about 25 including 4 stars in the Large Magellanic Cloud (LMC).

At about the time of the Harvard survey, a group of similar objects were discovered spectroscopically, the first being HD 182040 (Rufus 1923), that had the spectroscopic characteristics of the RCB stars, but did not have declines. These stars were clumsily called the cool hydrogen deficient carbon (HdC) stars which was unfortunate since most of the RCB stars are also cool hydrogen deficient carbon stars, but the lack of declines in the HdC stars delineate these two types of objects. Although HdC stars do not have declines, 2 HdC stars have infrared excesses due to circumstellar material similar to the RCB stars. The RCB and HdC stars are almost certainly related (Bidelman 1953) but details of why they should show some different characteristics is in dispute. The five HdC stars known prior to the recent reclassification of XX Cam as an HdC star, rather than an RCB star (see Section 2.4.3), were analysed by Warner (1967).

A group of hotter objects, generally called the extreme helium (eHe) stars (Drilling 1986), are presumed to be the hot extension of the RCB and HdC stars. The eHe stars have effective temperatures ($T_{eff}$) greater than 9500 K, and are thus delineated from the HdC stars and most of the RCB stars. [Most RCB stars and all HdC stars have $T_{eff}$ between

5000–7500 K, but there are several RCB or RCB–like stars (e.g., DY Cen, MV Sgr and V348 Sgr) with $T_{eff}$ as high as 20000 K.] Like the HdC stars, the eHe stars do not have declines and, in most cases, have no infrared excess.

The evolution status of all these stars is in dispute. The hydrogen deficiency has been explained, within the context of conventional post–Asymptotic Giant Branch (AGB) evolution, by mixing and nuclear burning (Wheeler 1978) or an envelope shedding process (Schönberner 1979). However, Schönberner (1986) has argued that the linking of these stars back to the AGB fails to explain the observed abundances, masses and evolutionary lifetimes. The most favoured hypothesis for the origin of these stars is the coalescence of a He–CO white dwarf binary (Webbink 1984). Such a proposal avoids the problem of evolving the hydrogen deficient star progenitor from the AGB and the subsequent loss of the hydrogen envelope. [The scheme of Webbink can also explain the rarity of binary systems in these stars (Jeffery, Drilling & Heber 1987).] We consider the implications of this model further in Chapters 2 and 6.

## 1.2 INTRODUCTION TO THE THESIS

IAU Colloquium No. 87, held in Mysore, India during 1985 was the first conference to specifically address the current knowledge on hydrogen deficient stars in general and how this knowledge might be advanced. Much of the proceedings of the Colloquium were devoted to the RCB, HdC and eHe stars.

Due to the attendance of the author at this meeting, we were aware of areas where an observational programme based around the existing facilities at Mount John University Observatory (MJUO), and at that time, soon to be commissioned 1.0–m reflector and the 1872 element Reticon–based detector (MacQueen 1986), would be able to advance the understanding of the RCB stars.

The programme was initially based around three proposals, but it was later expanded to include the study of other characteristics of cool hydrogen deficient carbon stars. These initial proposals were: a study of the pulsation–related photometric variations of a large sample of RCB (and later) HdC stars; a spectroscopic study of the line–splitting in RY Sgr and an extension of existing work on the pulsation period rate of change of RY Sgr. Later work included much effort on the declines of several RCB stars, in particular the 1988 decline R CrB, and the characteristics of the recently identified RCB star NSV 6708.

This type of programme had not been attempted before, mainly because of the difficulty of securing observations of these stars. There was already some appreciation, from existing photometry of R CrB (Fernie 1982) and RY Sgr (Alexander *et al.* 1972) and visual estimates for other RCB stars (Bateson 1975, 1978), that the periods for most RCB stars were in the range 40–120 d and that the light curves were probably semi–regular. In addition to the semi–regular variations at maximum light, the large amplitude (5–7 mag) declines of these stars occur unpredictably. Thus, the obtaining of observations for these stars is difficult due to the duration and nature of these variations and is affected by telescope time and instrument scheduling constraints at most observatories. At MJUO, resident observers ensure a continuous supply of observations and have the ability to respond to unforseen events, e.g. declines. The willingness of the Observatory to support such long term programmes has been essential for the acqusition of observations of these objects.

Prior to this survey of the cool hydrogen deficient stars, much of the information on these objects came from visual estimates obtained by amateurs, and then communicating their data to organisations as the Variable Star Section of the Royal Astronomical Society (VSSRASNZ) and the American Association of Variable Star Observers (AAVSO). These estimates, in particular the VSSRASNZ estimates, have been published in a continuing series by Bateson (1975, 1978) and Lawson, Cottrell & Bateson (1988, 1989). Such estimates continue to be of great value to the study of these stars, as they form the most homogenous set of observations available and the most frequent source of announcements of declines.

In Chapter 2, we analyse the photometric variations of 16 RCB and HdC stars including the 4 RCB stars in the LMC. Data for a further 4 stars are sourced from the literature. Prior to the MJUO survey of these stars, few long timescale observations had been attempted and there was a lack of information about their periodic nature. Photometry was obtained over intervals of 700–1100 d for many of these stars, permitting a more accurate analysis of the light and colour curves than had been possible with previously published data. More than 1100 nightly mean observations are reported. The discussion of the RCB stars emphasises the properties of these stars when they are at maximum light. (The declines of these objects are considered in Chapter 3.) Properties of the low amplitude variations, observed in all of these stars, are described and analysed using Fourier techniques. Synthetic light curves are produced for several stars.

Preliminary results of a spectroscopic survey of these stars are also discussed, in so far as these results influence the interpretation of the photometry (Section 2.5.1). For the 20 galactic stars for which spectra are available, 13 stars appear similar to the RCB stars R CrB and RY Sgr which have $T_{\rm eff} \approx 7000$ K. By combining the observed periods and estimated temperatures, we produce a period–temperature relationship for these stars. Most of these stars have periods that compare with theoretical radial modes for hydrogen deficient carbon stars in this temperature range.

Theoretical period decrease rates for hydrogen deficient carbon stars indicate that cooler ($T_{\rm eff} \approx 5000$ K) stars should dominate the temperature distribution. This is not observed. In Section 2.5.2, we discuss the reasons for this apparent lack of cooler stars and implications for the numbers of these objects in the Galaxy. If the evolutionary models are correct, we predict that there should be many more cool hydrogen deficient carbon stars still to be discovered.

Another implication of the estimated temperatures is that many of these stars are not as cool as suggested by their photometric colour indices. Consequently, there must be large amounts of reddening in the directions of these stars, many of which have low galactic latitudes. This is not surprising given their assumed luminosity ($M_{\rm bol} \approx -5$), which has been deduced from observations of RCB stars in the LMC. From the general appearance of the spectra, we deredden available photometry for these stars to produce intrinsic magnitudes, and hence distance estimates.

In Chapter 3, we discuss the 1988 decline of R CrB (Section 3.1) and the 1989 decline of S Aps and the 1988 decline of V CrA (Section 3.2).

The observations of the 1988 decline of R CrB are significant in that they represent the first occasion where both photometric and spectroscopic observations were obtained from prior to, and throughout, the onset of the decline. As noted by other authors, we see a gradual filling–in of the photospheric absorption spectrum and the appearance of

blue–shifted (10 $kms^{-1}$) emission lines. Our data of the early decline stages showed that there was an initial slow filling–in of photospheric absorption lines, followed by a rapid change in the spectra about 18 d after the decline onset. At this time the photospheric absorption lines were rapidly filled–in, emission lines appeared, as did extensive emission which was the cause of the significantly bluer colours noted in the photometry of this decline. High velocity ($\sim$ 150 $kms^{-1}$) blue–shifted material appeared in emission at the same time.

Photometrically, this decline had some similarities to the 1983 decline of this object, but it was dramatically different from the 1985 decline. We compare the 1988 decline with these events and the declines of other RCB stars, in particular RY Sgr, NSV 6708 and UW Cen. Most importantly, we find two extreme types of colour behaviour, which we call 'blue' (the 1983 and 1988 events) and 'red' (the 1985 event) types, since both the $(U–B)$ and $(B–V)$ colours initially move to bluer and redder values, respectively. The 'blue' type has been well documented in the literature and forms the basis for the standard eclipse model for this phenomenon. The interpretation of the 'red' type is an extension of the eclipse model which possibly involves the obscuration of the entire visible hemisphere (photosphere and much of the chromosphere) of the star upon the onset of the decline.

These interpretations may place constraints on the physical processes causing the formation of dust in these stars. The various methods for dust formation and the eventual dispersion of this dust are considered. The cause of a 'blue' decline is the broad emission feature ($\lambda\lambda$3900–5700Å) which appears in low–resolution spectra obtained during the initial decline phase. This emission feature could be due to unresolved chromospheric emission lines or continuum emission or both. This feature disappears as the decline progresses, suggesting that its location may be close to the photosphere. No such feature is believed to be observed during the early stages of a 'red' decline. We also present arguments and some simple decline models which show that the decline onset does not always occur at the same phase of the smaller amplitude pulsations.

In Section 3.2 we analyse photometry of the 1989 decline of S Aps and the 1988 decline of V CrA. Although we have no spectroscopic observations of these declines, we compare the photometry of these events within the framework of other such events. We derive the reddening law $A_V/E(B–V)$, due to extinction on the rising branch of these events, and for a number of other declines. The range of extinction varies by more than a factor of 3 between observed limits of 3.2 (i.e. similar to the interstellar value) and 10.3. We discuss this range of observed values for $A_V/E(B–V)$, with reference to recent work on the extinction caused by particles of amorphous carbon, or graphite (Borghesi, Bussoletti & Colangeli 1985). We also note that near–visual photometry is a poor indicator for the determination of particle size, or particle type, and that such information will only be forthcoming from ultraviolet data.

In Chapter 4, we discuss the charateristics of the recently identified RCB star NSV 6708 (= V854 Cen). The photometric and spectroscopic data of this star have been obtained at maximum light as well as during declines of this star. The data for this star are considered separately because of the recent identification of NSV 6708 and the types, and the sources, of observations. MJUO *UBVRI* and South African Astronomical Observatory (SAAO) *JHKL* photometry (Kilkenny & Marang 1989) obtained during 1988 revealed a period of $\sim$ 110 d before the star entered a 7 mag amplitude decline. The Fourier analysis of MJUO *UBVRI* photometry obtained during 1989 extracted several possible periodicities,

which suggests that NSV 6708 may be multi–periodic with periods ranging between 45 and 110 d. Spectra of NSV 6708 show much stronger hydrogen lines than published spectra of other RCB stars, but we indicate that NSV 6708 may not be unique in this respect. The presence of significant hydrogen in one other suspected RCB star, and in one HdC star, indicates that there may be a considerable variation in the degree of hydrogen deficiency for these stars.

In Chapter 5, we discuss two aspects of the behaviour of the RCB star RY Sgr that are currently known to be unique to this star.

In Section 5.1, we discuss the results of an O–C analysis to the times of maxima on the light curve of RY Sgr. The observations extend over 90 yrs and are mainly based upon visual estimates. The analysis was undertaken after we noted that the observed times of maxima were deviating from the quadratic solutions derived by Kilkenny (1982) and Marraco & Milesi (1982). The quadratic solutions infer a linear period rate of change towards shorter periods. We consider revised quadratic, cubic and a series of linear piecewise solutions to the times of maxima. Only a series of linear piecewise solutions satisfy the O–C residuals to within the observational uncertainty. Four such solutions have been determined for the times of maxima since 1948. These solutions have lifetimes of $\sim$ 100 cycles ($\sim$ 10 yrs) which suggests that the period changes may be semi–periodic. The polynomial solutions give the mean period rate of change over the 90 yrs of observations and these give a mean value of $-1.4 \times 10^{-3}$ d cycle$^{-1}$. The observed rate is consistent with the theoretical rate of change determined for model hydrogen deficient stars evolving through the region of the H–R diagram occupied by the RCB and HdC stars, towards the region occupied by the eHe stars (Schönberner 1977; Weiss 1987a).

In Section 5.2, we discuss the absorption line splitting observed in spectra of RY Sgr, which is due to a shock wave occurring near $V_{\max}$ on the pulsation cycle. We compare the pulsations of RY Sgr with those of other RCB stars and discuss the attempts to model the pulsations of these stars. We also consider the possible linking of the pulsations to the declines of RCB stars.

Much of this work has been published, or is awaiting publication, in *Monthly Notices of the Royal Astronomical Society*. Chapter 2 will appear as *'The photometric characteristics of cool hydrogen deficient carbon stars'* by W.A. Lawson, P.L. Cottrell, P.M. Kilmartin and A.C. Gilmore. Section 3.1 will appear as *'The 1988 decline of R Coronae Borealis'* by P.L. Cottrell, W.A. Lawson and M. Buchhorn. The 1988 data on NSV 6708 (Chapter 4) has appeared as *'The R Coronae Borealis star NSV 6708'* by W.A. Lawson and P.L. Cottrell (1989, *M.N.*, **240**, 689). Section 5.1 has appeared in two parts. The first, *'RY Sgr: pulsation period variations reinterpreted'* by W.A. Lawson and P.L. Cottrell (1988, *M.N.*, **231**, 609), analysed observations obtained up to 1986 October. The second, *'A change in the pulsation period of the R Coronae Borealis star RY Sgr'* by W.A. Lawson and P.L.Cottrell (1990, *M.N.*, **242**, 259), covers observations of RY Sgr up to 1989 April. In Chapter 4 and Section 5.1, in particular, the availablity of additional data and improved data analysis techniques have enhanced the conclusions reached in the original papers. Much effort has been placed upon retaining the flavour of the original papers. Hence, the individual Chapters or major Sections are largely self–contained and may be read without substantial reference to other parts of the thesis. The References for all Chapters and Sections are listed together at the end of the thesis.

# Chapter 2

# The photometric characteristics of cool hydrogen deficient carbon stars

## 2.1 INTRODUCTION

Prior to the observations discussed in this Chapter, little long timescale photoelectric photometry of the cool hydrogen deficient carbon stars had been attempted. These objects include the R Coronae Borealis (RCB) and the (commonly called) hydrogen deficient carbon (HdC) stars. The HdC stars are distinct from the RCB stars in that they have no large amplitude declines in light due to progressive obscuration by expanding clouds of dust (see Section 3.1) and some do not have infrared excesses indicative of the presence of circumstellar material (Walker 1986). The RCB and HdC stars are spectroscopically similar (Lambert 1986). The two groups of stars are almost certainly related (Bidelman 1953), but details of why they show some different characteristics have not been confirmed (see Section 1.1). Both groups are generally considered to be the low temperature extension of the extreme helium (eHe) stars (Drilling 1986). However, the evolutionary status of all of these stars is in dispute. The causes of such strong hydrogen deficiency have been explained by mixing and nuclear burning (Wheeler 1978), an envelope shedding process (Schönberner 1979), or mass exchange between a white dwarf binary producing a common hydrogen deficient envelope (Webbink 1984; Iben & Tutukov 1985).

Photometrically, the best studied cool hydrogen deficient carbon star has remained the RCB star RY Sgr. This star was observed extensively (both photometrically and spectroscopically) by Alexander *et al.* (1972) throughout the 1967 decline, which included observations until after RY Sgr had recovered to maximum light during 1971. These photometric data confirmed that RY Sgr was varying with a mean period of 38.6 d and an amplitude in $V$ of 0.3–0.5 mag. Variability of this order had first been noted in the visual light curves of Jacchia (1933), whose own observations of RY Sgr from 1920–1932 had shown a period of 39 d with an amplitude of 0.5 mag. More recent photometry of RY Sgr, obtained during the interval 1984–1986, was published by Lawson *et al.* (1987). The $(U–B)$ and $(B–V)$ colour amplitude observed by both Alexander *et al.* and Lawson *et al.* are comparable to the $V$ amplitude (0.3–0.5 mag). In addition, the colour curves lead the light curve by 4–8 d.

The long term period of RY Sgr has been analysed using photometry and visual estimates to find times of maxima or minima on the light curve. O–C analyses of the times of maxima, and minima, on the light curve of RY Sgr have shown that the pulsation period of RY Sgr is decreasing (see Section 5.1). The observed rate ($\sim -1.4 \times 10^{-3}$ d cycle$^{-1}$) is consistent with the period decrease rate determined from evolutionary models for helium stars evolving through the region of the H–R diagram occupied by the RCB stars and towards the region occupied by the eHe stars (Schönberner 1977, Weiss 1987a). (We also

show in Section 5.1 that the period of RY Sgr varies by discrete values on a timescale of ~10 yrs.)

Radial velocity variations of RY Sgr, with an amplitude of typically 30 $kms^{-1}$, were observed by Alexander *et al.* (1972), and were in phase with the photometric variations. High resolution ($\Delta\lambda \approx 0.15$Å) échelle spectra of RY Sgr obtained by Cottrell & Lambert (1982b) and Lawson (1986) showed line–splitting at certain phases, which were interpreted as a shock wave occurring near $V_{max}$. These data confirmed that RY Sgr was a radially pulsating star. (The radial velocity variations of RY Sgr are considered further in Section 5.2.)

The RCB star prototype R CrB has been monitored regularly by Fernie and his collaborators (see, in particular, Fernie 1989) mainly using the APT service at Fairborn Observatory (see Genet, Boyd & Hall 1986). Fernie Fourier analysed photometry of R CrB obtained between 1971–1986 and concluded that R CrB varied with a mean period of 45 d. The $V$ and colour amplitude appeared to be highly variable from cycle–to–cycle, but there was no evidence for more than one significant periodicity in the photometry (except possibly during 1972). The amplitude range of the light curve was typically 0.1–0.3 mag, but that of the colour curves was generally less than 0.1 mag. Photometric observations of R CrB at, or near, maximum light have also been published recently by Ashoka & Pukalenthi (1986), Böhme (1986, 1987) and Lawson, Kilmartin & Gilmore (1988a). R CrB was shown to have a radial velocity amplitude of 4–8 $kms^{-1}$ by Raveendran, Ashoka & Rao (1986).

Many of the RCB and HdC stars were observed at SAAO for short time intervals during 1982–83 (Kilkenny *et al.* 1985) and 1986 (Marang *et al.* 1989). All of the RCB stars observed were found to be varying with light amplitudes ranging from 0.1–0.8 mag and colour amplitudes comparable to those observed in R CrB, i.e. $< 0.1$ mag. Marang *et al.* concluded from these observations that the periods of the RCB stars fell into either 'short' ($\sim$ 40 d) or 'long' ($> 65$ d) groups. Although many RCB stars do appear to have characteristic periods of about 40 d, our photometry indicates that some of the Marang *et al.* conclusions were influenced by the short duration of the SAAO observations. In addition, one of the stars observed by Marang *et al.* (RS Tel) was rising towards maximum from a large amplitude decline and was incorrectly assigned to the 'long' period group. The most important result from the SAAO observations was the discovery of variability in the HdC stars (see also Kilkenny, Marang & Menzies 1988) which had been previously thought to be non–variable. The amplitude of the light variations of the HdC stars were generally very low ($< 0.1$ mag). In this respect the HdC stars appeared to differ from most RCB stars.

Photometry has also been obtained of the recently identified RCB star NSV 6708 (Section 4.3.6). An analysis of this photometry suggests that the star may have a period ranging between 45–110 d. Spectra were obtained prior to, and during the early stages of, the 1988 decline of this star, and also during 1989. There was no positive detection of radial velocity variations above the 2–4 $kms^{-1}$ uncertainty in the measurements (Section 4.3.7). This suggests the possibility that NSV 6708 may not be radially pulsating, and that some caution must be exercised when interpreting the photometric variations observed in all RCB and HdC stars as being due to radial pulsations.

Photometry of the RCB star GU Sgr, obtained during 1986 and 1987, have been published by Lawson, Kilmartin & Gilmore (1988b). These data indicated that the $V$

amplitude of GU Sgr was 0.2–0.3 mag. A linear fit to the times of maxima on the light curve gave a mean period of 37.8 d. This value was similar to the period of 38 d determined from visual estimates obtained on the rising branch of declines of GU Sgr by Bateson & Jones (1975).

For a majority of the RCB stars, visual estimates and light curves have been published by organisations such as the American Association of Variable Star Observers (AAVSO), the Variable Star Section of the Royal Astronomical Society of New Zealand (VSSRASNZ) and the British Astronomical Association (BAA). These data sometimes give an indication of periodicity but only for those stars with amplitudes larger than 0.2–0.3 mag. These estimates, in particular the VSSRASNZ estimates, have been used to examine the pulsation period of RY Sgr (see Section 5.1), S Aps (Kilkenny 1983) and UW Cen (Kilkenny & Flanagan 1983). The VSSRASNZ estimates and light curves have been published in a continuing series by Bateson (1975, 1978) and Lawson, Cottrell & Bateson (1988, 1989).

Recent attempts to model the 'pulsations' of RCB stars (see Saio & Wheeler 1985) have generally compared their results to the well studied characteristics of RY Sgr. The properties of this star have been taken as being somewhat representative of the behaviour of RCB stars in general although, as we will show (Sections 2.4.1.5 and 5.2), this is not the case. (RY Sgr has the most extreme photometric variations of any known hydrogen deficient carbon star. Most other RCB stars have variations that are 2–5 times less in $V$ amplitude and 5–10 times less in colour.) Even though there was some success in replicating the behaviour of RY Sgr (see fig. 3 of Saio 1986), the best models still gave light variations that were larger than those observed, and the theoretical phase relationship between the light and radial velocity curves did not agree with the observed phase difference.

In this Chapter we present photoelectric observations of 16 RCB and HdC stars (Section 2.2, with individual stars discussed in Section 2.4). The Fourier analysis technique is described in Section 2.3. We then consider the implication of our observations in terms of a period–temperature relation (Section 2.5.1) and the likelihood of discovering additional RCB and HdC stars in the Galaxy (Section 2.5.2).

## 2.2 OBSERVATIONS

The photometric (generally *UBV* or *UBVRI*) observations of the RCB and HdC stars were obtained with the two 0.6–m and the 1.0–m reflectors at MJUO using automated single channel photometers. The RCB and HdC stars discussed here are listed in Table 2.1. The observations extended from 1986 May until 1989 July, although not all stars were observed throughout this interval. As our main emphasis was on observing these stars at, or near, maximum light, the RCB stars were not generally observed during declines, unless the decline onset was observed. The 1988 declines of R CrB of NSV 6708 are analysed in Sections 3.1 and 4 respectively. Photometric observations obtained during the 1989 decline of S Aps and the 1988 decline of V CrA are discussed in Section 3.2.

Several combinations of telescope and photomultiplier tube were used throughout this programme. Observations made between 1986 June–November were obtained with the 0.6–m Optical Craftsman reflector and EMI 6094B tube; between 1986 November and

**Table 2.1.** Programme stars and adopted comparison star magnitudes.

| Star | Comparison | $V$ | $(U–B)$ | $(B–V)$ | $(V–R)$ | $(V–I)$ | Check |
|---|---|---|---|---|---|---|---|
| S Aps | 104[1] | 9.880 | 0.730 | 1.060 | 0.590 | 1.125 | 112 |
| U Aqr | 106[2] | 10.470 | 0.070 | 0.660 | | | 112 |
| V CrA | d[3] | 10.070 | 0.250 | 0.265 | | | e |
| Y Mus | d[4] | 8.900 | 0.200 | 0.320 | | | e |
| RY Sgr | 74[1] | 7.520 | 0.045 | 0.015 | 0.010 | 0.000 | 75 |
| RS Tel | 95[5] | 9.470 | 1.610 | 1.385 | | | 97 |
| RT Nor | c[6] | 9.970 | 0.025 | 0.130 | | | g |
| RZ Nor | g[5] | 10.900 | | 1.070 | | | h |
| SU Tau | a[7] | 9.990 | | 0.360 | 0.220 | 0.220 | b |
| W Men | 139[8] | 14.000 | | 0.510 | | | 117 |
| HV 5637 | a[7] | 14.170 | | 0.740 | | | b |
| HV 12842 | a[7] | 13.700 | | 0.610 | | | b |
| HV 12671 | a[7] | 13.430 | | 0.600 | | | b |
| HD 137613 | HD 138600 | 7.590 | 0.160 | 0.570 | 0.330 | | HD 137319 |
| HD 148839 | HD 148725 | 8.570 | -0.290 | -0.015 | 0.000 | | HD 148813 |
| HD 182040 | HD 180409 | 6.930 | 0.070 | 0.540 | | | HD 181235 |

(1) Bateson (1958)
(2) Chart No. 587; Bateson *et al.* (1981)
(3) Chart No. 474; Bateson *et al.* (1979a)
(4) Chart No. 603; Bateson, Morel & Sumner (1982)
(5) Chart No. 377; Bateson *et al.* (1977)
(6) Chart No. 936; Bateson & Morel (1988)
(7) Chart available from the author
(8) Chart No. 444; Bateson, Morel & Winnett (1979b)

1988 January with the 1.0–m reflector and EMI 6094B tube; thereafter with either the 0.6–m Optical Craftsman reflector and EMI 9558B tube or the 0.6–m Boller & Chivens reflector and RCA C31034A tube. The filters used were similar to those described by Bessell (1976).

The observations were obtained differentially with respect to nearby comparison stars. The differential magnitudes of the variable star, and those of a nearby check star, were then transformed to the standard system using mean coefficients determined from observations of E–region standards (Cousins 1983). The reduction of the differential magnitudes to the standard system were done at MJUO using software written by A.C. Gilmore. The observations were then transferred to the University of Canterbury VAX 6230 computer for further reduction. The comparison star chosen for each variable, and the adopted comparison star magnitude and colours, are listed in Table 2.1. The zero point errors for the comparison $V$ magnitudes (and hence the differentially determined check and variable star magnitudes) are less than 0.03 mag. For the colour indices they are less than 0.02 mag. The internal accuracy for each field was determined from the constancy of the check star magnitudes and the scatter between the (typically) 3–6 observations obtained of the

variable and check star on each night of observation. These 3–6 observations were then averaged to produce a nightly mean magnitude. The internal accuracy of the $V$ magnitudes and all colours [except for $(U–B)$] were generally less than 0.02 mag for stars brighter than $V = 11$, and 0.03 mag for stars fainter than $V = 11$. For $(U–B)$, the corresponding errors were typically 0.03 and 0.04 mag respectively.

We note that there was some overlap for some of the stars with SAAO photometry (Marang *et al.* 1989). Their observations were obtained from 1986 June–August. Small differences (typically less than 0.05 mag) remain in the zero points between the MJUO and SAAO data which should be considered if these data are compared.

## 2.3 ANALYSIS TECHNIQUES

In order to analyse the photometry in an objective manner, we applied the Lomb–Scargle Fourier method for non–equally spaced data (Lomb 1976; Scargle 1982). The Lomb–Scargle method has the advantage of considering the data on a per point basis and not on a per time interval basis. Thus, there is no need to equi–space the data by interpolation, or fill out gaps in the data file with zeros or some other value. Accordingly, the Fourier spectrum of the data is not convolved with the spectrum of a window function. This problem afflicts the method of Deeming (1975) which is commonly used in the Fourier analysis of astronomical data. The difficulties of interpreting the convolved data and window spectrum have been demonstrated by Fernie (1989).

The Lomb–Scargle method has been coded by Press & Teukolsky (1988), who also discuss the general aspects of this method. The code of Press & Teukolsky searches for periodicities between frequency limits, and at a particular frequency resolution, determined from a user–supplied oversampling rate and a multiple of the mean Nyquist frequency (see Press & Teukolsky for details). A FORTRAN program written by the author, followed a modified Press & Teukolsky code. The code was changed to permit user–inputted initial and final frequencies, as well as the stepping frequency. These modifications enable the user to examine photometry of a star after the addition of new data, or to analyse photometry for several stars with differing mean Nyquist frequencies, but at a fixed frequency resolution. The Lomb–Scargle routine of Press & Teukolsky outputs a normalised power spectrum as a function of frequency. The routine also returns a 'false alarm' probability for the most significant frequency (see Horne & Baliunas 1986), where a small value for this probability indicates the presence of a highly significant periodicity (see the Appendix).

Synthetic light curves are produced for some stars. We have adopted the method of Poretti (1989), where the amplitude and phase of the most significant frequency are calculated, and this constituent is then subtracted from the photometry. Ideally, the procedure is repeated until the standard deviation of the residual data is comparable to the standard deviation of the noise in the photometry (generally 0.02–0.03 mag). In practice, this ideal is difficult to achieve with a realistic number of fitted sine waves. Clearly, all data points could be fitted by constructing a synthetic curve using all peaks in the original power spectrum. However, this approach can give rise to unrealistic variability across data gaps and difficulties in interpretation since we are looking for physical connections between these periods and pulsation modes in the star. The approach adopted here was to monitor parameters such as the decrease in the amplitude of the sine wave and the increase

of the false alarm probability for each identified peak, in comparison to those frequencies identified by previous iterations. The iterative procedure was stopped when the amplitude of the identified periodicity was somewhat less than the remaining residuals, but still larger than the observational uncertainty, and the probability of this periodicity was (generally) several orders of magnitude larger than the initially identified (and the most significant) period. This point was usually achieved after 3–4 iterations on the larger data sets (100–200 observations), and 1–2 iterations on the shorter data sets (20–30 observations). A synthetic light curve can then be constructed as the sum $\sum_i M_i + A_i\cos(2\pi f_i + \phi_i)$ of the identified periodicities at frequency $f_i$, with mean magnitude $M_i$, amplitude $A_i$ and onset phase $\phi_i$. Note that, in this form, the amplitude $A_i$ is half the peak–to–peak amplitude of the sine wave.

Some stars, e.g. S Aps (Section 2.4.1.1) and V CrA (Section 2.4.1.3), show changes in mean magnitude from year to year that are generally attributable to the effects of the star rising from a decline. The interpretation of the power spectrum for these data is made more difficult if the year–to–year variations are significant when compared to the amplitude of the multi–periodic variations seen in the light curve. The effects of these year–to–year variations can be seen in the power spectrum as significant power at frequencies generally less than an inverse year ($2.7 \times 10^{-3}$ d$^{-1}$). For essentially continuous data this effect was counteracted by removing the low frequency content by applying the step–wise reduction procedure discussed above. If the data were obtained seasonally, or were of only short duration, then an option was to detrend these data by applying a number of linear least squares fits to the photometry and offsetting the photometry to a specified magnitude. It was not found necessary, nor thought desirable, to apply more than one least squares fit per year of data. The results, if the data were obtained over a short duration (200–300 d), were generally preferable to attempting to remove the low frequency contribution via the Fourier method.

## 2.4 PHOTOMETRY OF HYDROGEN DEFICIENT CARBON STARS

Of the 16 cool hydrogen deficient stars for which data is presented here, 9 are galactic RCB stars (Section 2.4.1), 4 are RCB stars in the Large Magellanic Cloud (LMC; Section 2.4.2) and 3 are HdC stars (Section 2.4.3). The LMC RCB stars and the HdC stars are considered separately from the galactic RCB stars in this Section mainly because, as conveniently studied groups of stars, they have received some attention to date (although primarily spectroscopic). All these stars were listed in Table 2.1. For each of these stars, the observations are listed and then analysed and discussed.

### 2.4.1 Galactic R Coronae Borealis stars

#### 2.4.1.1 S Aps

The *UBVRI* observations of S Aps from JD 2446769–2447652 are listed in Table 2.2. The data are listed until after the onset of the 1989 decline of this star near JD 2447650 (Section 3.2.3.1). The $V$ light curve and the ($U$–$B$), ($B$–$V$), ($V$–$R$) and ($V$–$I$) colour curves

**Table 2.2.** MJUO *UBVRI* photometry of S Aps.

| JD–2440000 | *V* | (*U–B*) | (*B–V*) | (*V–R*) | (*V–I*) | JD–2440000 | *V* | (*U–B*) | (*B–V*) | (*V–R*) | (*V–I*) |
|---|---|---|---|---|---|---|---|---|---|---|---|
| 6769.032 | 9.840 | 0.712 | 1.257 | | | 6904.094 | 9.750 | | 1.180 | | |
| 6837.189 | 9.799 | 0.639 | 1.203 | | | 6905.090 | 9.758 | 0.578 | 1.177 | | |
| 6846.164 | 9.833 | 0.594 | 1.184 | | | 6923.830 | 9.814 | 0.556 | 1.184 | | |
| 6847.162 | 9.809 | 0.598 | 1.200 | | | 6928.948 | 9.800 | 0.519 | 1.171 | | |
| 6848.090 | 9.811 | 0.585 | 1.197 | | | 6946.961 | 9.836 | 0.643 | 1.219 | | |
| 6873.216 | 9.896 | 0.618 | 1.235 | | | 6954.899 | 9.831 | 0.635 | 1.212 | | |
| 6874.199 | 9.885 | 0.637 | 1.235 | | | 6960.859 | 9.897 | 0.625 | 1.217 | | |
| 6876.178 | 9.902 | 0.660 | 1.212 | | | 6963.989 | 9.881 | 0.613 | 1.211 | | |
| 6896.079 | 9.787 | 0.567 | 1.184 | | | 6966.001 | 9.864 | 0.614 | 1.213 | | |
| 6897.171 | 9.783 | 0.578 | 1.154 | | | 6981.846 | 9.703 | 0.608 | 1.239 | | |
| 6982.931 | 9.703 | 0.637 | 1.211 | | | 7069.131 | 9.683 | 0.631 | 1.214 | | |
| 6985.950 | 9.689 | 0.656 | 1.213 | | | 7083.868 | 9.807 | 0.637 | 1.211 | | |
| 7003.051 | 9.832 | 0.650 | 1.246 | | | 7110.121 | 9.713 | 0.654 | 1.219 | | |
| 7017.142 | 9.912 | 0.622 | 1.234 | | | 7136.044 | 9.789 | 0.714 | 1.225 | 0.802 | |
| 7019.977 | 9.876 | 0.672 | 1.228 | | | 7138.025 | 9.760 | 0.758 | 1.246 | 0.769 | |
| 7021.979 | 9.847 | 0.644 | 1.238 | | | 7163.944 | 9.802 | 0.765 | 1.235 | | |
| 7030.939 | 9.701 | 0.639 | 1.216 | | | 7166.048 | 9.796 | 0.688 | 1.207 | | |
| 7032.010 | 9.692 | 0.639 | 1.212 | | | 7176.040 | 9.798 | 0.689 | 1.209 | 0.790 | |
| 7042.916 | 9.773 | 0.662 | 1.213 | | | 7185.046 | 9.771 | 0.679 | 1.220 | 0.772 | |
| 7062.922 | 9.707 | 0.675 | 1.199 | | | 7188.046 | 9.768 | 0.636 | 1.215 | 0.782 | |
| 7197.062 | 9.771 | 0.629 | 1.214 | | | 7259.010 | 9.860 | 0.666 | 1.244 | 0.765 | 1.510 |
| 7213.054 | 9.806 | 0.620 | 1.233 | 0.733 | | 7263.975 | 9.921 | 0.665 | 1.221 | 0.765 | 1.535 |
| 7221.043 | 9.778 | 0.678 | 1.224 | 0.788 | 1.512 | 7268.993 | 9.884 | | 1.233 | 0.772 | 1.513 |
| 7223.939 | 9.766 | 0.737 | 1.225 | 0.787 | 1.541 | 7272.979 | 9.883 | 0.620 | 1.232 | 0.774 | 1.523 |
| 7227.014 | 9.774 | 0.710 | 1.230 | 0.779 | 1.492 | 7283.005 | 9.873 | 0.664 | 1.237 | 0.777 | 1.518 |
| 7237.110 | 9.789 | 0.716 | 1.217 | 0.774 | 1.503 | 7297.849 | 9.626 | 0.609 | 1.202 | 0.764 | 1.472 |
| 7240.920 | 9.784 | 0.618 | 1.215 | 0.785 | 1.473 | 7301.935 | 9.624 | 0.613 | 1.191 | 0.769 | 1.448 |
| 7246.880 | 9.770 | 0.618 | 1.213 | 0.773 | | 7305.955 | 9.659 | 0.608 | 1.196 | 0.761 | 1.464 |
| 7254.946 | 9.837 | 0.609 | 1.219 | 0.775 | 1.491 | 7306.912 | 9.678 | 0.650 | 1.201 | 0.765 | |
| 7255.953 | 9.839 | 0.705 | 1.229 | 0.775 | 1.501 | 7308.036 | 9.684 | 0.581 | 1.196 | 0.758 | 1.481 |
| 7312.994 | 9.689 | 0.628 | 1.212 | 0.761 | 1.473 | 7354.849 | 9.800 | 0.650 | 1.217 | 0.763 | 1.507 |
| 7316.851 | 9.635 | 0.599 | 1.216 | 0.761 | 1.472 | 7360.923 | 9.795 | | 1.237 | | |
| 7322.140 | 9.645 | 0.650 | 1.209 | 0.759 | 1.467 | 7367.924 | 9.714 | 0.608 | 1.221 | 0.770 | 1.471 |
| 7325.901 | 9.659 | 0.604 | 1.198 | 0.765 | 1.496 | 7370.885 | 9.631 | 0.609 | 1.210 | 0.760 | 1.447 |
| 7333.883 | 9.637 | | 1.192 | | | 7372.908 | 9.596 | 0.635 | 1.199 | 0.774 | 1.469 |
| 7334.883 | 9.634 | | 1.196 | | | 7375.983 | 9.576 | 0.599 | 1.198 | 0.765 | 1.480 |
| 7337.027 | 9.633 | | 1.225 | | | 7380.088 | 9.581 | | 1.201 | | |
| 7343.939 | 9.650 | 0.631 | 1.225 | 0.753 | 1.453 | 7394.890 | 9.695 | 0.622 | 1.210 | 0.765 | 1.491 |
| 7346.084 | 9.682 | 0.611 | 1.217 | 0.760 | 1.473 | 7397.123 | 9.722 | 0.662 | 1.226 | 0.753 | 1.485 |
| 7352.843 | 9.784 | 0.600 | 1.220 | 0.768 | 1.518 | 7400.915 | 9.739 | 0.584 | 1.209 | 0.775 | 1.487 |
| 7408.092 | 9.684 | 0.644 | 1.221 | 0.774 | 1.490 | 7488.963 | 9.749 | | 1.169 | 0.775 | 1.464 |
| 7417.972 | 9.597 | 0.601 | 1.210 | 0.764 | 1.450 | 7489.978 | 9.732 | 0.582 | 1.186 | 0.764 | 1.461 |
| 7427.942 | 9.642 | 0.650 | 1.198 | 0.762 | 1.469 | 7556.130 | 9.824 | | 1.193 | 0.786 | 1.464 |
| 7435.922 | 9.738 | 0.585 | 1.168 | 0.729 | 1.422 | 7570.011 | 9.804 | | 1.194 | 0.784 | 1.463 |
| 7439.913 | 9.735 | 0.622 | 1.196 | 0.752 | 1.469 | 7571.152 | 9.812 | | 1.194 | 0.783 | 1.460 |
| 7464.916 | 9.595 | 0.627 | 1.205 | 0.754 | 1.420 | 7572.963 | 9.795 | 0.688 | 1.204 | 0.766 | 1.496 |
| 7466.912 | 9.673 | 0.622 | 1.204 | 0.772 | 1.470 | 7588.198 | 9.772 | 0.687 | 1.186 | 0.777 | |
| 7479.964 | 9.749 | 0.617 | 1.212 | 0.757 | 1.492 | 7590.137 | 9.781 | | 1.172 | 0.779 | |
| 7481.955 | 9.738 | | 1.205 | 0.764 | 1.472 | 7592.104 | 9.762 | | 1.204 | 0.787 | |
| 7486.970 | 9.746 | 0.613 | 1.193 | 0.750 | 1.493 | 7611.035 | 9.754 | 0.666 | 1.202 | 0.772 | 1.459 |
| 7612.161 | 9.725 | 0.661 | 1.209 | 0.767 | 1.448 | 7628.064 | 9.708 | 0.704 | 1.225 | 0.779 | 1.462 |
| 7616.177 | 9.668 | 0.612 | 1.207 | 0.771 | 1.504 | 7636.037 | 9.827 | 0.659 | 1.230 | 0.775 | 1.389 |
| 7620.065 | 9.626 | 0.712 | 1.192 | 0.777 | 1.475 | 7644.060 | 9.878 | | 1.232 | 0.796 | |
| 7620.971 | 9.612 | 0.673 | 1.214 | 0.759 | 1.459 | 7652.149 | 10.091 | | 1.254 | 0.795 | 1.501 |
| 7623.059 | 9.636 | 0.694 | 1.222 | 0.776 | | | | | | | |

are plotted in Fig. 2.1. Throughout most of our photometry, S Aps was slowly recovering from a decline which occurred prior to JD 2446450. A light curve of the recovery of the star from a minimum magnitude of $V = 13.2$ from JD 2446455–2446660 was shown by Marang *et al.* (1989).

Fig. 2.2a shows the power spectrum for the $V$ data obtained prior to JD 2447630 (the three observations covering the decline onset were ignored). The power spectrum shows significant low frequency power due to the star rising from the earlier decline and a number of higher frequency peaks. The two peaks at $f = 0.0009$ d$^{-1}$ and 0.0031 d$^{-1}$

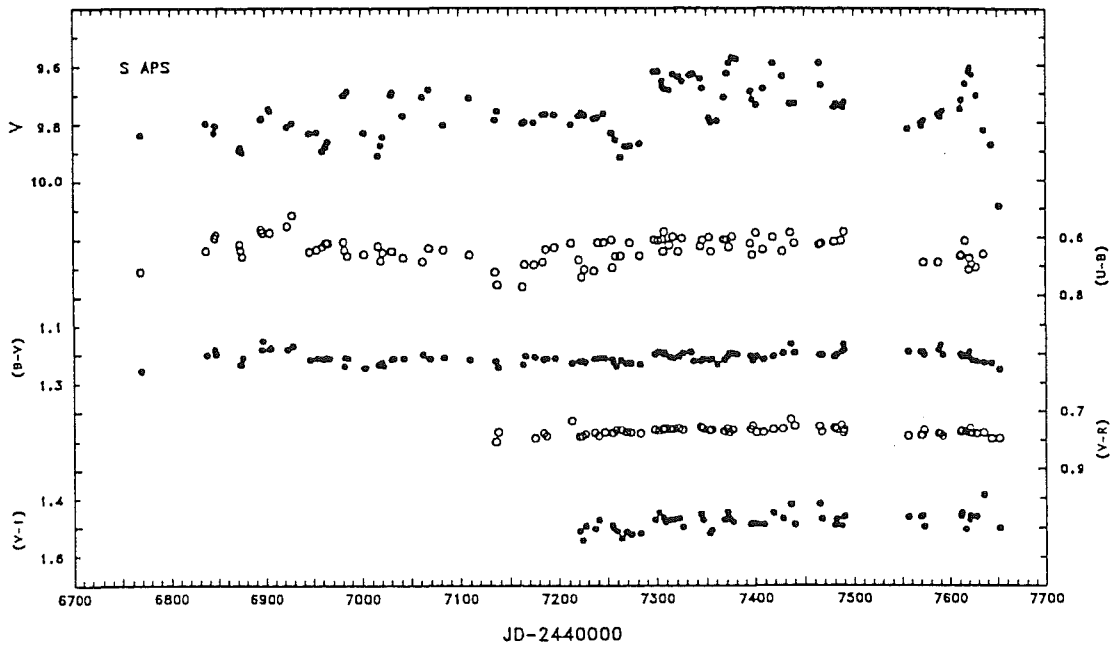


Figure 2.1. $V$ light and ($U$–$B$), ($B$–$V$), ($V$–$R$) and ($V$–$I$) colour curves for S Aps plotted against Julian Date.

were initially presumed to represent the low frequency contribution. These two frequencies were successively removed (Fig. 2.2b) as known constituents, where the frequency to be removed is shown within each panel, and the spectrum was recalculated (Fig. 2.2c). It shows the presence of a periodicity at $f_1 = 0.0125$ d$^{-1}$ (period $P_1 = 80.0$ d). Power spectra resulting from successive iterations are shown in Figs. 2.2d, 2.2e and 2.2f. Fig. 2.2d reveals a second periodicity at $f_2 = 0.0232$ d$^{-1}$ ($P_2 = 43.1$ d). Fig. 2.2e contains a peak at $f_3 = 0.0257$ d$^{-1}$ ($P_3 = 38.9$ d). As $f_3 \approx 2f_1$ it is probably the harmonic of that frequency. The values of these latter two frequencies raise the possibility that the low frequency periodicity at $f = 0.0031$ d$^{-1}$ may be the coupling term $f_{32} = f_3 - f_2$. None of the peaks in Fig. 2.2f was considered to be significant (see Section 2.3). The frequencies $f$ identified by this successive iteration, and the corresponding period $P$, amplitude $A$, onset phase $\phi$ and probability ($F$) of these frequencies, are summarised in Table 2.11 (at the end of Section 2.4.1).

A synthetic light curve (Fig. 2.3), consisting of the periods $P_1$, $P_2$ and $P_3$, is compared to the $V$ photometry of S Aps (with the two low frequency components removed). As expected, the general features of the light curve are reproduced by the synthetic curve although large residuals are still evident. As the inclusion of additional periods in the synthetic curve does not result in a substantially improved fit to the photometry, it is possible that the values for the three most significant periods will be improved, or that a currently unidentified period will be revealed, with the availability of additional data. A further possibility is that there is some modulation of the amplitudes of these three periods (also see Sections 2.4.1.5 and 2.5.1).

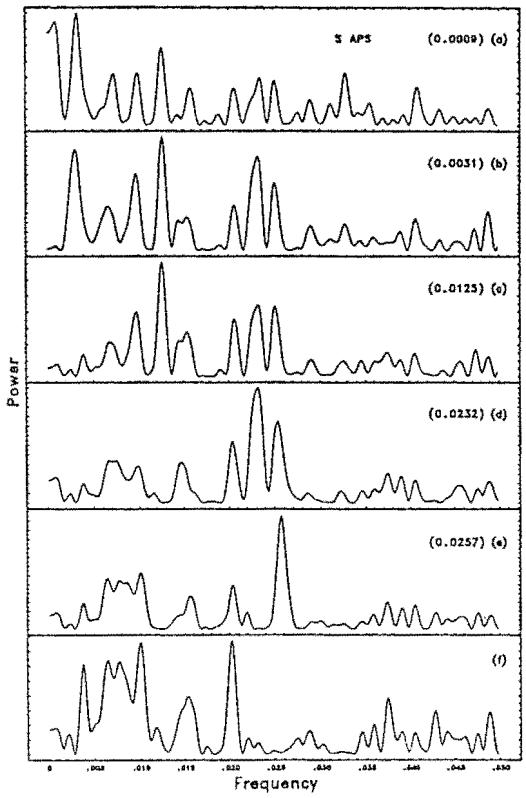


**Figure 2.2.** Power spectra from the Fourier analysis of $V$ photometry of S Aps obtained between JD 2446769–2447628. (a) is the power spectrum of the original dataset. Panels (b)–(f) show the spectra after the removal of identified constituent frequencies. The frequency to be removed is indicated within each panel. The unit of frequency is $d^{-1}$.

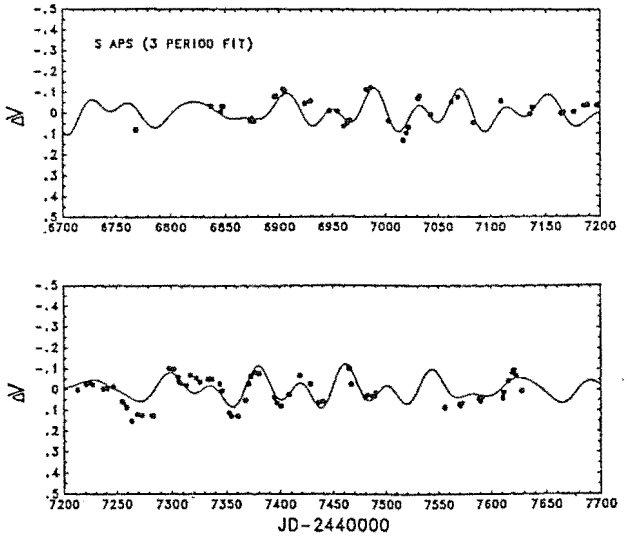


**Figure 2.3.** Comparison of a 3 period synthetic curve to the $V$ photometry of S Aps obtained between JD 2446769–2447628 (with the two low frequency components of Fig. 2.2 removed).

#### 2.4.1.2 U Aqr

The *UBV* observations of U Aqr from JD 2446598–2447700 are listed in Table 2.3. The light and colour curves are plotted in Fig. 2.4.

The photometry obtained during 1986 and 1987 showed the $V$ curve varying on a timescale of $\sim$ 40 d with alternately low (0.1–0.3 mag) and large (generally 0.5–0.7 mag) amplitude cycles. During 1988 U Aqr appeared almost inactive, but there was some indication that the amplitude of the variations increased during 1989. We note that the maximum magnitude of the star remained almost constant (at $V \approx 10.85$) throughout the duration of our observations. In these respects, the behaviour of U Aqr resembled that of an RV Tauri–type star (Wallerstein, personal communication to the author). The amplitude of the variations of U Aqr is, however, lower than most RV Tauri stars (see fig. 1 of Gillet *et al.* 1989). Wallerstein indicated that the low activity phase observed in U Aqr has also been observed to occur in RV Tauri stars. This phase is possibly caused by a decoupling of the outer envelope from the inner pulsations. When the larger amplitude variations return in RV Tauri stars they are in phase with earlier larger amplitude cycles.

The power spectrum for the 1986 and 1987 $V$ photometry (Fig. 2.5) clearly shows periodicities at $f_1 = 0.0123$ d$^{-1}$ ($P_1 = 81.30$ d) and $f_2 = 0.0249$ d$^{-1}$ ($P_2 = 40.16$ d). Note that $f_2 \approx 2f_1$ which is probably an harmonic of that frequency.

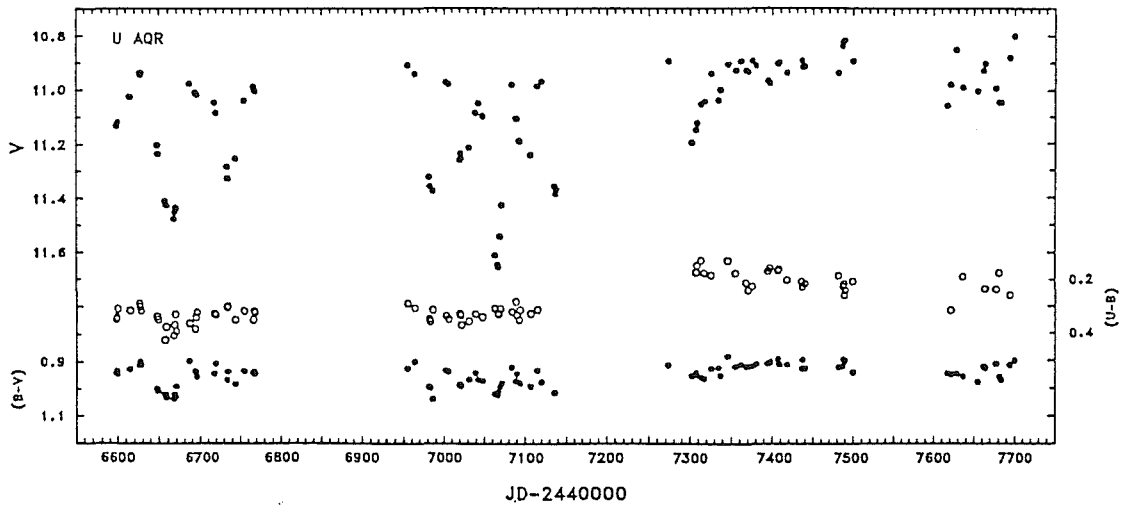


**Figure 2.4.** $V$ light and ($U$–$B$) and ($B$–$V$) colour curves for U Aqr plotted against Julian Date.

Table 2.3. MJUO *UBV* photometry of U Aqr.

| JD-2440000 | *V* | (*U*-*B*) | (*B*-*V*) | JD-2440000 | *V* | (*U*-*B*) | (*B*-*V*) |
|---|---|---|---|---|---|---|---|
| 6598.134 | 11.133 | 0.345 | 0.941 | 6658.165 | 11.425 | 0.371 | 1.030 |
| 6599.198 | 11.134 | 0.338 | 0.933 | 6667.183 | 11.477 | 0.401 | 1.035 |
| 6600.164 | 11.120 | 0.307 | 0.945 | 6668.070 | 11.451 | 0.363 | 1.017 |
| 6615.161 | 11.026 | 0.314 | 0.927 | 6669.152 | 11.435 | 0.326 | 1.027 |
| 6626.192 | 10.939 | 0.288 | 0.910 | 6670.104 | 11.439 | 0.387 | 0.990 |
| 6627.168 | 10.946 | 0.300 | 0.900 | 6687.013 | 10.978 | 0.358 | 0.894 |
| 6628.176 | 10.938 | 0.314 | 0.910 | 6694.104 | 11.009 | 0.378 | 0.932 |
| 6648.154 | 11.205 | 0.334 | 0.998 | 6694.993 | 11.016 | 0.336 | 0.933 |
| 6649.175 | 11.236 | 0.345 | 1.006 | 6696.124 | 11.019 | 0.318 | 0.952 |
| 6657.104 | 11.411 | 0.418 | 1.018 | 6718.058 | 11.047 | 0.322 | 0.942 |
| 6719.995 | 11.085 | 0.326 | 0.905 | 6982.021 | 11.317 | 0.340 | 0.990 |
| 6733.974 | 11.282 | 0.299 | 0.964 | 6983.096 | 11.351 | 0.350 | 0.993 |
| 6734.922 | 11.325 | 0.294 | 0.934 | 6986.072 | 11.368 | 0.308 | 1.034 |
| 6743.935 | 11.252 | 0.344 | 0.980 | 7003.072 | 10.970 | 0.329 | 0.928 |
| 6754.956 | 11.040 | 0.312 | 0.931 | 7006.162 | 10.977 | 0.341 | 0.932 |
| 6766.917 | 10.988 | 0.343 | 0.939 | 7020.128 | 11.254 | 0.321 | 0.981 |
| 6767.931 | 11.002 | 0.311 | 0.934 | 7021.082 | 11.231 | 0.328 | 0.987 |
| 6768.931 | 11.005 | 0.318 | 0.942 | 7022.112 | 11.248 | 0.362 | 0.985 |
| 6955.069 | 10.907 | 0.284 | 0.920 | 7031.049 | 11.210 | 0.349 | 0.962 |
| 6964.112 | 10.939 | 0.301 | 0.896 | 7039.144 | 11.081 | 0.323 | 0.939 |
| 7043.007 | 11.047 | | 0.963 | 7092.986 | 11.183 | 0.344 | 0.972 |
| 7047.920 | 11.095 | 0.334 | 0.967 | 7093.945 | 11.186 | 0.308 | 0.975 |
| 7062.976 | 11.609 | 0.303 | 1.015 | 7106.911 | 11.236 | 0.322 | 0.989 |
| 7066.070 | 11.642 | 0.319 | 1.018 | 7114.907 | 10.984 | 0.307 | 0.928 |
| 7066.913 | 11.652 | 0.325 | 1.007 | 7119.972 | 10.967 | | 0.971 |
| 7068.918 | 11.538 | 0.304 | 0.988 | 7135.940 | 11.351 | | 1.011 |
| 7070.949 | 11.421 | | 0.977 | 7136.946 | 11.379 | | |
| 7083.913 | 10.979 | 0.315 | 0.918 | 7137.935 | 11.363 | | |
| 7088.901 | 11.102 | 0.278 | 0.968 | 7273.218 | 10.891 | | 0.915 |
| 7089.977 | 11.104 | 0.327 | 0.942 | 7302.175 | 11.194 | | 0.953 |
| 7307.170 | 11.146 | 0.169 | 0.942 | 7367.984 | 10.925 | 0.207 | 0.920 |
| 7308.197 | 11.121 | 0.144 | 0.949 | 7371.070 | 10.930 | 0.235 | 0.919 |
| 7313.172 | 11.050 | 0.126 | 0.960 | 7376.082 | 10.891 | 0.219 | 0.917 |
| 7317.118 | 11.040 | 0.171 | 0.965 | 7380.175 | 10.908 | | 0.909 |
| 7326.099 | 10.936 | 0.179 | 0.927 | 7395.002 | 10.962 | 0.165 | 0.909 |
| 7335.025 | 11.035 | | 0.924 | 7397.092 | 10.971 | 0.153 | 0.903 |
| 7337.238 | 10.996 | | 0.952 | 7407.104 | 10.901 | 0.164 | 0.892 |
| 7346.063 | 10.904 | 0.126 | 0.883 | 7408.172 | 10.897 | 0.157 | 0.913 |
| 7355.096 | 10.925 | 0.172 | 0.920 | 7418.068 | 10.934 | 0.197 | 0.912 |
| 7361.120 | 10.892 | | 0.911 | 7435.994 | 10.889 | 0.202 | 0.927 |
| 7436.995 | 10.913 | 0.223 | 0.895 | 7628.244 | 10.850 | | 0.947 |
| 7440.007 | 10.910 | 0.211 | 0.926 | 7636.197 | 10.989 | 0.187 | 0.958 |
| 7461.936 | 10.934 | 0.182 | 0.922 | 7655.196 | 11.003 | | 0.978 |
| 7486.949 | 10.835 | 0.222 | 0.918 | 7662.189 | 10.927 | | 0.923 |
| 7487.946 | 10.820 | 0.212 | 0.894 | 7664.257 | 10.902 | 0.234 | 0.930 |
| 7488.946 | 10.817 | 0.254 | 0.904 | 7677.167 | 10.992 | 0.236 | 0.913 |
| 7489.959 | 10.816 | 0.236 | 0.898 | 7681.049 | 11.045 | 0.175 | 0.959 |
| 7499.929 | 10.892 | 0.203 | 0.941 | 7683.247 | 11.045 | | 0.971 |
| 7617.213 | 11.056 | | 0.946 | 7694.222 | 10.880 | 0.258 | 0.918 |
| 7621.228 | 10.977 | 0.313 | 0.951 | 7700.213 | 10.800 | | 0.901 |

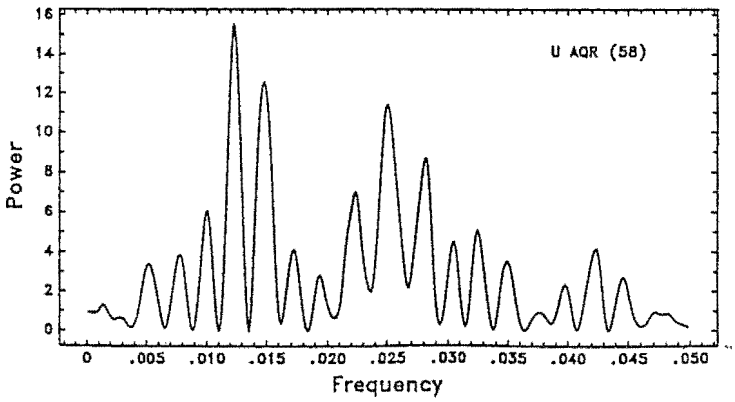


Figure 2.5. Power spectrum for the 1986–1987 *V* photometry of U Aqr. The number of data points is indicated.

#### 2.4.1.3 V CrA

The *UBV* observations of V CrA from JD 2446598–2447440 are listed in Table 2.4. The photometry is listed until about 10 d after the onset of the 1988 decline of this star near JD 2447430 (Section 3.2.2). The light and colour curves are shown in Fig. 2.6.

The periodic nature of the light curve of V CrA changes from year to year. During 1986 the period of the star was $\sim$ 50 d. During 1987 the period doubled to $\sim$ 100 d while in 1988, prior to the decline, the behaviour was complex although there appeared to be a period of $\sim$ 75 d and possibly variations of shorter duration. The amplitude of the $V$ light curve during 1986 ($\Delta V \sim 0.13$ mag) was lower than during 1987 ($\Delta V \sim 0.25$ mag) and 1988 ($\Delta V \sim 0.20$ mag). However, the colour amplitude was similar during all three years. The mean $V$ magnitude of V CrA brightened slowly during the interval examined here due to the rise from a decline which occurred near JD 2446330 (see fig 4 of Lawson, Cottrell & Bateson 1989).

The power spectra obtained from the analysis of the $V$ photometry obtained during the individual years, with the exception of the final two observations made during 1988, are shown in Fig. 2.7. The year and the number of data points (bracketted) are indicated within each panel. The data obtained during 1986 were detrended. The power spectra have peaks at $f = 0.0175$ d$^{-1}$ ($P = 57.1$ d), 0.0089 d$^{-1}$ ($P = 112.4$ d) and 0.0130 d$^{-1}$ ($P = 76.9$ d) during 1986, 1987 and 1988 respectively. Note the near 2:1 ratio of the frequencies identified during 1986 and 1987. These periodicities are summarised in Table 2.11. The 76.9 d period does not reflect the apparent range of variations observed in the light curve during 1988, but we note that this value is similar to the period of $\sim$ 75 d determined from visual estimates of V CrA obtained between JD 2435448–2441629 (Bateson 1975).

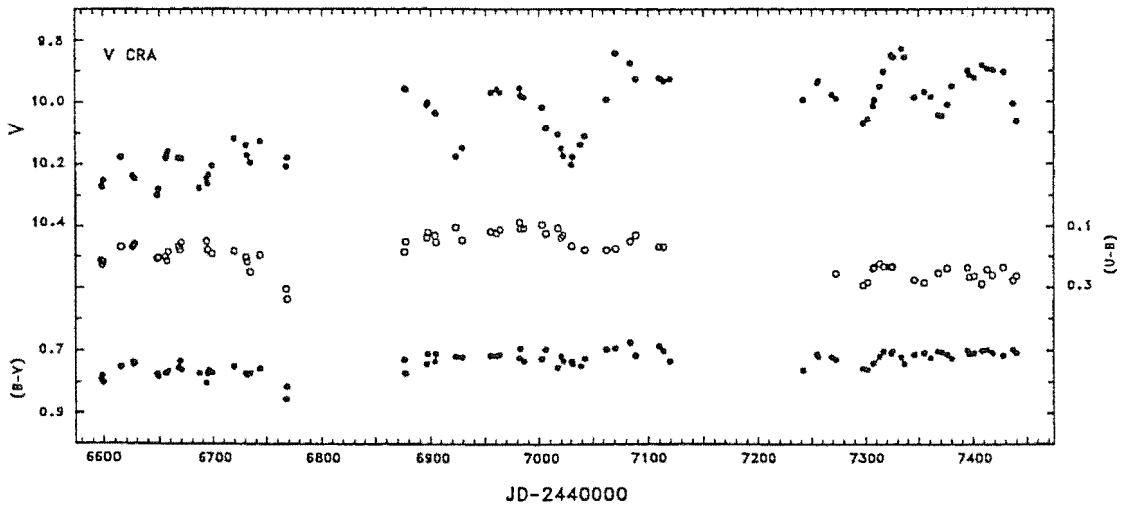


**Figure 2.6.** $V$ light and ($U$–$B$) and ($B$–$V$) colour curves for V CrA plotted against Julian Date.

Table 2.4. MJUO *UBV* photometry of V CrA.

| JD-2440000 | *V* | (*U*-*B*) | (*B*-*V*) | JD-2440000 | *V* | (*U*-*B*) | (*B*-*V*) |
|---|---|---|---|---|---|---|---|
| 6598.085 | 10.271 | 0.212 | 0.791 | 6657.061 | 10.170 | 0.212 | 0.771 |
| 6599.115 | 10.273 | 0.226 | 0.780 | 6658.130 | 10.160 | 0.185 | 0.766 |
| 6600.074 | 10.251 | 0.217 | 0.801 | 6668.029 | 10.180 | 0.166 | 0.753 |
| 6615.116 | 10.177 | 0.168 | 0.752 | 6669.103 | 10.181 | 0.178 | 0.734 |
| 6626.147 | 10.236 | 0.169 | 0.736 | 6670.076 | 10.183 | 0.155 | 0.760 |
| 6627.099 | 10.242 | 0.164 | 0.743 | 6686.993 | 10.276 | | 0.772 |
| 6628.106 | 10.246 | 0.158 | 0.739 | 6694.078 | 10.246 | 0.149 | 0.801 |
| 6648.122 | 10.299 | 0.206 | 0.774 | 6694.970 | 10.262 | 0.177 | 0.774 |
| 6649.118 | 10.280 | 0.202 | 0.782 | 6696.084 | 10.234 | | 0.761 |
| 6656.059 | 10.181 | 0.200 | 0.772 | 6698.994 | 10.205 | 0.189 | 0.769 |
| 6719.978 | 10.118 | 0.180 | 0.750 | 6897.226 | 10.003 | 0.118 | 0.710 |
| 6730.954 | 10.139 | 0.201 | 0.771 | 6904.149 | 10.035 | 0.129 | 0.732 |
| 6731.953 | 10.171 | 0.214 | 0.776 | 6905.147 | 10.038 | 0.151 | 0.710 |
| 6734.891 | 10.194 | 0.248 | 0.770 | 6923.189 | 10.175 | 0.103 | 0.718 |
| 6743.919 | 10.127 | 0.193 | 0.756 | 6929.063 | 10.147 | 0.144 | 0.720 |
| 6767.904 | 10.207 | 0.302 | 0.854 | 6955.026 | 9.970 | 0.116 | 0.714 |
| 6768.907 | 10.179 | 0.335 | 0.813 | 6960.927 | 9.958 | 0.121 | 0.715 |
| 6876.225 | 9.957 | 0.182 | 0.728 | 6964.069 | 9.969 | 0.110 | 0.711 |
| 6877.236 | 9.960 | 0.149 | 0.771 | 6981.928 | 9.955 | 0.085 | 0.721 |
| 6896.154 | 10.010 | 0.136 | 0.742 | 6983.012 | 9.979 | 0.106 | 0.692 |
| 6986.022 | 9.984 | 0.106 | 0.731 | 7063.013 | 9.991 | 0.177 | 0.696 |
| 7002.893 | 10.017 | 0.093 | 0.725 | 7071.019 | 9.842 | 0.172 | 0.691 |
| 7006.134 | 10.083 | 0.122 | 0.696 | 7083.882 | 9.873 | 0.148 | 0.674 |
| 7017.027 | 10.103 | 0.104 | 0.752 | 7088.926 | 9.925 | 0.128 | 0.715 |
| 7020.026 | 10.148 | 0.135 | 0.717 | 7109.935 | 9.922 | 0.166 | 0.686 |
| 7022.023 | 10.170 | 0.127 | 0.730 | 7113.909 | 9.932 | 0.167 | 0.700 |
| 7031.010 | 10.198 | 0.162 | 0.732 | 7119.936 | 9.925 | | 0.734 |
| 7031.881 | 10.175 | | 0.740 | 7242.131 | 9.993 | | 0.761 |
| 7039.080 | 10.135 | | 0.748 | 7255.138 | 9.938 | | 0.711 |
| 7042.969 | 10.109 | 0.176 | 0.725 | 7256.098 | 9.932 | | 0.718 |
| 7269.133 | 9.976 | | 0.719 | 7333.991 | 9.828 | | 0.720 |
| 7273.126 | 9.989 | 0.253 | 0.728 | 7337.130 | 9.854 | | 0.740 |
| 7298.055 | 10.069 | 0.291 | 0.756 | 7345.928 | 9.986 | 0.274 | 0.712 |
| 7302.080 | 10.056 | 0.282 | 0.759 | 7354.977 | 9.967 | 0.283 | 0.706 |
| 7307.020 | 10.012 | 0.238 | 0.739 | 7361.093 | 9.984 | | 0.722 |
| 7308.233 | 9.993 | 0.232 | 0.737 | 7367.951 | 10.043 | 0.252 | 0.702 |
| 7313.130 | 9.949 | 0.220 | 0.719 | 7370.919 | 10.045 | | 0.704 |
| 7316.974 | 9.901 | 0.229 | 0.702 | 7376.013 | 10.010 | 0.237 | 0.712 |
| 7323.971 | 9.847 | 0.231 | 0.707 | 7380.112 | 9.949 | | 0.725 |
| 7326.012 | 9.855 | 0.230 | 0.701 | 7394.986 | 9.899 | 0.235 | 0.698 |
| 7397.060 | 9.912 | 0.266 | 0.711 | 7418.009 | 9.897 | 0.260 | 0.707 |
| 7401.008 | 9.922 | 0.263 | 0.709 | 7427.998 | 9.903 | 0.235 | 0.716 |
| 7408.125 | 9.881 | 0.288 | 0.700 | 7436.958 | 10.006 | 0.277 | 0.697 |
| 7413.009 | 9.892 | 0.242 | 0.697 | 7439.985 | 10.064 | 0.263 | 0.707 |

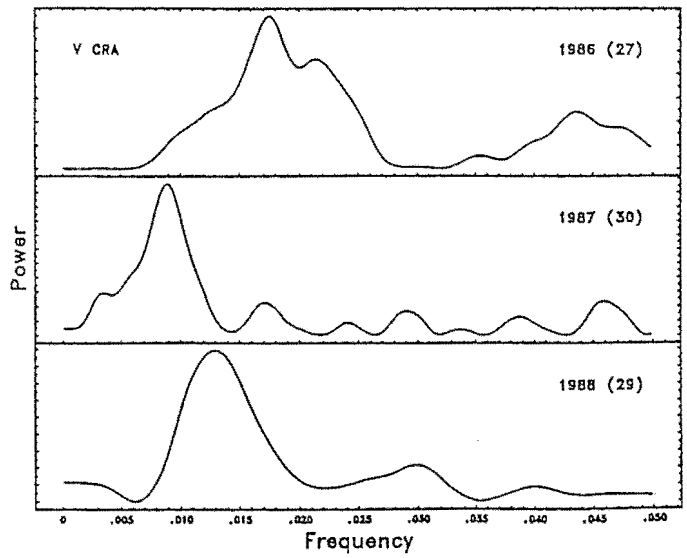


**Figure 2.7.** Power spectra for the 1986, 1987 and 1988 (to JD 2447428) *V* photometry of V CrA. The year and the number of data points obtained during each year is indicated within each panel.

#### 2.4.1.4 Y Mus

The *UBV* observations of Y Mus from JD 2446598–2447714 are listed in Table 2.5. The light and colour curves are shown in Fig. 2.8.

The $V$ and $(B–V)$ curves appear almost irregular, with some variability apparent in the $(U–B)$ curve on timescales of 100–200 d. The amplitude of the colour curves exceeds that of the $V$ curve. In Fig. 2.9 we show power spectra for the $V$, $(U–B)$ and $(B–V)$ photometry of Y Mus. The number in brackets within each panel is the number of data points in each analysis.

The dominant frequencies identified in these data are summarised in Table 2.11. A periodicity at $f \approx 0.090$ d$^{-1}$ ($P \approx$110 d) was detected in all three datasets, namely $V$, $(U–B)$ and $(B–V)$. The spectral analysis isolated two significant periodicities in the $(U–B)$ dataset at $f_1 = 0.0044$ d$^{-1}$ ($P_1 = 227.3$ d) and $f_2 = 0.0093$ d$^{-1}$ ($P_2 = 107.5$ d).

**Table 2.5.** MJUO *UBV* photometry of Y Mus.

| JD–2440000 | $V$ | $(U–B)$ | $(B–V)$ | JD–2440000 | $V$ | $(U–B)$ | $(B–V)$ |
|---|---|---|---|---|---|---|---|
| 6597.894 | 10.426 | 0.446 | 0.984 | 6648.940 | 10.275 | 0.332 | 0.882 |
| 6598.930 | 10.431 | 0.467 | 0.987 | 6655.887 | 10.271 | 0.335 | 0.875 |
| 6599.860 | 10.439 | 0.448 | 0.975 | 6656.934 | 10.263 | 0.327 | 0.879 |
| 6614.886 | 10.286 | 0.372 | 0.900 | 6667.868 | 10.307 | 0.316 | 0.871 |
| 6615.857 | 10.290 | 0.383 | 0.908 | 6668.873 | 10.302 | 0.325 | 0.874 |
| 6625.956 | 10.314 | 0.414 | 0.939 | 6669.884 | 10.303 | 0.307 | 0.874 |
| 6626.894 | 10.303 | 0.416 | 0.931 | 6686.874 | 10.290 | 0.363 | 0.903 |
| 6627.904 | 10.297 | 0.416 | 0.934 | 6694.903 | 10.312 | 0.423 | 0.913 |
| 6637.864 | 10.364 | 0.381 | 0.950 | 6698.887 | 10.263 | 0.329 | 0.871 |
| 6647.974 | 10.301 | 0.322 | 0.886 | 6731.157 | 10.332 | 0.429 | 0.942 |
| 6768.999 | 10.284 | 0.383 | 0.889 | 6877.132 | 10.330 | 0.360 | 0.923 |
| 6814.103 | 10.324 | 0.427 | 0.939 | 6896.057 | 10.325 | 0.337 | 0.884 |
| 6827.153 | 10.349 | 0.406 | 0.959 | 6897.156 | 10.306 | 0.325 | 0.884 |
| 6835.116 | 10.366 | 0.394 | 0.913 | 6904.081 | 10.292 | 0.314 | 0.879 |
| 6837.015 | 10.340 | 0.359 | 0.944 | 6905.078 | 10.287 | 0.332 | 0.920 |
| 6846.070 | 10.386 | 0.410 | 0.959 | 6923.975 | 10.322 | 0.365 | 0.914 |
| 6847.061 | 10.359 | 0.398 | 0.985 | 6946.938 | 10.432 | 0.506 | 1.014 |
| 6867.170 | 10.258 | 0.357 | 0.880 | 6954.870 | 10.291 | 0.429 | 0.944 |
| 6874.082 | 10.282 | 0.335 | 0.898 | 6960.875 | 10.270 | 0.411 | 0.923 |
| 6876.131 | 10.316 | 0.369 | 0.925 | 6963.973 | 10.267 | 0.429 | 0.922 |
| 6965.985 | 10.279 | 0.437 | 0.928 | 7162.078 | 10.307 | 0.408 | 0.955 |
| 6981.857 | 10.338 | 0.386 | 0.905 | 7164.105 | 10.291 | 0.411 | 0.933 |
| 6985.938 | 10.339 | 0.415 | 0.928 | 7176.059 | 10.366 | 0.415 | 0.968 |
| 7003.031 | 10.336 | 0.417 | 0.945 | 7185.023 | 10.400 | | 0.970 |
| 7019.954 | 10.316 | 0.411 | 0.917 | 7188.022 | 10.342 | | 0.944 |
| 7021.953 | 10.302 | 0.399 | 0.914 | 7197.081 | 10.272 | 0.408 | 0.919 |
| 7030.927 | 10.352 | 0.406 | 0.959 | 7213.031 | 10.291 | 0.407 | 0.908 |
| 7042.884 | 10.304 | 0.444 | 0.905 | 7220.974 | 10.283 | | 0.930 |
| 7062.911 | 10.318 | 0.483 | 0.897 | 7222.017 | 10.286 | | 0.936 |
| 7138.124 | 10.227 | 0.378 | 0.918 | 7226.982 | 10.276 | 0.442 | 0.938 |
| 7235.938 | 10.231 | 0.469 | 0.924 | 7354.832 | 10.335 | 0.425 | 0.914 |
| 7241.048 | 10.243 | | 0.933 | 7362.957 | 10.293 | | 0.910 |
| 7248.917 | 10.274 | | 0.960 | 7370.953 | 10.311 | 0.408 | 0.895 |
| 7255.091 | 10.271 | | 0.958 | 7375.917 | 10.310 | 0.435 | 0.918 |
| 7258.992 | 10.270 | | 0.976 | 7394.873 | 10.297 | 0.372 | 0.906 |
| 7263.997 | 10.325 | | 0.998 | 7400.893 | 10.302 | 0.363 | 0.900 |
| 7268.973 | 10.312 | | 0.967 | 7406.888 | 10.354 | 0.404 | 0.907 |
| 7273.228 | 10.324 | 0.488 | 0.956 | 7418.165 | 10.345 | | 0.935 |
| 7325.878 | 10.258 | 0.420 | 0.887 | 7427.925 | 10.275 | 0.429 | 0.932 |
| 7343.861 | 10.320 | | 0.932 | 7435.831 | 10.274 | 0.431 | 0.926 |
| 7480.140 | 10.251 | 0.473 | 0.952 | 7611.002 | 10.237 | 0.366 | 0.891 |
| 7489.119 | 10.275 | 0.377 | 0.915 | 7623.024 | 10.282 | 0.380 | 0.928 |
| 7490.125 | 10.282 | 0.404 | 0.904 | 7636.011 | 10.330 | 0.338 | 0.926 |
| 7569.998 | 10.295 | | 0.955 | 7644.026 | 10.267 | 0.421 | 0.932 |
| 7571.103 | 10.266 | | 0.945 | 7655.932 | 10.265 | 0.414 | 0.905 |
| 7572.982 | 10.256 | 0.360 | 0.914 | 7676.900 | 10.268 | 0.420 | 0.921 |
| 7592.048 | 10.366 | | 0.981 | 7713.904 | 10.373 | 0.444 | 0.942 |

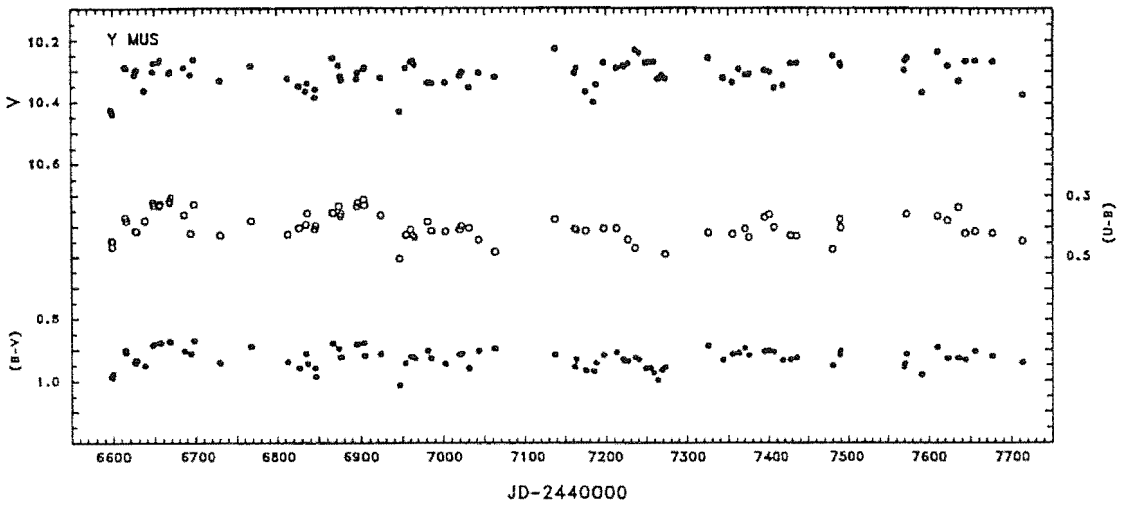


Figure 2.8. $V$ light and $(U\text{-}B)$ and $(B\text{-}V)$ colour curves for Y Mus plotted against Julian Date.

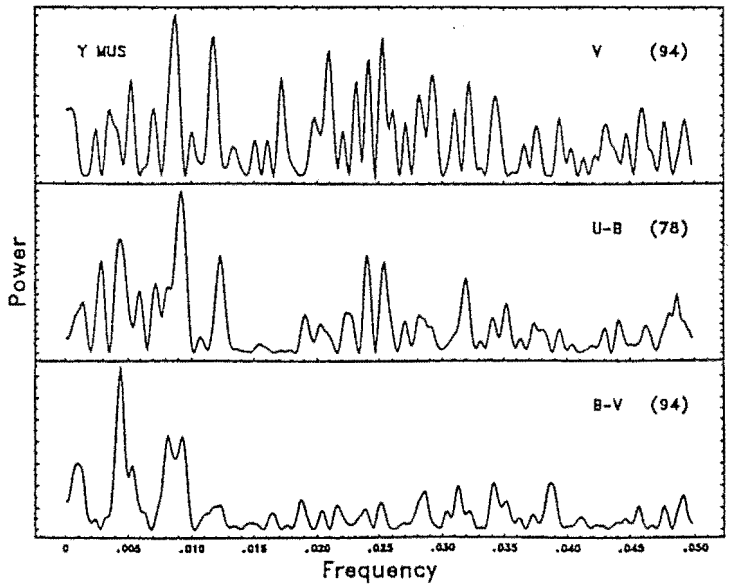


**Figure 2.9.** Power spectra for $V$, $(U\text{-}B)$ and $(B\text{-}V)$ photometry of Y Mus. The number of data points for the magnitudes and colours are indicated within each panel.

### 2.4.1.5 RY Sgr

The MJUO *UBVRI* observations of RY Sgr from JD 2446583–2447781 are listed in Tables 2.6a and 2.6b. The $V$ light curve and $(U–B)$ and $(B–V)$ colour curves for those data obtained during 1986 and 1987 are plotted in Fig. 2.10. The $V$ light curve and $(U–B)$, $(B–V)$, $(V–R)$ and $(V–I)$ colour curves for those data obtained during 1988 and 1989 are plotted in Figs. 2.11a and 2.11b. Much of the 1986 photometry for RY Sgr was published by Lawson *et al.* (1987), but has been included here due to the availability of additional data obtained during 1986 and a revision of the comparison star magnitude and colours.

Several aspects characterise the light and colour curves of RY Sgr. The amplitudes of both the light and colour curves are greater than any other known RCB star. While it is apparent that the pulsation period of RY Sgr varies from cycle to cycle, the regularity of the mean period of the star, at least over ~100 cycles, is well demonstrated (see Section 5.1).

**Table 2.6a.** MJUO *UBV* photometry of RY Sgr during 1986 and 1987.

| JD–2440000 | $V$ | $(U–B)$ | $(B–V)$ | JD–2440000 | $V$ | $(U–B)$ | $(B–V)$ |
|---|---|---|---|---|---|---|---|
| 6582.950 | 6.250 | 0.045 | 0.440 | 6633.876 | 6.418 | 0.272 | 0.697 |
| 6584.080 | 6.200 | 0.045 | 0.430 | 6638.012 | 6.483 | 0.252 | 0.682 |
| 6586.980 | 6.170 | 0.065 | 0.470 | 6638.879 | 6.491 | 0.248 | 0.670 |
| 6598.105 | 6.255 | 0.202 | 0.625 | 6647.928 | 6.375 | -0.053 | 0.420 |
| 6599.125 | 6.289 | 0.197 | 0.623 | 6648.888 | 6.354 | -0.076 | 0.404 |
| 6600.082 | 6.324 | 0.199 | 0.619 | 6655.959 | 6.229 | 0.004 | 0.475 |
| 6615.085 | 6.429 | 0.019 | 0.506 | 6656.932 | 6.226 | 0.029 | 0.506 |
| 6627.077 | 6.284 | 0.241 | 0.665 | 6658.099 | 6.246 | 0.091 | 0.524 |
| 6628.043 | 6.296 | 0.252 | 0.676 | 6662.835 | 6.275 | 0.206 | 0.629 |
| 6628.889 | 6.316 | 0.269 | 0.678 | 6667.117 | 6.391 | 0.305 | 0.699 |
| 6667.976 | 6.405 | 0.321 | 0.720 | 6694.813 | 6.265 | 0.071 | 0.506 |
| 6669.016 | 6.440 | 0.341 | 0.734 | 6696.084 | 6.258 | 0.110 | 0.523 |
| 6669.906 | 6.473 | 0.353 | 0.746 | 6696.900 | 6.278 | 0.071 | 0.536 |
| 6672.833 | 6.562 | 0.386 | 0.769 | 6698.922 | 6.282 | 0.123 | 0.563 |
| 6676.130 | 6.590 | 0.396 | 0.754 | 6710.852 | 6.512 | 0.283 | 0.687 |
| 6678.913 | 6.582 | 0.315 | 0.720 | 6717.942 | 6.571 | 0.265 | 0.656 |
| 6682.874 | 6.555 | 0.120 | 0.562 | 6719.880 | 6.520 | 0.228 | 0.636 |
| 6683.829 | 6.535 | 0.084 | 0.542 | 6722.945 | 6.461 | 0.119 | 0.512 |
| 6686.855 | 6.448 | -0.001 | 0.470 | 6724.876 | 6.372 | 0.062 | 0.469 |
| 6694.089 | 6.283 | 0.060 | 0.452 | 6730.876 | 6.266 | 0.122 | 0.544 |
| 6731.892 | 6.268 | 0.142 | 0.550 | 6877.217 | 6.276 | -0.052 | 0.446 |
| 6733.934 | 6.251 | 0.199 | 0.620 | 6896.167 | 6.641 | 0.425 | 0.787 |
| 6734.907 | 6.280 | 0.187 | 0.603 | 6897.188 | 6.746 | 0.450 | 0.798 |
| 6743.863 | 6.363 | 0.304 | 0.692 | 6904.159 | 6.879 | 0.457 | 0.805 |
| 6744.935 | 6.387 | 0.292 | 0.689 | 6912.145 | 6.727 | 0.274 | 0.666 |
| 6766.886 | 6.179 | | 0.456 | 6914.023 | 6.598 | 0.206 | 0.611 |
| 6767.886 | 6.115 | | 0.452 | 6923.119 | 6.156 | 0.104 | 0.541 |
| 6768.889 | 6.154 | 0.003 | 0.455 | 6924.012 | 6.157 | 0.110 | 0.571 |
| 6874.222 | 6.302 | -0.026 | 0.433 | 6925.003 | 6.153 | 0.150 | 0.564 |
| 6876.194 | 6.281 | -0.045 | 0.436 | 6929.079 | 6.162 | 0.184 | 0.615 |
| 6945.058 | 6.588 | 0.274 | 0.630 | 7016.893 | 6.519 | 0.284 | 0.688 |
| 6955.042 | 6.397 | 0.060 | 0.524 | 7020.016 | 6.554 | 0.228 | 0.650 |
| 6960.911 | 6.295 | 0.132 | 0.591 | 7021.054 | 6.546 | 0.208 | 0.611 |
| 6964.028 | 6.318 | 0.197 | 0.636 | 7022.054 | 6.559 | 0.167 | 0.590 |
| 6981.938 | 6.534 | 0.147 | 0.582 | 7030.953 | 6.264 | -0.082 | 0.429 |
| 6983.021 | 6.510 | 0.113 | 0.559 | 7031.860 | 6.246 | -0.011 | 0.451 |
| 6986.030 | 6.464 | 0.045 | 0.503 | 7036.835 | 6.217 | 0.102 | 0.518 |
| 7002.875 | 6.319 | 0.213 | 0.643 | 7039.057 | 6.214 | 0.189 | 0.553 |
| 7006.095 | 6.364 | 0.295 | 0.686 | 7042.979 | 6.281 | 0.263 | 0.637 |
| 7015.155 | 6.511 | 0.331 | 0.688 | 7045.891 | 6.397 | 0.348 | 0.681 |
| 7047.900 | 6.453 | 0.373 | 0.691 | 7106.896 | 6.386 | 0.115 | 0.519 |
| 7062.934 | 6.641 | 0.222 | 0.575 | 7113.880 | 6.443 | 0.148 | 0.659 |
| 7064.941 | 6.529 | 0.206 | 0.540 | 7114.878 | 6.441 | 0.175 | 0.676 |
| 7065.910 | 6.421 | 0.199 | 0.557 | 7116.903 | 6.447 | 0.223 | 0.744 |
| 7068.903 | 6.363 | 0.181 | 0.551 | 7119.954 | 6.477 | 0.376 | 0.740 |
| 7070.935 | 6.272 | 0.179 | 0.562 | 7135.915 | 6.602 | 0.299 | 0.621 |
| 7083.890 | 6.333 | 0.401 | 0.704 | 7137.923 | 6.547 | 0.102 | 0.566 |
| 7088.866 | 6.422 | 0.368 | 0.682 | | | | |
| 7089.938 | 6.425 | 0.347 | 0.658 | | | | |
| 7092.966 | 6.475 | 0.240 | 0.564 | | | | |

**Table 2.6b.** MJUO *UBVRI* photometry of RY Sgr during 1988 and 1989.

| JD-2440000 | *V* | (*U*-*B*) | (*B*-*V*) | (*V*-*R*) | (*V*-*I*) | JD-2440000 | *V* | (*U*-*B*) | (*B*-*V*) | (*V*-*R*) | (*V*-*I*) |
|---|---|---|---|---|---|---|---|---|---|---|---|
| 7241.191 | 6.576 | 0.420 | 0.719 | 0.418 | 0.682 | 7302.053 | 6.211 | 0.192 | 0.577 | 0.365 | 0.546 |
| 7242.164 | 6.580 | 0.403 | 0.703 | 0.410 | 0.657 | 7303.148 | 6.199 | 0.200 | 0.591 | 0.364 | 0.557 |
| 7255.173 | 6.362 | 0.093 | 0.529 | 0.347 | 0.533 | 7306.003 | 6.194 | 0.242 | 0.614 | 0.369 | 0.576 |
| 7256.112 | 6.326 | 0.097 | 0.541 | 0.340 | 0.532 | 7307.044 | 6.209 | 0.259 | 0.613 | 0.384 | 0.572 |
| 7264.094 | 6.252 | 0.205 | 0.607 | 0.358 | 0.590 | 7308.056 | 6.206 | 0.239 | 0.628 | 0.370 | 0.592 |
| 7269.152 | 6.260 | 0.226 | 0.630 | 0.368 | 0.587 | 7309.116 | 6.221 | 0.262 | 0.648 | 0.368 | 0.586 |
| 7273.080 | 6.307 | 0.327 | 0.650 | 0.376 | 0.601 | 7313.018 | 6.253 | 0.253 | 0.625 | 0.379 | 0.565 |
| 7283.216 | 6.475 | 0.201 | 0.601 | 0.360 | 0.606 | 7316.995 | 6.314 | 0.231 | 0.607 | 0.371 | 0.569 |
| 7284.125 | 6.460 | 0.185 | 0.601 | 0.365 | 0.614 | 7318.063 | 6.330 | 0.211 | 0.591 | 0.366 | 0.551 |
| 7296.192 | 6.288 | 0.086 | 0.534 | 0.348 | 0.537 | 7322.249 | 6.333 | 0.130 | 0.510 | 0.334 | 0.518 |
| 7323.989 | 6.319 | 0.075 | 0.469 | 0.326 | 0.508 | 7362.873 | 6.286 | 0.111 | 0.494 | 0.341 | 0.487 |
| 7327.206 | 6.277 | 0.014 | 0.433 | 0.317 | 0.487 | 7367.856 | 6.154 | 0.036 | 0.413 | 0.324 | 0.474 |
| 7333.935 | 6.267 | | 0.507 | | | 7370.841 | 6.179 | 0.082 | 0.464 | 0.327 | 0.510 |
| 7334.935 | 6.245 | | 0.533 | | | 7372.834 | 6.228 | 0.145 | 0.495 | 0.344 | 0.498 |
| 7337.170 | 6.283 | | 0.565 | | | 7375.933 | 6.349 | 0.230 | 0.592 | 0.371 | 0.583 |
| 7345.913 | 6.440 | 0.432 | 0.723 | 0.431 | 0.650 | 7379.921 | 6.448 | | 0.664 | | |
| 7352.823 | 6.531 | 0.489 | 0.741 | 0.467 | 0.677 | 7388.928 | 6.747 | 0.564 | 0.802 | 0.482 | 0.687 |
| 7354.991 | 6.545 | 0.470 | 0.749 | 0.450 | 0.678 | 7390.840 | 6.798 | 0.578 | 0.820 | 0.493 | 0.708 |
| 7355.988 | 6.531 | 0.448 | 0.728 | 0.436 | 0.654 | 7392.809 | 6.817 | | 0.829 | 0.487 | 0.696 |
| 7360.900 | 6.333 | | 0.532 | | | 7394.903 | 6.804 | 0.599 | 0.806 | 0.476 | 0.687 |
| 7395.884 | 6.844 | 0.574 | 0.792 | 0.469 | 0.668 | 7413.854 | 6.197 | 0.216 | 0.544 | 0.363 | 0.518 |
| 7396.995 | 6.845 | 0.570 | 0.791 | 0.470 | 0.670 | 7417.922 | 6.267 | 0.293 | 0.593 | 0.376 | 0.543 |
| 7398.828 | 6.804 | 0.483 | 0.765 | 0.410 | 0.666 | 7420.921 | 6.327 | 0.340 | 0.628 | 0.394 | 0.576 |
| 7400.936 | 6.690 | 0.443 | 0.701 | 0.379 | 0.629 | 7423.924 | 6.389 | 0.397 | 0.671 | 0.398 | 0.590 |
| 7404.850 | 6.469 | 0.360 | 0.613 | 0.391 | 0.557 | 7425.949 | 6.447 | 0.430 | 0.679 | 0.404 | 0.615 |
| 7405.848 | 6.408 | 0.325 | 0.592 | 0.376 | 0.538 | 7428.014 | 6.499 | 0.461 | 0.698 | 0.416 | 0.624 |
| 7408.066 | 6.313 | 0.276 | 0.547 | 0.371 | 0.516 | 7435.880 | 6.587 | 0.402 | 0.663 | 0.404 | 0.614 |
| 7409.938 | 6.242 | 0.197 | 0.527 | 0.364 | 0.502 | 7436.891 | 6.570 | 0.372 | 0.654 | 0.393 | 0.593 |
| 7411.947 | 6.207 | 0.186 | 0.526 | 0.360 | 0.538 | 7439.934 | 6.471 | 0.262 | 0.584 | 0.381 | 0.557 |
| 7412.855 | 6.205 | 0.199 | 0.529 | 0.367 | 0.525 | 7455.847 | 6.128 | 0.214 | 0.540 | 0.356 | 0.523 |
| 7464.876 | 6.255 | 0.302 | 0.592 | 0.391 | 0.573 | 7588.211 | 6.469 | 0.214 | 0.538 | 0.349 | 0.535 |
| 7466.893 | 6.282 | 0.308 | 0.605 | 0.381 | 0.567 | 7590.177 | 6.447 | 0.157 | 0.514 | 0.326 | 0.465 |
| 7479.874 | 6.369 | 0.153 | 0.505 | 0.347 | 0.513 | 7592.192 | 6.436 | 0.143 | 0.501 | 0.321 | 0.424 |
| 7481.903 | 6.333 | 0.168 | 0.520 | 0.350 | 0.505 | 7611.151 | 6.530 | | 0.745 | 0.410 | 0.630 |
| 7486.878 | 6.325 | 0.206 | 0.546 | 0.371 | 0.580 | 7612.180 | 6.548 | | 0.772 | 0.392 | 0.621 |
| 7487.890 | 6.336 | 0.224 | 0.568 | 0.358 | 0.534 | 7616.190 | 6.644 | 0.478 | 0.773 | 0.448 | 0.666 |
| 7488.893 | 6.366 | 0.290 | 0.556 | 0.369 | 0.595 | 7620.181 | 6.698 | 0.470 | 0.755 | 0.437 | 0.664 |
| 7489.892 | 6.375 | 0.290 | 0.593 | 0.384 | 0.560 | 7621.151 | 6.692 | 0.450 | 0.742 | 0.427 | 0.608 |
| 7496.888 | 6.530 | 0.404 | 0.667 | 0.387 | | 7623.169 | 6.652 | 0.398 | 0.695 | 0.407 | 0.597 |
| 7498.886 | 6.580 | 0.455 | 0.689 | 0.408 | 0.653 | 7628.166 | 6.500 | | 0.562 | 0.317 | 0.503 |
| 7636.118 | 6.192 | 0.171 | 0.506 | 0.341 | 0.491 | 7683.192 | 6.335 | | 0.713 | 0.365 | 0.579 |
| 7644.219 | 6.125 | 0.346 | 0.637 | 0.369 | 0.518 | 7690.947 | 6.561 | 0.557 | 0.800 | 0.459 | 0.667 |
| 7652.176 | 6.331 | | 0.779 | 0.388 | 0.607 | 7694.108 | 6.652 | 0.558 | 0.813 | 0.463 | 0.694 |
| 7655.131 | 6.439 | 0.414 | 0.718 | 0.411 | 0.614 | 7697.083 | 6.705 | | 0.767 | 0.482 | 0.699 |
| 7657.204 | 6.458 | 0.391 | 0.686 | 0.417 | 0.574 | 7700.183 | 6.658 | | 0.697 | 0.376 | 0.595 |
| 7662.157 | 6.510 | 0.287 | 0.609 | 0.363 | 0.562 | 7705.179 | 6.390 | | 0.537 | 0.314 | 0.464 |
| 7664.075 | 6.454 | 0.200 | 0.517 | 0.353 | 0.539 | 7708.238 | 6.206 | 0.119 | 0.466 | 0.317 | 0.451 |
| 7674.229 | 6.200 | | 0.540 | 0.309 | 0.491 | 7713.958 | 6.078 | 0.155 | 0.499 | 0.322 | 0.461 |
| 7677.027 | 6.179 | 0.237 | 0.581 | 0.351 | 0.487 | 7722.049 | 6.173 | 0.435 | 0.652 | 0.391 | 0.491 |
| 7680.964 | 6.269 | 0.358 | 0.651 | 0.385 | 0.576 | 7724.952 | 6.274 | 0.436 | 0.718 | 0.411 | 0.588 |
| 7727.014 | 6.397 | 0.480 | 0.742 | 0.430 | 0.632 | 7756.867 | 6.120 | 0.291 | 0.595 | 0.367 | 0.517 |
| 7729.142 | 6.478 | 0.512 | 0.771 | 0.441 | 0.634 | 7758.934 | 6.170 | 0.350 | 0.617 | 0.337 | 0.545 |
| 7730.139 | 6.523 | 0.517 | 0.766 | 0.457 | 0.650 | 7760.057 | 6.176 | 0.371 | 0.659 | 0.402 | 0.565 |
| 7731.124 | 6.545 | 0.517 | 0.776 | 0.438 | 0.652 | 7765.963 | 6.388 | 0.432 | 0.747 | 0.418 | 0.626 |
| 7731.933 | 6.575 | 0.512 | 0.769 | 0.442 | 0.652 | 7771.059 | 6.596 | 0.473 | 0.758 | 0.434 | 0.633 |
| 7735.125 | 6.631 | 0.441 | 0.726 | 0.411 | 0.626 | 7774.013 | 6.661 | 0.438 | 0.715 | 0.420 | 0.621 |
| 7735.976 | 6.627 | 0.425 | 0.706 | 0.420 | 0.623 | 7779.015 | 6.607 | 0.267 | 0.570 | 0.385 | 0.548 |
| 7736.983 | 6.625 | 0.381 | 0.687 | 0.402 | 0.616 | 7780.013 | 6.565 | 0.192 | 0.547 | 0.346 | 0.531 |
| 7744.081 | 6.459 | 0.168 | 0.533 | 0.330 | 0.494 | 7781.047 | 6.510 | 0.161 | 0.513 | 0.338 | 0.480 |
| 7747.003 | 6.280 | 0.094 | 0.457 | 0.330 | 0.452 | | | | | | |

A Fourier analysis of the photometry of RY Sgr shows a dominant peak with a periodicity at $f_1 = 0.0265$ d$^{-1}$ ($P_1 = 37.74$ d; see Fig. 2.12), which is in close agreement with the period of the LP4 solution determined in Chapter 5.1.3.2 ($P = 37.81 \pm 0.04$ d). [The LP4 solution is valid for pulsation cycles of RY Sgr since JD$\sim$2446128 (1985 February).] The other peaks in the power spectrum contribute to the cycle–to–cycle variations observed in the light curve.

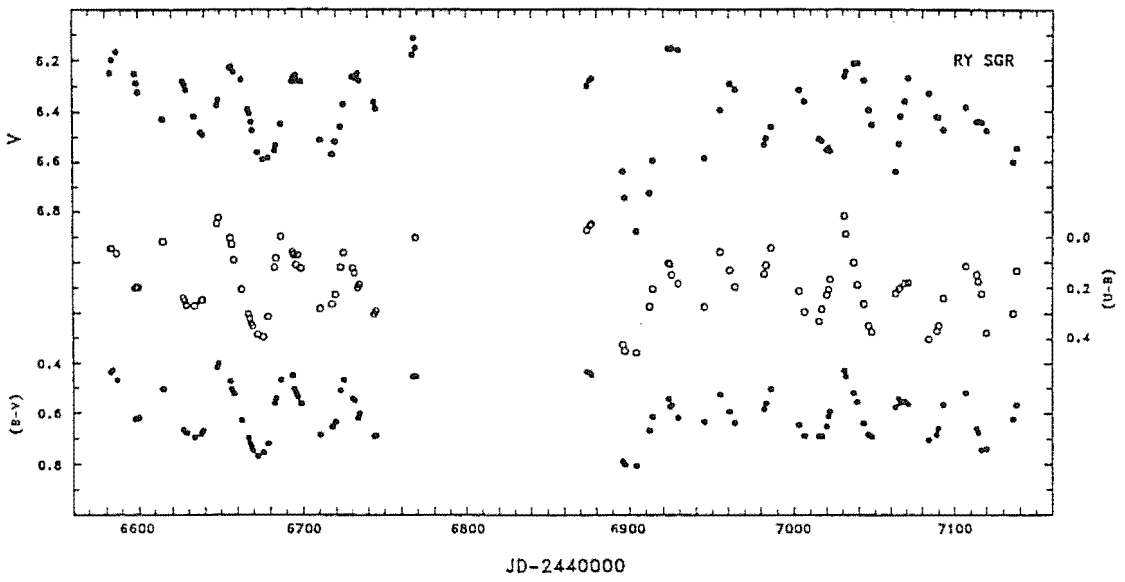


Figure 2.10. $V$ light and ($U$-$B$) and ($B$-$V$) colour curves for RY Sgr during 1986–1987 plotted against Julian Date.

By introducing $f_1$ as a known constituent, an iterative analysis of the $V$ photometry of RY Sgr extracted three additional periodicities at $f_2 = 0.0181$ d$^{-1}$ ($P_2 = 55.25$ d), $f_3 = 0.0203$ d$^{-1}$ ($P_3 = 49.26$ d) and $f_4 = 0.0141$ d$^{-1}$ ($P_4 = 70.92$ d), respectively. These periodicities are summarised in Table 2.11. A synthetic curve constructed from these four periods offers a reasonable fit to the RY Sgr photometry when the light curve is more regular, e.g. during 1986. The curve does not fit the 1988 data particularly well although the general shape of the light curve is reproduced. This synthetic curve is compared to the RY Sgr $V$ photometry and is shown as a dashed line in Fig. 2.13.

To examine the year–to–year irregularity in the light curve of RY Sgr we Fourier analysed the data obtained in individual years. The power spectra are shown in Fig. 2.14, where the year and the number of data points (bracketted) are indicated within each panel. There are notable differences in the power spectra. There are small shifts in the values of the periodicities near $f = 0.019$ d$^{-1}$ ($P \approx 52$ d) and 0.026 d$^{-1}$ ($P \approx 38$ d), but the mean values are consistent with the peaks in Fig. 2.12. The amplitude of both these major frequencies varied from year to year, in particular the amplitude of the $f \approx 0.019$ d$^{-1}$ frequency varied by a factor of four. During 1988 the amplitude of that periodicity was greater than the amplitude of the $f \approx 0.026$ d$^{-1}$ periodicity.

The values of the periodicities near $f = 0.019$ d$^{-1}$ may suggest that $f_2$ and $f_3$ represent the same periodicity. The periodicity observed each year near these frequencies was

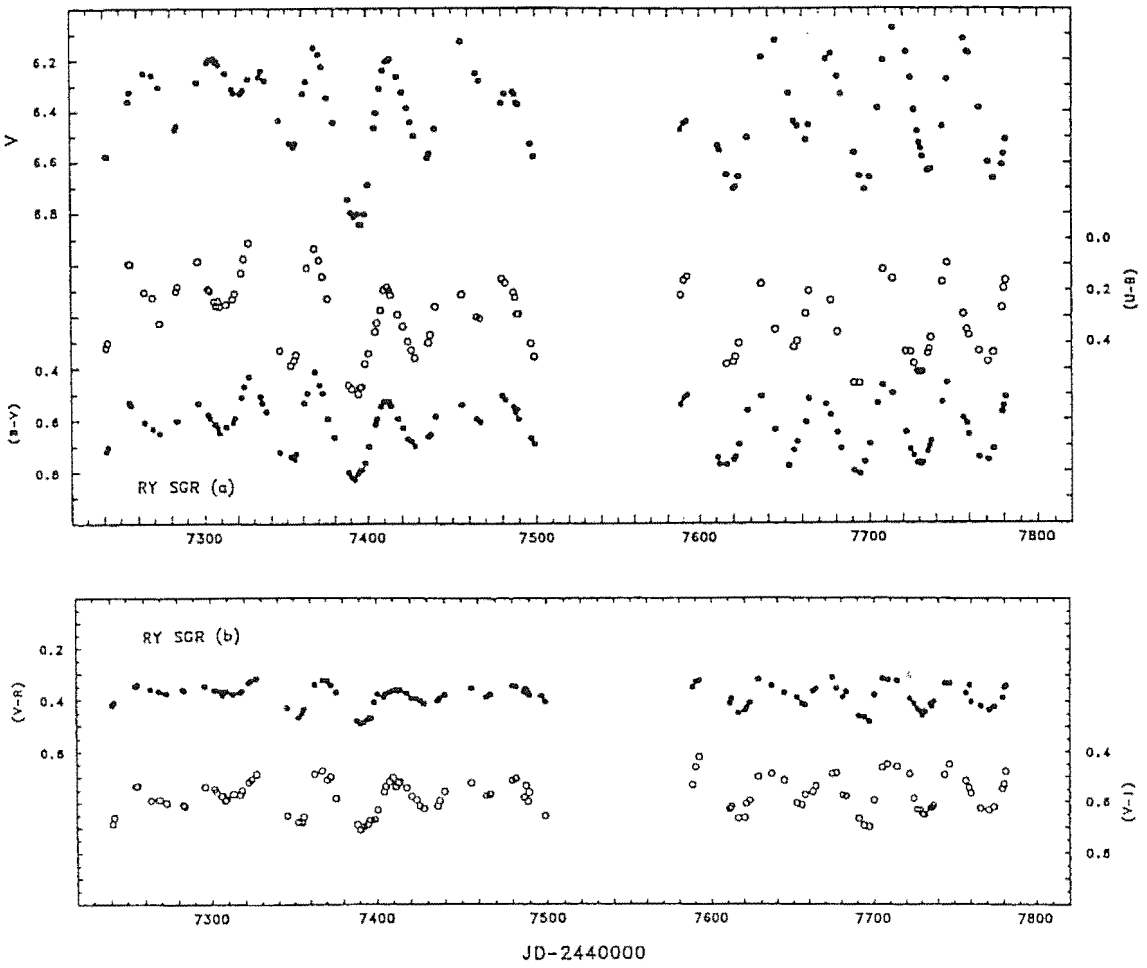


Figure 2.11. $V$ light and $(U\text{–}B)$, $(B\text{–}V)$ (a), $(V\text{–}R)$ and $(V\text{–}I)$ (b) colour curves for RY Sgr during 1988–1989 plotted against Julian Date.

approximately the mean of these two values. We summarise the dominant frequencies identified in the data for each year in Table 2.11. The synthetic curves for each year are shown as solid lines in Fig. 2.13. Note the generally improved fit, in comparison to the dashed line four–period fit. The remaining residuals are probably due to the modulation of the amplitudes of the fitted periods.

The $(U\text{–}B)$ and $(B\text{–}V)$ colour curves have been shown to lead (by about 8 d) the $V$ light curve (Alexander *et al.* 1972). We extend this identification to the $(V\text{–}R)$ and $(V\text{–}I)$ colour curves. Our photometry suggests that the lead varies from 0–10 d. All the colour curves appeared to be in phase. This implies that the $U$ mag leads the $B$ mag, which leads the $V$ mag, which in turn leads the $R$ mag. However, similar phase leads for the $(V\text{–}R)$ and $(V\text{–}I)$ colour curves indicate that the $R$ and $I$ curves have a similar phase relationship. The amplitude of the colour curves decreases towards redder colours, with the exception of the $(V\text{–}I)$ curve which has a amplitude similar to that of the $(V\text{–}R)$

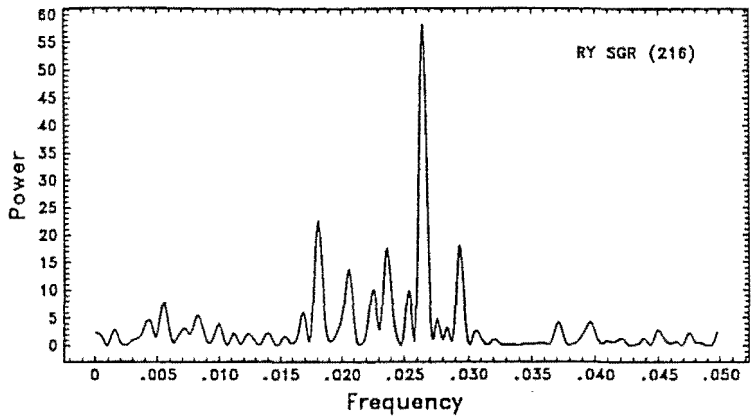


Figure 2.12. Power spectra for $V$ photometry of RY Sgr. The number of data points is indicated.

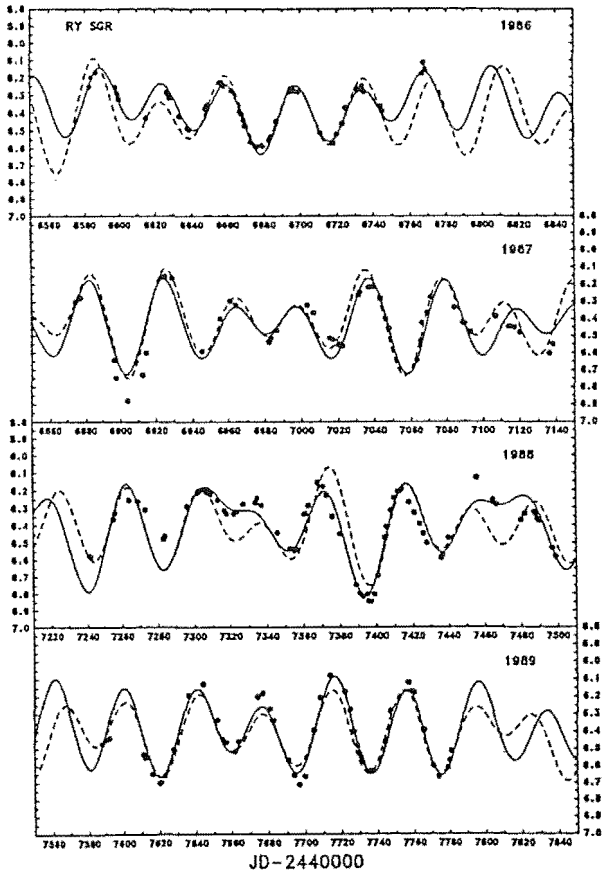


**Figure 2.13.** Comparison of synthetic light curves to $V$ photometry of RY Sgr obtained during 1986, 1987, 1988 and 1989. The dashed line is a 4 period fit to the entire dataset. The solid lines are 2 or 3 period fits obtained from spectral analyses for data obtained during the individual years (see Table 2.11).

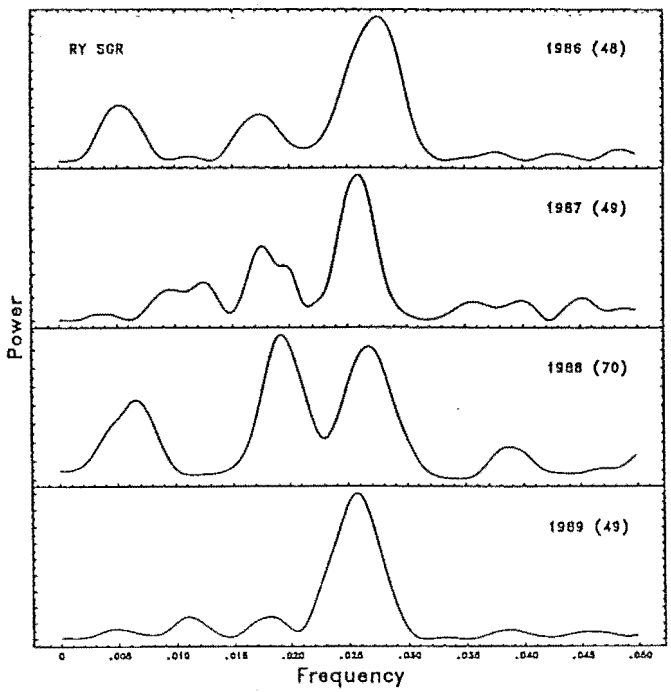


Figure 2.14. Power spectra for $V$ photometry of RY Sgr obtained during individual years. The year and the number of data points obtained during each year is indicated within each panel.

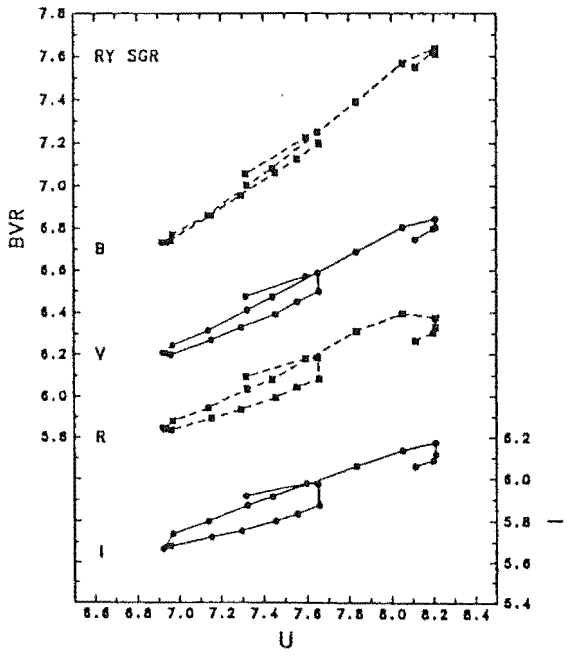


Figure 2.15. 'Loop' diagram of $BVRI$ magnitudes, plotted against $U$, from photometry of RY Sgr obtained between JD 2447389–2447440. The amplitude and phase relationship between these 5 individual filter magnitudes is discussed in the text.

curve. This, in turn, implies that the the amplitude of the individual filter light curves decreases towards increasing wavelength, with the exception that the $R$ and $I$ amplitudes are similar. The decreasing amplitudes, and the lag of the longer wavelength magnitudes with respect to the $U$ magnitude, can be seen in a 'loop' diagram for photometry obtained between JD2447389–2447440 (see Fig. 2.15). These data cover nearly two cycles and are representative of the behaviour of RY Sgr at maximum light. By way of an example, if the individual filter light curves were in phase, then no loop would be apparent in the magnitude–magnitude plane. Also, if the amplitude was constant with wavelength then the relationship in this plane would have unit slope. In the case of RY Sgr neither of these is true. [There is no unambiguous evidence for phase differences with respect to wavelength occurring in any other RCB star and, with the exception of NSV 6708 (see Section 4.3.1), all other RCB stars show a general decrease in amplitude towards longer wavelengths.]

For RY Sgr, we also noted a change in the mean ($U$–$B$) index of ~0.2 mag from a mean value of 0.14 during 1986 to a mean of 0.32 during 1989. An examination of the check star ($U$–$B$) index showed a change of less than 0.02 mag during this time. Small changes in the check star indices (at the 0.01–0.02 mag level) were not uncommon over the 3 years for which data were obtained at MJUO, and probably indicated some low amplitude long–term variation in either the local comparison star or check star magnitudes. As any significant variation in the comparison star colour index would be apparent in both the variable star and the check star photometry we conclude that the change in the ($U$–$B$) index is intrinsic to RY Sgr. We are unable to test if this trend was apparent during 1984 and 1985, for which we have some data (Lawson *et al.* 1987), as the star was rising from a decline in 1984 causing some reddening of the colour indices and we made only infrequent observations in 1985. No such effect was seen in the other colour indices, indicating that the cause of this change was affecting only the $U$ magnitude.

#### 2.4.1.6 RS Tel

The $UBV$ observations of RS Tel from JD 2446598–2447714 are listed in Table 2.7. Our observations of RS Tel were begun during a rise from a decline that commenced near JD 2446290 (see fig 9 of Lawson, Cottrell & Bateson 1989). Because of this rise, the $V$ light curve for those data obtained during 1986 and 1987 is shown separately (Fig. 2.16a) from the colour curves (Fig. 2.16b). The light and colour curves for 1988 and 1989 are shown in Fig. 2.17. Variations on timescales of 40–100 d are visible in the 1986 and 1987 data but these data were not Fourier analysed due to the irregular rise towards maximum light. A Fourier analysis of the $V$ photometry obtained during 1988 and 1989 showed a marginally significant peak at $f = 0.0261$ d$^{-1}$ ($P = 38.31$ d; Table 2.11). We note that Marang *et al.* (1989) concluded, from SAAO observations of RS Tel obtained between JD 2446595–2446658, that the star had a period $P > 65$ d. Their data were obtained during the rising branch of the decline, which gave rise to an inappropriate value for the period. Bateson (1975) obtained an average period of 45.8 d from visual estimates of RS Tel obtained between JD 2435000–2442290.

**Table 2.7.** MJUO *UBV* photometry of RS Tel.

| JD-2440000 | *V* | (*U*-*B*) | (*B*-*V*) | JD-2440000 | *V* | (*U*-*B*) | (*B*-*V*) |
|---|---|---|---|---|---|---|---|
| 6597.960 | 11.492 | 0.810 | 1.132 | 6658.107 | 10.576 | 0.673 | 0.973 |
| 6599.097 | 11.472 | 0.713 | 1.115 | 6667.137 | 10.465 | 0.617 | 0.965 |
| 6600.048 | 11.499 | 0.782 | 1.122 | 6667.979 | 10.412 | 0.544 | 0.933 |
| 6615.095 | 11.434 | 0.868 | 1.169 | 6669.122 | 10.447 | 0.566 | 0.978 |
| 6627.053 | 11.170 | 0.804 | 1.102 | 6670.047 | 10.400 | 0.546 | 0.938 |
| 6628.079 | 11.145 | 0.809 | 1.108 | 6686.971 | 10.492 | 0.611 | 0.979 |
| 6648.081 | 10.719 | 0.685 | 1.027 | 6694.030 | 10.478 | 0.620 | 0.991 |
| 6649.043 | 10.696 | 0.701 | 1.023 | 6694.954 | 10.532 | 0.663 | 0.948 |
| 6655.997 | 10.609 | 0.649 | 0.997 | 6696.059 | 10.466 | 0.619 | 1.007 |
| 6657.037 | 10.576 | 0.663 | 0.990 | 6698.970 | 10.442 | 0.633 | 0.986 |
| 6718.010 | 10.290 | 0.629 | 0.914 | 6904.139 | 10.294 | 0.509 | 0.895 |
| 6719.962 | 10.225 | | 0.910 | 6905.137 | 10.294 | 0.520 | 0.895 |
| 6731.972 | 10.443 | | 0.960 | 6923.208 | 10.559 | 0.559 | 0.912 |
| 6733.953 | 10.472 | 0.587 | 0.988 | 6955.013 | 10.015 | 0.475 | 0.865 |
| 6743.903 | 10.257 | 0.430 | 0.893 | 6964.054 | 9.921 | 0.421 | 0.831 |
| 6744.912 | 10.279 | 0.425 | 0.864 | 6981.915 | 9.935 | 0.402 | 0.847 |
| 6876.208 | 10.190 | 0.421 | 0.845 | 6983.003 | 9.947 | 0.448 | 0.830 |
| 6877.226 | 10.181 | 0.388 | 0.861 | 6986.011 | 9.953 | 0.427 | 0.831 |
| 6896.140 | 10.358 | 0.482 | 0.947 | 7002.927 | 10.075 | 0.407 | 0.846 |
| 6897.214 | 10.409 | 0.509 | 0.936 | 7020.003 | 10.159 | 0.444 | 0.859 |
| 7022.015 | 10.193 | 0.463 | 0.866 | 7269.112 | 10.019 | | 0.836 |
| 7030.990 | 10.015 | 0.402 | 0.828 | 7273.102 | 9.967 | 0.486 | 0.849 |
| 7039.103 | 10.050 | 0.405 | 0.855 | 7283.231 | 10.007 | | 0.825 |
| 7042.954 | 10.022 | 0.433 | 0.826 | 7298.001 | 9.929 | | 0.816 |
| 7062.998 | 10.134 | 0.492 | 0.865 | 7302.031 | 9.969 | 0.541 | 0.826 |
| 7071.002 | 9.969 | 0.361 | 0.804 | 7306.992 | 10.077 | 0.529 | 0.858 |
| 7083.902 | 9.958 | 0.445 | 0.854 | 7308.073 | 10.082 | 0.549 | 0.863 |
| 7088.890 | 9.825 | 0.421 | 0.831 | 7313.112 | 10.048 | 0.516 | 0.837 |
| 7255.117 | 10.039 | | 0.846 | 7316.946 | 10.021 | 0.499 | 0.834 |
| 7256.078 | 10.042 | | 0.835 | 7322.233 | 10.076 | 0.501 | 0.843 |
| 7325.979 | 10.082 | 0.495 | 0.808 | 7372.940 | 9.842 | | 0.790 |
| 7333.965 | 9.900 | | 0.800 | 7375.999 | 9.856 | 0.434 | 0.792 |
| 7334.965 | 9.924 | | 0.772 | 7380.101 | 9.896 | | 0.820 |
| 7337.112 | 9.872 | | 0.830 | 7394.973 | 9.942 | | 0.829 |
| 7345.940 | 9.917 | 0.453 | 0.839 | 7397.044 | 9.980 | 0.466 | 0.826 |
| 7352.988 | 9.887 | 0.485 | 0.808 | 7400.992 | 9.965 | 0.462 | 0.821 |
| 7354.963 | 9.900 | 0.526 | 0.813 | 7408.143 | 9.894 | 0.457 | 0.792 |
| 7363.022 | 9.963 | | 0.840 | 7412.936 | 9.880 | 0.369 | 0.772 |
| 7367.938 | 9.926 | 0.470 | 0.800 | 7417.991 | 9.850 | 0.386 | 0.777 |
| 7370.978 | 9.887 | 0.508 | 0.800 | 7425.986 | 9.945 | 0.417 | 0.797 |
| 7427.983 | 9.972 | 0.476 | 0.833 | 7496.909 | 9.905 | | 0.867 |
| 7435.939 | 9.937 | 0.473 | 0.851 | 7573.150 | 9.872 | | 0.829 |
| 7436.925 | 9.965 | 0.480 | 0.827 | 7611.125 | 10.021 | 0.393 | 0.803 |
| 7439.970 | 9.919 | 0.479 | 0.808 | 7620.122 | 10.184 | 0.353 | 0.847 |
| 7464.934 | 9.930 | 0.443 | 0.794 | 7628.154 | 10.035 | 0.432 | 0.821 |
| 7481.915 | 9.898 | | 0.812 | 7636.083 | 9.930 | 0.509 | 0.796 |
| 7486.930 | 9.778 | 0.549 | 0.794 | 7644.209 | 9.957 | 0.562 | 0.762 |
| 7487.927 | 9.765 | 0.520 | 0.814 | 7655.178 | 9.944 | | 0.839 |
| 7488.927 | 9.752 | | 0.808 | 7664.207 | 10.054 | 0.509 | 0.850 |
| 7489.933 | 9.733 | 0.516 | 0.783 | 7674.213 | 9.856 | | 0.784 |
| 7677.131 | 9.837 | 0.433 | 0.775 | 7700.159 | 9.952 | | 0.801 |
| 7683.171 | 9.882 | | 0.801 | 7705.169 | 10.065 | | 0.865 |
| 7694.096 | 9.896 | 0.423 | 0.781 | 7713.994 | 9.958 | 0.520 | 0.799 |

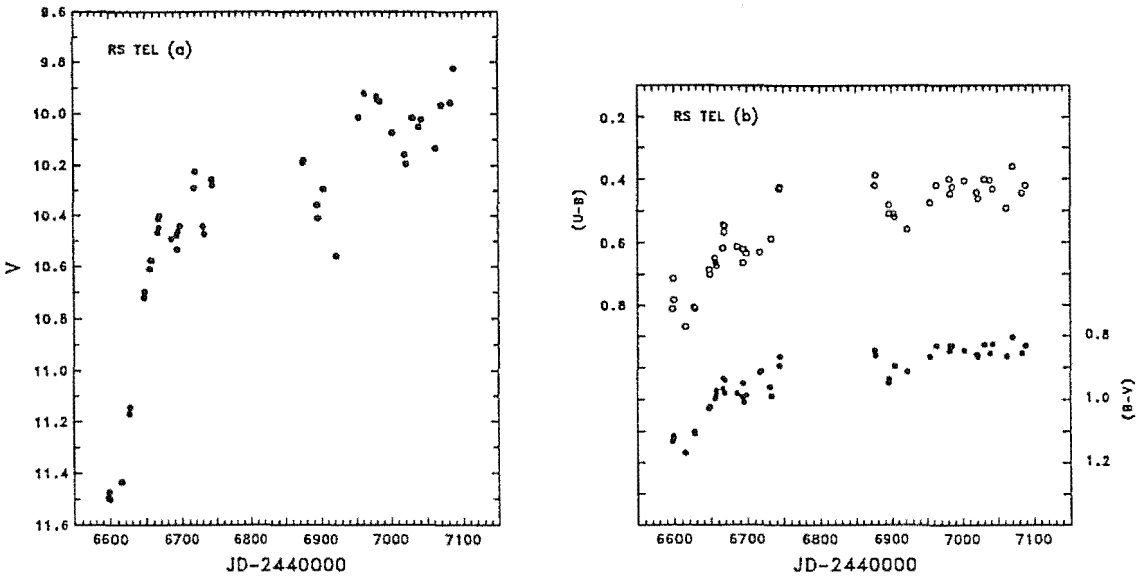


**Figure 2.16.** $V$ light (a) and $(U\text{-}B)$ and $(B\text{-}V)$ colour (b) curves for RS Tel during 1986–1987 plotted against Julian Date.

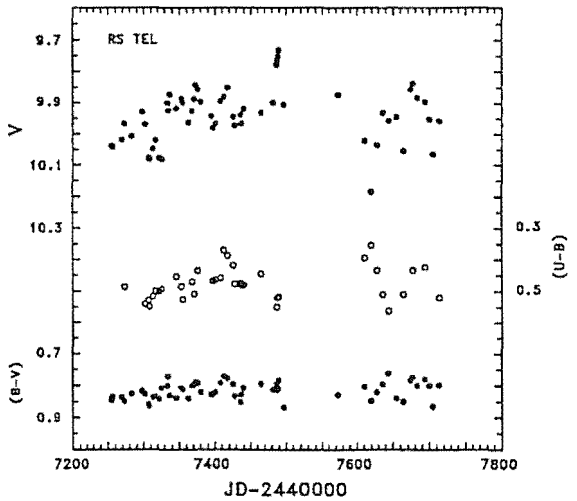


**Figure 2.17.** $V$ light and $(U\text{-}B)$ and $(B\text{-}V)$ colour curves for RS Tel during 1988–1989 plotted against Julian Date.

### 2.4.1.7 RT Nor, RZ Nor and SU Tau

We list $UBV$ photometry of RT Nor in Table 2.8 and in Fig. 2.18 we show the $V$ light and colour curves. A power spectrum for these $V$ data (see Fig. 2.19) identifies periodicities at $f_1 = 0.0221$ d$^{-1}$ ($P = 45.3$ d) and $f_2 = 0.0518$ d$^{-1}$ ($P_2 = 19.3$ d) respectively. The star was observed by Marang *et al.* (1989), who found that the star had an amplitude in $V$ exceeding 0.6 mag. Our data indicated a lower level of activity, with a maximum recorded amplitude of 0.4 mag. Including the SAAO data in the Fourier analysis gave similar values to those of the MJUO data alone. Periodicities were identified in the combined dataset at $f_1 = 0.0217$ d$^{-1}$ ($P_1 = 46.1$ d) and $f_2 = 0.0511$ d$^{-1}$ ($P_2 = 19.6$ d) respectively (Table 2.11). Note that sometimes there is a similarity of the light curve of RT Nor (in particular fig 1 of Marang *et al.*) to that of U Aqr (see Fig. 2.4).

The $BV$ observations of RZ Nor are listed in Table 2.9 and in Fig. 2.20 we show the light and colour curves. A power spectrum for these $V$ data had a maximum peak at $f = 0.0236$ d$^{-1}$ ($P = 42.37$ d, Table 2.11.).

In Table 2.10 we list the $BVRI$ photometry of SU Tau. The light and colour curves from JD 2447070–2447270 are shown in Fig. 2.21. The light curve showed the final stages of a rise from a decline. Variations on timescales of 40–70 d can be seen in the $V$ curve. A power spectrum of the $(B-V)$ data showed a periodicity at $f = 0.0238$ d$^{-1}$ ($P = 40.32$ d, Table 2.11).

**Table 2.8.** MJUO $UBV$ photometry of RT Nor.

| JD-2440000 | $V$ | $(U-B)$ | $(B-V)$ | JD-2440000 | $V$ | $(U-B)$ | $(B-V)$ |
|---|---|---|---|---|---|---|---|
| 7573.079 | 10.125 | 0.677 | 1.030 | 7683.077 | 10.147 | | 1.089 |
| 7592.156 | 9.896 | | 0.941 | 7690.978 | 10.184 | 0.804 | 1.084 |
| 7611.092 | 10.153 | | 1.059 | 7699.068 | 10.388 | | 1.129 |
| 7617.113 | 10.258 | 0.777 | 1.081 | 7705.080 | 10.263 | | 1.117 |
| 7623.116 | 10.274 | | 1.063 | 7714.015 | 10.174 | 0.733 | 1.075 |
| 7628.092 | 10.050 | | 1.025 | 7724.986 | 9.969 | | 1.020 |
| 7644.139 | 10.205 | | 1.090 | 7729.002 | 10.018 | 0.743 | 1.066 |
| 7655.954 | 10.303 | | 1.098 | 7730.027 | 10.051 | 0.739 | 1.050 |
| 7664.142 | 10.144 | 0.838 | 1.074 | 7731.036 | 10.036 | | 1.053 |
| 7674.079 | 10.034 | | 1.021 | 7734.956 | 10.079 | 0.756 | 1.039 |
| 7676.964 | 10.142 | 0.770 | 1.055 | | | | |

**Table 2.9.** MJUO $BV$ photometry of RZ Nor.

| JD-2440000 | $V$ | $(B-V)$ | JD-2440000 | $V$ | $(B-V)$ |
|---|---|---|---|---|---|
| 7571.180 | 10.328 | 1.055 | 7683.103 | 10.615 | 1.094 |
| 7592.184 | 10.470 | 1.064 | 7691.002 | 10.581 | 1.113 |
| 7611.109 | 10.376 | 1.069 | 7700.088 | 10.404 | 1.021 |
| 7620.111 | 10.367 | 1.066 | 7705.104 | 10.321 | 0.998 |
| 7623.139 | 10.407 | 1.065 | 7714.070 | 10.385 | 1.017 |
| 7628.114 | 10.476 | 1.071 | 7725.019 | 10.427 | 1.078 |
| 7644.160 | 10.472 | 1.062 | 7729.030 | 10.432 | 1.069 |
| 7655.985 | 10.306 | 1.066 | 7730.054 | 10.408 | 1.087 |
| 7664.166 | 10.376 | 1.048 | 7731.057 | 10.389 | 1.079 |
| 7674.131 | 10.483 | 1.064 | 7734.977 | 10.371 | 1.056 |
| 7676.985 | 10.501 | 1.062 | | | |

**Table 2.10.** MJUO *BVRI* photometry of SU Tau.

| JD−2440000 | *V* | (*B*−*V*) | (*V*−*R*) | (*V*−*I*) | JD−2440000 | *V* | (*B*−*V*) | (*V*−*R*) | (*V*−*I*) |
|---|---|---|---|---|---|---|---|---|---|
| 7069.152 | 10.146 | 1.219 | | | 7187.896 | 9.822 | | 0.682 | |
| 7093.089 | 9.958 | 1.153 | | | 7190.894 | 9.855 | 1.167 | 0.696 | |
| 7110.060 | 9.941 | 1.114 | | | 7196.947 | 9.870 | 1.130 | 0.683 | |
| 7115.002 | 9.913 | 1.129 | | | 7212.912 | 9.844 | 1.148 | 0.681 | |
| 7120.132 | 9.807 | 1.146 | 0.680 | | 7220.874 | 9.790 | 1.162 | 0.682 | |
| 7137.987 | 9.839 | 1.163 | 0.664 | 1.083 | 7221.871 | 9.796 | 1.156 | 0.717 | 1.061 |
| 7161.925 | 9.831 | 1.138 | 0.692 | | 7223.879 | 9.787 | 1.135 | 0.702 | |
| 7166.005 | 9.816 | 1.067 | | | 7225.874 | 9.738 | 1.165 | 0.700 | 1.063 |
| 7175.974 | 9.758 | 1.135 | 0.674 | | 7226.866 | 9.751 | 1.153 | 0.700 | |
| 7184.899 | 9.775 | 1.174 | 0.692 | | 7240.855 | 9.675 | 1.135 | 0.652 | 1.073 |
| 7246.853 | 9.715 | 1.117 | 0.664 | 1.043 | 7482.100 | 9.578 | 1.048 | 0.639 | 0.978 |
| 7248.849 | 9.731 | 1.115 | 0.689 | 1.066 | 7487.094 | 9.609 | | 0.647 | 0.955 |
| 7254.838 | 9.722 | 1.138 | 0.694 | 1.072 | 7489.064 | 9.620 | 1.045 | 0.655 | 0.954 |
| 7258.841 | 9.674 | 1.143 | 0.669 | 1.045 | 7490.079 | 9.634 | 1.059 | 0.650 | 0.931 |
| 7268.817 | 9.768 | 1.182 | 0.654 | | 7500.024 | 9.641 | 1.060 | 0.637 | 1.005 |
| 7480.104 | 9.590 | 1.030 | 0.662 | 1.048 | 7552.923 | 9.661 | 1.074 | | |

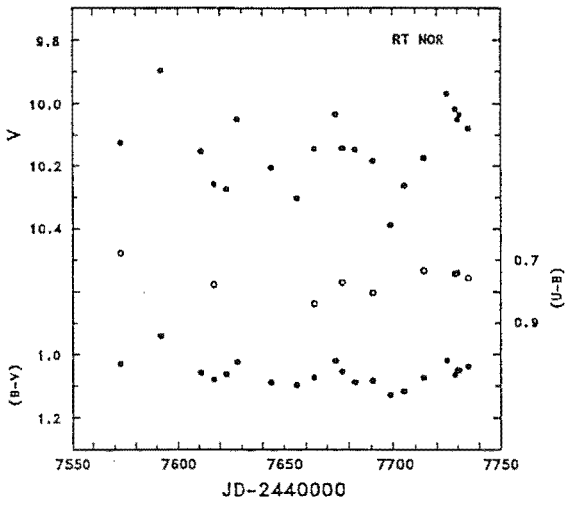


**Figure 2.18.** *V* light and (*U*−*B*) and (*B*−*V*) colour curves for RT Nor plotted against Julian Date.

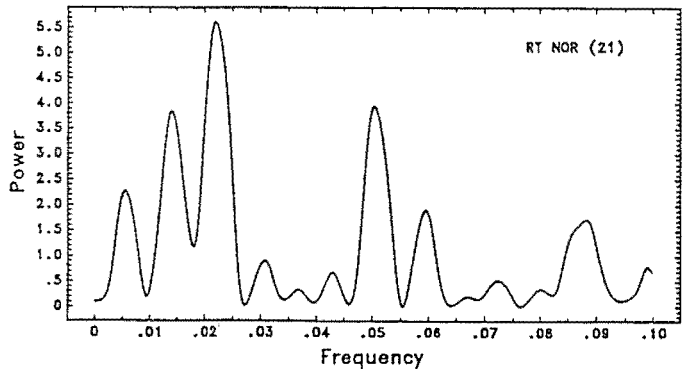


**Figure 2.19** Power spectrum for *V* photometry of RT Nor. The number of data points is indicated.

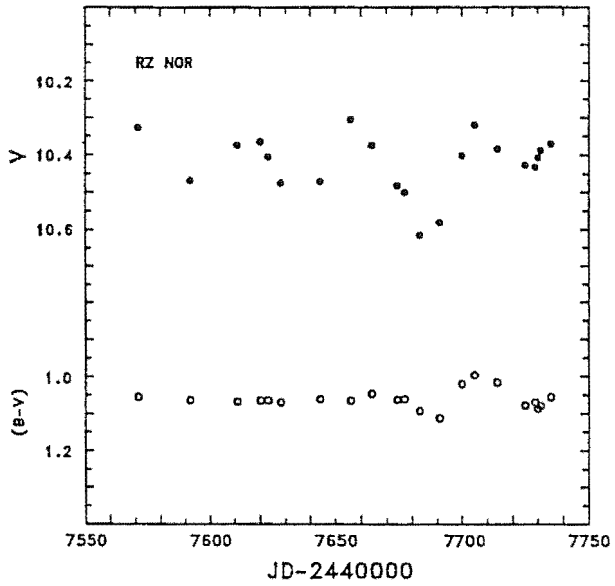


**Figure 2.20.** $V$ light and $(B–V)$ colour curves for RZ Nor plotted against Julian Date.

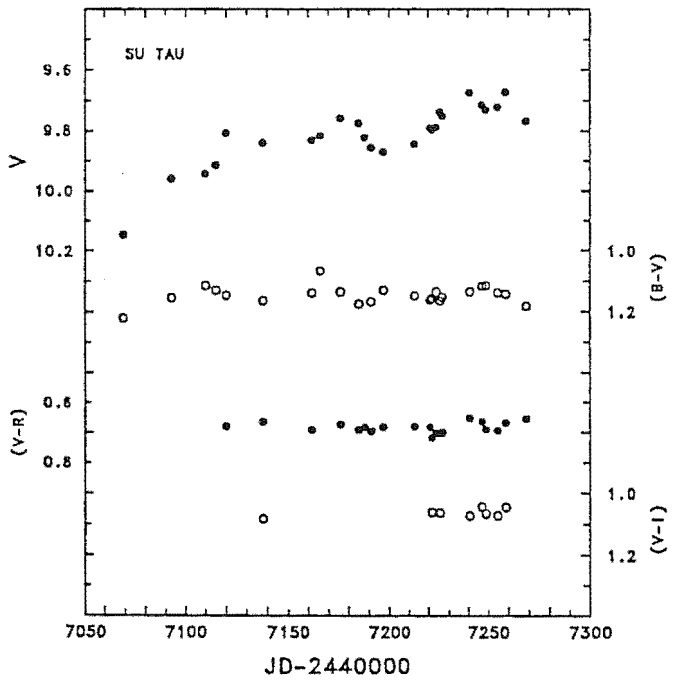


**Figure 2.21.** $V$ light and $(B–V)$, $(V–R)$ and $(V–I)$ colour curves for SU Tau from JD 2447069–2447269 plotted against Julian Date.

**Table 2.11.** Fourier components of galactic RCB star photometry.

| Star | Data | | $f$ (d$^{-1}$) | $P$ (d) | $A$ (mag) | $\phi$ (rad) | $F$ |
|---|---|---|---|---|---|---|---|
| S Aps | | | 0.0009 | l.f. | 0.0640 | 5.34071 | |
| | | $f_{32}$? | 0.0031 | 322.58 | 0.0456 | 3.83274 | |
| | | $f_1$ | 0.0125 | 80.00 | 0.0494 | 5.02655 | 5.9 E–5 |
| | | $f_2$ | 0.0232 | 43.10 | 0.0401 | 2.63894 | 5.2 E–4 |
| | | $f_3 = 2f_1$ | 0.0257 | 38.91 | 0.0329 | 4.77522 | 3.1 E–4 |
| U Aqr | 1986–1987 | $f_1$ | 0.0123 | 81.30 | 0.2127 | 1.44513 | 9.9 E–6 |
| | | $f_2 = 2f_1$ | 0.0249 | 40.16 | 0.1299 | 2.51327 | 1.5 E–4 |
| V CrA | 1986 | | 0.0175 | 57.14 | 0.0390 | 1.63363 | 2.5 E–2 |
| | 1987 | | 0.0089 | 112.36 | 0.1179 | 3.76991 | 5.8 E–4 |
| | 1988 | | 0.0130 | 76.92 | 0.0753 | 2.13628 | 2.5 E–3 |
| Y Mus | $V$ | | 0.0088 | 113.64 | 0.0259 | 5.90619 | 3.6 E–2 |
| | ($U$–$B$) | $f_1$ | 0.0044 | 227.27 | 0.0378 | 1.19381 | 4.6 E–5 |
| | | $f_2 = 2f_1$ | 0.0093 | 107.53 | 0.0244 | 5.21504 | 9.8 E–3 |
| | ($B$–$V$) | | 0.0092 | 108.70 | 0.0217 | 5.46637 | 1.9 E–3 |
| RY Sgr | all data | $f_1$ | 0.0265 | 37.74 | 0.1808 | 2.95310 | 5.7 E–24 |
| | | $f_2$ | 0.0181 | 55.25 | 0.0870 | 1.82212 | 4.6 E–11 |
| | | $f_3$ | 0.0203 | 49.26 | 0.0565 | 3.14159 | 7.4 E–7 |
| | | $f_4$ | 0.0141 | 70.92 | 0.0523 | 2.26195 | 7.2 E–5 |
| | 1986 | | 0.0276 | 36.23 | 0.1505 | 2.26195 | 2.2 E–6 |
| | | | 0.0055 | 181.82 | 0.0652 | 2.63894 | 1.6 E–4 |
| | | | 0.0191 | 52.36 | 0.0491 | 1.31947 | 4.5 E–6 |
| | 1987 | | 0.0259 | 38.61 | 0.1719 | 1.57080 | 7.2 E–5 |
| | | | 0.0193 | 51.81 | 0.1195 | 2.82743 | 1.5 E–4 |
| | 1988 | | 0.0192 | 52.08 | 0.1737 | 0.50265 | 4.4 E–6 |
| | | | 0.0264 | 37.88 | 0.1412 | 6.03186 | 1.1 E–6 |
| | | | 0.0069 | 144.93 | 0.0961 | 6.09469 | 3.6 E–6 |
| | 1989 | | 0.0257 | 38.91 | 0.2236 | 1.19381 | 2.9 E–7 |
| | | | 0.0136 | 73.53 | 0.0589 | 4.20973 | 9.3 E–3 |
| | | | 0.0197 | 50.76 | 0.0603 | 0.87965 | 2.0 E–4 |
| RS Tel | 1988–1989 | | 0.0261 | 38.31 | 0.0701 | 2.38761 | 1.2 E–2 |
| RT Nor | MJUO | $f_1$ | 0.0221 | 45.25 | 0.1300 | 0.94248 | 1.1 E–1 |
| | | $f_2$ | 0.0518 | 19.31 | 0.0734 | 3.07876 | 1.7 E–1 |
| | MJUO + SAAO | $f_1$ | 0.0217 | 46.08 | 0.2047 | 6.15752 | 8.0 E–5 |
| | | $f_2$ | 0.0511 | 19.57 | 0.0706 | 3.64425 | 4.5 E–2 |
| RZ Nor | | | 0.0236 | 42.37 | 0.0734 | 2.63894 | 1.5 E–1 |
| SU Tau | ($B$–$V$) | | 0.0238 | 40.32 | 0.0264 | 0.87965 | 1.3 E–1 |

### 2.4.2 R Coronae Borealis stars in the Large Magellanic Cloud

Four RCB stars have been identified in the Large Magellanic Cloud (LMC). These stars are W Men (HV 966), HV 5637, HV 12842 and HV 12671 (Payne–Gaposchkin 1971). W Men was first identified by Luyten (1927) and has been observed by Eggen (1970) and Sherwood (1975). Several declines of these stars have been detected. Declines of W Men have been noted by Milone (1975) and Glass (*IAU* Circ. 4572). Hodge & Wright (1969) showed a $B$ light curve of HV 5637 derived from Harvard plates, with a decline occurring near JD 2425000. Morgan, Nandy & Rao (1986) have used UK Schmidt $I$ plates to examine the behaviour of HV 12842 between 1976 and 1985 and have recorded several declines.

Feast (1972) obtained low resolution spectra of three of these stars and, from the $C_2$ band strength, concluded that W Men and HV 12842 resembled R CrB and RY Sgr. Strong absorption bands were observed in the spectra of HV 5637, indicating some similarity to cool galactic RCB stars, e.g. S Aps. Feast was unable to detect HV 12671, presumably because the star was in decline. HV 12671 is unique since it is also a symbiotic star (Allen 1980) and is thus the only known star with both RCB and symbiotic star characteristics. Unpublished spectra of HV 12671 (Wood, personal communication) show that the star has a photospheric spectrum indicative of a cool RCB star.

Despite the interest in these stars, and the information that they give to studies of the galactic RCB stars (the $M_{\rm bol}$ estimate of –5), there have been few attempts to observe these stars photoelectrically. Prior to this study there has been no attempt to observe the LMC RCB stars over a long timescale to search for periodicities.

The LMC RCB stars were included on the MJUO survey as early as 1986 June (W Men) and 1986 October (the other three stars). We continued observing only W Men and HV 12842 on a regular basis as the faintness of HV 5637 ($V$ = 14.5) and HV 12671 ($V$ = 15.5) prevented accurate photometry being obtained on enough nights to derive useful results. W Men declined late in 1987 (*IAU* Circ. 4572) and unfortunately we did not observe the decline onset. Further observations of W Men have only been obtained after the recovery of the star to near maximum light. For HV 12842 we have an essentially continuous light curve. This is due to the favourable declination of these stars ($\delta$ = –69° to –71°) such that they are circumpolar objects at MJUO (latitude = –44°).

The $BV$ observations of W Men and HV 12842 are listed in Table 2.12 and 2.13 respectively. For W Men, the light and colour curves from JD 24465499–2447138 are shown in Fig. 2.22. The light and colour curves for HV 12842 are shown in Fig. 2.23.

An analysis of the $V$ photometry of W Men reveals several possible periodicities. The power spectrum of the dataset from JD 2446599–2447138 has a periodicity at $f$ = 0.0016 d$^{-1}$ ($P$ = 625 d) which is due to the variations in the $V$ magnitude between 14.0–14.3 during the time of these observations. The cause of this periodicity is uncertain as the star was not known to be recovering from a decline. After removing this constituent, an iterative analysis revealed peaks at $f$ = 0.0057 d$^{-1}$ ($P$ = 175.4 d) and $f$ = 0.0271 d$^{-1}$ ($P$ = 36.9 d). The latter periodicity was of marginal significance (Table 2.16).

The $V$ light curve for HV 12842 shows evidence of a strong beating phenomenon with a beat envelope period of $\sim$ 700 d, assuming that the peaks of the outer envelope occurred near JD 2446800 and JD 2447500. If this behaviour is retained in the longer term, then there are at least two dominant modes of pulsation for this star. A Fourier

**Table 2.12.** MJUO $BV$ photometry of W Men (HV966).

| JD−2440000 | $V$ | $(B-V)$ | JD−2440000 | $V$ | $(B-V)$ | JD−2440000 | $V$ | $(B-V)$ |
|---|---|---|---|---|---|---|---|---|
| 6599.243 | 14.026 | 0.361 | 6667.217 | 14.042 | 0.356 | 6745.025 | 13.829 | 0.389 |
| 6600.206 | 14.035 | 0.367 | 6668.181 | 14.093 | 0.362 | 6755.038 | 13.878 | 0.355 |
| 6615.240 | 14.003 | 0.375 | 6669.187 | 14.083 | 0.353 | 6767.003 | 13.759 | 0.375 |
| 6626.230 | 13.989 | 0.392 | 6670.143 | 14.057 | 0.373 | 6768.000 | 13.764 | 0.380 |
| 6627.204 | 13.985 | 0.353 | 6687.106 | 13.957 | 0.347 | 6787.021 | 13.888 | 0.330 |
| 6628.210 | 13.996 | 0.330 | 6694.163 | 14.085 | 0.345 | 6800.939 | 13.833 | 0.344 |
| 6648.218 | 13.950 | 0.348 | 6696.186 | 14.046 | 0.357 | 6827.008 | 13.897 | 0.401 |
| 6649.210 | 13.928 | 0.364 | 6718.112 | 13.926 | 0.343 | 6834.950 | 13.837 | 0.328 |
| 6657.162 | 13.989 | 0.383 | 6734.969 | 13.825 | 0.381 | 6836.049 | 13.837 | 0.388 |
| 6658.201 | 14.030 | 0.433 | 6744.036 | 13.875 | 0.373 | 6836.926 | 13.834 | 0.385 |
| 6845.918 | 13.862 | 0.383 | 6925.163 | 13.826 | 0.334 | 7030.845 | 13.950 | 0.376 |
| 6847.004 | 13.865 | 0.348 | 6954.804 | 13.867 | 0.406 | 7039.209 | 13.947 | 0.421 |
| 6867.051 | 13.784 | 0.370 | 6963.894 | 13.863 | 0.346 | 7043.044 | 13.911 | 0.404 |
| 6873.935 | 13.817 | 0.342 | 6982.090 | 13.850 | 0.355 | 7063.108 | 13.942 | 0.412 |
| 6875.942 | 13.803 | 0.348 | 6982.877 | 13.825 | 0.390 | 7065.035 | 13.890 | 0.373 |
| 6876.970 | 13.831 | 0.362 | 6985.869 | 13.817 | 0.374 | 7088.966 | 13.880 | 0.384 |
| 6895.887 | 13.813 | 0.357 | 7003.138 | 13.886 | 0.369 | 7090.033 | 13.849 | 0.329 |
| 6897.124 | 13.837 | 0.451 | 7019.832 | 13.929 | 0.413 | 7093.973 | 13.831 | 0.344 |
| 6904.044 | 13.805 | 0.330 | 7020.982 | 13.945 | 0.339 | 7106.977 | 13.909 | 0.408 |
| 6905.042 | 13.828 | 0.338 | 7021.836 | 13.936 | 0.393 | 7120.105 | 13.915 | 0.394 |
| 7138.070 | 13.827 | 0.422 | 7572.939 | 14.428 | 0.505 | 7627.890 | 14.765 | 0.601 |
| 7466.967 | 16.055 | 0.714 | 7591.894 | 14.461 | 0.456 | 7653.860 | 14.554 | 0.507 |
| 7482.049 | 15.805 | | 7609.851 | 14.551 | | 7655.858 | 14.548 | 0.603 |
| 7500.081 | 14.879 | 0.663 | 7610.839 | 14.728 | | 7682.824 | 14.699 | 0.466 |
| 7564.939 | 14.388 | 0.502 | 7615.979 | 14.631 | 0.379 | 7699.685 | 14.575 | 0.543 |
| 7565.971 | 14.398 | 0.514 | 7619.873 | 14.449 | 0.660 | 7705.975 | 14.483 | 0.574 |
| 7570.968 | 14.454 | 0.508 | 7620.869 | 14.675 | 0.581 | | | |

**Table 2.13.** MJUO $BV$ photometry of HV 12842.

| JD−2440000 | $V$ | $(B-V)$ | JD−2440000 | $V$ | $(B-V)$ | JD−2440000 | $V$ | $(B-V)$ |
|---|---|---|---|---|---|---|---|---|
| 6731.127 | 13.797 | | 6835.017 | 13.963 | 0.547 | 6905.014 | 13.706 | 0.509 |
| 6744.065 | 13.701 | 0.459 | 6836.984 | 13.970 | 0.518 | 6923.859 | 13.710 | 0.526 |
| 6745.055 | 13.657 | 0.507 | 6846.003 | 13.796 | 0.507 | 6925.187 | 13.721 | 0.464 |
| 6755.074 | 13.572 | 0.438 | 6847.033 | 13.819 | 0.524 | 6928.854 | 13.701 | 0.476 |
| 6767.108 | 13.707 | 0.426 | 6867.110 | 13.684 | 0.508 | 6947.026 | 13.963 | 0.485 |
| 6768.095 | 13.721 | 0.494 | 6874.034 | 13.727 | 0.514 | 6954.832 | 13.859 | 0.465 |
| 6792.046 | 13.700 | 0.481 | 6876.032 | 13.722 | 0.524 | 6982.128 | 13.777 | 0.461 |
| 6801.050 | 13.720 | 0.537 | 6895.998 | 13.732 | 0.482 | 6985.831 | 13.699 | 0.499 |
| 6814.027 | 13.959 | 0.529 | 6897.093 | 13.685 | 0.508 | 7002.994 | 13.875 | 0.484 |
| 6827.114 | 14.133 | 0.581 | 6904.019 | 13.704 | 0.522 | 7006.246 | 13.823 | 0.499 |
| 7019.860 | 13.744 | 0.488 | 7094.002 | 13.667 | 0.480 | 7190.938 | 13.767 | 0.489 |
| 7021.024 | 13.715 | 0.479 | 7109.981 | 13.715 | 0.445 | 7196.986 | 13.746 | 0.481 |
| 7021.866 | 13.687 | 0.510 | 7120.074 | 13.788 | 0.479 | 7212.971 | 13.663 | 0.489 |
| 7030.877 | 13.658 | 0.523 | 7137.958 | 13.688 | 0.463 | 7221.969 | 13.652 | 0.511 |
| 7043.082 | 13.741 | 0.466 | 7155.979 | 13.747 | 0.495 | 7226.916 | 13.693 | 0.480 |
| 7043.875 | 13.740 | 0.483 | 7162.008 | 13.738 | 0.521 | 7240.949 | 13.712 | 0.498 |
| 7063.070 | 13.817 | 0.470 | 7164.005 | 13.733 | 0.428 | 7244.951 | 13.680 | 0.481 |
| 7065.000 | 13.820 | 0.470 | 7175.934 | 13.778 | 0.498 | 7258.887 | 13.664 | 0.536 |
| 7089.010 | 13.661 | 0.481 | 7184.958 | 13.769 | 0.506 | 7263.918 | 13.693 | 0.473 |
| 7090.062 | 13.675 | 0.472 | 7187.935 | 13.788 | 0.487 | 7268.871 | 13.699 | 0.522 |
| 7282.892 | 13.608 | 0.480 | 7375.862 | 13.794 | 0.473 | 7436.065 | 13.951 | 0.408 |
| 7297.894 | 13.722 | 0.527 | 7380.222 | 13.763 | 0.536 | 7465.016 | 13.745 | 0.577 |
| 7301.833 | 13.718 | 0.500 | 7395.158 | 13.744 | 0.467 | 7466.995 | 13.767 | 0.515 |
| 7306.832 | 13.771 | 0.487 | 7397.163 | 13.686 | 0.514 | 7479.995 | 13.753 | 0.452 |
| 7316.812 | 13.810 | 0.469 | 7401.110 | 13.654 | 0.476 | 7481.983 | 13.750 | 0.475 |
| 7323.899 | 13.749 | 0.533 | 7407.150 | 13.692 | 0.458 | 7487.013 | 13.701 | 0.494 |
| 7325.832 | 13.784 | 0.505 | 7408.214 | 13.725 | 0.448 | 7488.993 | 13.773 | 0.460 |
| 7343.841 | 13.688 | 0.514 | 7418.127 | 13.759 | 0.527 | 7490.010 | 13.733 | 0.470 |
| 7355.192 | 13.640 | 0.544 | 7420.984 | 13.780 | 0.509 | 7500.045 | 13.901 | 0.457 |
| 7363.052 | 13.637 | 0.540 | 7428.113 | 13.832 | 0.495 | 7552.948 | 13.690 | 0.494 |
| 7564.974 | 13.608 | 0.467 | 7619.902 | 13.734 | 0.543 | 7655.901 | 13.744 | 0.463 |
| 7570.994 | 13.555 | 0.468 | 7622.917 | 13.697 | | 7663.862 | 13.719 | 0.468 |
| 7572.910 | 13.568 | 0.417 | 7627.920 | 13.732 | 0.467 | 7682.845 | 13.755 | 0.493 |
| 7588.021 | 13.714 | 0.330 | 7635.870 | 13.692 | 0.545 | 7699.869 | 13.667 | 0.479 |
| 7609.876 | 13.711 | 0.510 | 7643.908 | 13.760 | 0.523 | 7706.001 | 13.649 | 0.445 |
| 7610.881 | 13.714 | 0.496 | 7653.843 | 13.793 | 0.459 | | | |

analysis of the $V$ photometry (Fig. 2.24) reveals three dominant periodicities at $f_1 = 0.0168$ d$^{-1}$ ($P_1 = 59.5$ d), $f_2 = 0.0086$ d$^{-1}$ ($P_2 = 116.3$ d) and $f_3 = 0.0184$ d$^{-1}$ ($P_3 = 54.3$ d) respectively. Note that $f_1 \approx 2f_2$, which indicates that $f_1$ may be an harmonic of $f_2$. The amplitudes of these two periodicities are almost equal (see Table 2.16). A synthetic light curve based upon these three periodicities did not convincingly reproduce the observed variations of HV 12842, in particular any long-term beating phenomenon. The $(B-V)$ colour curve appeared to be variable only when the corresponding $V$ amplitude was large, e.g. near JD 2446800.

The limited $BV$ observations of HV 5637 and HV 12671 are listed in Tables 2.14 and 2.15 respectively. Note that, for HV 12671, there were times when the $V$ magnitude and the $(B-V)$ index changed rapidly (e.g., near JD 2446875). This type of behaviour is unusual for an RCB star at maximum and we suspect that these changes are due to the symbiotic characteristics of the system.

Table 2.14. MJUO $BV$ photmetry of HV 5637.

| JD-2440000 | $V$ | $(B-V)$ | JD-2440000 | $V$ | $(B-V)$ | JD-2440000 | $V$ | $(B-V)$ |
|---|---|---|---|---|---|---|---|---|
| 6767.074 | 14.752 | 1.162 | 6836.080 | 14.757 | 1.238 | 6873.964 | 14.783 | 1.384 |
| 6768.031 | 14.821 | 1.174 | 6836.953 | 14.732 | 1.343 | 6876.102 | 14.803 | 1.115 |
| 6792.015 | 14.780 | 1.148 | 6845.976 | 14.816 | 1.174 | 6877.035 | 14.826 | 1.266 |
| 6800.988 | 14.825 | 1.236 | 6846.977 | 14.816 | 1.233 | 6895.917 | 14.722 | 1.366 |
| 6813.971 | 14.840 | 1.178 | 6847.994 | 14.889 | 1.153 | 6903.992 | 14.795 | 1.305 |
| 6835.049 | 14.774 | 1.233 | 6867.078 | 14.794 | 1.301 | 6904.987 | 14.747 | 1.136 |

Table 2.15. MJUO $BV$ photometry of HV 12671.

| JD-2440000 | $V$ | $(B-V)$ | JD-2440000 | $V$ | $(B-V)$ | JD-2440000 | $V$ | $(B-V)$ |
|---|---|---|---|---|---|---|---|---|
| 6768.064 | 15.976 | 0.933 | 6835.084 | 15.515 | 0.649 | 6876.066 | 15.646 | 0.775 |
| 6801.020 | 15.668 | 0.617 | 6837.136 | 15.712 | 0.747 | 6877.003 | 15.543 | 0.650 |
| 6813.985 | 15.679 | 0.692 | 6845.948 | 15.616 | 0.572 | 6895.958 | 15.702 | 0.816 |
| 6827.082 | 15.651 | 0.626 | 6873.999 | 15.814 | 0.856 | 6904.950 | 15.540 | 0.595 |

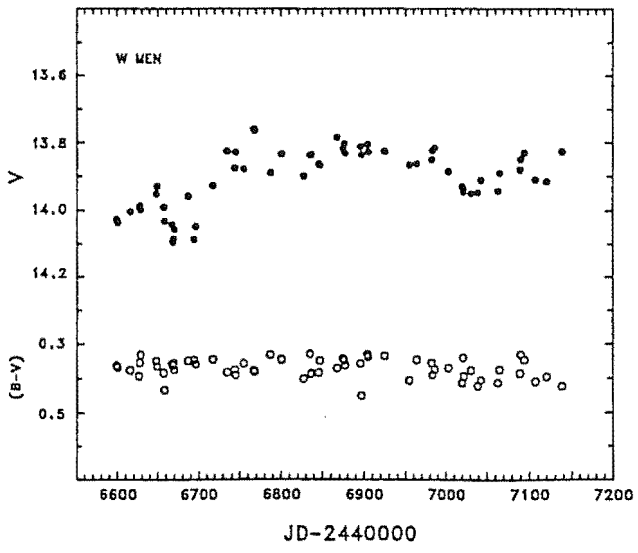


**Figure 2.22.** $V$ and $(B-V)$ colour curves for W Men from JD 2446599–2447138 plotted against Julian Date.

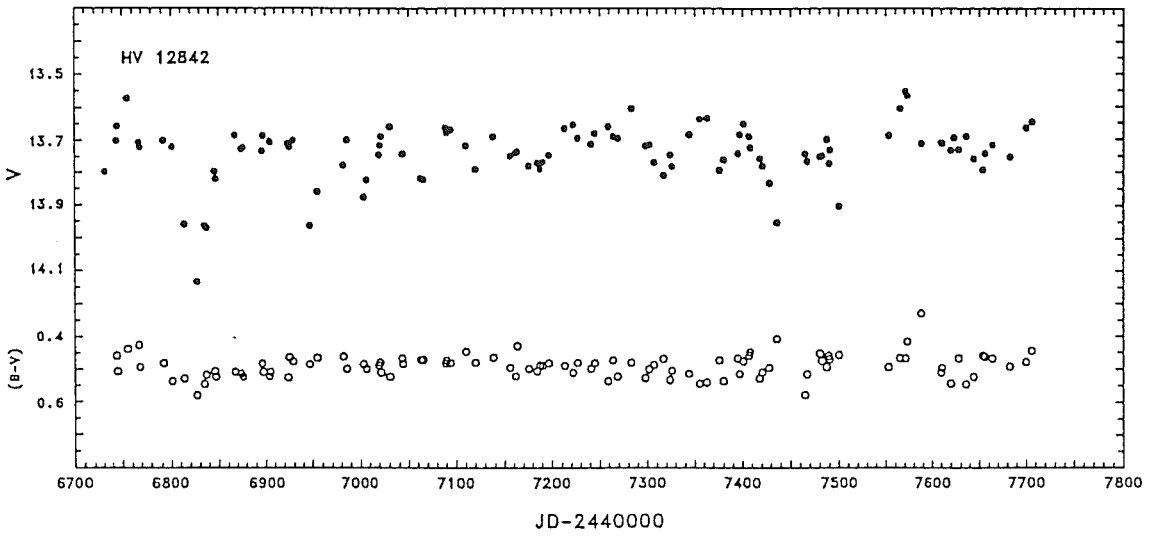


Figure 2.23. $V$ and $(B-V)$ colour curves for HV 12842 plotted against Julian Date.

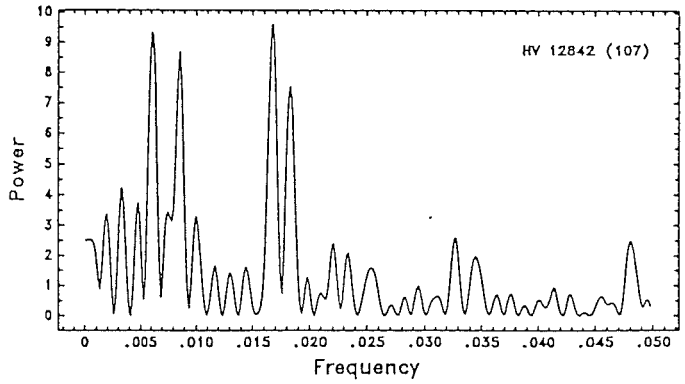


Figure 2.24. Power spectrum for $V$ photometry of HV 12842. The number of data points is indicated.

**Table 2.16.** Fourier components of LMC RCB star photometry.

| Star | | $f$ (d$^{-1}$) | $P$ (d) | $A$ (mag) | $\phi$ (rad) | $F$ |
|---|---|---|---|---|---|---|
| W Men | | 0.0016 | l.f. | 0.0880 | 0.06283 | 5.4 E–6 |
| | | 0.0057 | 175.4 | 0.0511 | 3.64425 | 1.2 E–3 |
| | | 0.0271 | 36.9 | 0.0328 | 0.50265 | 6.7 E–2 |
| HV 12842 | $f_1$ | 0.0168 | 59.5 | 0.0531 | 2.01062 | 6.6 E–3 |
| | $f_2 = 0.5f_1$ | 0.0086 | 116.3 | 0.0487 | 0.87965 | 3.4 E–3 |
| | $f_3$ | 0.0184 | 54.3 | 0.0366 | 0.62832 | 7.5 E–2 |

### 2.4.3 The hydrogen deficient carbon (HdC) stars

The HdC stars have long been associated with the RCB stars, principally due to their spectral similarities. The possible connection between these two groups of stars was initially recognised by Bidelman (1953), and was further enhanced by Warner's (1967) spectral analysis of the HdC stars known at that time. The star XX Cam, initially classified as an RCB star, appears to have characteristics more closely aligned to those of the HdC stars (see Rao, Ashok & Kulkarni 1980; Walker 1986) and was not recognised at the time of Warner's analysis as a possible HdC star.

Warner's spectral analysis revealed that one star, HD 148839, possessed an intermediate hydrogen deficiency with a C/H ratio of $\sim$ 0.05, compared with C/H ratios in excess of 1000 for the other stars. Warner postulated that HD 148839 may be a star intermediate between normal cool carbon stars and the other HdC stars (and by inference the RCB stars). The alternative viewpoint is that there is a range of hydrogen abundance in these classes of objects. The detection of hydrogen lines in the RCB star NSV 6708 (Section 4.3.8), stronger than those present in most other RCB stars supports this viewpoint. The spectral similarities between the HdC stars and RCB stars were recently reviewed by Lambert (1986).

The HdC stars had been generally thought to be non-variable stars, but variability was discovered in four of the five southern HdC stars by Kilkenny, Marang & Menzies (1988) using facilities at SAAO. The only possible exception was HD 173409, for which variability was not detected with certainty. The expression 'non-variable' originally referred to the lack of RCB star–type declines in these stars, and the survey of Kilkenny, Marang & Menzies (1988) was the first such attempt to detect low amplitude variations similar to those observed in the RCB stars. The SAAO survey observed the five HdC stars for short intervals during 1982–83 and 1986. Kilkenny, Marang & Menzies found evidence for variability on timescales of 20–100 d in these stars, although the short duration of the observations prevented any conclusive argument about the range of variation of period and amplitude. It was apparent from these data that, with the exception of HD 175893, these stars had amplitudes lower than those RCB stars observed during the same survey. HD 175893 was discovered to have variations in $V$ of $\sim$ 0.3 mag over timescales of 20–40 d, and thus was similar in appearance to many RCB stars. The SAAO photometry of the HdC stars and RCB stars were compiled by Marang *et al.* (1989). Totochava (1973) obtained limited photometry for XX Cam and claimed variability on the order of 0.1 mag over timescales of $\sim$40 d. Additional photometry of this star would be extremely valuable.

The three brightest southern HdC stars, HD 137613, HD 148839 and HD 182040, were scheduled into the MJUO survey during 1988. The $V$ magnitude and colour indices for these stars are tabulated in Table 2.17, 2.18 and 2.19, and the light and colour curves are shown in Figs. 2.25, 2.26 and 2.27 respectively. Our observations were obtained for about 200 d for HD 137613 and HD 182040, and 300 d for HD 148839. Whilst our photometry supported the general conclusions reached by Kilkenny, Marang & Menzies (1988), the longer duration of our dataset enables us to make several additional comments about these stars.

The $V$ light curves for all three stars show variability of the order of 0.1 mag over timescales apparently similar to those noted by Kilkenny, Marang & Menzies (1988). Surprisingly, the colour curves, in particular the $(B–V)$ curves, showed more regular changes

**Table 2.17.** MJUO *UBVR* photometry of HD 137613.

| JD–2440000 | *V* | (*U–B*) | (*B–V*) | (*V–R*) | JD–2440000 | *V* | (*U–B*) | (*B–V*) | (*V–R*) |
|---|---|---|---|---|---|---|---|---|---|
| 7237.140 | 7.447 | 0.951 | 1.161 | | 7275.117 | 7.449 | 0.957 | 1.175 | |
| 7241.127 | 7.445 | 0.923 | 1.177 | 0.633 | 7281.101 | 7.516 | 0.961 | 1.182 | |
| 7242.209 | 7.481 | 0.928 | 1.172 | | 7282.132 | 7.508 | 0.948 | 1.187 | |
| 7244.190 | 7.473 | 0.946 | 1.182 | | 7283.141 | 7.503 | 0.967 | 1.187 | |
| 7255.053 | 7.452 | 0.916 | 1.176 | | 7297.958 | 7.456 | 0.978 | 1.179 | |
| 7256.052 | 7.471 | 0.962 | 1.176 | 0.649 | 7302.008 | 7.430 | 0.984 | 1.186 | |
| 7268.123 | 7.472 | 0.988 | 1.173 | | 7306.961 | 7.448 | 0.985 | 1.188 | |
| 7269.056 | 7.459 | 0.987 | 1.182 | | 7309.068 | 7.459 | 0.980 | 1.183 | |
| 7273.167 | 7.452 | 0.949 | 1.178 | | 7313.095 | 7.457 | 0.962 | 1.181 | |
| 7274.119 | 7.459 | 0.955 | 1.175 | | 7322.157 | 7.472 | | 1.158 | |
| 7325.928 | 7.476 | | 1.173 | | 7394.957 | 7.496 | 0.924 | 1.187 | |
| 7329.043 | 7.474 | | 1.165 | | 7396.972 | 7.470 | 0.918 | 1.172 | |
| 7337.073 | 7.446 | | 1.167 | 0.603 | 7400.875 | 7.472 | 0.935 | 1.189 | |
| 7354.923 | 7.467 | 0.908 | 1.179 | | 7406.917 | 7.511 | 0.985 | 1.204 | |
| 7361.032 | 7.490 | | 1.168 | 0.611 | 7412.870 | 7.500 | 0.988 | 1.200 | |
| 7367.896 | 7.547 | 0.929 | 1.200 | | 7417.931 | 7.519 | 0.949 | 1.195 | |
| 7370.937 | 7.464 | 0.957 | 1.187 | | 7420.906 | 7.507 | 0.984 | 1.194 | |
| 7372.869 | 7.474 | 0.957 | 1.195 | | 7423.905 | 7.496 | 0.966 | 1.163 | |
| 7375.968 | 7.484 | 0.945 | 1.195 | | 7427.898 | 7.519 | 0.975 | 1.188 | |
| 7379.906 | 7.485 | | 1.184 | 0.628 | 7439.876 | 7.494 | | 1.180 | |
| 7388.953 | 7.508 | 0.940 | 1.199 | 0.639 | | | | | |

**Table 2.18.** MJUO *UBVR* photometry of HD 148839.

| JD–2440000 | *V* | (*U–B*) | (*B–V*) | (*V–R*) | JD–2440000 | *V* | (*U–B*) | (*B–V*) | (*V–R*) |
|---|---|---|---|---|---|---|---|---|---|
| 7162.119 | 8.350 | 0.689 | 0.936 | 0.487 | 7255.031 | 8.368 | 0.702 | 0.928 | |
| 7164.123 | 8.344 | | 0.913 | 0.480 | 7256.000 | 8.346 | 0.724 | 0.920 | 0.491 |
| 7176.104 | 8.339 | 0.688 | 0.924 | 0.482 | 7259.030 | 8.351 | 0.698 | 0.921 | |
| 7185.077 | 8.324 | 0.705 | 0.927 | 0.478 | 7263.006 | 8.342 | 0.729 | 0.924 | |
| 7188.074 | 8.347 | 0.708 | 0.927 | 0.488 | 7264.012 | 8.354 | 0.686 | 0.921 | |
| 7197.104 | 8.349 | 0.702 | 0.920 | 0.481 | 7267.068 | 8.331 | 0.704 | 0.914 | 0.480 |
| 7221.024 | 8.349 | 0.698 | 0.932 | 0.488 | 7269.028 | 8.326 | 0.699 | 0.914 | |
| 7227.044 | 8.354 | 0.724 | 0.927 | | 7273.000 | 8.348 | 0.709 | 0.912 | |
| 7237.156 | 8.355 | 0.699 | 0.927 | | 7274.073 | 8.335 | 0.685 | 0.913 | |
| 7241.078 | 8.334 | 0.705 | 0.918 | 0.480 | 7275.015 | 8.364 | 0.706 | 0.916 | |
| 7281.023 | 8.339 | 0.712 | 0.909 | | 7322.176 | 8.359 | 0.682 | 0.929 | |
| 7283.023 | 8.342 | 0.690 | 0.908 | | 7325.948 | 8.359 | 0.681 | 0.924 | |
| 7297.981 | 8.337 | 0.696 | 0.912 | | 7354.938 | 8.359 | 0.703 | 0.937 | |
| 7301.958 | 8.335 | 0.684 | 0.906 | | 7362.984 | 8.366 | 0.699 | 0.936 | 0.490 |
| 7306.943 | 8.345 | 0.681 | 0.916 | | 7371.005 | 8.378 | 0.711 | 0.941 | |
| 7309.043 | 8.345 | 0.682 | 0.911 | | 7401.052 | 8.389 | 0.720 | 0.941 | |
| 7313.075 | 8.358 | 0.696 | 0.922 | | 7412.993 | 8.351 | 0.715 | 0.922 | |
| 7316.921 | 8.335 | 0.700 | 0.908 | | 7427.970 | 8.338 | 0.665 | 0.902 | |
| 7318.143 | 8.367 | 0.709 | 0.917 | | 7439.894 | 8.337 | 0.670 | 0.904 | |

**Table 2.19.** MJUO *UBV* photometry of HD 182040.

| JD–2440000 | *V* | (*U–B*) | (*B–V*) | JD–2440000 | *V* | (*U–B*) | (*B–V*) |
|---|---|---|---|---|---|---|---|
| 7255.192 | 6.996 | 0.684 | 1.037 | 7307.067 | 7.011 | 0.676 | 1.035 |
| 7256.133 | 6.992 | 0.694 | 1.037 | 7309.148 | 7.007 | 0.690 | 1.031 |
| 7268.203 | 6.976 | 0.607 | 1.014 | 7317.022 | 7.030 | 0.694 | 1.051 |
| 7269.172 | 6.978 | 0.624 | 1.012 | 7318.183 | 7.027 | 0.704 | 1.037 |
| 7273.189 | 6.961 | 0.592 | 1.006 | 7322.213 | 7.005 | 0.680 | 1.042 |
| 7274.157 | 6.952 | 0.602 | 1.011 | 7326.068 | 7.012 | 0.672 | 1.040 |
| 7275.140 | 6.951 | 0.612 | 1.016 | 7346.028 | 6.990 | 0.689 | 1.047 |
| 7282.244 | 6.992 | 0.641 | 1.019 | 7355.012 | 6.999 | 0.674 | 1.042 |
| 7283.201 | 6.988 | 0.656 | 1.017 | 7371.021 | 6.995 | 0.648 | 1.045 |
| 7302.102 | 6.992 | 0.633 | 1.022 | 7376.028 | 6.994 | 0.662 | 1.042 |
| 7395.019 | 7.015 | 0.639 | 1.043 | 7418.049 | 6.984 | 0.648 | 1.027 |
| 7397.032 | 6.999 | 0.644 | 1.044 | 7428.046 | 6.997 | | 1.054 |
| 7401.025 | 6.969 | 0.632 | 1.028 | 7435.977 | 7.028 | 0.665 | 1.058 |
| 7407.084 | 6.969 | 0.637 | 1.016 | | | | |

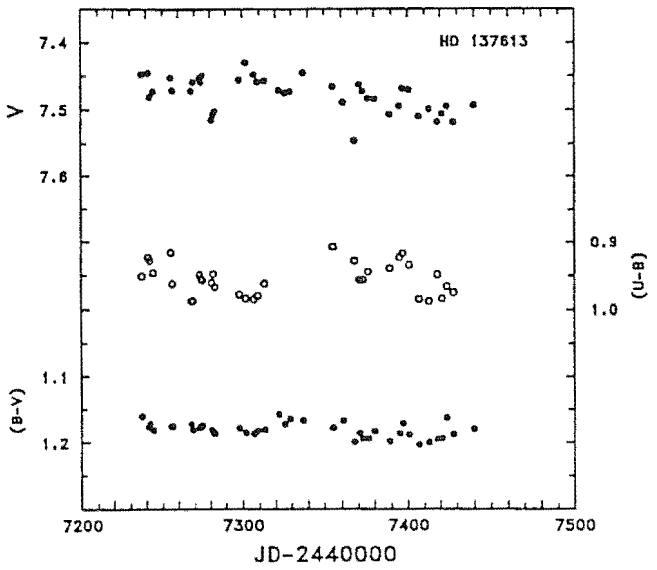


**Figure 2.25.** $V$ light and $(U\text{–}B)$ and $(B\text{–}V)$ colour curves for HD 137613 plotted against Julian Date.

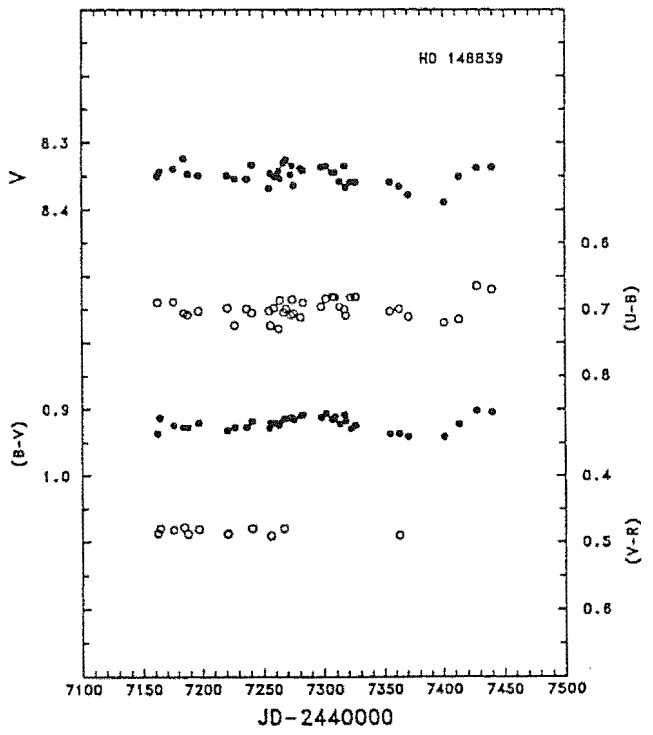


**Figure 2.26.** $V$ light and $(U\text{–}B)$, $(B\text{–}V)$ and $(V\text{–}R)$ colour curves for HD 148839 plotted against Julian Date.

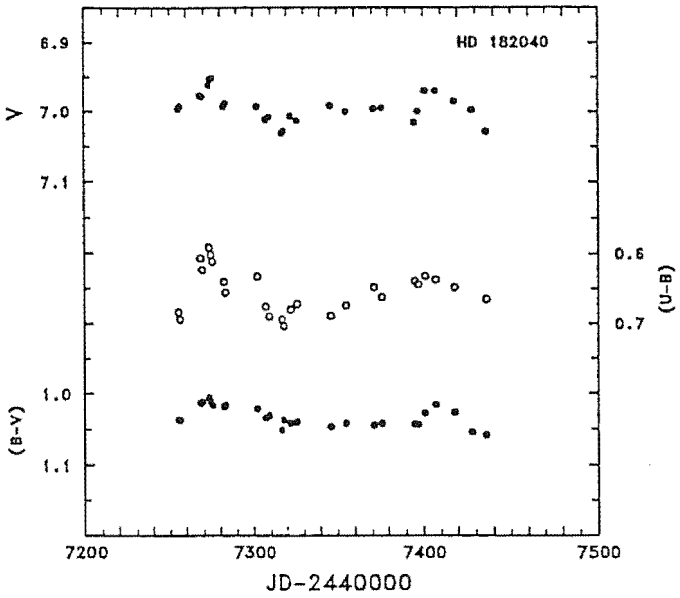


**Figure 2.27.** $V$ light and $(U\text{-}B)$ and $(B\text{-}V)$ colour curves for HD 182040 plotted against Julian Date.

in colour over much longer timescales. This variability was particularly evident in the $(U\text{-}B)$ and the $(B\text{-}V)$ colour curves of HD 148839. A Fourier analysis of the HD 148839 $(B\text{-}V)$ data extracted a periodicity at $f = 0.0062$ d$^{-1}$ ($P = 161$ d; see Fig. 2.28). Including the SAAO photometry of HD 148839 gave a peak at $f = 0.0063$ d$^{-1}$ ($P = 158$ d).

A Fourier analysis of the $V$ photometry of HD 182040 had a peak at $f = 0.0092$ d$^{-1}$ ($P = 109$ d), but the $(B\text{-}V)$ photometry had a peak at $f = 0.0148$ d$^{-1}$ ($P = 67.57$ d). This latter periodicity is supported by the inclusion of SAAO photometry for this star ($f = 0.0146$ d$^{-1}$ for $V$, $f = 0.0159$ d$^{-1}$ for $B\text{-}V$; see Table 2.20). (Note that the 109 d period in the MJUO $V$ photometry of HD 182040 is the least significant periodicity.)

The $V$ photometry for HD 137613 showed a distinct downward trend ($\Delta V = 0.05$ mag) throughout the dataset. We concluded, after an analysis of the comparison star and check star observations obtained concurrently with the data for this star, that this downward trend was intrinsic to HD 137613. This downward trend may indicate that the mean $V$ magnitude of HD 137613 varies over a longer timescale than the current set of observations. A Fourier analysis of the $(B\text{-}V)$ photometry showed a periodicity at $f = 0.0096$ d$^{-1}$ ($P = 104$ d). Including the SAAO photometry for this star gave a peak at $f = 0.0091$ d$^{-1}$ ($P = 110$ d). The Fourier components of the MJUO and SAAO photometry of these three HdC stars are summarised in Table 2.20.

It was also apparent that the colour amplitudes of these stars varied greatly with time. There were several occasions where the colour amplitudes of the MJUO photometry exceeded the colour amplitudes observed by Kilkenny, Marang & Menzies (1988). In all three stars, the $(U\text{-}B)$ and $(B\text{-}V)$ colour curves were observed to be generally in phase with the $V$ curve.

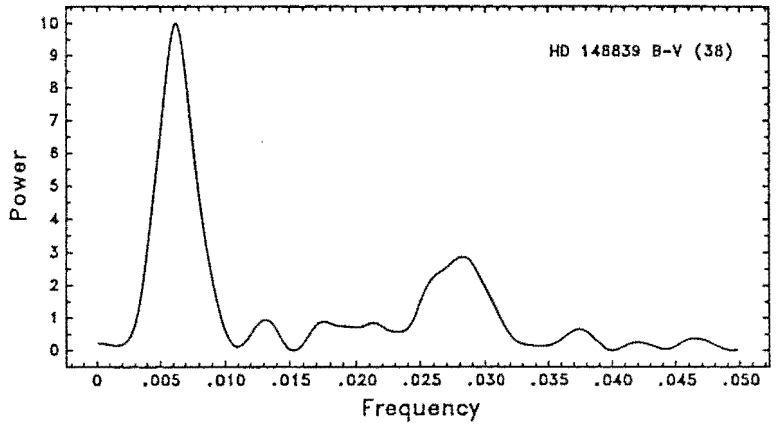


Figure 2.28. Power spectrum for MJUO ($B$–$V$) photometry of HD 148839. The number of data points is indicated.

Table 2.20. Fourier components of HdC star photometry.

| Star | Data | | $f$ (d$^{-1}$) | $P$ (d) | $A$ (mag) | $\phi$ (rad) | $F$ |
|---|---|---|---|---|---|---|---|
| HD 137613 | MJUO | ($B$–$V$) | 0.0096 | 104.17 | 0.0073 | 3.07876 | 1.5 E–1 |
| | MJUO + SAAO | ($B$–$V$) | 0.0091 | 109.89 | 0.0043 | 4.71239 | 3.3 E–1 |
| HD 148839 | MJUO | ($B$–$V$) | 0.0062 | 161.29 | 0.0099 | 4.46106 | 1.2 E–3 |
| | MJUO + SAAO | $V$ | 0.0064 | 156.25 | 0.0075 | 0.31416 | 2.8 E–1 |
| | MJUO + SAAO | ($B$–$V$) | 0.0063 | 158.73 | 0.0068 | 0.69115 | 5.5 E–3 |
| HD 182040 | MJUO | $V$ | 0.0092 | 108.70 | 0.0133 | 1.63363 | 7.0 E–2 |
| | MJUO | ($B$–$V$) | 0.0148 | 67.57 | 0.0222 | 1.13097 | 1.8 E–2 |
| | MJUO + SAAO | $V$ | 0.0146 | 68.49 | 0.0178 | 3.51858 | 5.7 E–4 |
| | MJUO + SAAO | ($B$–$V$) | 0.0159 | 62.89 | 0.0104 | 3.26726 | 4.3 E–3 |

## 2.5 DISCUSSION

A preliminary appraisal of the photometric characteristics of these objects indicates an apparent diversity in the properties of these stars. In particular, there is a considerable range in the degree of regularity and in the amplitude of the light and colour curves. This diversity of activity is interesting as there are also many common characteristics between these stars. In particular, the RCB stars all have documented declines, have circumstellar shells that are typically 6–8 mag brighter at 12 $\mu$m than at $V$ (Section 2.5.2) and share common spectroscopic characteristics. The HdC stars, although spectroscopically similar to the RCB stars (Section 2.4.3), do not have declines and some do not have infrared excesses indicative of the presence of circumstellar shells (Walker 1986). Although *most* HdC stars have lower amplitude variations than *most* RCB stars, this is not always the

case, e.g. the amplitude of the light curve of the HdC star HD 175893 [fig 1 of Kilkenny, Marang & Menzies (1988); comments in Section 2.4.3] is greater than that of the RCB star Y Mus (Section 2.4.1.4).

RCB and HdC stars with known photometric characteristics, but not observed here, are included in our discussions of the overall properties of hydrogen deficient carbon stars in the Galaxy. These additional stars include R CrB and GU Sgr (see Section 2.1); NSV 6708 (see Section 4.3.6); WX CrA (Marang *et al.* 1989); XX Cam, HD 173409 and HD 175893 (see Section 2.4.3).

In Section 2.5.1 we show evidence for a period–temperature relationship for these stars. This relationship offers further evidence for similarities between the RCB and the HdC stars. In Section 2.5.2 we seek, through theoretical and observational arguments, reasons for the apparent difference between the predicted and observed population distribution as a function of effective temperature. The main implication of these arguments is that there may be many more cooler hydrogen deficient stars still to be discovered. An alternative viewpoint is that theoretical models require revision to explain the observed temperature distribution. We also discuss possible origins for these stars.

### 2.5.1 A period–temperature relationship for cool hydrogen deficient carbon stars

A major obstacle in the effort to understand the evolutionary status of the RCB and HdC stars has been a lack of knowledge of the temperatures of these objects. Spectroscopically derived temperatures are available for only three RCB stars (R CrB, $T_{\rm eff}$ = 7000 K, Cottrell & Lambert 1982a; RY Sgr, 7000 K, Schönberner 1975; UW Cen, 6800 K, Giridhar & Rao 1986) and one HdC star (XX Cam, 7000 K, Cottrell & Lambert 1982a). Note that all four stars have effective temperatures near 7000 K and for that reason they will be loosely termed F–type stars. Marang *et al.* (1989) coarsely separated the periods of these stars into 'short' and 'long' period groups by noting that there was some relationship between the period type and the $C_2$ and CN band strength in unpublished blue spectra of some of the RCB stars. Specifically, those stars with weak $C_2$ and CN features belonged to the 'short' period ($P \sim 40$ d) group. Those stars with strong $C_2$ and CN features belonged to the 'long' period ($P > 65$ d) group. The two apparent exceptions were RS Tel (weak $C_2$ and CN, 'long' period) and S Aps (strong $C_2$, 'short' period). The discrepancy for RS Tel can be explained since the star was rising from a decline (see Section 2.4.1.6). For S Aps, Kilkenny (1983) noted that the star may have changed pulsation period as a result of a changing mode of pulsation. The earlier period of $\sim$ 120 d claimed by Waters (1966) and Kilkenny & Flanagan (1983) would be consistent with a strong spectral feature, 'long' period grouping.

To overcome the lack of spectroscopic data for these stars, a spectroscopic survey of most of the accessible RCB and HdC stars was undertaken by Dr P.L. Cottrell at Mount Stromlo and Siding Spring Observatories. These spectra were obtained with the 1.9–m telescope, at the coudé focus, at resolutions $\Delta\lambda \sim 0.3$–$0.7$Å and at similar wavelength intervals to those observed by Cottrell & Lambert (1982a). These intervals target the Na *D*, H$\alpha$ and 6707Å Li I regions. [These spectra are being used to derive abundances for these stars using similar techniques to Cottrell & Lambert (1982a).] In the context of

the work presented in this Chapter, these spectra permit us to make some comparative estimates of the temperatures of these stars. The survey showed that most of the RCB and HdC stars had spectra similar to those of R CrB and RY Sgr (which have $T_{eff}$ = 7000 K). Those stars with $T_{eff} \approx 7000$ K belonged to the 'short' period group of Marang *et al.* (1989) indicating that the 'short' and 'long' period division was also a coarse temperature division.

By combining estimated temperatures for the galactic RCB and HdC stars from these spectra, and the dominant periods for these stars from the MJUO survey and elsewhere, we have produced a provisional period–temperature diagram (Fig. 2.29). Basic data for those stars plotted in Fig. 2.29 are listed in Table 2.21. These temperatures are estimated by comparing the spectra with those of the four stars with temperature determinations and by assuming that the apparently coolest star (S Aps) has $T_{eff}$ = 5000 K[1]. The estimated temperatures should only be taken as a guide, but an uncertainty of at least 500 K does not compromise the interpretation of the figure. (The points near $T_{eff}$ = 7000 K have been separated slightly to show the large number of stars with similar periods near this temperature.) Two eHe stars with known temperatures and periods are also included in this figure (BD +1°4381, 9500 K, 21.5 d; BD −1°3438, 10900 K, 5–8 d; see Jeffery, Hill & Morrison 1986). Those stars which are multi–periodic are plotted twice and joined by dashed lines. The figure key denotes those symbols used for the various classes of stars, and an uncertainty of 500 K. The relationships shown on this figure are theoretical periods for the fundamental (labelled 'F') and second harmonic (labelled 'H2') radial pulsations from 'Case 1' of Weiss (1987a) ($M = 0.825\ M_{\odot}$, 'R1' composition $X{:}Y{:}X_c{:}X_o{:}Z$ = 0.0:0.972:0.012:0.010:0.0006) and correspond to RCB–type stars in this temperature range. These two modes are pulsationally unstable (pulsation predicted) at the temperatures of the RCB and HdC stars. (The first harmonic of 'Case 1' is pulsationally stable for $T_{eff} >$ 4200 K.)

Three main points arise from this graph:

(i) Significantly, most of the RCB and HdC stars have periods that are consistent with the theoretical relationship for fundamental (F–mode) radial pulsations.

(ii) The 43.1 d period for S Aps lies near the relationship for second harmonic pulsations (H2–mode). This identification would appear to support the suggestion of Kilkenny (1983) that the pulsation mode of the star changed from the fundamental to an harmonic between 1967 and 1971. The predicted F–mode period would be $\sim$ 130 d, which is similar to the period ($\sim$ 120 d) prior to 1967 claimed by Waters (1966) and Kilkenny & Flanagan (1983). However, Kilkenny (1983) claimed an instantaneous period, $P_o = 39.8 \pm 0.2$ d for S Aps. This period appears inconsistent with the 43.1 d H2–mode, but is closer in value to the 38.9 d harmonic of the 80.0 d periodicity (see Section 2.4.1.1). While the H2–mode period of S Aps may have increased between 1972–1988, we believe that there are more likely explanations. There was either an error in the $P_o$ calculated by Kilkenny (our own experience with O–C analyses for RY Sgr suggests that it is very difficult to determine $P_o$ and the period rate of change using instantaneous periods; see fig 3 of Kilkenny 1983), or the 38.9 d harmonic dominated the 43.1 d mode during the early 1970s. The latter would be

[1]Kilkenny & Whittet (1984) found that the blackbody temperature for S Aps was $T_{BB}$ = 4000 K from broadband photometry. However, $T_{eff}$ have been found to be $\sim$ 1000 K higher than $T_{BB}$ for these stars (see Kilkenny & Flanagan 1983; Weiss 1987a).

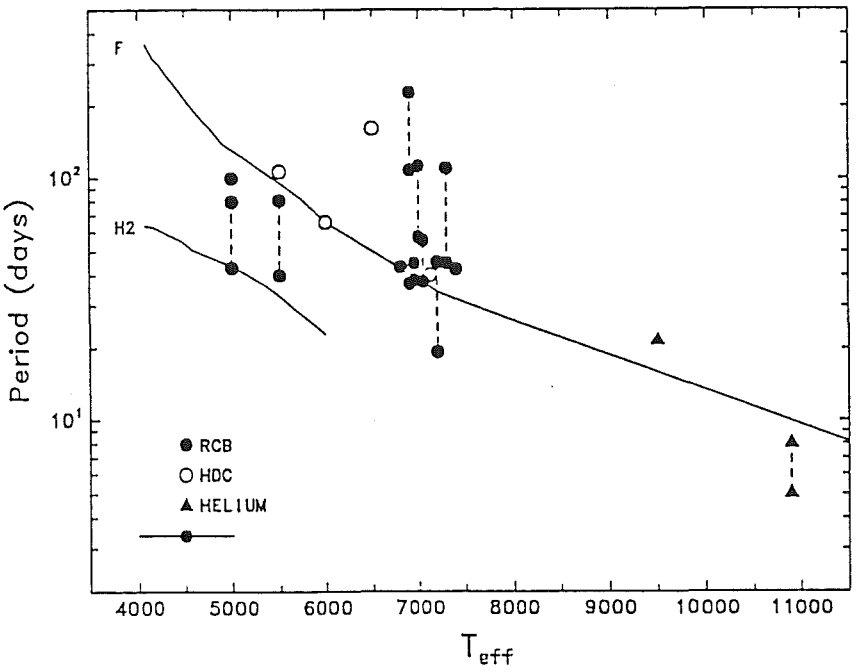


**Figure 2.29.** Period–temperature relationship for galactic RCB stars (•) and HdC stars (o). Two eHe stars (▲) are also plotted. Those stars which are multi-periodic are plotted twice and joined by dashed lines. The solid lines are the theorectical relationships for fundamental (labelled 'F') and second harmonic (labelled 'H2') radial pulsations from 'Case 1' of Weiss (1987a) (see Section 2.5.1).

similar to the changes noted in the amplitude of the two most significant periods of RY Sgr (see Section 2.4.1.5). A change in the dominant periodicity from the 38.9 d period to the 43.1 d period, either a stepwise or gradual change, would mimic the effect of an increasing period.

(iii) Many of the stars analysed in Section 2.4 have periodicities that are not consistent with the radial modes according to Weiss (1987a).

(a) For S Aps, the 80.0 d period and the 38.9 d harmonic were not near predicted radial modes.
(b) The dominant period for U Aqr (81.3 d) was near the predicted F–mode period near 5500 K. The 40.2 d period is probably an harmonic (due to the near 2:1 ratio of these periods) rather than an H2–mode period.
(c) The $\sim$ 52 d period for RY Sgr; $\sim$ 110 d and 227 d periods for Y Mus; 57 d, 77 d and 112 d periods for V CrA; $\sim$ 110 d periodicity for NSV 6708 (Section 4.3.1) and the $\sim$ 160 d period for HD 148839 are longer than the predicted F–mode periods.
(d) The $\sim$ 19 d period for RT Nor was near the predicted first harmonic mode even though the 'Case 1' of Weiss (1987a) did not predict that this mode was unstable for $T_{eff} > 4200$ K. However, we note that for 'Case 2' of Weiss ($M = 0.800\ M_{\odot}$, 'R1' composition), the first harmonic mode is pulsationally unstable for $T_{eff} \gtrsim 7500$ K. This indicates that the assigning of periods to unstable modes may be model dependent.

**Table 2.21.** Basic data for galactic hydrogen deficient carbon stars.

| Star | Type | Period (d) | | Temp. (K) | $V$ | $(B-V)$ | $V_o$ | $(B-V)_o$ | $V_o$–[12] | BC | $\ell$ | b | dist. (kpc) |
|---|---|---|---|---|---|---|---|---|---|---|---|---|---|
| BD $-1°3438$ | eHe | 5–8 | F | 10900[1] | | | | | | | | | |
| BD $+1°4361$ | eHe | 21.5 | F | 9500[1] | | | | | | | | | |
| NSV 6708 | RCB | ~110[2] | | 7000[3] | 7.10 | 0.50 | 7.1 | 0.5 | 6.9 | 0.2 | 324 | 19 | 2.4 |
| | | ~45[4] | F | | | | | | | | | | |
| RZ Nor | RCB | ~42[3] | F | 7000[3] | 10.42 | 1.06 | 8.7 | 0.5 | 6.3 | 0.2 | 332 | –4 | 5.0 |
| R CrB | RCB | ~45[5] | F | 7000[6] | 5.83 | 0.59 | 5.8 | 0.6 | 6.0 | 0.2 | 45 | 51 | 1.3 |
| RY Sgr | RCB | 37.74[3,7] | F | 7000[8] | 6.40 | 0.62 | 6.4 | 0.6 | 7.3 | 0.2 | 4 | –19 | 1.7 |
| | | 55.25[3] | | | | | | | | | | | |
| V CrA | RCB | ~112[3] | | 7000[3] | 9.95 | 0.72 | 9.6 | 0.6 | 7.7 | 0.2 | 358 | –16 | 7.6 |
| | | ~57[3] | | | | | | | | | | | |
| RS Tel | RCB | ~38[3] | F | 7000[3] | 9.94 | 0.82 | 9.2 | 0.6 | 5.9 | 0.2 | 348 | –14 | 6.3 |
| RT Nor | RCB | ~46[3] | F | 7000[3] | 10.14 | 1.06 | 8.7 | 0.6 | 4.9 | 0.2 | 327 | –7 | 5.0 |
| | | ~20[3] | H1 | | | | | | | | | | |
| SU Tau | RCB | ~40[3] | F | 7000[3] | 9.70 | 1.11 | 8.1 | 0.6 | 6.9 | 0.2 | 189 | –4 | 3.8 |
| Y Mus | RCB | ~227[3] | | 7000[3] | 10.31 | 0.93 | 9.3 | 0.6 | 5.5 | 0.2 | 304 | –3 | 6.6 |
| | | ~109[3] | | | | | | | | | | | |
| GU Sgr | RCB | 37.8[9] | F | 7000[3,10] | 10.11 | 1.17 | 8.3 | 0.6 | 4.7 | 0.2 | 8 | –5 | 4.2 |
| XX Cam | HdC | ~40[11] | F | 7000[6] | 7.30 | 0.87 | 6.5 | 0.6 | 1.3 | 0.2 | 150 | 1 | 1.8 |
| HD 173409 | HdC | – | | 7000[3] | 9.49 | 0.82 | 8.8 | 0.6 | 4.5 | 0.2 | 4 | –13 | 5.2 |
| UW Cen | RCB | 42.8[12] | F | 6800[13] | 9.11 | 0.67 | 8.9 | 0.6 | 7.5 | 0.2 | 302 | 8 | 5.5 |
| HD 148839 | HdC | ~162[3] | | 6500[3] | 8.35 | 0.89 | 7.8 | 0.7 | – | 0.4 | 322 | –13 | 3.0 |
| HD 175893 | HdC | – | | 6000[3] | 9.35 | 1.14 | 8.3 | 0.8 | 3.8 | 0.5 | 7 | –14 | 3.6 |
| HD 182040 | HdC | ~68[3] | F | 6000[3] | 6.99 | 1.03 | 6.3 | 0.8 | 2.1 | 0.5 | 27 | –12 | 1.4 |
| U Aqr | RCB | 81.3[3] | F | 5500[3] | 11.19 | 0.95 | 11.0 | 0.9 | 7.5 | 0.6 | 39 | –50 | 13.2 |
| | | 40.2[3] | | | | | | | | | | | |
| HD 137613 | HdC | ~105[3] | F | 5500[3] | 7.48 | 1.18 | 6.9 | 1.0 | 2.3 | 0.6 | 342 | 26 | 1.8 |
| WX CrA | RCB | ~100[10] | F | 5000[3] | 10.43 | 1.26 | 10.2 | 1.2 | 7.3 | 0.8 | 355 | –8 | 7.6 |
| S Aps | RCB | 80.0[3] | | 5000[3] | 9.72 | 1.21 | 9.7 | 1.2 | 7.2 | 0.8 | 313 | –12 | 6.0 |
| | | 43.1[3] | H2 | | | | | | | | | | |

(1) Jeffery, Hill & Morrison (1986)
(2) Section 4.3.1
(3) this Chapter
(4) Section 4.3.6
(5) Fernie (1989)
(6) Cottrell & Lambert (1982a)
(7) Section 5.1
(8) Schönberner (1975)
(9) Lawson, Kilmartin & Gilmore (1988b)
(10) Marang *et al.* (1989)
(11) Totochava (1973)
(12) Kilkenny & Flanagan (1983)
(13) Giridhar & Rao (1986)

In an attempt to explain some of the discrepancies in the observed periods for these stars, in particular (a) and (c), we consider the possibility that many of these stars are non–radial pulsators, possibly in conjunction with radial modes. There is support for non–radial pulsations. Firstly, several non–radially pulsating eHe stars are known (e.g., BD–9° 4395, Jeffery *et al.* 1985; HD 160641, Lynas–Gray *et al.* 1986). Secondly, the radial velocity variations of RY Sgr appear to be related to the 37.74 d period (see Chapter 2.5.2) and not locked to the $\sim$ 52 d period in the photometry. The $\sim$ 52 d period may be a non–radial mode. Finally, the non–detection of radial velocity variations in NSV 6708 (see Section 4.3.7) may indicate a non–radial pulsation mode as a source of the photometric variations. Wheeler (personal communication to the author) suggested that the radial velocity amplitude due to such long period non–radial pulsations would be very low, which would be consistent with the non–detection in NSV 6708.

Employing the arguments of Jeffery *et al.* (1985), non–radial $g$–modes (Cox 1980) are the modes that give periods many times longer than the radial F–modes. (In fact there appears to be no upper limit.) In addition, the non–radial $f$–mode can give a period that is about 10 per cent longer than the F–mode (see table 17.2 of Cox 1980). Consequently,

non–radial $g$–mode (and possibly $f$–mode) pulsations may explain these longer periods. (Conversely, the 80.0 d period for S Aps, which is shorter than the F–mode period, could be explained by a non–radial $p$–mode.) The major difficulty in invoking non-radial pulsations is that these periods are usually detectable in the colour curves of these stars. This would appear to be inconsistent with the type of variability usually associated with non–radially pulsating stars i.e., large $V$ amplitude, low (and usually undetectable) colour amplitude.

### 2.5.2 The distribution and number of cool hydrogen deficient carbon stars in the Galaxy

The spectroscopic observations indicate that most RCB and HdC stars have temperatures near $T_{eff}$ = 7000 K. An important question is whether the sample for these stars is complete, and therefore whether the observed temperature distribution is the correct one? We will attempt to answer this question from both theoretical and observational viewpoints.

Evolutionary models predict shorter periods at higher temperatures (Schönberner 1977; Weiss 1987a). Weiss (1987a) has also calculated the theoretical period changes for some models (see his table 7), in particular his 'Case 1'. This model predicts a period change of $-1.4 \times 10^{-3}$ d cycle$^{-1}$ for a 7218 K, $P$ = 34 d model star. This value is in general agreement with the observed period decrease rate for RY Sgr (see Chapter 5.1). Despite there being only three temperatures with theoretical period decrease rates for 'Case 1', the rate changes slowly enough to enable some prediction of the crossing time for these stars, and therefore a prediction of the relative number of stars at each temperature. By calculating the mean period rate of change across 1000 K intervals centered on 5000 K, 6000 K, and 7000 K, we calculate mean crossing times of about $5 \times 10^4$ yrs, $8 \times 10^3$ yrs and $1.5 \times 10^3$ yrs respectively at these temperatures, giving a total crossing time between $T_{eff}$ = 4500–7500 K of about $6 \times 10^4$ yrs. (These crossing times also indicate that it is the F–type RCB stars that should be targetted photoelectrically to determine their period rate of change.) These crossing times also give the respective ratio of about 30:5:1 for the number of stars within each temperature interval. Unless current theoretical models give unrealistic period decrease rates[2], the predicted ratio is far from the observed ratio of about 1:1:4.

The observation that most RCB and HdC stars have $T_{eff} \approx 7000$ K contrasts with the $(B–V)$ photometric colours for these stars which indicate a range for the RCB stars (with the exception of the few hotter members) of typically 0.5–1.2. For the HdC stars the range is 0.9–1.2. These colours give the impression that these are mainly cool groups of stars, and that the HdC stars are generally a cooler group than are the RCB stars. The discrepancy arises due to the high luminosity of these stars. Observations of the RCB

[2]We must note that one of the other models of Weiss (1987a) ($M$ = 0.850 $M_\odot$, 'R1' composition, $T_{eff}$ = 4412 K, see his table 7) gives a period decrease rate about 4 times faster than that of 'Case 1' at this temperature. However, in order for this model to be valid, there would have to be a deceleration of the period decrease rate to satisfy the observed period decrease rate of RY Sgr and this has not been anticipated by models to date. Schönberner (1986) noted that enhanced mass loss in cool RCB stars might considerably decrease the crossing time, which would in turn give a lower number of cool RCB stars. A speculative point is that these stars may not all commence the RCB star decline phase at cooler temperatures ($T_{eff}$ < 5000 K) and so will be seen as HdC stars.

stars in the LMC indicate $M_{bol} \sim -5$ (Section 5.1.4.2). If the galactic RCB and HdC stars have similar luminosities to the LMC RCB stars then they must be quite distant (1–10 kpc). Many have low galactic latitudes ($|b| < 10°$) and are thus heavily reddened. [Note the redder colour index of XX Cam ($B$–$V = 0.87$; b = +1°) due to reddening, despite the star having a similar temperature to R CrB ($B$–$V = 0.59$; b = +51°) and RY Sgr ($B$–$V = 0.62$; b = −19°).] Several examples of our spectra are shown in Fig. 2.30, where we show spectra for four stars in the interval λλ6620–6700 Å. RY Sgr is essentially unreddened. Y Mus (b = −3°) appears spectroscopically similar to RY Sgr, but has a mean ($B$–$V$) index of 0.93 (see Section 2.4.1.4) and thus a colour excess $E(B-V) \sim 0.3$ mag. HD 175893 ($B$–$V = 1.15$, see Marang *et al.* 1989; b = −14°) is an HdC star that appears cooler than RY Sgr and RT Nor, probably indicating $T_{eff} \sim 6000$ K. Spectra of the RCB star S Aps ($B$–$V = 1.21$, see Section 2.4.1.1; b = −12°) indicate that this star is probably the coolest of the stars surveyed (including the HdC stars).

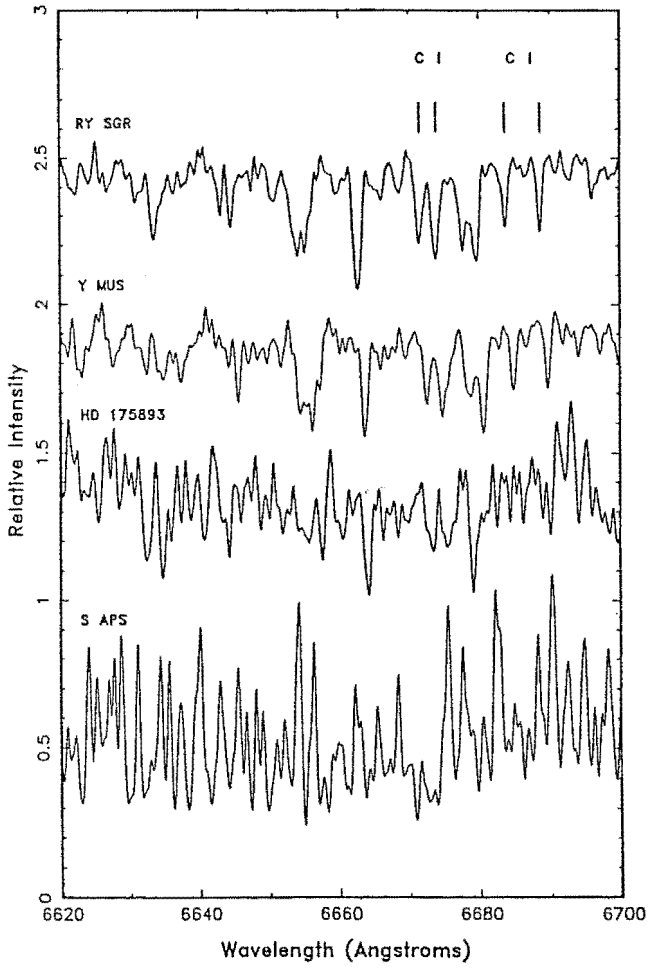


**Figure 2.30.** Comparison spectra of four hydrogen deficient carbon stars in the interval λλ6620–6700Å. Key spectral features are indicated. Note the similarity of the spectra of RY Sgr and Y Mus. RY Sgr, Y Mus and S Aps are RCB stars and HD 175893 is an HdC star (see Section 2.5.2).

Most of the RCB stars were discovered prior to the 1930s on Harvard Observatory survey plates and as a consequence of the declines of these objects (see Kholopov *et al.* 1985 for many of the original references for these stars). The limiting magnitude for this survey to detect a decline, and to identify an RCB star, was about $B = 11.8$. Some RCB stars will have redder $(B-V)$ indices (thus increasing the chance of non–detection) due to their intrinsic colour, reddening, or a combination of these two effects. Cool RCB stars such as S Aps and WX CrA have $B$ magnitudes of $\sim$ 10.9 and 11.7 respectively and were detected only because there is little reddening in the direction of these two stars (colour excesses of $E(B-V) < 0.1$ and $\approx 0.2$ respectively). Consequently, cool RCB stars at low galactic latitudes, and with colour excesses in the range 0.2–0.6, as we have observed in the F–type RCB and HdC stars, were unlikely to have been detected by the Harvard plate survey. This effect may explain the apparent lack of cooler RCB stars in the Galaxy. (HdC stars have only been detected spectroscopically due to the low degree of variability of these stars, see Section 2.4.3.)

The reddening in the directions of these stars can be estimated by comparison with spectra of high galactic latitude (and presumably unreddened) stars and, if the galactic latitude exceeded $|b| = 10°$, by an inspection of the reddening maps of Burnstein & Heiles (1982). The mean $V$ and $(B-V)$, and estimated intrinsic $V_o$ and $(B-V)_o$ for these stars are listed in Table 2.21. The $V_o$ magnitude can be used to derive the distance to these stars if we assume that $M_{bol} \approx -5$ (as for the LMC RCB stars)[3] and an appropriate bolometric correction (Allen 1976). These distances are listed in Table 2.21 and the positions for these stars in the Galaxy (assuming a distance of 8 kpc to the centre of the Galaxy) are shown in Fig. 2.31. Considerable uncertainties are involved in the calculation of these distances but two points are worthy of note. There is a limited volume of the Galaxy within which these stars have been identified and there is an asymetry in the distribution, with an apparent scarcity of stars between $\ell = 20$–$70°$ at distances of 2–6 kpc. [The star at $\ell = 39°$, distance = 10 kpc is the Sr– and Y–rich RCB star U Aqr (Bond, Luck & Newman 1979) which has a galactic latitude of +51°.] Two of the major omissions from this figure, the northern RCB stars SV Sge and V482 Cyg (Gustad *et al.* 1988), are in this region. However, this region may be a potential search area for new RCB stars.

While the limiting magnitude of the Harvard survey would preclude the detection of heavily reddened stars, the infrared flux from the circumstellar shells surrounding all RCB stars may make them *IRAS* sources (Walker 1986). Hence, the *IRAS Point Source Catalog* may provide a source for additional RCB stars. RCB stars have intrinsic $V$–[12] colours of typically 6 to 8. Reddening will increase this index, and alter the position of the star in the $V$–[12]/$(B-V)$ plane. In Fig. 2.32 we show mean observed and estimated unreddened colours for the RCB and HdC stars in this colour–colour plane. The direction of redddening is indicated. This figure identifies the region where reddened RCB stars will be located in this plane. HdC stars will be difficult to detect via this method due to the weakness, or absence, of a circumstellar shell surrounding these objects. We note that two HdC stars (HD 173409 and HD 175893) have intrinsic $V$–[12] colours that are near the lower limit of the range of colours for the RCB stars.

The volume presently surveyed for RCB and HdC stars represents only a small fraction

[3]Gustad *et al.* (1988) derived $M_V = -2.8$ for V482 Cyg based upon the assumption that the RCB star and a nearby star (star B) were part of a physical system, possibly a cluster. This would imply $M_{bol} = -3$ to –4.

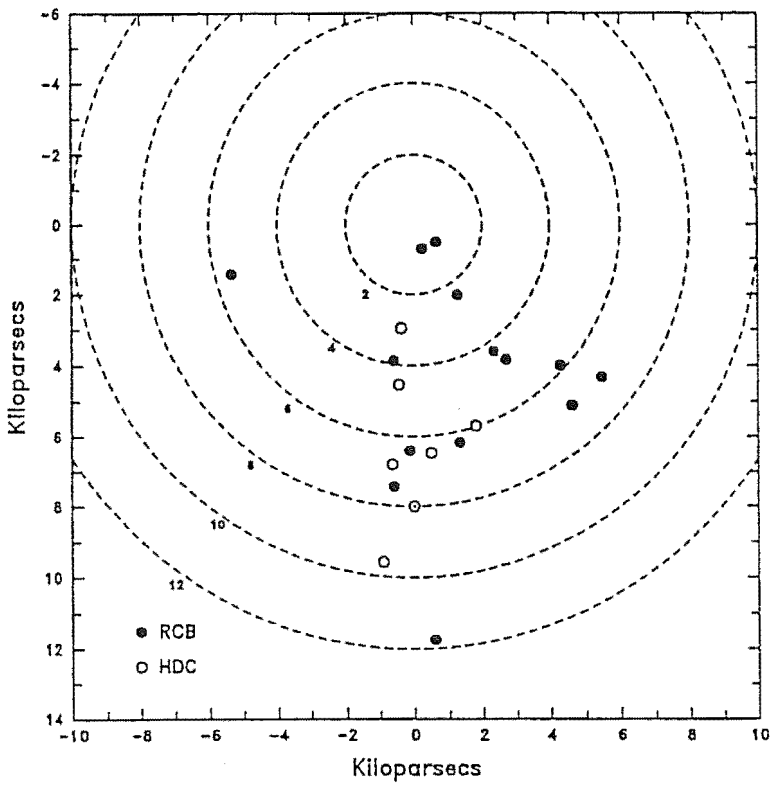


**Figure 2.31.** Galactic map of the positions for the RCB (•) and HdC (o) stars listed in Table 21 assuming a distance to the centre of the Galaxy of 8 kpc. The position of the Sun is indicated (⊙). Radii of 2, 4, 6, 8, 10 and 12 kpc from the galactic centre are drawn as dashed lines. Note that the distances of Table 21 are radial, and that to produce this figure we have compressed the $z$–components of these radial distances onto the galactic plane.

of the total volume of the Galaxy, and a lack of cooler stars would indicate that there are a significant number of undetected cooler stars in the Galaxy. Schönberner (1986) discussed the various evolutionary schemes proposed for hydrogen deficient carbon stars. He found that all current schemes linking the hydrogen deficient carbon stars back to the AGB failed to explain the observed abundances, masses and evolutionary lifetimes. The scheme of Webbink (1984) and Iben & Tutukov (1985), which is based upon the coalescence of a He–CO white dwarf binary system, appeared to meet many of these objections and can also explain the rarity of binary systems in the RCB, HdC and eHe stars (Jeffery, Drilling & Heber 1987). The only known binary is the LMC RCB/symbiotic star HV 12671 (Section 2.4.2). Webbink (1984) estimated the birthrate for such systems to be 0.015 $yr^{-1}$ for the Galaxy. Given a lifetime for an RCB star or HdC star of $\sim$ 6 x $10^4$ yrs (Section 2.5.1) this would lead to a galactic population of $\sim 10^3$ stars. Extrapolating the number of currently known RCB and HdC stars over the entire volume of the Galaxy gives $\sim$ 200–300 objects. An increase in the number of cool hydrogen deficient stars (even to a ratio of stars at 5000 K, 6000 K and 7000 K of 1:1:1) would, to within a factor of 2, give the required number of stars. A further effect increasing the population could be the

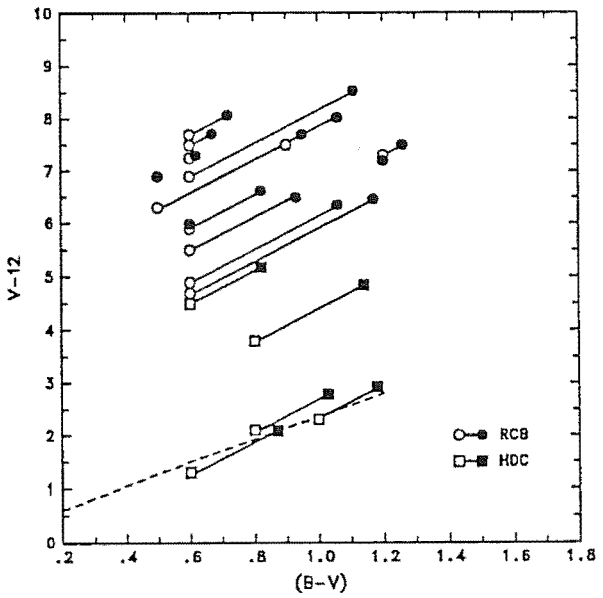


**Figure 2.32.** The positions of the RCB and HdC stars in the $V$–[12]/($B$–$V$) plane. The measured, and estimated intrinsic, colours for the RCB stars are shown as • and o respectively. The corresponding symbols for the HdC stars are ■ and □ respectively. The solid lines connecting the measured and intrinsic colours, indicating the reddening law, has a slope of 3.14 (Schultz & Weimer 1975). The dashed line is the relationship for stars with no infrared excess (Waters, Cote & Aumann 1987).

assumption of a bulge population distribution (Drilling 1986) of these stars. Support for the evolutionary scheme of Webbink (1984), and also the models of Weiss (1987a), rests heavily upon the identification of additional cool hydrogen deficient carbon stars and the determination of the crossing times from the variation in the period of these stars.

## 2.6 CONCLUSIONS

We have been monitoring the photometric variations of 16 cool hydrogen deficient carbon stars, including 8 stars for timescales longer than 2 yrs. The analysis of this photometry has shown the benefit of such a long–term programme. Some stars were observed to change period from year to year (V CrA), have differing degrees of variability (U Aqr) or have multi–periodic light curves (S Aps, HV 12842). Short duration light curves could give incomplete or misleading results. A period–temperature relationship for these stars indicates that most have dominant periods consistent with fundamental (F–mode) radial pulsations. Several stars have periods that are longer than the predicted F–mode periods, possibly indicating the presence of non–radial $f$– or $g$–mode pulsations. S Aps has a 43.1 d period consistent with second harmonic radial pulsations.

There is a need to continue monitoring many of the stars reported here to more accurately determine periods and modes of pulsation, and also to commence observations

of RCB and HdC stars currently not on this programme. Northern hemisphere RCB and HdC stars should be observed in a parallel programme.

Theoretical period rates of change for hydrogen deficent carbon stars in the temperature range $T_{eff}$ = 4500–7500 K indicate that cooler ($T_{eff} \approx$ 5000 K) stars should dominate the temperature distribution. This is not observed. Consequently, current models may give inappropriate period rates of change or effects such as extreme mass loss may reduce the crossing times for cooler stars, and therefore decrease the total number of such objects. Alternatively, the cooler stars may have been preferentially excluded from detection by reddening effects or their faint blue ($B$<12) magnitude precluding their detection in the major discovery survey.

The galactic distribution of known RCB and HdC stars suggest that only a small volume of the Galaxy has been sampled for these stars. Extrapolating the number of known RCB and HdC stars over the entire volume of the Galaxy gives a population of 200–300 objects. Making allowances for the lack of cooler stars, and possibly a bulge population distribution, could give a population comparable to the number predicted ($\sim 10^3$) by the evolutionary scheme of Webbink (1984) where hydrogen deficient carbon stars are produced from white dwarf binary progenitors.

# Chapter 3

# Declines of R Coronae Borealis stars

## 3.1 The 1988 decline of R Coronae Borealis

### 3.1.1 INTRODUCTION

The R Coronae Borealis (RCB) stars have such bizarre properties that they have attracted a large amount of attention ever since they were first identified as a distinct class of objects. At first glance they appear spectroscopically similar to late F– to M–type supergiants. Typically they have $M_{\rm bol}$ of about –5, derived from observations of RCB stars in the LMC. However, they exhibit strong hydrogen deficiency, with a hydrogen abundance of up to $10^{-5}$ the solar abundance. In addition, they have helium and carbon overabundances and some also have lithium enhancement, all relative to the solar abundance distribution (Cottrell & Lambert 1982a). Spectroscopically, they appear to be closely related to the hydrogen deficient carbon (HdC) stars (Lambert 1986). The RCB and HdC stars are generally presumed to be evolving towards the hot helium stars (Schönberner 1977; Weiss 1987a). The main feature distinguishing the RCB stars from the HdC stars are the sudden and irregular declines in brightness of typically 5 mag in around a month (although 7 mag declines are not unknown), and a return to maximum light taking of the order of several months to a year. Some of the members of this class go through one of these major declines every few years, e.g. the prototype R CrB, while others can remain at maximum light for 5–10 yr (see Lawson, Cottrell & Bateson 1988, 1989). The times between declines of R CrB, UW Cen and SU Tau have been shown statistically to occur at random intervals (Sterne 1935; Howarth 1976, 1977). However, Pugach (1977) has suggested that the declines occur at the same pulsation phase, i.e. maximum light, in RY Sgr and therefore that the interval between declines is a random integer number of pulsation periods.

In addition to these major declines, all RCB stars are known to have variations of the order of 0.1–0.7 mag with a semi–regular period of 40–100 d (see Section 2.4). These variations, which show a great diversity in behaviour, are usually thought to be associated with radial pulsations of the star. We note, however, that some RCB stars may have very low, and possibly no, radial velocity variations, e.g. NSV 6708 (see Section 4.3.7). [Most HdC stars also appear to be photometrically variable but with a much smaller amplitude (Kilkenny, Marang & Menzies 1988; Section 2.4.2).]

The most successful model which explains the observed decline behaviour considers a gas cloud, which cools and condenses into carbon grains, as the obscuring element in these stars (see e.g., Feast 1986; Holm *et al.* 1987). The normal form of the model considers that the dust cloud is seen initially as a near line–of–sight optically thick occulting disk that grows and eventually obscures the visible disk of the star. These dust clouds are

proposed to occur in random directions about once every 40 d, possibly commensurate with the optical pulsation period, and cover approximately 1/30th of the stellar surface (Feast 1986). As the cloud expands, the photospheric spectrum is obscured and emission from the chromosphere becomes visible, which is also then progressively obscured. In Sections 3.1.4 and 3.1.5 we will discuss this simple model which can explain the observed characteristics of some declines. Other declines require a modification to this model.

Because of the unpredictability of the decline onset it is impossible to schedule telescope time to cover these sorts of events, so photometric coverage will only be obtained by a concerted effort to capture the decline phase, or by a good deal of luck. A detailed spectroscopic study of the early stages has not previously been achieved. In particular, only declines of the three brightest RCB stars, R CrB (Payne–Gaposchkin 1963; Herbig 1949; Holm *et al.* 1987), RY Sgr (Alexander *et al.* 1972) and NSV 6708 (Kilkenny & Marang 1989; Chapter 4) have been studied spectroscopically in any detail. With the exception of the 1988 decline of NSV 6708, for which only limited spectroscopy was obtained near the decline onset, the observations only started about 20 d *after* the decline onset.

In this Chapter, we discuss the 1988 decline of R CrB and include, for the first time, extensive photometry (Section 3.1.4.2) and spectroscopy (Section 3.1.4.3) during the 20 d either side of the decline onset. The spectroscopic data has been extended to over 250 d after the decline onset, when R CrB had recovered to $V = 6.2$ (compared to $V = 5.8$ at maximum). We have reduced these data to velocities (Section 3.1.3.1) for most of the readily identifiable features.

Comparison will be made to previous declines of this object that have been covered in some detail with photoelectric photometry and spectroscopy. These declines will also be compared with those of other RCB stars (Section 3.1.5.1). Finally, we discuss (Section 3.1.6) certain key areas where considerable progress could be made in our understanding of the major declines, and indeed all aspects, of RCB star behaviour.

## 3.1.2 OBSERVATIONS

### 3.1.2.1 Photometry

Photometric (*UBVRI*) observations were made of R CrB ($\delta \approx +28°$), and its comparison star SAO 84005, as it skimmed the northern horizon at MJUO, which is at a latitude of $\approx -44°$. The observations covered the period 1988 June to 1989 July, with the decline event occurring during 1988 July (Lawson, Kilmartin & Gilmore; *IAU* Circ. 4633). The observations were obtained with the two 0.6–m reflectors at MJUO, using automated single channel photometers, filters according to the Bessell (1976) recipe and either EMI 9558B or RCA C31034A photomultiplier tubes. The transformed $V$, ($U$–$B$), ($B$–$V$), ($V$–$R$) and ($V$–$I$) photometry, obtained relative to SAO 84005, are listed in Table 3.1, and are plotted against Julian Date in Figs. 3.1a and 3.1b. The photometric accuracy is 1–2 per cent when the star is near maximum light ($V \approx 6$), increasing to 2–3 per cent when the star is faint ($V \approx 11$). In addition, we plot the visual estimates of Pereira (*IAU* Circ. 4633, 4636, 4645, 4650, 4666, 4689, 4753) in Fig. 3.1a as near the decline minimum these form a more extensive series of observations than do our photometry.

**Table 3.1.** MJUO *UBVRI* photometry of R CrB.

| JD-2440000 | *V* | (*U-B*) | (*B-V*) | (*V-R*) | (*V-I*) | JD-2440000 | *V* | (*U-B*) | (*B-V*) | (*V-R*) | (*V-I*) |
|---|---|---|---|---|---|---|---|---|---|---|---|
| 7326.946 | 5.825 | 0.145 | 0.585 | 0.383 | 0.597 | 7379.848 | 9.894 | | 0.386 | 0.306 | 0.818 |
| 7336.937 | 5.923 | | 0.606 | | 0.596 | 7388.836 | 10.317 | -0.183 | 0.649 | 0.498 | 1.010 |
| 7343.888 | 5.937 | 0.126 | 0.583 | 0.382 | 0.620 | 7394.815 | 10.763 | -0.160 | 0.837 | 0.576 | 1.087 |
| 7354.872 | 6.016 | 0.039 | 0.515 | 0.370 | 0.581 | 7400.820 | 10.163 | | 0.927 | 0.556 | 1.093 |
| 7362.853 | 6.428 | 0.016 | 0.517 | 0.344 | 0.583 | 7404.828 | 10.739 | -0.124 | 0.931 | 0.596 | 1.176 |
| 7366.892 | 6.821 | 0.005 | 0.534 | 0.365 | 0.617 | 7405.825 | 10.837 | | 0.880 | 0.637 | 1.174 |
| 7367.817 | 6.956 | 0.014 | 0.554 | 0.359 | 0.608 | 7406.823 | 10.802 | | 0.832 | 0.585 | 1.207 |
| 7370.816 | 7.446 | -0.049 | 0.551 | 0.351 | 0.635 | 7407.821 | 10.756 | | 0.840 | 0.523 | |
| 7372.823 | 7.902 | -0.104 | 0.537 | 0.396 | 0.690 | 7409.823 | 10.847 | | 0.838 | 0.549 | 1.164 |
| 7375.835 | 8.651 | -0.205 | 0.497 | 0.314 | 0.668 | 7412.819 | 10.919 | | 0.920 | 0.556 | 1.175 |
| 7611.178 | 6.337 | | 0.703 | 0.397 | 0.705 | 7677.006 | 5.994 | 0.112 | 0.624 | 0.373 | 0.576 |
| 7616.147 | 6.220 | 0.183 | 0.656 | 0.415 | 0.694 | 7682.973 | 6.020 | | 0.605 | 0.378 | 0.589 |
| 7620.145 | 6.079 | 0.172 | 0.692 | 0.307 | 0.596 | 7693.997 | 6.103 | 0.203 | 0.690 | 0.417 | 0.662 |
| 7621.170 | 6.104 | 0.145 | 0.623 | 0.401 | 0.611 | 7699.959 | 6.152 | | 0.644 | 0.406 | 0.692 |
| 7623.157 | 6.048 | 0.169 | 0.653 | 0.368 | 0.589 | 7704.992 | 6.214 | | 0.680 | 0.403 | 0.680 |
| 7644.079 | 6.051 | 0.164 | 0.628 | 0.391 | 0.650 | 7724.879 | 5.957 | 0.095 | 0.584 | 0.352 | 0.560 |
| 7655.062 | 6.134 | 0.212 | 0.636 | 0.444 | 0.671 | 7728.929 | 5.967 | 0.102 | 0.587 | 0.346 | 0.578 |
| 7664.036 | 6.049 | 0.204 | 0.639 | 0.368 | 0.603 | 7730.873 | 6.002 | 0.116 | 0.603 | 0.367 | 0.559 |

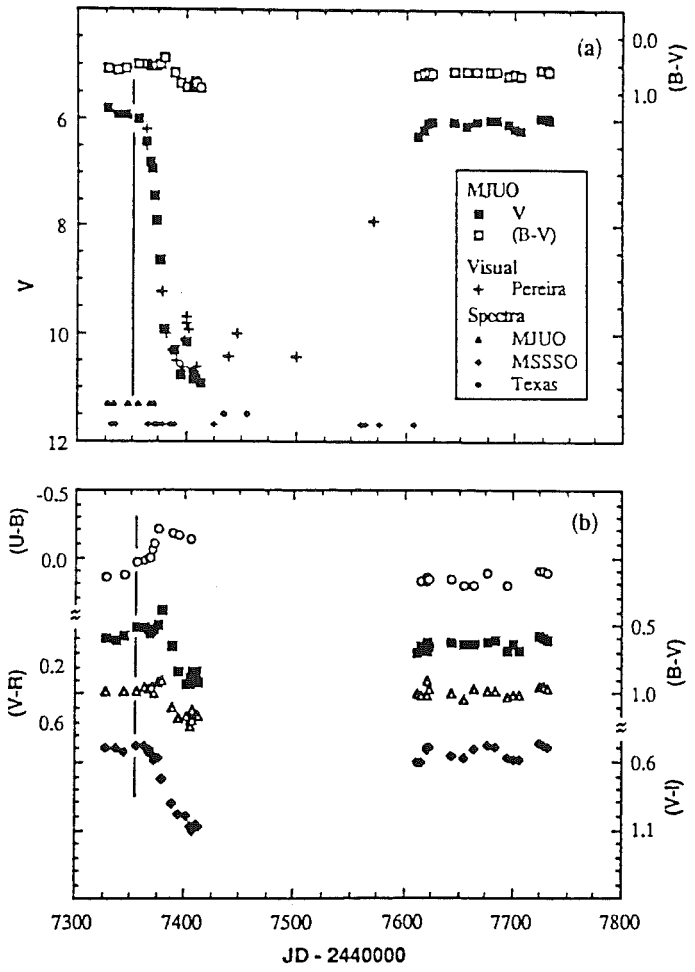


**Figure 3.1.** Magnitude (a) and (b) colour photometry of the 1988 decline of R CrB. The vertical line indicates JD 2447355, which we have defined as day number 0 (the day when the *V* mag first drops below the average pulsation minimum, see Section 3.1.4.1). The dates of the spectra are shown along the bottom of (a). Note the strong 'blueing' of the colours of the star around JD 2447380.

### 3.1.2.2 Spectroscopy

The spectroscopic data came from three sources: (i) the 1.0–m telescope at MJUO using a 1872 element Reticon–based Linear Diode Array (LDA) detector system (MacQueen 1986) giving a resolution, $\Delta\lambda \approx 0.15$Å, (ii) the 1.9–m telescope at Mount Stromlo and Siding Spring Observatories (MSSSO) using both the coudé ($\Delta\lambda \approx 0.3$–$0.7$Å) and Cassegrain ($\Delta\lambda \approx 0.5$ and 10Å) foci and the Photon Counting Array (PCA, see Stapinski, Rodgers & Ellis 1981), and (iii) the University of Texas at Austin, where D.L. Lambert kindly provided us with two spectra in advance of publication. The spectra are summarised in Table 3.2, indicating the dates and wavelength regions covered. The $V$ mags are also listed. The comments indicate the prominent features of each spectrum. The times and places at which spectra were obtained are also shown in Fig. 3.1a. The vertical line in this figure and in Fig. 3.1b indicates the point on the $V$ light curve where the decline can be considered to have begun (see Section 3.1.4.1).

**Table 3.2.** Summary of spectroscopic observations of the 1988 decline.

| Date | JD-2440000 | Day[1] | $V$ | $\lambda\lambda$ (Å) | Source | Equipment | S/N[2] | Comments |
|---|---|---|---|---|---|---|---|---|
| Mar 21 | 7242.179 | -113 | 5.8 | 6540-6600 | MJUO | LDA | 20 | normal photospheric spectrum |
| Jun 19 | 7332.073 | -23 | 5.8 | 6500-6720 | MSO | 16" coude | 16 | normal photospheric spectrum |
| Jun 21 | 7333.973 | -21 | 5.9 | 6550-6610 | MJUO | LDA | 60 | normal photospheric spectrum |
| Jun 21 | 7334.008 | -21 | | 5855-5910 | MJUO | LDA | 40 | normal Na D absorption, 70% central depth (c.d.) |
| Jun 23 | 7336.025 | -19 | 5.9 | 6500-6720 | MSO | 16" coude | 20 | normal photospheric spectrum |
| Jul 4 | 7346.953 | -8 | 6.0 | 6550-6610 | MJUO | LDA | 15 | normal photospheric spectrum |
| Jul 12 | 7354.884 | 0 | 6.0 | 6550-6610 | MJUO | LDA | 30 | *day number 0*, normal photospheric spectrum |
| Jul 22 | 7364.970 | 10 | 6.6 | 6340-6450 | MSO | 32" coude | 14 | filling in of photospheric C I lines |
| Jul 22 | 7364.985 | 10 | | 5830-5940 | MSO | 32" coude | 13 | filling in of photospheric Na D lines |
| Jul 24 | 7366.841 | 12 | 6.8 | 6550-6610 | MJUO | LDA | 10 | filling in of lines by >10% |
| Jul 27 | 7369.954 | 15 | 7.3 | 6610-6720 | MSO | 32" coude | 17 | further filling in of lines |
| Jul 27 | 7369.965 | 15 | | 5830-5940 | MSO | 32" coude | 17 | Na D lines reduced to a c.d. of 30% |
| Jul 28 | 7370.898 | 16 | 7.4 | 6510-6620 | MSO | 32" coude | 17 | Sc II, Ti II and Fe II in emission |
| Jul 28 | 7370.915 | 16 | | 6340-6450 | MSO | 32" coude | 20 | Fe II in emission |
| Jul 29 | 7371.933 | 17 | 7.7 | 6510-6620 | MSO | 32" coude | 21 | increasing Sc II, Ti II and Fe II emission |
| Jul 30 | 7372.926 | 18 | 7.9 | 6510-6620 | MSO | 32" coude | 19 | strong Sc II, Ti II and Fe II emission |
| Jul 30 | 7372.943 | 18 | | 5830-5940 | MSO | 32" coude | 19 | Na D, stellar and cloud ($-110$ km s$^{-1}$) emission |
| Jul 31 | 7373.880 | 19 | 8.1 | 6340-6450 | MSO | 32" coude | 13 | Fe I emission, PLC birthday, Fe II emission |
| Jul 31 | 7373.894 | 19 | | 6510-6620 | MSO | 32" coude | 12 | Fe II, Ti II emission decaying, Sc II emission still rising |
| Jul 31 | 7373.911 | 19 | | 5830-5940 | MSO | 32" coude | 15 | Na D, stellar and cloud, Ba II, Fe II emission |
| Jul 31 | 7373.930 | 19 | | 6610-6720 | MSO | 32" coude | 15 | Fe I in emission, very little photospheric absorption |
| Aug 1 | 7374.926 | 20 | 8.4 | 5660-5860 | MSO | Cass high | 19 | Sc II, Ba II emission |

**Table 3.2** – *continued*

| Date | JD-2440000 | Day[1] | $V$ | λλ (Å) | Source | Equipment | S/N[2] | Comments |
|---|---|---|---|---|---|---|---|---|
| Aug 1 | 7374.946 | 20 | | 6270-6450 | MSO | Cass high | 21 | several Sc II emission, Fe I, Fe II emission |
| Aug 1 | 7374.972 | 20 | | 6470-6665 | MSO | Cass high | 17 | Fe I, Fe II, Ti II, Sc II, Ba II emission |
| Aug 3 | 7376.867 | 22 | 8.7 | 6470-6665 | MSO | Cass high | 12 | Ti II, Fe I, Fe II, Sc II, Ba II emission, still C I and Hα absorption |
| Aug 3 | 7376.888 | 22 | | 5800-6000 | MSO | Cass high | 15 | strong, broad Na D emission, Ba II emission |
| Aug 3 | 7376.906 | 22 | | 3870-4000 | MSO | Cass high | 4 | Ca II H and K in absorption |
| Aug 4 | 7377.870 | 23 | 9.3 | 3500-5500 | MSO | Cass low | 11 | Flux calibrated spectra. |
| Aug 4 | 7377.888 | 23 | | 5500-7500 | MSO | Cass low | 8 | Broad (λλ3900 – 5700 Å) emission |
| Aug 4 | 7377.896 | 23 | | 7500-9000 | MSO | Cass low | 7 | |
| Aug 12 | 7385.855 | 31 | 10.2 | 6470-6660 | MSO | Cass high | 11 | only Sc II and Ba II in emission, *cf* Aug 3 |
| Aug 12 | 7385.873 | 31 | | 5800-6000 | MSO | Cass high | 10 | very strong and broad Na D emission, Ba II disappeared |
| Aug 12 | 7385.886 | 31 | | 3870-4000 | MSO | Cass high | 3 | Ca II H and K now in emission |
| Aug 14 | 7387.857 | 33 | 10.3 | 3500-5500 | MSO | Cass low | 17 | Flux calibrated spectra. |
| Aug 14 | 7387.872 | 33 | | 5500-7500 | MSO | Cass low | 10 | Broad emission from Aug 4 disappeared |
| Aug 14 | 7387.877 | 33 | | 6500-9000 | MSO | Cass low | 11 | |
| Sep 21 | 7425.879 | 71 | 11 | 5830-5940 | MSO | 32" coude | 3 | extremely strong and broad Na D emission |
| Sep 30 | 7434.625 | 80 | 10.5 | 5860-5910 | Texas | | > 50 | multiple component (broad *and* narrow) Na D absorption and emission, photospheric absorption spectrum visible |
| Oct 20 | 7454.625 | 100 | 10 | 5860-5910 | Texas | | > 50 | as for Sep 30, but with broad high velocity absorption |
| Feb 2 | 7560.257 | 205 | 8 | 5750-6000 | MSO | 16" coude | 30 | Na D absorption, 40% c.d., strong high velocity absorption |
| Feb 5 | 7563.260 | 208 | 8 | 3850-4000 | MSO | 16" coude | 10 | stellar Ca II H and K in absorption, strong core emission |
| Feb 17 | 7575.220 | 220 | 7.5 | 5830-5940 | MSO | 32" coude | 40 | Na D absorption, 70% c.d., high velocity absorption, 30% c.d. |
| Feb 17 | 7575.264 | 220 | | 3900-3975 | MSO | 32" coude | 25 | normal stellar H and K absorption, weak core emission |
| Feb 18 | 7576.216 | 221 | 7.5 | 5830-5940 | MSO | 32" coude | 30 | As for Feb 17 |
| Feb 18 | 7576.241 | 221 | | 3900-3975 | MSO | 32" coude | 20 | As for Feb 17 |
| Mar 21 | 7607.163 | 252 | 6.5 | 5830-5940 | MSO | 32" coude | 17 | stellar Na D absorption only |
| Mar 21 | 7607.189 | 252 | | 3900-3975 | MSO | 32" coude | 25 | stellar Ca II H and K absorption |

[1] Number of days after day number 0 (JD 2447355)
[2] Signal to Noise ratio in continuum

## 3.1.3 SPECTROSCOPIC ANALYSIS

### 3.1.3.1 Reduction

All spectroscopic data were reduced using the FIGARO reduction package (Keith Shortridge, Anglo–Australian Observatory). The already wavelength–calibrated spectra from the LDA were transferred to the MSSSO VAX 11/785 and converted to the required FIGARO format. The Texas spectra were hand–digitised and the wavelength calibration was carried out in FIGARO using telluric lines from the spectrum of a hot star. This technique is not as precise as for the other spectra and the velocities measured from these spectra have an uncertainty of about 10 $kms^{-1}$.

The MSSSO spectra were wavelength–calibrated with a Th–Ar arc for the coudé spectra and He–Ar or Fe–Ar arcs for the Cassegrain spectra. There are two facts that should be realised with respect to this calibration: (i) Near the ends of each spectrum the error in the dispersion solution increases. This is important when determining velocities from lines in these regions. Typically, the rms error in the solution was $< 0.2$ of a pixel, there being 750 pixels across each spectrum. Near the edges, this error can rise up to 0.4 of a pixel. This corresponds to errors in the velocity measurements (on the 32–inch camera of the 1.9–m coudé system) of between 1.4 $kms^{-1}$ and 2.8 $kms^{-1}$. (ii) The rms error in the Cassegrain spectra is around 0.3 of a pixel (0.6 near the edges) due to the scarcity of arc lines in the Cassegrain arc lamps on the MSSSO 1.9–m. This leads to velocity errors of 4.0–8.0 $kms^{-1}$.

On each of two dates, JD 2447378 and JD 2447388, three low dispersion spectra were taken, centred on the blue (4500Å), green (6000Å) and red (7800Å) regions. While the observations were not carried out under full spectrophotometric conditions it was possible to 'pseudo flux–calibrate' these spectra in FIGARO using a standard star, LDS749. The three spectra in each set were then merged into a single spectrum (see Figs. 3.2a and 3.2b).

### 3.1.3.2 Line identifications and velocities

The spectra were corrected to the heliocentric reference frame in the usual way using techniques outlined in Gordon (1976) and then the line positions were measured using FIGARO routines. The line identifications, wavelengths and multiplets, came from several sources:

(i) *A Multiplet Table of Astrophysical Interest*, C.E. Moore, 1959, NBS Technical Note 36
(ii) *The Solar Spectrum 2935Å to 8770Å*, C.E. Moore, M.G.J. Minnaert & J. Houtgast, 1966, NBS Monograph 61
(iii) *A Table of Semi–empirical gf Values*, R.L. Kurucz & E. Peytremann, 1975, SAO Special Report 362
(iv) *Wavelength and Transition Probabilities for Atoms and Atomic Ions*, J. Reader, C.H. Corliss, W.L. Wiese & G.A. Martin, 1980, NSRDS–NBS 68
(v) *Selected Tables of Atomic Spectra*, C.E. Moore, 1970, NSRDS–NBS 3
(vi) *The Chromospheric Spectrum at the 1962 Eclipse*, R.B. Dunn *et al.*, 1967
(vii) *The Chemical Composition of R CrB and XX Cam*, P.L. Cottrell & D.L. Lambert, 1982a
(viii) *The Line Spectrum of R CrB λλ3700–8600Å*, P.C. Keenan & J.L. Greenstein, 1963

(The full references for sources vi, vii and viii are given in the References.) Comparisons of lines from the same multiplet, as well as their measured intensities, allowed most lines to be uniquely identified.

Table 3.3 lists the identified lines and classifies each line as being in absorption, emission, doubtful, or absent, and in the case of sodium, of complex structure. Table 3.4

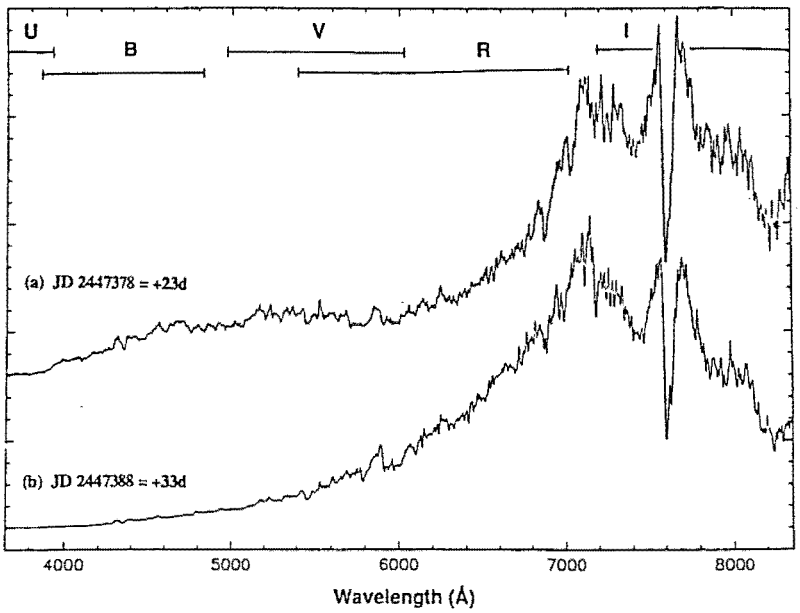


**Figure 3.2.** Calibrated spectra (on an arbitrary scale) of R CrB taken on (a) JD 2447378 (day 23, see Section 3.1.4.1) and (b) JD 2447388 (day 33). Each spectrum is a composite of 3 spectra matched at 5000 and 7000 Å. On JD 2447378 R CrB was $\sim$ 4 times brighter in $V$ than on JD 2447388. The broad emission hump is clearly visible in (a). The wavelength range for each of the filters, $UBVRI$, is shown at the top of the figure.

**Table 3.3.** Summary of line evolution as a function of day number.

| Line | λ | -113 | -23 | -21 | -19 | -8 | 0 | +10 | +12 | +15 | +16 | +17 | +18 | +19 | +20 | +22 | +31 | +80 | +100 |
|---|---|---|---|---|---|---|---|---|---|---|---|---|---|---|---|---|---|---|---|
| Ba II 2 | 5853.69 | | | | | | | a | | a | | | a | e | e | e | ? | | |
| Ba II 2 | 6496.91 | | | | | | | | | | | | | | e | e | e | | |
| C I | 6578.77 | a | a | a | a | a | a | | a | | a | a | a | a | - | - | - | | |
| C I 6 | 6568.71 | a | a | a | a | a | a | | a | | a | a | a | a | - | - | - | | |
| C I 21.01 | 6711.28 | | a | | a | | | | | | | | | | | | | | |
| C I 22 | 6587.62 | a | a | a | a | a | a | | a | | a | a | a | a | - | - | - | | |
| C I 22.03 | 5720.78 | | | | | | | | | | | | | | a | | | | |
| C I 29.04 | 6397.98 | | | | | | | a | | | a | | | a | a | | | | |
| C I 29.04 | 6413.55 | | | | | | | a | | | a | | | a | - | | | | |
| C I 29.04 | 6417.54 | | | | | | | a | | | a | | | - | - | | | | |
| C I 29.05 | 6389.87 | | | | | | | a | | | - | | | a | - | | | | |
| C I 29.06 | 6378.79 | | | | | | | a | | | a | | | - | - | | | | |
| C I 29.07 | 6342.32 | | | | | | | a | | | a | | | a | - | | | | |
| C I 29.08 | 5877.31 | | | a | | | | a | | a | | | a | a | | - | - | a | a |
| C I 29.09 | 5870.66 | | | a | | | | a | | a | | | a | - | - | ? | - | a | a |
| C I 29.10 | 5864.95 | | | a | | | | a | | a | | | a | ? | | - | - | a | a |
| C I 29.11 | 5846.35 | | | | | | | - | | - | | | a | a | - | - | - | | |
| C I 29.11 | 5850.25 | | | | | | | a | | a | | | a | a | a | - | - | | |
| C I 33 | 6662.73 | | a | | a | | | | | a | | | | a | | | | | |
| C I 33 | 6671.84 | | a | | - | | | | | a | | | | a | | | | | |
| C I 33 | 6674.11 | | a | | a | | | | | a | | | | a | | | | | |
| C I 33 | 6679.64 | | a | | - | | | | | - | | | | - | | | | | |
| C I 33 | 6683.95 | | a | | a | | | | | a | | | | a | | | | | |
| C I 33 | 6688.79 | | a | | a | | | | | a | | | | a | | | | | |
| C I 35 | 6591.45 | a | ? | a | - | a | a | | a | | a | a | a | a | - | - | - | | |
| C I 35 | 6595.24 | a | - | a | - | a | a | | a | | a | - | a | - | - | a | - | | |
| C I 35 | 6596.85 | a | - | a | a | a | a | | a | | a | a | a | - | - | a | a | | |
| C I 35 | 6602.42 | | a | | a | a | a | | a | | a | a | a | - | - | a | a | | |
| C I 35 | 6611.35 | | a | | a | | | | | a | a | a | a | a | a | a | a | | |
| C I 59 | 6586.27 | a | - | a | - | a | a | | a | | a | a | a | a | - | - | a | | |
| C I 71 | 5912.58 | | | | | | | a | | a | | | a | ? | | - | - | | |
| C I 72 | 5910.34 | | | | | | | a | | a | | | a | ? | | - | - | | |

**Table 3.3.** – *continued*

| Line | λ | -23 | -21 | -19 | +10 | +15 | +16 | +17 | +18 | +19 | +20 | +22 | +31 | +80 | +100 |
|---|---|---|---|---|---|---|---|---|---|---|---|---|---|---|---|
| Ca I | 6717.69 | a | | a | | | | | | | | | | | |
| Ca I 18 | 6439.08 | | | | a | | a | | | | | | | | |
| Ca I 47 | 5857.46 | | a | | a | a | | | a | a | | | | a | a |
| Ca II 1 | 3933.66 | | | | | | | | | | | a | e | | |
| Ca II 1 | 3968.47 | | | | | | | | | | | a | e | | |
| Fe I | 6383.68 | | | | a | | a | | | a | | | | | |
| Fe I 62 | 6430.86 | | | | a | | a | | | e | e | | | | |
| Fe I 111 | 6421.36 | | | | a | | a | | | e | | | | | |
| Fe I 168 | 6393.61 | | | | | | | | | e | e | | | | |
| Fe I 168 | 6494.99 | | | | | | | | | | e | e | | | |
| Fe I 268 | 6678.00 | | | a | | a | | | | e | | | | | |
| Fe I 816 | 6400.01 | | | | a | | a | | | e? | | | | | |
| Fe I 982 | 5934.67 | | | | ? | a | | | ? | ? | | | | | |
| Fe I 1161 | 5708.10 | | | | | | | | | | a | | | | |
| Fe I 1180 | 5862.37 | | a | | a | a | | | ? | | | | | a | a |
| Fe I 1180/1 | 5914.16 | | | | a | a | | | ? | | | | | | |
| Fe I 1180 | 5930.19 | | | | a | a | | | a | | | | | | |
| Fe I 1181 | 5859.60 | | a | | | a | | | a | | | | | a | a |
| Fe I 1253 | 6385.71 | | | | a | | a | | | a | | | | | |
| Fe II | 5930.36 | | | | | | | | | | | e | | | |
| Fe II | 6517.01 | | | | | | a | a | a | a | | | | | |
| Fe II 40 | 6369.45 | | | | a | | a | | | e | e | | | | |
| Fe II 40 | 6432.68 | | | | | | e | | | e | e | | | | |
| Fe II 40 | 6516.08 | | | | | | e | e | e | e | e | e | | | |
| Fe II 46 | 5991.38 | | | | | | | | | | | e | | | |
| Fe II 74 | 6416.93 | | | | | | | | | e | e | | | | |
| Fe II 183 | 5856.45 | | | | | | | | | e | | | | | |

**Table 3.3.** – *continued*

| Line | λ | -113 | -23 | -21 | -19 | - 8 | 0 | +10 | +12 | +15 | +16 | +17 | +18 | +19 | +20 | +22 | +31 | +71 | +80 | +100 |
|---|---|---|---|---|---|---|---|---|---|---|---|---|---|---|---|---|---|---|---|---|
| H I | 6562.82 | a | a | | a | a | a | | | | a | a | a | a | a | a | ? | | | |
| Li I 1 | 6707.79 | | a | | a | | | | | a | | | | - | | | | | | |
| Na I 1 | 5889.97 | | | a | | | | * | | * | | | * | * | | * | * | * | * | * |
| Na I 1 | 5895.94 | | | a | | | | * | | * | | | * | * | | * | * | * | * | * |
| Ni I 231 | 5760.84 | | | | | | | | | | | | | | e | | | | | |
| Sc II 19 | 6604.60 | | a | a | a | a | a | | | | e | e | e | e | e | e | e | | | |
| Sc II 28 | 6279.75 | | | | | | | | | | | | | | e | | | | | |
| Sc II 28 | 6300.68 | | | | | | | | | | | | | | e | | | | | |
| Sc II 28 | 6309.89 | | | | | | | | | | | | | | e | | | | | |
| Sc II 28 | 6320.84 | | | | | | | | | | | | | | e | | | | | |
| Sc II 29 | 5684.19 | | | | | | | | | | | | | | e | | | | | |
| Si I 9 | 5780.39 | | | | | | | | | | | | | | a | | | | | |
| Si I | 6555.47 | a | - | | a | a | a | | | | a | a | - | a | a | - | - | | | |
| Si II 2 | 6347.10 | | | | | | | a | | | a | | | a | a | | | | | |
| Si II 2 | 6371.35 | | | | | | | a | | | a | | | a | a | | | | | |
| Ti I 72 | 5899.30 | | | | | | | a | | a | | | a | a | | - | - | | | |
| Ti II 91 | 6491.58 | | | | | | | | | | | | | | e | e | - | | | |
| Ti II 91 | 6559.57 | a | a | a | a | a | a | | a | | e | e | e | e | e | e | - | | | |
| Ti II 91 | 6606.98 | | - | | - | a | a | | a | - | a | a | a | - | e | e | a | | | |
| Ti II 112 | 6680.26 | | - | | a | | | | | a | | | | a | | | | | | |

Notes:

a : absorption
e : emission
? : doubtful identification
* : complex structure
– : no feature found

**Table 3.4a.** Measured velocities ($kms^{-1}$) of all identified lines as a function of day number.

| Line | λ | -113 | -23 | -21 | -19 | -8 | 0 | +10 | +12 | +15 | +16 | +17 | +18 | +19 | +20 | +22 | +31 | +80 |
|---|---|---|---|---|---|---|---|---|---|---|---|---|---|---|---|---|---|---|
| Ba II 2 | 5853.69 | | | | | | | 37.39 | | 40.46 | | | 16.90 | 23.06 | 23.56 | 15.38 | | |
| Ba II 2 | 6496.91 | | | | | | | | | | | | | | 20.75 | 22.15 | 21.67 | |
| C I | 6578.77 | 20.15 | | 23.25 | | 23.41 | 24.72 | | | | | | | | | | | |
| C I 6 | 6568.71 | 23.75 | 29.66 | 24.51 | 33.78 | 26.14 | 28.75 | | 22.49 | | 29.22 | 29.22 | 27.39 | 20.08 | | | | |
| C I 21.01 | 6711.28 | | 17.89 | | 23.23 | | | | | | | | | | | | | |
| C I 22 | 6587.62 | 23.04 | 16.38 | 24.22 | | 24.44 | 27.01 | | | | 23.20 | 35.49 | 34.13 | 33.22 | | | | |
| C I 22.03 | 5720.78 | | | | | | | | | | | | | | 22.54 | | | |
| C I 29.04 | 6397.98 | | | | | | | 17.34 | | | 30.93 | | | 30.93 | 28.12 | | | |
| C I 29.04 | 6413.55 | | | | | | | 27.59 | | | 32.73 | | | 37.41 | | | | |
| C I 29.04 | 6417.54 | | | | | | | | | | 23.81 | | | | | | | |
| C I 29.05 | 6389.87 | | | | | | | 18.76 | | | | | | 38.01 | | | | |
| C I 29.06 | 6378.79 | | | | | | | 13.15 | | | 18.79 | | | | | | | |
| C I 29.07 | 6342.32 | | | | | | | 26.47 | | | 32.15 | | | 35.45 | | | | |
| C I 29.08 | 5877.31 | | | 36.71 | | | | 29.07 | | 26.00 | | | 35.19 | 36.71 | | | | 31.11 |
| C I 29.09 | 5870.66 | | | 34.21 | | | | 25.53 | | 23.49 | | | 20.42 | | | 10.72 | | 25.53 |
| C I 29.10 | 5864.95 | | | 35.77 | | | | 36.79 | | 21.46 | | | 26.06 | 24.53 | | | | 19.92 |
| C I 29.11 | 5846.35 | | | | | | | | | | | | 18.45 | | | | | |
| C I 29.11 | 5850.25 | | | | | | | 23.07 | | 32.28 | | | 27.67 | 33.83 | 27.67 | | | |
| C I 33 | 6662.73 | | 31.95 | | 37.35 | | | | | | | | | | | | | |
| C I 33 | 6671.84 | | 28.76 | | | | | | | | | | | 26.53 | | | | |
| C I 33 | 6674.11 | | 22.02 | | 30.99 | | | | | 13.03 | | | | 30.09 | | | | |
| C I 33 | 6679.64 | | 17.49 | | | | | | | | | | | | | | | |
| C I 33 | 6683.95 | | 23.76 | | 40.36 | | | | | | | | | 31.38 | | | | |
| C I 33 | 6688.79 | | 22.41 | | 21.51 | | | | | 16.59 | | | | 38.54 | | | | |
| C I 35 | 6591.45 | 24.43 | 29.56 | 25.68 | | 21.29 | 27.59 | | 27.52 | | 34.11 | 30.47 | 30.47 | 36.82 | | | | |
| C I 35 | 6595.24 | 19.28 | | 23.78 | | | 24.17 | | | | 28.63 | | 30.45 | | | 21.82 | | |
| C I 35 | 6596.85 | | | 24.13 | 22.72 | | | | | | 24.54 | 19.53 | 24.08 | | | 20.90 | 26.36 | |
| C I 35 | 6602.42 | | 37.69 | | 33.61 | | | | | | 17.71 | 22.70 | 22.70 | | | 12.26 | 28.16 | |
| C I 35 | 6611.35 | | | | 23.12 | | | | | 15.88 | 29.03 | 29.47 | 22.67 | 33.54 | | | 12.69 | |
| C I 59 | 6586.27 | 27.50 | | 26.10 | | 27.25 | | | | | 29.14 | 32.32 | 34.58 | 30.96 | | | 39.14 | |
| C I 71 | 5912.58 | | | | | | | 18.25 | | 19.26 | | | 19.26 | 26.37 | | | | |
| C I 72 | 5910.34 | | | | | | | 23.85 | | 24.87 | | | 28.41 | 31.97 | | | | |

Table 3.4a – *continued*

| Line | λ | -23 | -21 | -19 | +10 | +15 | +16 | +17 | +18 | +19 | +20 | +22 | +31 |
|---|---|---|---|---|---|---|---|---|---|---|---|---|---|
| Ca I | 6717.69 | 21.88 | | 16.06 | | | | | | | | | |
| Ca I 18 | 6439.08 | | | | 22.80 | | 32.12 | | | | | | |
| Ca I 47 | 5857.46 | | 34.29 | | 26.12 | 36.34 | | | 29.69 | 37.89 | | | |
| Fe I | 6383.68 | | | | 21.60 | | 25.36 | | | 17.36 | | | |
| Fe I 62 | 6430.86 | | | | 33.10 | | 10.27 | | | 17.73 | | | |
| Fe I 111 | 6421.36 | | | | 31.76 | | 35.95 | | | 19.15 | | | |
| Fe I 168 | 6393.61 | | | | | | | | | 18.29 | 14.54 | | |
| Fe I 168 | 6494.99 | | | | | | | | | | 24.90 | 25.83 | |
| Fe I 268 | 6678.00 | | | 26.94 | | 37.26 | | | | 21.55 | | | |
| Fe I 816 | 6400.01 | | | | 20.15 | | 32.34 | | | 15.46 | | | |
| Fe I 982 | 5934.67 | | | | 19.19 | 17.17 | | | 26.79 | 35.37 | | | |
| Fe I 1161 | 5708.10 | | | | | | | | | | 14.69 | | |
| Fe I 1180 | 5862.37 | | 35.28 | | | 23.00 | | | 34.76 | | | | |
| Fe I 1180/1 | 5914.16 | | | | 23.32 | 25.84 | | | 32.94 | | | | |
| Fe I 1180 | 5930.19 | | | | 26.81 | 28.81 | | | 33.37 | | | | |
| Fe I 1181 | 5859.60 | | 32.23 | | | 19.96 | | | 16.36 | | | | |
| Fe I 1253 | 6385.71 | | | | 10.34 | | 14.56 | | | 15.01 | | | |
| Fe II | 5930.36 | | | | | | | | | | | 18.71 | |
| Fe II | 6517.01 | | | | | | 18.42 | 21.63 | 32.21 | 38.66 | | | |
| Fe II 40 | 6369.45 | | | | 23.53 | | 23.05 | | | 14.57 | 10.82 | | |
| Fe II 40 | 6432.68 | | | | | | 15.84 | | | 18.64 | | | |
| Fe II 40 | 6516.08 | | | | | | 11.95 | 17.03 | 17.48 | 18.87 | 18.87 | 18.87 | |
| Fe II 46 | 5991.38 | | | | | | | | | | | 28.02 | |
| Fe II 74 | 6416.93 | | | | | | | | | | 16.81 | | |
| Fe II 183 | 5856.45 | | | | | | | | | 12.80 | | | |

**Table 3.4a** – *continued*

| Line | λ | -113 | -23 | -21 | -19 | -8 | 0 | +10 | +12 | +15 | +16 | +17 | +18 | +19 | +20 | +22 | +31 |
|---|---|---|---|---|---|---|---|---|---|---|---|---|---|---|---|---|---|
| H I | 6562.82 | 18.65 | 22.39 | 21.53 | 22.39 | | 20.54 | | | | 28.80 | 24.67 | 25.58 | 33.81 | 15.99 | 14.16 | |
| Li I 1 | 6707.79 | | 15.65 | | 25.47 | | | | | 33.52 | | | | | | | |
| Ni I 231 | 5760.84 | | | | | | | | | | | | | | 15.63 | | |
| Sc II 19 | 6604.60 | | | 26.30 | 31.32 | 22.83 | 27.94 | | 26.70 | | | | 14.52 | 16.80 | 29.50 | 23.14 | 17.24 |
| Sc II 28 | 6300.68 | | | | | | | | | | | | | | 19.03 | | |
| Sc II 28 | 6309.89 | | | | | | | | | | | | | | 18.51 | | |
| Sc II 28 | 6320.84 | | | | | | | | | | | | | | 16.60 | | |
| Sc II 29 | 5684.19 | | | | | | | | | | | | | | 13.19 | | |
| Si I | 6555.47 | 21.85 | | | | 21.59 | 26.32 | | 29.23 | | 18.29 | 29.72 | | 15.99 | 35.66 | | |
| Si I 9 | 5780.39 | | | | | | | | | | | | | | 14.00 | | |
| Si II 2 | 6347.10 | | | | | | | 22.19 | | | 32.10 | | | 40.15 | 15.59 | | |
| Si II 2 | 6371.35 | | | | | | | 21.16 | | | 31.98 | | | 32.92 | 27.29 | | |
| Ti I 72 | 5899.30 | | | | | | | 16.28 | | 23.37 | | | 22.88 | 25.93 | | | |
| Ti II 91 | 6491.58 | | | | | | | | | | | | | | 30.94 | 27.24 | |
| Ti II 91 | 6559.57 | 25.01 | 19.21 | 25.48 | 28.81 | 21.92 | 27.21 | | 28.64 | | 10.06 | 11.43 | 11.43 | 16.92 | 17.83 | 12.34 | |
| Ti II 91 | 6606.98 | | | | | | | | | | 37.66 | 40.39 | 39.92 | | 27.23 | 26.32 | 30.40 |
| Ti II 112 | 6680.26 | | | | 10.78 | | | | | 21.10 | | | | 20.20 | | | |

**Table 3.4b.** Measured velocities of all components of Na $D$ as a function of day number.

| Line | λ | -21 | +10 | +15 | +18 | +19 | +22 | +31 | +71 | +80 | +100 | | Comments |
|---|---|---|---|---|---|---|---|---|---|---|---|---|---|
| Na I 1 | 5889.97 | | | | -113.01 | -105.87 | | -130.83 | | -119.72 | -172.61 | | high velocity component |
| Na I 1 | 5889.97 | -8.67 | -10.19 | -15.78 | -23.93 | -26.99 | | | | -25.03 | -20.44 | | interstellar component |
| Na I 1 | 5889.97 | 20.85 | 20.35 | 37.16 | 16.78 | 18.81 | 22.39 | 29.00 | 23.41 | 18.21 | 21.81 | } | |
| Na I 1 | 5889.97 | 48.34 | | | | | | | | 45.20 | 42.17 | } | stellar component |
| Na I 1 | 5889.97 | | | | | | | | | 55.36 | 66.10 | } | |
| Na I 1 | 5895.94 | | | | -131.79 | -131.28 | | | | | | | high velocity component |
| Na I 1 | 5895.94 | -6.60 | | | | | | | | -29.59 | -20.92 | | interstellar component |
| Na I 1 | 5895.94 | 24.41 | 22.89 | 34.06 | 8.14 | 13.73 | 19.32 | 31.53 | 22.37 | 17.19 | 20.79 | } | |
| Na I 1 | 5895.94 | 47.79 | | | | | | | | 44.64 | 44.68 | } | stellar component |
| Na I 1 | 5895.94 | | | | | | | | | 60.41 | 73.15 | } | |

presents all the measured velocities. Note that the sodium lines are listed by themselves due to the complex structure that they exhibit. The different components (stellar, interstellar and high velocity) are indicated. We have excluded any values $< 10$ and $> 40$ kms$^{-1}$ (except for sodium). These discrepant values usually arose due to the dispersion solution problems outlined above or the low signal–to–noise ratio of some of the spectra.

A large fraction of the spectra have been plotted into time series, to show the evolution of the spectra with time. Figs. 3.3 and 3.4, respectively, show the rise and decay of the Na I $D$ emission, while Fig. 3.5 illustrates the behaviour of the Na I $D$ region on the rise to maximum light. Figs. 3.6, 3.7, 3.8 and 3.9 respectively show the evolution of the Ca II $K$ line (during both the decline and the rise back to maximum light), the H$\alpha$ line region and the wavelength intervals $\lambda\lambda$6340–6450Å and $\lambda\lambda$6610–6720Å. Fig. 3.10 shows three pre–decline spectra and we note that there is very little change leading up to the decline onset. The bar at the edge of each time series plot shows the scale of the intensity as a percentage of the continuum.

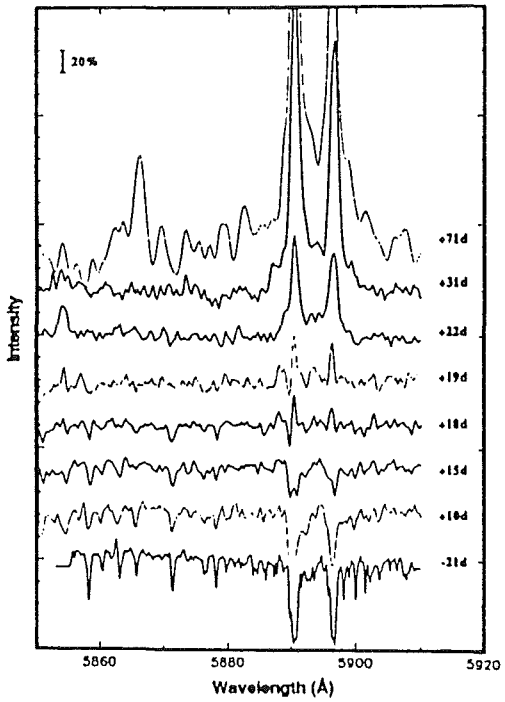


**Figure 3.3.** Time series, on the day numbers shown, of the rise of the Na I $D$ emission during the decline of R CrB. Note the high velocity (blueshifted by $\lambda \sim 3$ Å) Na I $D$ emission line on day 18 and 19.

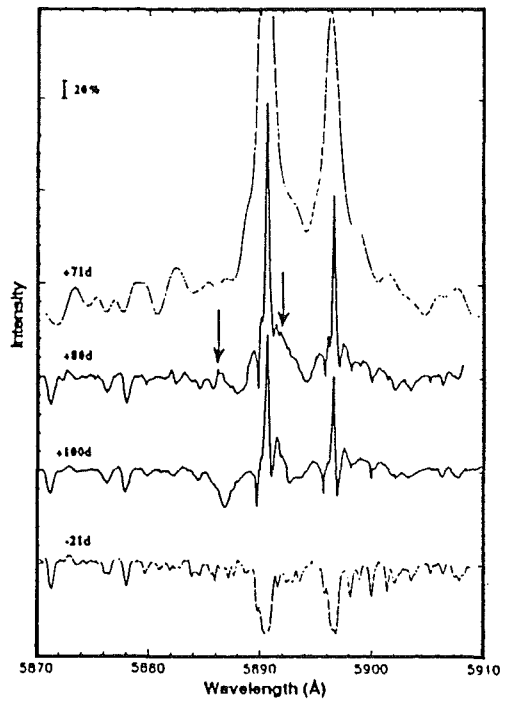


**Figure 3.4.** Time series, on the day numbers shown, of the decay of the Na I $D$ emission near the decline minimum of R CrB. The arrows indicate the position of excess emission (see Section 3.1.4.3).

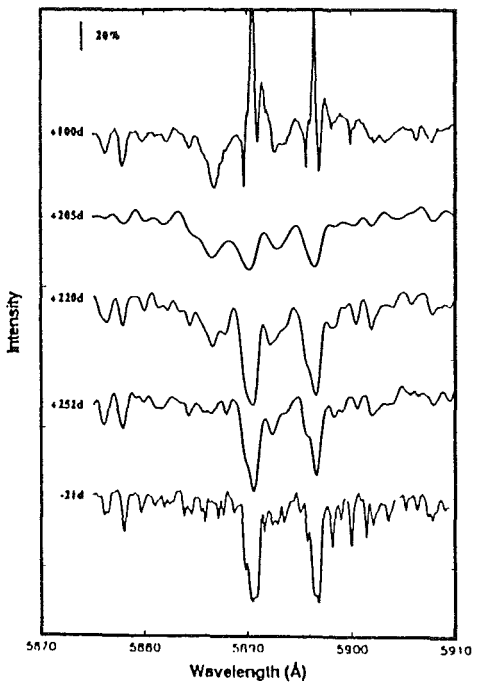


**Figure 3.5.** Time series, on the day numbers shown, of the spectral evolution of the Na I $D$ lines during the recovery to maximum light. The data is of varying spectral resolution.

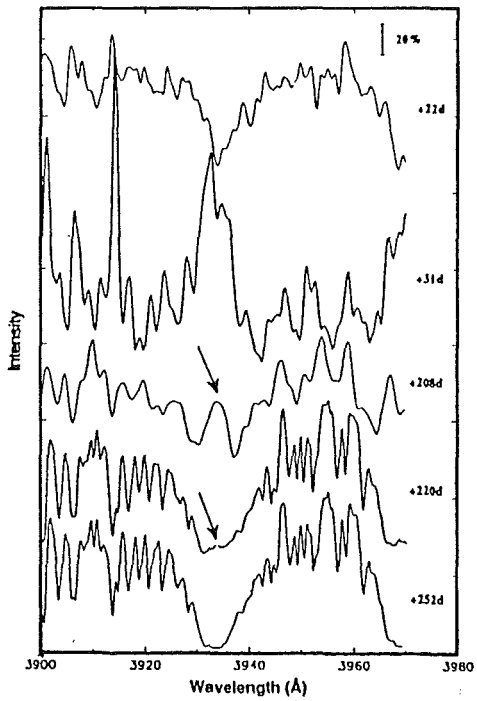


**Figure 3.6.** Time series, on the day numbers shown, of the spectral evolution of the Ca II $K$ line throughout the decline. The core emission (arrowed) is still visible on day 220.

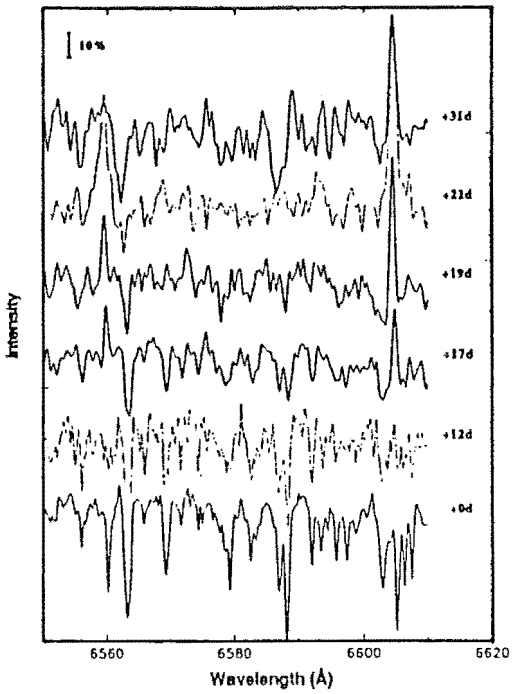


**Figure 3.7.** Time series, on the day numbers shown, of the spectral evolution in the wavelength interval $\lambda\lambda$6550–6620Å. Of particular note are H$\alpha$ ($\lambda$6562.8Å) and the Sc II line at $\lambda$6604.6Å.

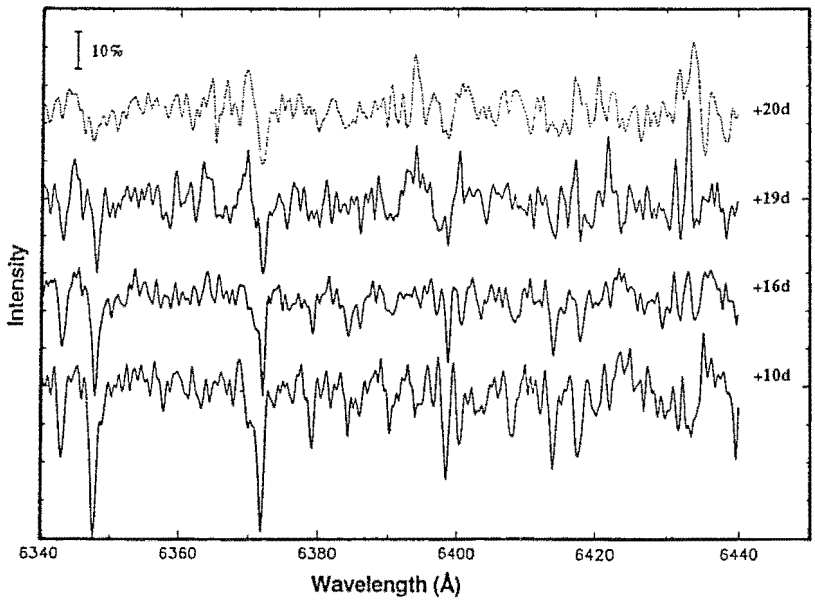


**Figure 3.8.** Time series, on the day numbers shown, of the spectral evolution in the wavelength interval $\lambda\lambda$6340–6450Å. Note the appearance of the emission lines on day 19.

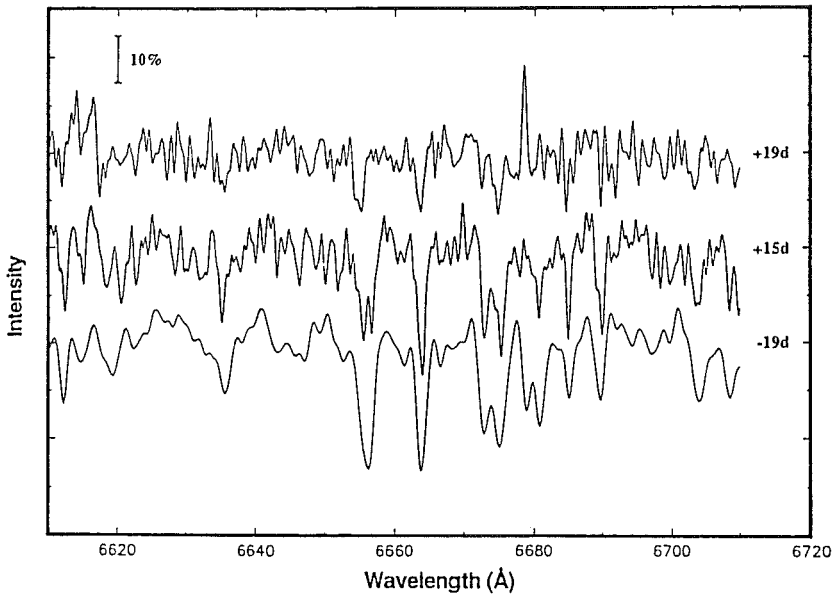


**Figure 3.9** Time series, on the day numbers shown, of the spectral evolution in the wavelength interval $\lambda\lambda$6610–6720 Å.

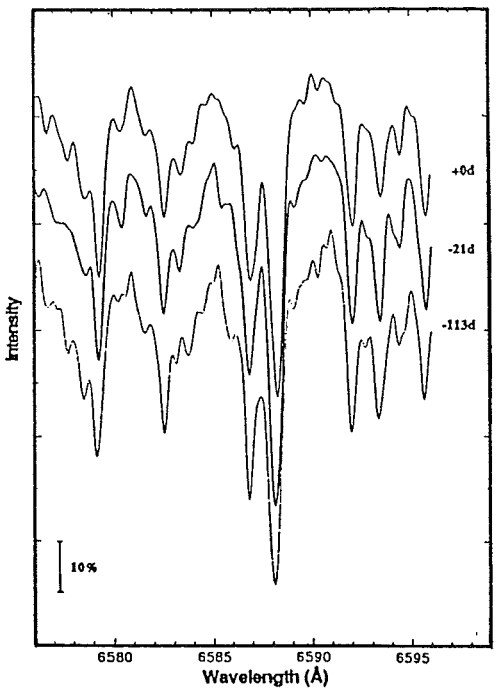


**Figure 3.10.** Pre–decline time series spectra which demonstrate that there is no change in the spectra prior to day 0.

## 3.1.4 ASPECTS OF THE DECLINE PHASE

### 3.1.4.1 Defining the 'decline onset'

As indicated in Section 3.1.1, there have been few detailed analyses of the initial decline phases of RCB stars. In fact, there has previously been no extensive spectroscopic coverage of this phase until about 15–20 d after the decline onset, when the stars are already 2.5–3.0 mag below their value at maximum light. The term 'decline onset' needs to be defined in some manner that permits a comparison to be made with other declines. If photoelectric photometry is available (as we have here) then some estimate of the actual decline onset time can be made (see Section 3.1.5.3). For those declines for which no photoelectric data are available during the initial decline, and these include all other declines for which spectroscopy is available, the actual decline onset time will be very uncertain. Defining the decline onset poses some difficulties because it is complicated by the stellar pulsations which continue after the obscuring cloud has formed. Where only less accurate visual estimates are available we have to devise a new definition for the decline onset which permits some comparison to be made with these less well covered declines. For our purposes here we define day number 0 as the Julian Date at which the $V$ mag (or visual estimate) first drops below the average pulsation minimum. In this decline this occurs on JD 2447355 and was shown as a vertical line in Figs. 3.1a and 3.1b. In discussing our data, in particular our extensive spectroscopy, we will use this zero point as it avoids the use of cumbersome Julian Dates. (We comment in Section 3.1.5.3 that this definition for the apparent decline onset may sometimes differ by 5–30 d from the onset time determined by photoelectric photometry.)

### 3.1.4.2 Photometry and low–resolution spectroscopy during the initial decline

Before the star was seen to be in decline, the light curve of R CrB (Fig. 3.1a) showed a 15 d interval (JD 2447335–2447350; day –20 to –5) at almost constant magnitude. We discuss this standstill in the $V$ mag in Sections 3.1.5.3 and 3.1.5.4. For 30 d (to JD 2447380; to day 25) after this standstill the star's brightness decreased rapidly. From JD 2447380–2447395 (day 25–40), the rate of decline of the $V$ curve decreased as R CrB approached its minimum mag of $V \approx 11$ near JD 2447420 (day 65). However, before the minimum mag was reached, the $V$ curve showed a peak near JD 2447400 (day 45). Although the decrease in light is the most noticeable effect of the decline, it is the colour curves (Fig. 3.1b), in conjunction with our spectra, that provide the key to our understanding of the evolution of R CrB during the early stages of the decline.

Prior to JD 2447365 (day 10) the colour curves showed no apparent indication that the light output of the star was decreasing. This supports the idea that only a fraction of the star's disk was initially obscured by an optically thick dust cloud and that the photosphere was still dominating the light output of the star. From JD 2447365–2447380 (day 10–25), there was a rapid change to bluer ($U$–$B$) and ($B$–$V$) colour indices. These changes can be seen in the $V/(B–V)$ diagram (Fig. 3.11a) and the $(U–B)/(B–V)$ diagram (Fig. 3.11b). In Fig. 3.12 we have plotted the flux distribution of R CrB throughout the decline. From the decline onset, through JD 2447373 (day 18), the flux distribution did not change significantly. On JD 2447376 (day 21), there was some indication of a departure from the

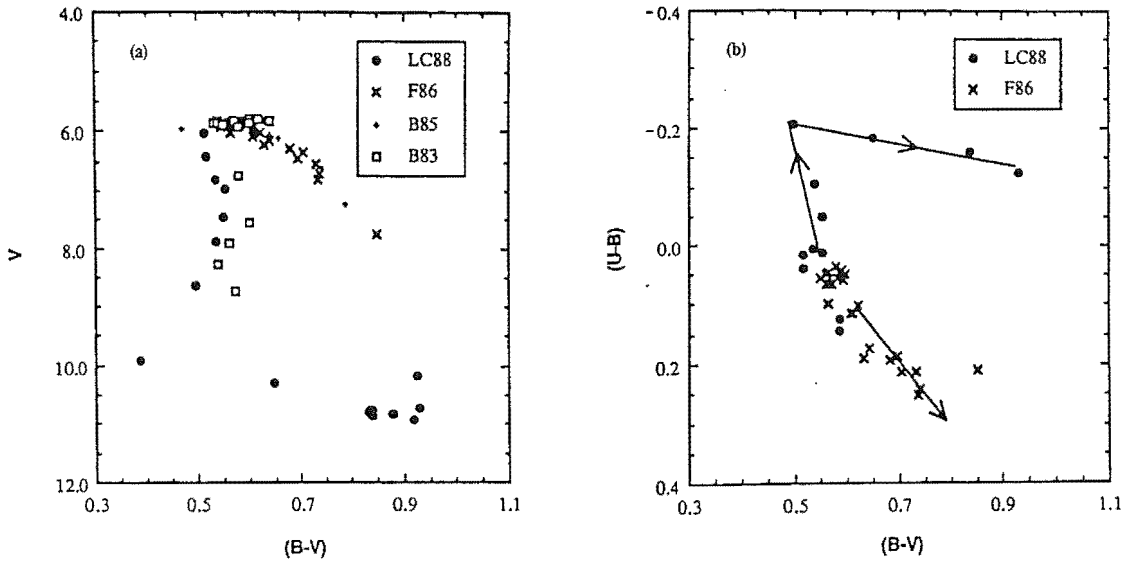


**Figure 3.11.** Comparison of R CrB declines in the (a) $V$ versus $(B–V)$ plane and (b) $(U–B)$ versus $(B–V)$ plane. In (b), the arrows show the difference between a 'blue' (LC88 – this decline) and 'red' (F86 = Fernie, Percy & Richer 1986) decline. B83 and B85 is the photometry of Böhme (1983) and Böhme (1985) respectively, for the 1983 and 1985 declines of R CrB.

normal energy distribution, but on JD 2447380 (day 25) the departure was significant. We interpret this complex behaviour as being due to the rapid domination of flux received from the chromosphere of the star as the expanding dust cloud obscures the photosphere. This interpretation is supported by our high–resolution spectra (Section 3.1.4.3) which show a gradual transition from a photospheric absorption line dominated spectrum to one dominated by chromospheric emission lines at about this time.

In Fig. 3.2a we plotted the low–resolution ($\Delta\lambda \approx 10$Å) spectra obtained on JD 2447378 (day 23) which shows broad emission in the interval $\lambda\lambda$3900–5700Å. This broad emission accounts for the blueing of the star as the peak $(B–V)$ colour occurs around this time. There must also be some UV excess emission as the $(U–B)$ colour also peaks at the same time. (Such a UV feature was observed by Holm *et al.* 1987 during the 1983 decline of R CrB.) The general form of the emission is consistent in appearance with the flux distribution at about this date. The feature may be due to unresolved chromospheric emission lines, continuum emission, or possibly a combination of both. The feature appears to be similar to that observed by Alexander *et al.* (1972) during the 1969 decline of RY Sgr (see Alexander *et al.* 1972; section 3b and 3c). Alexander *et al.* (1972) were unable to unequivocally identify the nature of this feature, but they considered both a continuum (emission and absorption) and unresolved emission lines as contributors. If the feature is at least partially continuum emission, the initial portion ($\lambda\lambda$3900–4000Å) may be similar to the continuum seen by Alexander *et al.* (1972) (see their fig. 9), and identified by them as the electron recombination spectrum of CN in a spectrum of RY Sgr taken $\approx$3 mag

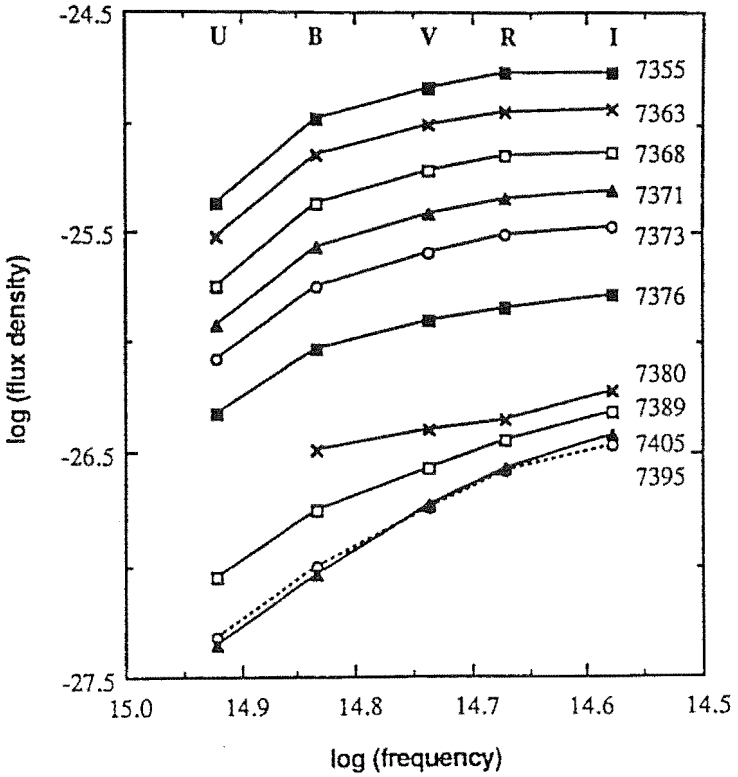


**Figure 3.12.** Flux Density ($Wm^2hz^{-1}$) versus frequency for the 1988 decline of R CrB. The numbers next to each curve are the (JD–2440000) of the observation. The filters are indicated at the top.

below maximum light. Work by Dunn *et al.* (1967) during the 1962 solar eclipse showed that the base of the chromosphere of the Sun exhibits very strong emission, with many lines in the blue, so the emission seen in R CrB can most probably be identified with the emission formed at the base of its chromosphere.

From JD 2447380–2447395 (day 25–40) the colour indices of R CrB rapidly reddened, coinciding with a slowing of the $V$ light curve decline rate. The effects of this slowing are seen dramatically in the $V/(B–V)$ and $(U–B)/(B–V)$ diagrams. A low–resolution spectrum obtained on JD 2447388 (day 33; see Fig. 3.2b) no longer showed the emission seen 10 d earlier. The flux distribution has returned to a more normal form, only reddened by the obscuring dust. At this phase the reddening approximates a $1/\lambda$ relationship. We interpret the reddening of the colour curves as the obscuration of both the photosphere and the inner chromosphere (which we have identified as the source of the broad emission). The rapid disappearance of the broad emission (inferred from the more normal flux distribution after JD 2447389; day 34) may support the identification of the dust cloud's initial location as being close to the photosphere, with subsequent rapid growth or motion obscuring the chromospheric emission regions.

### 3.1.4.3 High–resolution spectroscopy during the decline

No spectroscopic changes were seen until R CrB had begun to decline in light output (see Fig. 3.10). Thus, at least over a restricted wavelength interval, there does not appear to be any spectroscopic signature of the upcoming decline.

As the star declined, the photospheric absorption spectrum became weaker, and emission lines from the chromosphere became visible (see Figs. 3.3, 3.6, 3.7, 3.8 and 3.9). The identification of the chromosphere as the origin of these lines can be inferred from the emission lines that are blue–shifted by about 10 $kms^{-1}$ relative to the pre–decline absorption lines. This can be seen in the upper portion of Fig. 3.13 where the velocities for 3 lines; H$\alpha$, Sc II ($\lambda$6604.6Å) and Ti II ($\lambda$6559.6Å), have been averaged over various days and then plotted as a function of day number. A lower–velocity group of lines is visible (in emission, except for H$\alpha$) after day 15. Prior to this date these lines were all in absorption (see Table 3). This shift of about 10 $kms^{-1}$ is also exhibited by a number of other lines, in particular Ba II ($\lambda$5853.7Å) and a few lines of Fe I and Fe II, which also go into emission around day 15. (They were not plotted in the upper portion of Fig. 3.13 as they were not observed as frequently as those shown.) The lower portion of Fig. 3.13 shows the results for the high excitation ($\chi$ >8 eV) C I lines, which are always in absorption and exhibit no such shift. Hence, while the C I lines are visible (generally up until day 19), they must always be formed in the (deeper) photospheric layers. This blue–shifting of many of the lines was also noticed by Payne–Gaposchkin (1963), who showed that this value agreed with calculations for outward streaming chromospheric material. The H$\alpha$ line is only partially filled–in as it mainly forms high in the photosphere (or even in the lower chromosphere). For H$\alpha$ to appear in emission about 12 eV of energy would be required to excite the upper level of this transition.

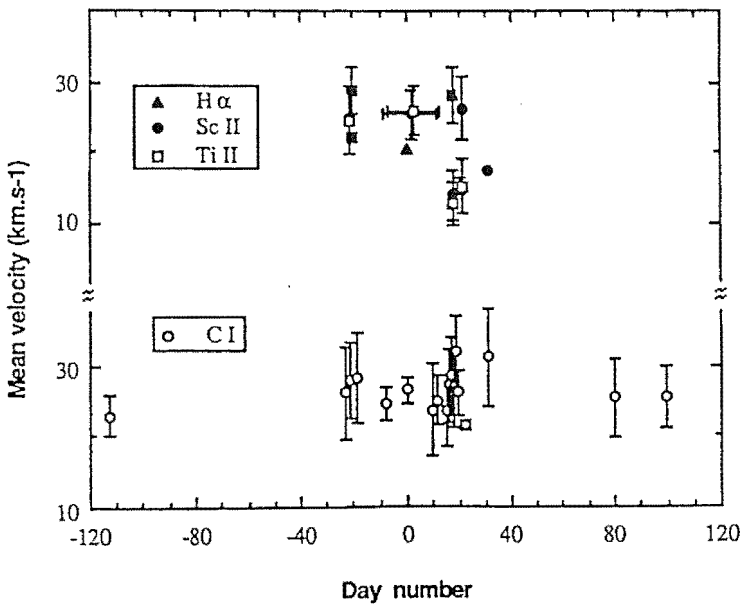


**Figure 3.13.** Mean velocities versus day number for 3 lines of the species shown (upper section) and various C I lines (lower section). Note the 'step' in velocity in the upper section on day 18 (see Section 3.1.4.3).

We see a weakening of the chromospheric emission lines from around day 30. The high excitation lines disappeared first, followed by the lower excitation lines, until only the zero volt lines of Na I *D* and Ca II *H* and *K* were still in emission. This weakening is consistent with the progressive blocking of the chromosphere by an expanding dust cloud.

The Ca II *H* and *K* lines (see Fig. 6) followed a slightly different trend to that of the majority of the lines. They were still in absorption around day 22, while the rest of the spectrum showed strong emission, and went into emission only when the other lines had already begun to decay. This can be explained by the fact that the *H* and *K* lines form quite high in the chromosphere (see Noyes & Avrett 1987, in particular their fig. 5.15). The veiling material only slowly obscures the region where these lines form. The *H* and *K* lines can still go into emission as they require very little energy to populate the upper level of the transition. This is in contrast to the higher excitation H$\alpha$ line which never goes into emission, although its velocity does shift to lower velocity, indicative of the outward streaming motion seen in the emission lines. When the cloud has obscured the highest regions of the chromosphere we should see the smoothly outflowing regions of the outer chromosphere, and these are the narrow Na I *D* emission lines visible around day 80 (see Fig. 3.4). [Lambert (personal communication) has indicated to us that some of this narrow low velocity emission may be due to night sky emission. However, the velocities measured for the Na I *D* lines on both day 80 and 100 are consistent with the stellar velocity.] A large fraction of the chromosphere is then obscured by the dust cloud, but there is still a large amount of turbulence present, shown by the very broad emission at the base of the narrow Na I *D* lines.

The strong, broad, high velocity emission feature due to sodium that we saw on day 18, and the absorption feature seen on day 100, have comparable velocities and are almost certainly the same material. The absorption feature is possibly due to the cooling of the material as it has moved away from the star. Its velocity of $\sim$150 kms$^{-1}$ is more than twice the escape velocity of the star. (The latter was derived from a mass estimate of 0.7–0.9$M_{\odot}$ and a radius ($R_{\star}$) of $\approx$ 70–85$R_{\odot}$. We can also deduce a radius of $\approx$50$R_{\star}$ for the circumstellar shell of R CrB from the infrared (3–60$\mu$m) flux received and its effective temperature of $\sim$650 K.) If we assume that it is the same material that we see on days 18 and 100, then during this time it will have moved out to about 50$R_{\star}$, which is the position that we have calculated for the circumstellar shell. This leads to several points.

Firstly, if there was no addition to the veiling material (dust cloud) and it had moved out as far as the circumstellar shell then we would expect to see the star brightening again. This was not observed. This implies that either more material has condensed into the veil or that the veil has not moved as far as the high velocity material, i.e. it is still nearer the star. Interestingly, we saw the photosphere reappear on day 80. From the photometric observations, the dust cloud was still obscuring around 98 per cent of the photospheric light. This indicates that the veiling material has now obscured enough of the chromosphere for the photospheric component of the total light to once again dominate the chromospheric contribution. Due to the poor signal–to–noise ratio obtained for the spectrum of day 71, it is impossible to say whether this return is gradual, or if it is a very rapid transition.

Secondly, unless high velocity material is slowed by its interaction with the circumstellar shell, it will leave the star. If all the material (obscuring dust plus high velocity gas) was moving at more than $\sim$ 100 kms$^{-1}$ then it could disrupt the circumstellar shell. We

speculate that it is more likely that the high velocity material was rather tenuous and was mostly composed of gas.

Finally, the centroid of the shorter wavelength high velocity sodium absorption feature appeared to shift from day 80 to day 100. This could be due to either a shock mechanism, that suddenly appears around day 80 and accelerates the material, or else the absorption profile is distorted in some way. There appear to be emission features (arrowed in Fig. 3.4) which are distorting the profiles of the high velocity material. These can easily be seen in Fig. 3.14, where we have endeavoured to show the extent of this emission. As the gas cloud has now reached the circumstellar shell we suggest that this emission is due to the gas cloud being heated as it interacts with the circumstellar shell. The fact that we have the gas cloud out at the circumstellar shell, yet the obscuring dust apparently nearer the star, means that any model for these declines has to explain how some material can be accelerated preferentially without moving the dust as much. Also, since we see the high velocity gas only during a decline (the high velocity absorption has decayed by day 252), they are most probably linked in some way.

The emission lines of sodium became very broad, peaking around day 70, and then appeared to collapse into very narrow lines but with a very broad multi–component emission base. Possibly the passage of the high velocity material causes a great deal of turbulent heating of the chromosphere due to shocks, as the speed of sound in the chromosphere is only about 4 $kms^{-1}$ (Payne–Gaposchkin 1963). (Some variations in this sound speed, increasing this value to $\approx$10 $kms^{-1}$, will result from the use of more recent abundance results, e.g. Cottrell & Lambert 1982a.) Once the material has passed, the chromosphere takes quite some time to return to its equilibrium state. We then see very narrow emission

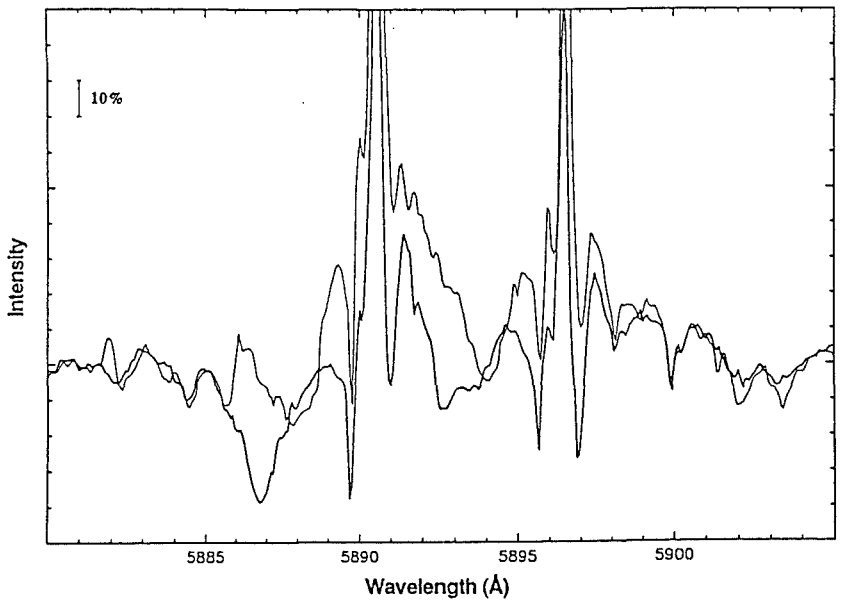


**Figure 3.14.** Overlay of the two Texas spectra, day 80 (thin line) and day 100 (thick line). The excess emission on day 80 is clearly visible.

lines superimposed on very broad emission bases. We have indicated that the narrow lines are probably from the smooth outflow of material at the very top of the chromosphere, and the broad base is the turbulent chromosphere, veiled by the slowly expanding (either by continual dust formation or outward motion or a combination of both) dust cloud. Another possible cause could be a very rapid (in the 9 day between day 71 and 80) cooling of the outer chromosphere due to some unknown mechanism.

By day 220 the spectrum of R CrB had almost returned to its appearance at maximum light. (The star had recovered to $V = 7.5$.) Two relatively small exceptions are the high velocity blue-shifted absorption components of the Na I $D$ lines (see Fig. 3.5) and the emission in the core of Ca II $H$ and $K$ lines (see arrows in Fig. 3.6). The latter is probably the remnant of the chromospheric emission which decays slower than the Na I $D$ lines. (This phase shift is similar to the delay which the Ca II lines exhibited when they first went into emission.) Both the high velocity absorption and the core emission had completely disappeared by day 252 when $V = 6.5$ and the colours were almost the same as those at maximum light (see Fig. 3.1).

#### 3.1.4.4 Photometry during the rise to maximum

Due to the limited observing season that we have for R CrB from MJUO, we were unable to monitor the rise from minimum light. Our observations obtained during 1989 showed the star at $V = 6.0$–$6.2$, or 0.2–0.4 mag fainter than the normal mean mag at maximum of $V = 5.8$. Pulsations with periods of 40–45 d were clearly evident in the photometry. Photometry obtained by Alexander *et al.* (1972) during the rising branch of the 1969 decline of RY Sgr suggested that an RCB star may take an additional 6–12 months to fully recover to its normal magnitude at maximum.

### 3.1.5 DISCUSSION

#### 3.1.5.1 Decline comparison

In Fig. 3.1 we showed the light and colour curves for the 1988 decline. Plotted in Fig. 3.15 are published $V$ and $(B–V)$ photometry and visual observations from the (a) 1983 decline (Böhme 1983; IAU Circ. 3857, 3859, 3884, 3900) and (b) 1985 decline (Fernie, Percy & Richer 1986; Böhme 1985; IAU Circ. 4108, 4116, 4143) of R CrB. These data, in conjunction with data for declines of other RCB stars, enable us to make some comparisons between these events. Initially it can be seen that there is a variety of decline rates for these events. The decline rate for the 1983 and 1988 declines of R CrB were somewhat more rapid than the 1985 event. The timescales for the star to fade 1 mag from maximum were $\sim$ 7, 7 and 12 d respectively. These values can also be compared to $\sim$ 8 d for the 1967 decline of RY Sgr and $\sim$ 10 d for the 1988 decline of NSV 6708. We will indicate in Sections 3.1.5.3 and 3.1.5.4 that the initial decline rate may be highly influenced by the phase of the semi-regular variations at which the decline onset occurs.

It is also clear from the table of spectroscopic observations that the 1988 decline of R CrB can be divided into distinct spectroscopic sequences. These are outlined in Table 3.5 (day numbers are approximate). Consequently, we can compare the spectroscopy

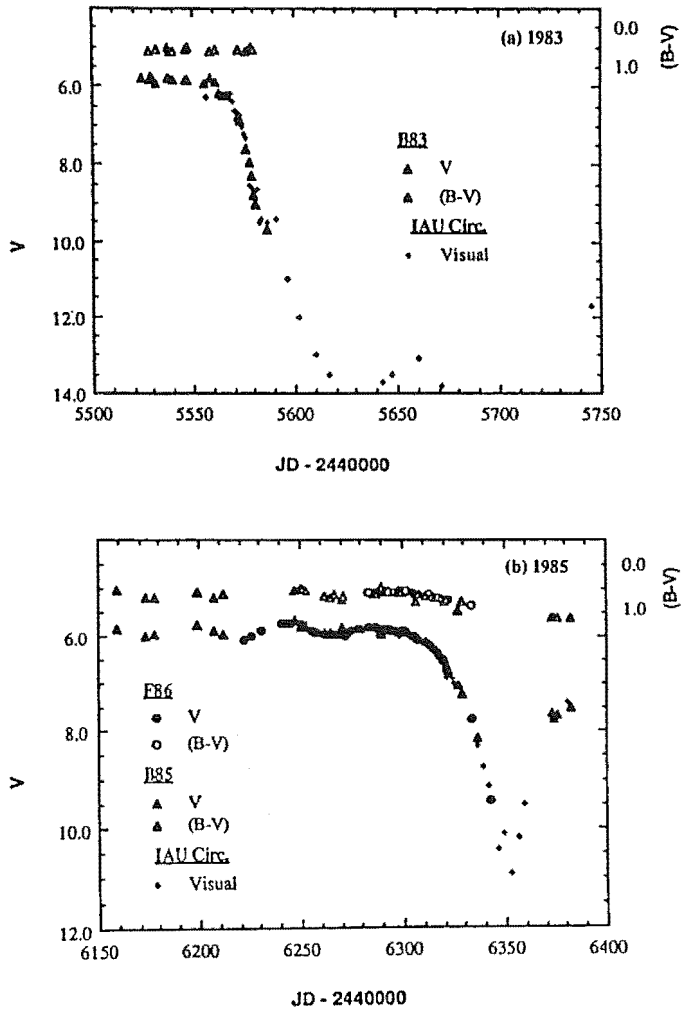


**Figure 3.15.** R CrB photoelectric data for the (a) 1983 and (b) 1985 declines. The codes used for the different sources are identified in the caption for Fig. 3.11.

obtained for this decline with other declines for which spectroscopic coverage is available; e.g., the 1948 (Herbig 1949) and 1963 (Payne–Gaposchkin 1963) declines of R CrB and the 1967 decline of RY Sgr (Alexander *et al.* 1972). Spectroscopically, these four declines showed some degree of similarity in their overall behaviour. In all cases there was a veiling of the photospheric continuum and the appearance of strong emission lines, probably chromospheric, most of which later decayed but with different timescales for different species. All declines showed a high velocity blue–shifted absorption feature due to sodium and calcium (with the exception of Herbig 1949, in which it may have been missed due to the unfortunate timing of this decline, which occurred shortly before R CrB passed behind the Sun). The timescales were also quite comparable. For example, the Ca II *H* and *K* lines lagged behind the other lines in going into emission. In the 1988 decline, this occurred between day 22 and day 31, Alexander *et al.* (1972) (1967 decline of RY Sgr) saw

**Table 3.5.** Summary of decline and recovery 'phases'.

| | |
|---|---|
| *Day 0 - 16* | Slow filling of lines, general dimming of star, very slow colour change towards the blue |
| *Day 16* | Emission lines appear |
| *Day 18* | Blueshifted Na D emission (–110 km $s^{-1}$) appears, strong blueing of star |
| *Day 18 - 22* | Strong chromospheric emission spectrum, Ca H and K lines still in absorption |
| *Day 23* | Broad emission ($\lambda\lambda$ 3900–5700Å) is seen (probably appeared a few days before) |
| *Day 23 - 31* | Decaying of chromospheric emission, Ca H and K lines in emission, broadening of stellar Na D emission |
| *Day 31* | Broad emission gone, star reddening, star reaches minimum brightness |
| *Day 71 - 80* | Narrowing of stellar Na D emission, appearance of blueshifted Na D absorption, reappearance of photospheric absorption spectrum |
| *Day 80-100* | Na D absorption appears to accelerate, possibly due to distortion of profile by emission |
| *Day 200-220* | Normal photospheric spectrum, star brightening, blueshifted Na D absorption, (–150 km $s^{-1}$), Ca H and K absorption with weak core emission |
| *Day 250* | All spectra normal, no high velocity absorption |

it sometime before day 30, Herbig (1949) (1948 of R CrB) between days 28 and 45, and Payne–Gaposchkin (1963) (1960 of R CrB) sometime before day 49. The fact that there are different decline rates indicates that the decline behaviour is due to a combination of mechanisms. Any single, simple mechanism would reproduce similar results for each decline. It is possible that the formation rate of the obscuring material is variable with rapid formation leading to a faster decline. It is also possible that there are competing mechanisms, such as the star behind the cloud causing variable dissociation of the cloud material depending upon the phase of the smaller amplitude variations of these stars.

An inspection of the comparative photometric diagrams (Figs. 3.1, 3.11 and 3.15) shows that the early behaviour of the 1983 decline closely resembled the behaviour of the 1988 decline. The 1983 decline was deeper than the 1988 decline, reaching $V = 14$ compared to $V = 11$, but the colour behaviour appears to be closely aligned to that of the 1988 decline. There was also a brief discontinuity of several day duration during the initial decline near $V = 9.5$ which may be comparable in origin to the peak seen in the 1988 decline near JD 2447400. We expect that the photometric and spectroscopic behaviour of the current decline should apply equally well to the 1983 decline.

In contrast, the 1985 decline differed markedly from the behaviour of the 1983 and 1988 declines. The most obvious difference was that the colours of R CrB became redder from the onset of the decline. Although photometry was not available throughout the entirety of the 1985 decline, Fernie, Percy & Richer (1986) commented that the reddening relationship derived on the initial declining branch closely resembled the reddening relationships seen

in photometry obtained during the rising branch (i.e. the rise back to maximum light) in other declines (for a more recent discussion, see Pugach 1988). Pugach found that an approximately interstellar reddening relationship could describe the reddening seen in the $V$ versus colour plane, for the rising branches of the 1977, 1981 and 1983 declines of R CrB. Fernie, Percy & Richer (1986) were aware that the photometry of this decline did not appear to agree with the observed photometric and spectroscopic behaviour of other declines but could offer no alternative interpretation of their observations.

The reddening behaviour of the 1985 decline of R CrB is not unique amongst RCB stars. Our observations of other recent declines of RCB stars has shown that this behaviour may be rather common and may occur at least as often as the 'blue' declines. During the 1988 decline of NSV 6708, the initial decline was well observed at *UBVRI* wavelengths (at MJUO, see Chapter 4), *JHKL* wavelengths (at SAAO, see Kilkenny & Marang 1989; Chapter 4) and spectroscopically at both observatories. In this decline, the decline onset was particularly easy to recognise as the colours turned sharply towards redder values (see Fig. 4.1) in phase with the change in the $V$ mag. The reddening during the initial decline closely resembled interstellar reddening. The 1989 decline of S Aps (see Section 3.2.1) was also a 'red' decline.

These 'red' declines pose difficulties for the usually accepted RCB decline model which assumes, as we have discussed in Section 3.1, that the dust cloud obscures a limited fraction of the visible hemisphere of the star.

The observed characteristics of the 'red' declines can be explained if the dust obscures the entire visible hemisphere of the star upon condensing. In this case the dust is optically thin and the cloud will act like a filter, causing both the $V$ mag to fade and the colour indices to redden. We also suggest that much of the inner chromosphere is obscured simultaneously with the photosphere and that this is the reason why we do not observe complex colour variations due to chromospheric emission. We would expect that only low excitation chromospheric lines would be present after the obscured (and combined) photospheric and inner chromospheric flux were sufficiently suppressed for these low excitation emission lines (from the outer chromosphere) to be visible. Secondly, we would anticipate that the transition from a photospheric– to a chromospheric–dominated spectrum would occur at a fainter magnitude, as the chromosphere is already largely obscured by the dust cloud. SAAO spectra of the decline of NSV 6708 certainly support this second point. The transition was observed in this star 4–5 mag below maximum light, which was a further 2–3 mag below maximum light when compared to the 1988 decline of R CrB. Spectra obtained prior to this transition appeared to show a normal photospheric spectrum even though the photometric colours were heavily reddened by this time.

SAAO (Marang *et al.* 1989) and unpublished MJUO photometry of the current decline of the RCB star UW Cen (which began in 1986 January) indicate that this star has experienced both types of declines. $V$/JD and $V/(B-V)$ diagrams for this decline are given in Figs. 3.16a and 3.16b respectively. The $(B-V)$ index of UW Cen became bluer [$\Delta(B-V)$ = –0.7] during the initial decline. Although UW Cen became considerably bluer than our observations indicate for R CrB, the $(B-V)$ excess was probably caused by the same source of emission seen in the low–resolution spectra of R CrB. After UW Cen reached $V$ = 14.5 (about 5 mag below its normal maximum), the star reddened rapidly, and during successive rises and falls in the $V$ magnitude showed a similar reddening relation in the $V/(B-V)$ plane (double headed arrow in Fig. 3.16b). The decline near JD 2447100

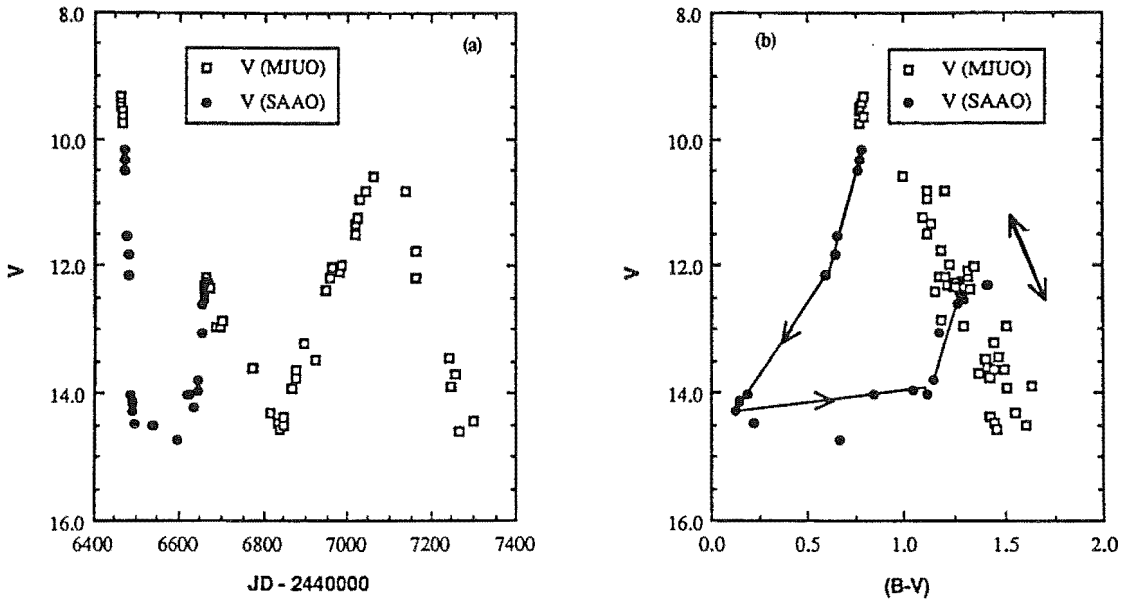


**Figure 3.16.** Photoelectric data for the 1986 decline of UW Cen. (a) $V$ versus Julian Date and (b) $V$ versus $(B–V)$. These data are from MJUO and SAAO. The arrows on the SAAO data show a 'blue' type initial decline of UW Cen.

(1987 November, when UW Cen was about 1 mag fainter than its normal magnitude at maximum light of $V = 9.3$) also described the same reddening relationship.

In describing the above declines by their colour curves, we have identified two extreme types of colour behaviour: 'blue' declines, where the $(U–B)$ and $(B–V)$ colours become substantially bluer before finally reddening, and 'red' declines, where the star reddens from the onset of the decline. However, we would expect that there may be a whole range of decline behaviour between these two extreme types. The 1988 decline of V CrA (see Section 3.2.3.2) may be of intermediate type in that the colours remained constant during the early decline stage, and reddened only after the star had declined by 2 mag in $V$.

### 3.1.5.2 Geometry of the decline

The generally accepted model for explaining the observed decline behaviour of RCB stars considers a dense dust cloud as the obscuring element in these stars. From purely geometrical considerations it is difficult to prefer either a cloud that *expands laterally* and probably also radially (Feast 1986), or one that is *ejected radially* and possibly with some lateral growth. The distinctions between these two approaches are not subtle in detail, but are difficult to identify with the observations currently available.

In the first case a dust cloud might form, possibly close to the star, due to a set

of conditions that favours the condensation of carbon gas into carbon grains, e.g. a temperature minimum. If the size of this cloud was less than the visible hemisphere of the star then the lateral growth of this cloud would first obscure the photosphere and then the chromosphere, giving rise to a 'blue' decline. The observed characteristics of a 'red' decline would need to be met by a more extensive cloud that obscures both the photosphere and the inner chromosphere almost simultaneously.

In the second case, gas is ejected radially through some mechanism. The gas cools and condenses into dust at some critical radius, and then progressively obscures the star and chromosphere as it expands radially. The fraction of the visible surface area of the star that is obscured depends upon both the ejection angle of the gas and the condensation radius. Fadayev (1988) has calculated the dust formation rate in RCB stars and favours condensation radii $> 20R_*$. Fadayev's calculations suggest that if the gas is ejected at angles between 20° and 40° (seen as a projection angle from the centre of the star), then the dust cloud, after condensing, will only partially eclipse the star which would give rise to a 'blue' decline (ejection angles less than 20° gave declines rates that were less than those observed). For ejection angles greater than 40°, the dust upon condensing will totally eclipse the photosphere, i.e. a 'red' decline. This approach to the decline phenomenon was also taken by Goldsmith & Evans (1985), although they were largely concerned with modelling the light curve decline rate. They did, however, consider cases where the size of the ejected dust cloud was both smaller than, and larger than, the visible hemisphere of the RCB star.

It is possible that combinations of condensation radius and/or projection angle of the dust with respect to the star can be rejected by careful infrared photometry during the decline. A dust cloud that is both close and large will occupy a greater solid angle with respect to the star and would be expected to reradiate absorbed radiation to a greater extent than a more distant cloud. Unfortunately, there are few published series of infrared data for RCB stars during declines. Shenavrin *et al.* (1979) obtained infrared photometry for a few dates during the 1977 minimum of R CrB and resolved a component with an estimated temperature of 1850 K in addition to the permanent 700 K shell. They assigned this 1850 K component to the obscuring dust and, by assuming that the dust was in the form of a circumstellar shell, found that the dust was close to the photosphere. They suggested that the dust was expelled through radiation pressure. Considering the circumstellar shell proposal as an alternative to the line of sight cloud model, to obscure the star by 5–7 mag, the radius of an 1850 K circumstellar shell would need to be $\sim$ 15 stellar radii (assuming $R_{\rm RCB}$ = 70–85 $R_\odot$). The radiation from such a shell with a temperature of 1850 K and a luminosity of $\sim 10^4$ $L_\odot$ (comparable to the luminosity of the obscured star) would be readily detected. Thus, we consider that the obscuring dust is not in the form of a circumstellar shell.

There was some indication of a weak $I$ band excess during the 1988 decline of NSV 6708 which may have been attributable to the obscuring cloud (Section 4.3.3). We note that a weak infrared source similar to that observed by Shenavrin *et al.* (1979) would be harder to detect in NSV 6708 as the circumstellar shell surrounding this star is hotter ($\sim$950 K) than that surrounding R CrB (650–700 K). A higher temperature shell would more effectively mask the flux of a hotter, but less luminous, cloud.

### 3.1.5.3 The decline onset phase

In Section 3.1.4.1 we adopted the approach of setting day 0 for the decline as the day when the $V$ mag was below the normal minimum of the semi–periodic variations. This approach permits some comparison of timescales to be made with declines that have not been covered in detail with photoelectric photometry. With access to photoelectric data a more accurate estimate of the actual time of decline onset can be made. The initial decline light curve will be affected by the phase of the semi–regular variations at which the decline begins as well as the colour type of the decline. In a 'red' decline the accuracy of the onset time is limited by the ability to determine the date at which the colour curves showed a redward trend. The 1985 decline of R CrB and the 1988 decline of NSV 6708 are examples. It is clear from the light and colour curves for the 1985 decline of R CrB (Fig. 3.15b; Fernie, Percy & Richer 1986) that the decline onset occurred near $V_{\rm max}$. In the 1988 decline of NSV 6708 (Section 4.3.2), we estimated the decline onset phase $\phi = 0.1$ assuming a period $P = 110$ d and that $V_{\rm max}$ defined $\phi = 0.0$. In a 'blue' decline the obscuring dust cloud is presumed to initially shield only a fraction of the photosphere. Correspondingly, if effects such as limb–darkening and the rising contribution from the chromosphere are initially small, the colour curves will show no initial indication that a decline is in progress. We see this effect in the colour curves of the 1988, and to a lesser extent the 1983, decline of R CrB. We note that if only visual estimates are available for a decline, or if photometry has only been obtained after the visual discovery of a decline, then the decline onset time is highly uncertain. The uncertainty may range from 5–10 d if the decline type can be confirmed to be an extreme 'red' type, to perhaps 20–30 d if the decline type is an extreme 'blue' type.

The photometric survey of RCB stars at MJUO (Chapter 2) has shown that, with the well documented exception of RY Sgr, the light and colour variations observed in all RCB stars are generally in phase. (In RY Sgr the colour curves lead the $V$ curve by 4–8 d; see Section 2.4.1.5.) Published photometry of R CrB (see e.g.; Fernie, Percy & Richer 1986, Böhme 1983, Böhme 1985) indicate that the light and colour variations of R CrB also appear to be in phase.

If we assume phase coherency between the light and colour variations in R CrB, we find that the actual decline onset for the 1988 decline most probably occurred around the time of the colour minimum near JD 2447335–2447340 (see Fig. 3.1b), which is 15–20 d prior to the 'day 0' defined in Section 3.1.4.1. These Julian Dates correspond to the beginning of the standstill in the $V$ mag (see Fig. 3.1a). We associate the colour maximum near JD 2447360 with the pulsations of R CrB, as the maximum occurred 20–25 d after the minimum near JD 2447335–2447340 (which corresponds to $\sim 0.5$ cycles assuming a mean pulsation period of 40–45 d). This maximum occurred when the $V$ mag was $V{\approx}6.3$, or when R CrB was already $\sim 0.5$ mag below its normal mean mag at maximum light. Using the same argument, the peak seen in the $V$ light curve near JD 2447400 could be due to the pulsation related maximum 1.5 cycles (60–65 d) after the standstill. This argument may also hold for the feature observed during the initial decline of the 1983 decline.

The identification of $V_{\rm min}$ as the actual decline onset phase would appear to be at odds with previous studies that have claimed that declines of RCB stars occur near $V_{\rm max}$. Pugach (1977) has shown visual light curves of RY Sgr that suggest that the declines start near $V_{\rm max}$ and are phase–locked to the pulsations of the star. Goncharova, Kovalchuk &

Pugach (1983) have claimed that a similar relationship exists in R CrB. Their analysis of decline onset times of R CrB suggested that the decline onset was related to a 40 d pulsation mode. Their interpretation has, however, been questioned by Percy, Carriere & Fabro (1987) who found little evidence for a 40 d period in more extensive data of R CrB. Recently, Fernie (1989) Fourier analysed photometry of R CrB obtained since 1971 and found evidence for a 45 d period with little indication for further frequency modulation of the light curve (except possibly during 1972).

While we believe that an accurate estimate for the decline onset phase demands high precision photometric data, it is possible that in the case of RY Sgr, visual light curves may be sufficiently accurate to determine the decline onset phase. RY Sgr has the largest amplitude light and colour variations of the stars surveyed during the RCB photometric survey at MJUO. The light and colour amplitudes regularly exceed 0.3 mag. (The large light amplitude, and the star's mean magnitude at maximum light of $V \approx 6.4$, has made RY Sgr a popular star to be observed by organisations such as the Variable Star Section of the Royal Astronomical Society of New Zealand.) It is known that RY Sgr has a radial velocity amplitude exceeding 30 $\mathrm{kms}^{-1}$ with a shock wave occurring near $V_{\mathrm{max}}$ (see Section 5.2). A possible correlation between these shock waves and the decline onsets has not been lost to us (see Section 5.2), nor to other workers (e.g. Hill 1987). (However, it is then difficult to relate the presence of shock waves in RY Sgr with the dust formation mechanism, with the low amplitude, or possible non–detection, of radial velocity amplitudes in other RCB stars.) The onset of a decline in RY Sgr has yet to be observed photoelectrically.

R CrB is known to have a radial velocity amplitude of less than 8 $\mathrm{kms}^{-1}$ (Raveendran, Ashoka & Rao 1986). Because this amplitude is too low to produce a shock wave in these helium–rich atmospheres, we might not expect the radial velocity variations to have the same phase relationship with the photometric variations that we see in RY Sgr. But it seems surprising that, despite being the subject of considerable photometric and spectroscopic study for several decades, the phase relationship between the photometric and radial velocity variations in R CrB has not been established.

#### 3.1.5.4 Decline curve models

Using simple models, we can test the hypothesis that the 1983 and 1988 declines of R CrB began near $V_{\mathrm{min}}$, and that the 1985 decline began near $V_{\mathrm{max}}$. We have assumed that the pulsational light curve of R CrB can be treated as a simple sine wave of appropriate period and amplitude, and the decline event as a simple polynomial (in our models a cubic) that gives an appropriate decline rate. In Figs. 3.17a and 3.17b, we compare $V$ photometry from the 1988 and 1985 declines with the model curves. In our model of the 1985 decline, we begin the decline at $V_{\mathrm{max}}$; in our model of the 1988 decline at $V_{\mathrm{min}}$. We have not used the same cubic function to duplicate the decline curve in both examples, but rather one that provides a 'best fit' to these data. A quick examination of the shape of the 1988 decline model shows that the standstill in the light curve (previously referred to in Sections 3.1.4.2 and 3.1.5.3), before the star rapidly decreases in brightness, is caused by the cancellation of the opposing effects of the pulsation light curve rising to $V_{\mathrm{max}}$ and the early effects of the decline curve. Likewise, the rapid decrease in the $V$ mag after this

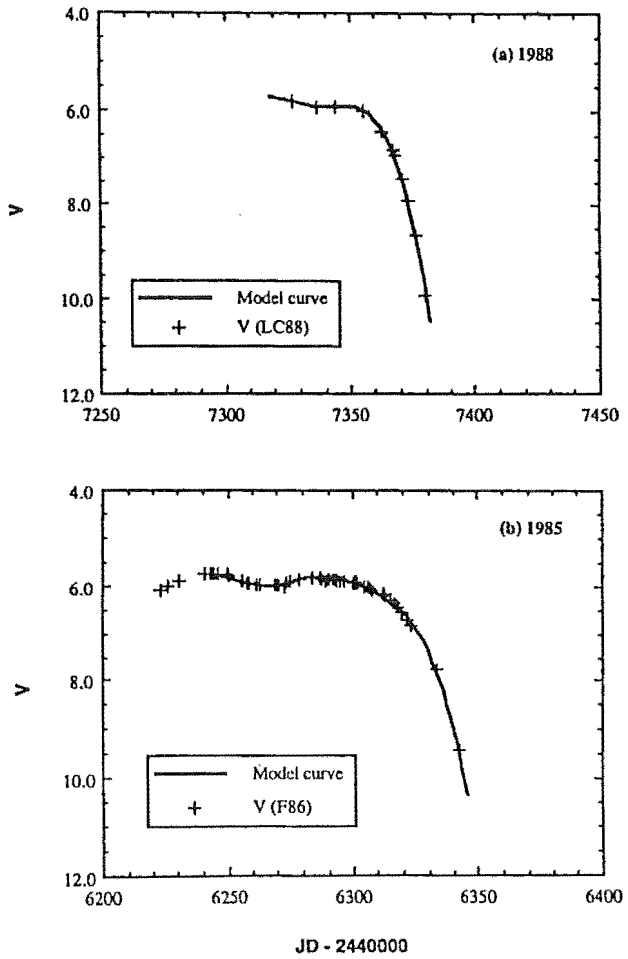


**Figure 3.17.** Decline curve models for the (a) 1988 and (b) 1985 declines of R CrB. These models indicate a decline from approximately a minimum of the pulsation cycle in (a) and a maximum of a pulsation cycle in (b).

standstill is enhanced by the star fading from $V_{\max}$ to $V_{\min}$ on its pulsation cycle as well as the effects of the decline.

### 3.1.5.5 Interaction between the declines and pulsations

The possible connection between the decline curves and the pulsations of RCB stars has been hinted at, but never seriously examined. Our observation of features in the early decline light curves of the 1983 and 1988 declines of R CrB almost certainly point towards some interplay between the varying luminosity of the underlying RCB star and the rate of obscuration due to the dust cloud. These features occur at times where we would expect a pulsation maximum in the light curve, if the star were not in decline.

RY Sgr provides the most compelling evidence that this interplay is not only confined to the initial decline of these stars. In the early stages of the 1967 decline, Alexander

*et al.* (1972) commented that the time difference between the decline onset and a hump observed in the decline light curve (see Alexander *et al.* 1972, fig. 1) was roughly 40 d, a value comparable to the pulsation period of RY Sgr (Sections 2.4.1.4 and 5.1.3). In Section 5.1.3, we found that between the years 1948 and 1989, the times of maxima on the light curve of RY Sgr were best represented by four linear solutions. Although the peak of the hump was not well observed, and there was some indication of structure in this feature, the peak occurred near JD 2439720. The predicted time of this maxima is JD 2439713.

The hump observed in the 1967 decline was dwarfed by the feature observed during the 1982 decline of RY Sgr (for a visual light curve, see Fig. 5.5). Although the onset of this decline was not observed, the visual estimates indicated that the magnitude of RY Sgr decreased to mag 12.5, in about 50 d, before rising to mag 8.5. The star remained between mag 8.5 and 8.7 for nearly 40 d before declining again to mag 12. The width of this feature hints at a relationship with the pulsation period of RY Sgr. The Julian Dates defining the width of this feature are approximately JD 2445052 and JD 2445088 and the times of maxima are predicted at JD 2445047 and JD 2445086 respectively. The differences between the observed and predicted times of maxima are comparable to the inherent variability of the pulsation period of RY Sgr of typically 4–8 d.

#### 3.1.5.6 Alternative models

Stanford *et al.* (1988) considered a number of other models for the cause of the major declines of RCB stars. In particular, they discussed the binary star and orbiting dust cloud scenarios. They rejected these in favour of a model which incorporates the idea that the semi–regular pulsations are the cause of the decline phases. However, their spectropolarimetry suggested that there was a preferred plane for the ejection of the obscuring dust cloud, which they in turn say is indicative of nonradial pulsations. If such nonradial pulsations are to be invoked then they may provide explanations for not only the spectroscopic picture described here during the decline phase, but also the semi–regular nature of the photometric variability at maximum light (see Section 2.5.1).

#### 3.1.5.7 Beyond the decline and evolutionary connections

If our interpretation of the spectroscopic data is correct, the obscuring cloud spends a long time close to the star. Even if the heating process is very slow, some parts of the cloud could become hot enough for the grains to dissociate. Thus we would see the grain size decreasing with time. This was possibly seen by Rao, Vasundhara & Ashoka (1986) in their spectrophotometric observations taken during the recovery of R CrB to maximum light from the 1972 and 1974 declines. Also, if the recovery to maximum light were due purely to the dispersal of the cloud, the optical depth of the cloud would be proportional to the inverse square of the time since the onset. It was pointed out by Holm *et al.* (1987) that the light curve did not follow such a shape, and they invoked several (rapid) successive minima of different depths to account for this. But the optical depth is related to the grain size, increasing as the grain size decreases. If there was a trend towards smaller grain sizes with time, without any dispersal, the light curve would tend to follow a slower recovery curve than the simple inverse square law. If we then include dispersal, the light curve

could fit anywhere between these two extremes.

The eventual fate of the carbon dust cloud is uncertain. If any radial motion is present, and the cloud is moving faster than $\approx$ 60 kms$^{-1}$ (the escape velocity of a 0.7–0.9$M_{\odot}$ supergiant) it will no longer be bound to the star. At any velocity much lower than this it will fall back onto the star, unless it interacts (by some as yet unidentified mechanism) with the energy from the semi–regular variations seen in these stars or with the material ejected by the next decline. But from only 50 $R_{\star}$ each cloud would have fallen onto the star within the three years or so until the next decline. If each cloud is at some intermediate velocity then it could become bound in orbit, but from conservation of angular momentum this material would tend to collapse into a ring or disk.

Little is known about the structure of the circumstellar shell, whether it is thin or thick, or even spherical in shape. If the circumstellar shell is spherical and is thick, this may imply that each dust cloud thrown off leaves the star and that the whole shell is actually many thin shells. On the other hand, a thin circumstellar shell could be due to the interaction between the expanding clouds and the local interstellar medium, where the thin shell is replenished from below as it diffuses away from its outer edge.

For R CrB, Gillett *et al.* (1986) found a very extensive shell, beyond the ordinary circumstellar shell, extending from 0.6–4.3 pc from the star. They suggested this was the old hydrogen envelope of R CrB and that whatever process had removed this envelope had finished about $3 \times 10^4$ yr ago. A similar shell was detected surrounding SU Tau (but not surrounding RY Sgr which appears as a point source at *IRAS* resolutions; see Walker 1986). If this mass loss event was separate from the current decline process then these declines would only have started after this time.

### 3.1.6 CONCLUSIONS

We have obtained and analysed photoelectric and both high ($\Delta\lambda \approx$ 0.2–0.7Å) and low ($\Delta\lambda \approx$ 10Å) resolution spectroscopic observations of the 1988 decline of R Coronae Borealis (R CrB).

The photometric data have enabled us to compare the colour curves of the present decline with those of previous declines of R CrB and also with the declines of other RCB stars, e.g., RY Sgr, NSV 6708 and UW Cen. We have identified two extreme types of colour decline, which we have termed 'blue' and 'red'.

The 'blue' type show a blueward trend in the ($U$–$B$) and ($B$–$V$) colours after the star begins to decline in $V$. The cause of the blue trend is increased flux in the $U$, $B$ and $V$ filter bands relative to the $R$ and $I$ bands. The enhancement of these fluxes is due to broad emission ($\lambda\lambda$3900–5700Å) which can be seen in one of our low resolution ($\Delta\lambda \approx$10Å) spectra. The appearance of this feature during a 'blue' decline and its subsequent disappearance as the decline progresses as well as its non–detection during 'red' declines leads us to believe that it is chromospheric in origin. It is probably due to unresolved chromospheric emission lines or continuum emission or a combination of both. From these observations a 'blue' decline follows the conventional model for an RCB star decline, as outlined by Feast (1986) for the 1969 decline of RY Sgr (Alexander *et al.* 1972).

In contrast, the 'red' type declines show all colours reddening as soon as the $V$ mag declines. We suggest that the 'red' declines will have no broad–band emission in their

spectra, as there is no indication of colour changes that could be attributed to such emission in the early stages of a 'red' decline (see Fig. 4.1b). This is further supported by spectroscopy of the 1988 decline of NSV 6708 which indicates that the transition from a photospheric to a chromospheric dominated spectrum occurred when the star was 4–5 mag below maximum light. By this time the star was heavily reddened by the intervening dust. We suggest that, in a 'red' decline, the entire visible hemisphere of the photosphere and much of the inner chromosphere (which may be the location of the broad emission observed in a 'blue' decline) is obscured almost simultaneously.

The identification of two extreme types of colour behaviour should not be taken to mean that there are just two types of decline. We suggest that this bifurcation is caused by the size of the dust cloud upon the initial condensation of the dust. In particular, the timescale for the spectral and photometric changes seen during a decline will be dependent upon the size of the cloud in comparison to that of the photosphere. If the size of the obscuring cloud, upon condensation, is less than the size of the photosphere, then a 'blue' decline will be observed and the decline will progress in a manner similar to that observed for the current decline. If the size of the obscuring cloud is larger than both the photosphere and the inner chromosphere upon condensation, then a 'red' decline will be observed. If the size of the cloud is comparable to the that of the photosphere, then the characteristics of the decline should appear intermediate to those of the extreme types.

The spectroscopic data for this decline includes, for the first time, observations obtained from immediately prior to the onset of the decline through the first 20 d of the decline.

At high resolution we have observed the gradual filling–in of the absoption spectrum, followed by a rapid transition to a chromospheric emission spectrum. This rapid phase coincides with the appearance of high velocity Na I *D* emission and a change in the velocity measured for many of the lines. There also seems to be a relationship between these effects and the broad emission feature.

As a consequence of this work, a number of additional observational tests have become evident. The relative occurrence of the different colour types in RCB star declines may yield important information about the dust formation process in RCB stars. Factors such as the projection angle of the cloud (with respect to the star), the condensation radius and the direction of growth (laterally or radially) of the cloud (see Section 3.1.5.2) may become resolvable with the availability of additional data. In particular, infrared data obtained during declines may offer clues about the size and location, and the eventual fate, of the dust cloud.

Confirmation of the findings of this chapter requires simultaneous spectroscopic and photometric observations at different wavelength regions during a number of declines, and quantitative modelling of the evolution of dust clouds in the vicinity of RCB stars. More specifically, it is useful to make some comments about the types of data that could be obtained in the future.

(i) We noted in Section 5.2 that it is very difficult to distinguish between a laterally expanding cloud and one that that expands radially. Spectroscopy (including the 1–5$\mu$m region), polarimetry and multi–colour photometry of the star and its circumstellar shell is needed to identify the structure, composition and development of the obscuring cloud during a decline. We still do not know in any detail what ultimately happens to the cloud

material.

(ii) To improve our understanding of the triggering mechanism we need more data during the very early stages of many more declines. For example, to identify the decline type photometry is needed in the first 20 d. By this stage the star has already undergone some significant spectroscopic changes, which need to be monitored. In particular, we need to explore any connection between the appearance of the high velocity emission, the 'step' in the velocities measured for the low velocity material and the rapid change from an absorption to emission line spectrum.

(iii) The abrupt appearance of the high velocity emission, and its possible interaction with the circumstellar material, needs to be probed in greater detail. As indicated in Section 4.3, it seems likely that there is high velocity gas at 50 $R_\star$, as well as the dust cloud much closer to (and still obscuring most of) the stellar photosphere. Any model of the decline phase must have a means by which this situation can be achieved from what appears to be a single triggering mechanism.

(iv) Another important feature of the early stages of the decline is the broad emission hump. More frequent and extensive spectrophotometry is required to determine its waxing and waning and also its extent in wavelength space. Also, is it a continuum emission, a very broad line emission, or a combination of many unresolved individual lines, or even a combination of all three of these?

(v) The detection by Gillett *et al.* (1986) of the very large (8 pc) circumstellar shell around R CrB, and their tentative connection of this with the old hydrogen envelope, suggests that high sensitivity and high spatial resolution (e.g. radio) maps of R CrB itself, and other members of the class, could provide information about the existence of shells around other members, the composition of this shell, and also the evolutionary status of these stars.

# 3.2 Declines of S Apodis and V Coronae Austrini

## 3.2.1 INTRODUCTION

There are relatively few declines where observations have been obtained throughout these events. Only two declines have been covered both photometrically *and* spectroscopically throughout a greater part of the duration of the decline. These declines are the 1967–1971 decline of RY Sgr (Alexander *et al.* 1972) and the 1988–1989 decline of R CrB, which was discussed in Section 3.1. The decline of RY Sgr was observed extensively throughout the decline minimum until after the star had returned to maximum light, but the initial decline phase was only observed visually. The decline of R CrB was observed extensively from prior to the decline onset until after the $V$ mag of the star had begun to brighten after the decline minimum. Thereafter only a few spectra, and little photometric data, were obtained as the star returned to maximum.

We noted in Section 3.1 that early decline phases have been observed photoelectrically in a number of declines, but due to factors such as telescope and instrument scheduling constraints, the faint $V$ mag of the star near minimum and seasonal breaks in observing, these observations have been continued throughout a decline in only a few cases. Examples of declines where published photoelectric data covers the initial decline include the 1983 (Böhme 1983) and 1985 (Böhme 1985; Fernie, Percy & Richer 1986) declines of R CrB and the 1988 decline of NSV 6708 (Kilkenny & Marang 1989; Chapter 4). Yefimov (1988) has published light curves derived from *UBVR* photometry that cover significant portions of the 1977, 1983 and 1986 declines of R CrB, but we are not aware that these data have been published in a tabular form except for some data of the 1977 decline (Shenavrin *et al.* 1979). In most cases, declines are only observed visually (Fig. 5.5).

Spectroscopic observations of declines have been limited to relatively few cases and, in addition to the 1967 decline of RY Sgr and the 1988 decline of R CrB, these include the 1948 (Herbig 1949), 1963 (Payne–Gaposchkin 1963) and 1983 (Holm *et al.* 1987) declines of R CrB.

Alexander *et al.* (1972) commented that the correct interpretation of the complex photometric behaviour observed during declines requires complementary spectroscopy. Much of this complex behaviour is observed in the colours of the star, which are driven by the relative contribution of the photosphere, chromosphere and the effects of the obscuring material, throughout the decline. Spectroscopic data are required to fully interpret the changes occurring throughout the decline.

However, a comparison of declines observed photoelectrically enable a comparative study of these events. In the absence of spectroscopic information, but with a knowledge of the *general characteristics* of these events, photometry of a decline can be interpreted within the framework of earlier such events. In addition, the ease of obtaining and analysing photometric data, compared to that of spectroscopic data, will always mean that more declines will be observed photometrically than spectroscopically.

In this Section we discuss MJUO photometry of the 1989 decline of S Aps and the 1988 decline of V CrA. These events were announced by Lawson, Kilmartin & Gilmore in *IAU* Circs. 4778 and 4671 respectively, with the decline onsets occurring near JD 2447650 (1989 April) and JD 2447430 (1988 September) respectively. We compare the photometry

of these events with photoelectric data for other declines, in particular; the 1977, 1981, 1983, 1985 and 1988 declines of R CrB (see Section 3.1.5.1); the 1967 decline of RY Sgr (Alexander *et al.* 1972); the 1986 decline of UW Cen (Section 3.1.5.1) and the 1988 decline of NSV 6708 (Section 4.3.2). These declines are discussed in Section 3.2.4.

### 3.2.2 OBSERVATIONS

The observations of these declines were obtained differentially at MJUO with respect to nearby comparison stars. These magnitudes were then reduced to the standard system as discussed in Section 2.2. The comparison and check stars used for each star were listed in Table 2.1. The *UBVRI* observations of S Aps from JD 2447556–2447916 are listed in Table 3.6 and the *UBV* observations of V CrA from JD 2447361–2447863 are listed in Table 3.7. We have listed observations obtained from about 100 d prior to the decline onset for both stars. Thus there is some overlap between the observations discussed here and those reported in Chapter 2 (Tables 2.2 and 2.4, for S Aps and V CrA, respectively). The $V$ light curve and the $(U–B)$, $(B–V)$, $(V–R)$ and $(V–I)$ colour curves for S Aps are plotted in Figs. 3.18a and 3.18b. S Aps is circumpolar from MJUO and hence we have achieved a particularly good coverage of this event. The $V$ light curve and the $(U–B)$ and $(B–V)$ colour curves for V CrA are plotted in Figs. 3.19a and 3.19b.

Table 3.6. MJUO *UBVRI* photometry of the 1989 decline of S Aps.

| JD–2440000 | $V$ | $(U–B)$ | $(B–V)$ | $(V–R)$ | $(V–I)$ | JD–2440000 | $V$ | $(U–B)$ | $(B–V)$ | $(V–R)$ | $(V–I)$ |
|---|---|---|---|---|---|---|---|---|---|---|---|
| 7556.130 | 9.824 | | 1.193 | 0.786 | 1.464 | 7620.065 | 9.626 | 0.712 | 1.192 | 0.777 | 1.475 |
| 7570.011 | 9.804 | | 1.194 | 0.784 | 1.463 | 7620.971 | 9.612 | 0.673 | 1.214 | 0.759 | 1.459 |
| 7571.152 | 9.812 | | 1.194 | 0.783 | 1.460 | 7623.059 | 9.636 | 0.694 | 1.222 | 0.776 | |
| 7572.963 | 9.795 | 0.688 | 1.204 | 0.766 | 1.496 | 7628.064 | 9.708 | 0.704 | 1.225 | 0.779 | 1.462 |
| 7588.198 | 9.772 | 0.687 | 1.186 | 0.777 | | 7636.037 | 9.827 | 0.659 | 1.230 | 0.775 | 1.389 |
| 7590.137 | 9.781 | | 1.172 | 0.779 | | 7644.060 | 9.878 | | 1.232 | 0.796 | 1.534 |
| 7592.104 | 9.762 | | 1.204 | 0.787 | | 7652.149 | 10.091 | 0.680 | 1.254 | 0.795 | 1.501 |
| 7611.035 | 9.754 | 0.666 | 1.202 | 0.772 | 1.459 | 7653.808 | 10.166 | 0.707 | 1.268 | 0.800 | 1.506 |
| 7612.161 | 9.725 | 0.661 | 1.209 | 0.767 | 1.448 | 7654.921 | 10.238 | | 1.280 | 0.789 | 1.460 |
| 7616.177 | 9.668 | 0.612 | 1.207 | 0.771 | 1.504 | 7655.851 | 10.268 | | 1.266 | 0.804 | 1.588 |
| 7657.111 | 10.359 | | 1.280 | 0.824 | 1.576 | 7693.960 | 13.361 | | 1.505 | 0.965 | 1.893 |
| 7659.954 | 10.479 | | 1.308 | 0.810 | 1.628 | 7699.992 | 14.176 | | 1.498 | 1.017 | 1.977 |
| 7661.854 | 10.611 | | 1.297 | 0.816 | 1.468 | 7705.018 | 14.471 | | 1.569 | 0.979 | 1.939 |
| 7663.997 | 10.773 | 0.684 | 1.331 | 0.844 | 1.519 | 7706.049 | 14.642 | | 1.499 | 1.045 | 2.014 |
| 7673.949 | 11.409 | | 1.351 | 0.876 | 1.658 | 7707.880 | 14.694 | | 1.523 | 1.070 | |
| 7676.938 | 11.673 | | 1.394 | 0.866 | 1.735 | 7713.930 | 14.996 | | | | |
| 7680.910 | 12.029 | 0.741 | 1.437 | 0.888 | 1.715 | 7728.845 | 15.176 | | | | |
| 7683.026 | 12.214 | 0.702 | 1.458 | 0.903 | 1.745 | 7729.850 | 15.164 | | | | |
| 7686.180 | 12.558 | | 1.506 | 0.920 | 1.756 | 7730.949 | 15.302 | | | | |
| 7690.856 | 13.162 | | 1.568 | 0.956 | 1.853 | 7731.895 | 15.268 | | | | |
| 7734.920 | 15.387 | | | | | 7795.931 | 13.296 | | 1.736 | 1.071 | |
| 7747.049 | 15.026 | | | | | 7817.948 | 13.158 | | 1.791 | 1.110 | |
| 7758.912 | 14.215 | | | | | 7829.939 | 13.181 | | 1.826 | 0.979 | |
| 7759.909 | 14.229 | | | | | 7880.134 | 10.809 | | 1.484 | 0.900 | |
| 7765.998 | 14.071 | | 1.802 | 1.019 | | 7900.936 | 10.517 | 0.810 | 1.341 | 0.873 | 1.673 |
| 7770.931 | 14.123 | | 1.716 | 1.059 | | 7910.115 | 10.477 | 0.885 | 1.340 | 0.866 | 1.637 |
| 7772.970 | 14.197 | | 1.859 | 1.118 | | 7912.079 | 10.475 | | 1.332 | 0.827 | 1.568 |
| 7773.879 | 14.124 | | 1.864 | | | 7914.139 | 10.484 | 0.856 | 1.344 | 0.841 | 1.627 |
| 7774.897 | 14.201 | | 1.786 | 1.009 | | 7916.113 | 10.454 | 0.840 | 1.349 | 0.842 | 1.630 |
| 7791.897 | 13.482 | | 1.693 | 1.105 | | 7922.039 | 10.411 | | 1.318 | 0.820 | 1.591 |
| 7923.157 | 10.413 | 0.812 | 1.333 | 0.828 | 1.593 | 7924.154 | 10.356 | 0.770 | 1.334 | 0.835 | 1.596 |

**Table 3.7.** MJUO *UBV* photometry of the 1988 decline of V CrA.

| JD-2440000 | *V* | (*U*-*B*) | (*B*-*V*) | JD-2440000 | *V* | (*U*-*B*) | (*B*-*V*) |
|---|---|---|---|---|---|---|---|
| 7361.093 | 9.984 | | 0.722 | 7418.009 | 9.897 | 0.260 | 0.707 |
| 7367.951 | 10.043 | 0.252 | 0.702 | 7427.998 | 9.903 | 0.235 | 0.716 |
| 7370.919 | 10.045 | 0.312 | 0.704 | 7436.958 | 10.006 | 0.277 | 0.697 |
| 7376.013 | 10.010 | 0.237 | 0.712 | 7439.985 | 10.064 | 0.263 | 0.707 |
| 7380.112 | 9.949 | | 0.725 | 7455.859 | 10.574 | 0.293 | 0.730 |
| 7394.986 | 9.899 | 0.235 | 0.698 | 7464.865 | 11.083 | 0.332 | 0.756 |
| 7397.060 | 9.912 | 0.266 | 0.711 | 7466.876 | 11.221 | 0.207 | 0.752 |
| 7401.008 | 9.922 | 0.263 | 0.709 | 7479.897 | 12.748 | 0.502 | 0.956 |
| 7408.125 | 9.881 | 0.288 | 0.700 | 7481.891 | 12.950 | | 1.092 |
| 7413.009 | 9.892 | 0.242 | 0.697 | 7486.912 | 13.181 | | 1.255 |
| 7487.907 | 13.236 | | 1.368 | 7731.158 | 13.638 | | 1.295 |
| 7488.909 | 13.228 | | 1.367 | 7735.089 | 13.557 | | 1.203 |
| 7489.907 | 13.085 | | 1.562 | 7771.042 | 12.539 | 0.655 | 1.072 |
| 7620.166 | 14.815 | | | 7792.969 | 11.395 | 0.677 | 0.999 |
| 7636.104 | 13.192 | | 1.220 | 7799.016 | 11.126 | 0.416 | 0.946 |
| 7657.185 | 13.226 | | 1.086 | 7818.991 | 10.870 | 0.525 | 0.917 |
| 7664.224 | 13.501 | | 1.227 | 7832.958 | 11.107 | 0.690 | 0.974 |
| 7677.151 | 14.001 | 0.630 | 1.145 | 7842.921 | 11.320 | 0.934 | 1.090 |
| 7729.125 | 13.637 | 0.650 | 1.047 | | | | |
| 7729.896 | 13.590 | 0.692 | 1.213 | | | | |

## 3.2.3 DESCRIPTION OF THE DECLINES

### 3.2.3.1 The 1989 decline of S Aps

The decline onset of S Aps occurred near JD 2447650 with the $V$ mag of the star fading on an initial timescale $t_{1/2} \approx 13$ d, where $t_{1/2}$ defines the time for the star to fade to half its brightness prior to the decline onset. The star faded from $V \approx 9.9$ to a minimum of $V \approx 15.3$ in 90 d. Note that the decline onset appears to occur near $V_{\rm min}$ on the pulsation–related light curve, but due to the complex nature of the variations of S Aps (see Section 2.4.1.1) we cannot be certain about the decline onset phase or if the decline appears linked to one of the modes of pulsation.

The colours of S Aps, with the possible exception of the ($U$–$B$) index, redden from JD 2447650 and therefore we classify the decline as being a 'red' type (Section 3.1.5.1). Note the linearity of the photometry obtained during the initial decline in the colour–mag diagram (Fig. 3.20). We have connected those data obtained during the initial decline with a solid line and those obtained during the rising branch with a dashed line. The reddening terms $A_V/E(B\text{–}V) \approx 10.3$ (prior to $V \sim 13$) and $A_V/E(V\text{–}R) \approx 20.0$ define the extinction characteristics of the obscuring cloud. Note that there is a deviation from the reddening relationship for the ($B$–$V$) index of $\sim 0.15$ mag when $V \sim 14.5$. This $B$ mag excess is similar to that noted for the 1988 decline of NSV 6708 (see Section 4.3.4 and Fig. 4.5) and may be due to chromospheric emission. Note that this deviation occurs about 3 mag below maximum for S Aps whereas it occurred about 4 mag below maximum for NSV 6708. Fig. 3.20 also indicates that the ($B$–$V$) colour reddened by $\sim 0.15$ mag, from the extrapolated reddening relationship, when the star was $V \sim 14.5$. Without accounting for the possible effects of emission, the star reddened by $\sim 0.3$ mag. Correspondingly, the ($V$–$R$) colour reddened by $\sim 0.07$ mag. Although the $V$ mag reached a minimum of $\sim 15.4$, the colour data was not considered to be reliable when $V > 15$. Despite fewer observations being made during the decline minimum and the rise in the $V$ mag, the reddening relationships for both colours appear similar to that of the initial decline between $V = 14.5$–$10.7$ but with the colours reddened by $\sim 0.15$ and 0.07 mag for the ($B$–$V$) and ($V$–$R$) colours

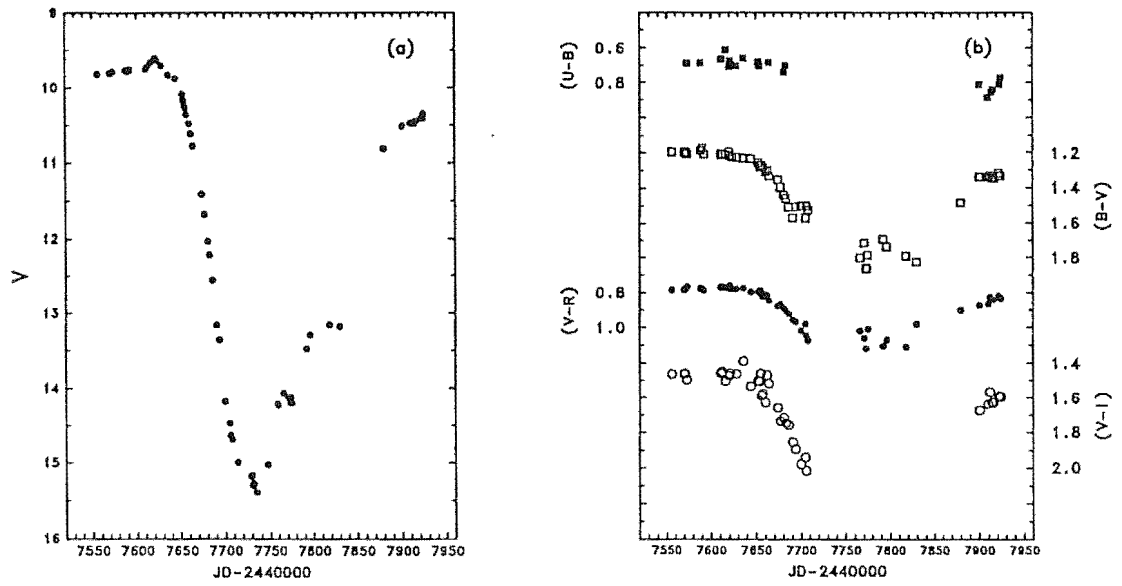


**Figure 3.18.** Light (a) and colour (b) curves for the 1989 decline of S Aps.

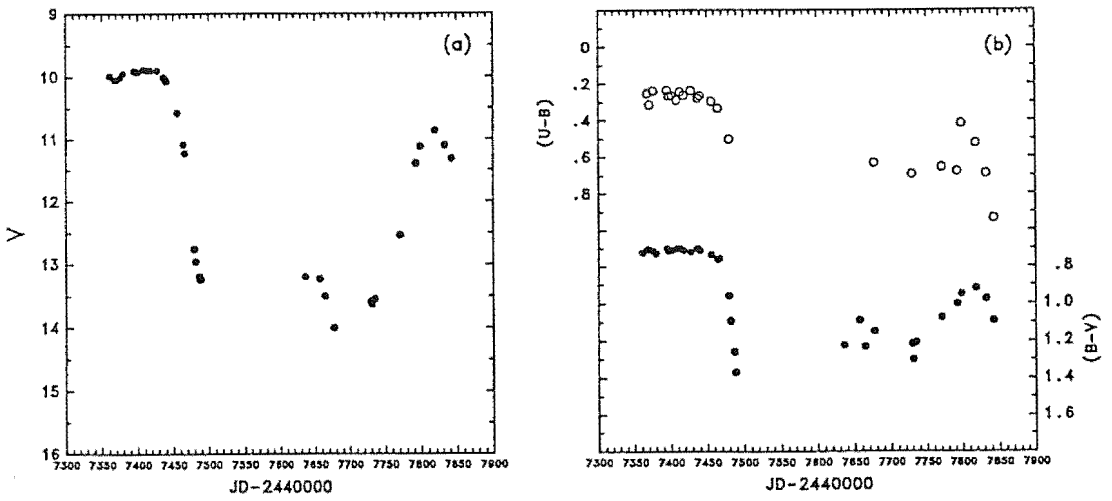


**Figure 3.19.** Light (a) and colour (b) curves for the 1988 decline of V CrA.

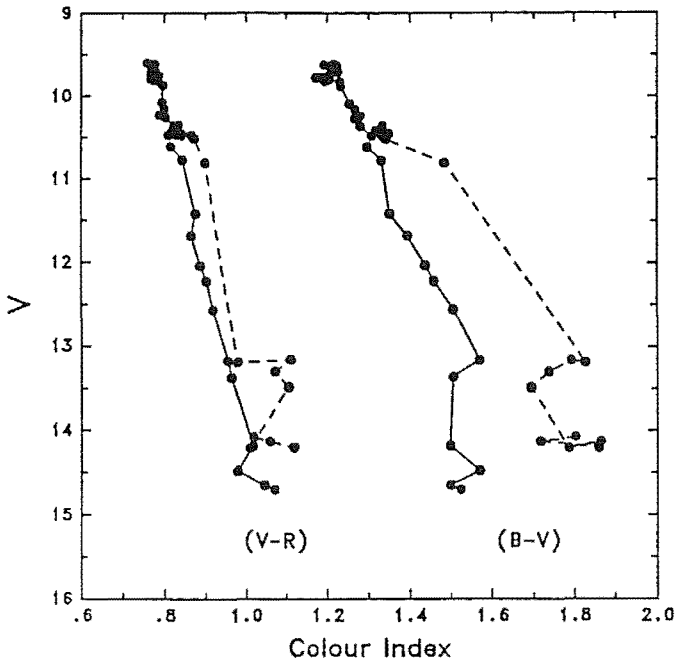


**Figure 3.20.** $(V\text{–}R)/V$ and $(B\text{–}V)/V$ colour–mag diagrams for the 1989 decline of S Aps. Note the linearity of the initial decline (points joined by solid lines) in $(V\text{–}R)$, and in $(B\text{–}V)$ prior to $V \approx 13$ (for reasons, see text). The points joined by dashed lines are those obtained during the rise to maximum light.

respectively. At $V < 10.7$, the colours show a rapid transition back to the relationship observed during the initial decline. At the end of the observations considered here, the $V$ mag had brightened to 10.4 which is 0.6–0.8 mag below the magnitude of the star at maximum.

In Fig. 3.21 we plot the photometry of S Aps in the colour versus $(B\text{–}V)$ plane. The slope of these data in these colour–colour planes, for those data obtained during the initial decline, were 0.0–0.1 for $(U\text{–}B)$, $\sim 0.3$ for $(V\text{–}R)$ and $\sim 1.2$ for $(V\text{–}I)$. These values are different from those observed during the 1988 decline of NSV 6708, which was also a 'red' decline (see Section 4.3.2). For NSV 6708 the slopes in the $(V\text{–}R)$, and $(V\text{–}I)$, versus $(B\text{–}V)$ planes were similar to those of interstellar reddening (0.78 and 1.60 respectively; see Schultz & Weimer 1975). We also note that Fernie, Percy & Richer (1986), who obtained photometry of the 1985 decline of R CrB, which was a 'red' decline (Section 3.1.5.1), observed that the reddening in the $V$ versus $(U\text{–}B)$, and $(B\text{–}V)$, planes were similar to the interstellar values.

Note that, in Fig. 3.21, the $(V\text{–}R)$ and $(V\text{–}I)$ colours obtained on the rising branch of the decline are similar to those obtained during the initial decline and hence are indistinguishable in this figure. However, the $(U\text{–}B)$ data obtained on the rising branch are $\sim 0.13$ mag bluer for a similar $(B\text{–}V)$, compared to those obtained during the initial decline, which may indicate some evolution of the obscuring material during the decline (see Section 3.2.5).

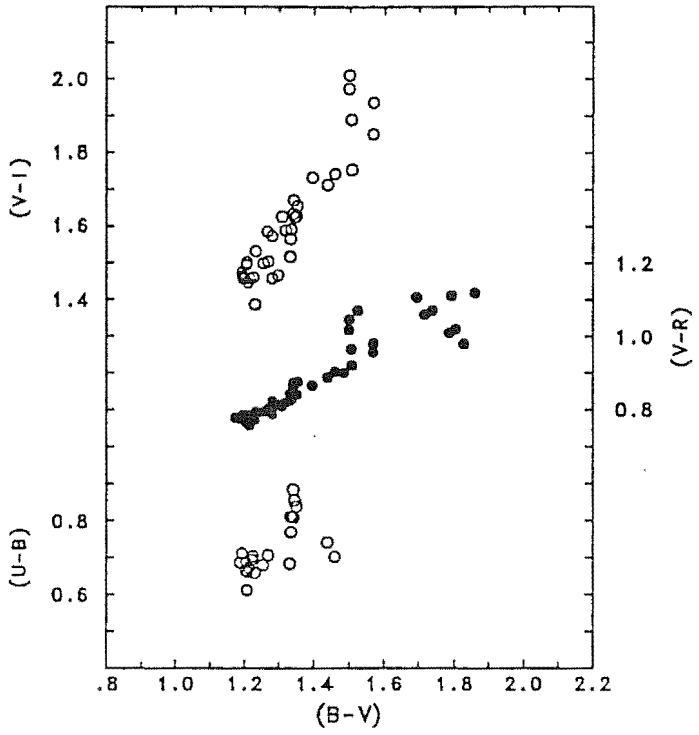


**Figure 3.21.** Colour–colour diagram for the 1989 decline of S Aps.

### 3.2.3.2 The 1988 decline of V CrA

The decline onset of V CrA occurred near JD 2447430 with the $V$ mag of the star fading on an initial timescale $t_{1/2} \approx 30$ d. The star faded from $V \approx 10.0$ to $V \approx 13.3$ in $\sim$ 60 d. The conjunction of V CrA with the Sun prevented photometry from being obtained between 1988 December and 1989 April. However, visual estimates are able to be obtained under twilight conditions, and these indicated that the magnitude of the star remained near $V = 14$ during this interval (Bateson 1989). A change in the $V$ mag of $\sim 1.0$ mag was observed near JD 2447650 before the star rose from $V = 14$–10.8. After JD 2447820 the $V$ mag faded to $V = 11.3$ which may signal another decline, or possibly pulsation–related variations similar to those discussed in Section 2.4.1.3.

For $\sim$ 35 d after the decline onset (to JD 2447465) the $(U\text{–}B)$ and $(B\text{–}V)$ colours of V CrA remained similar to the values observed at maximum light of 0.25 and 0.70 mag respectively. At JD 2447465 the $V$ mag of the star had faded to 11.1. Thereafter the colours reddened rapidly as the star faded to $V = 13.3$. Thus the decline of V CrA more closely resembled a 'blue' decline in that the colours did not redden at the decline onset (see Section 3.1.5.1). However, the colours did not become bluer than those at maximum light which may indicate that the decline type was an intermediate type with a colour behaviour between those of the 'blue' and 'red' types. A further comment is that the lack of changes in colour could be interpreted as the obscuring dust cloud having neutral

extinction [$A_V/E(B\text{-}V) = \infty$] during the initial decline. This interpretation is consistent with the model of a 'blue' type decline (Section 3.1.5.1) which assumes that the dust cloud is initially optically thick and obscures only a limited area of the photosphere. [Two contributions that might affect the colours during the initial stages of a 'blue' type decline are limb-darkening and chromospheric emission (although these will have an opposite effect upon the colours if both are present).]

The behaviour of the decline in the $V$ versus $(B\text{-}V)$ mag-colour plane is plotted in Fig. 3.22. As in Fig. 3.20 we have joined those data obtained during the initial decline with a solid line, and those obtained during the rise with a dashed line. Notice the colour behaviour during the initial decline as outlined above. During the rising branch the reddening term $A_V/E(B\text{-}V) \approx 9.7$. To calculate this value we ignored the two data points obtained after JD 2447820.

### 3.2.4 DECLINE COMPARSION

In the previous Section we calculated that the extinction due to the obscuring cloud $A_V/E(B\text{-}V)$ observed during the rising branch of the declines of S Aps and V CrA was $\approx$ 10.3 and 9.7 respectively. We can compare these values to those calculated for other declines. During the 1967–1971 decline of RY Sgr (Alexander *et al.* 1972) the extinction observed during 1969 was $A_V/E(B\text{-}V) = 4.3$. Pugach (1988) found that approximately

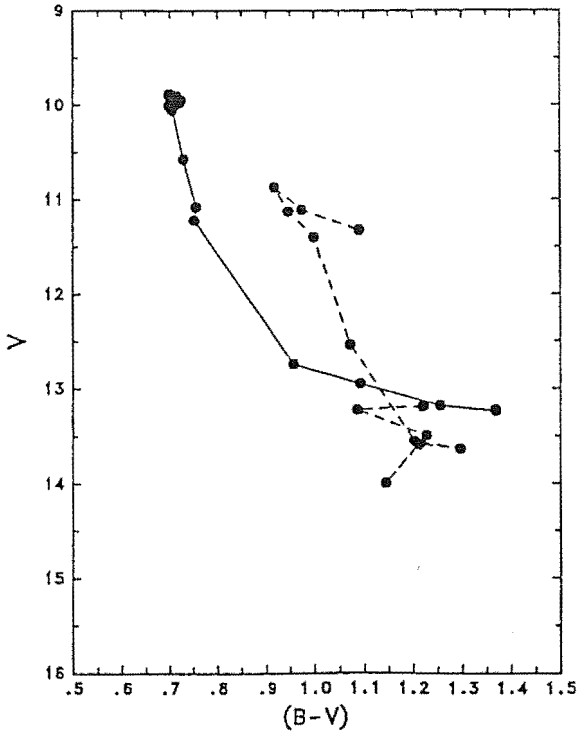


**Figure 3.22.** $(B\text{-}V)/V$ colour-mag diagram for the 1989 decline of V CrA. The data obtained during the initial decline are connected with a solid line. Those obtained during the rise to maximum are connected with a dashed line.

interstellar values could describe the reddening observed on the rising branches of the 1977, 1981 and 1983 declines of R CrB. The values determined by Pugach were $A_V/E(U–B) = 2.12$, $A_V/E(B–V) = 3.20$ and $A_V/E(V–R) = 3.81$ respectively. In Figure 3.16 we showed MJUO and SAAO $BV$ photometry of the 1986 decline of UW Cen and for this decline we derive $A_V/E(B–V) \approx 7.0$. Values of extinction for these declines and others, derived from the literature, are summarised in Table 3.8.

Feast (1986) compared the mean extinction at $UBVRIJ$ wavelengths for declines of 8 RCB stars with laboratory results for amorphous carbon particles with radii of 40Å and 150Å (Borghesi, Bussoletti & Colangeli 1985) together with ultraviolet results obtained with *IUE* for RY Sgr (Holm, Wu & Doherty 1982; Hecht *et al.* 1984). More recent ultraviolet results for the 1983 decline R CrB (Holm *et al.* 1987) are similar to those of RY Sgr. The mean extinction derived by Feast has a value for $A_V/E(B–V) \approx 4$, which is similar to the mean value for the declines of RY Sgr and R CrB in Table 3.8, but it does not reflect the more extreme values observed. In Fig. 3.23 we reproduce figure 4 of Feast (1986) but include the ultraviolet results for R CrB and, instead of a mean extinction at near–visual wavelengths, extinction at $UBVRI$ wavelengths for the declines with extreme values for $A_V/E(B–V)$, i.e. 3.2 and 10.3, in Table 3.8.

Holm *et al.* (1987) modelled the extinction of the 1983 decline of R CrB and obtained a best fit with glassy or amorphous carbon grains with a radius of 100Å (and a reasonable fit with 200Å graphite particles). There is some discrepancy between the model grain sizes of Holm *et al.* (1987) and the laboratory results of Borghesi, Bussoletti & Colangeli, but the general trend is that the extinction hump near 2400Å (4.1 $\mu m^{-1}$) is enhanced towards smaller grain sizes. Holm and his collaborators have generally preferred amorphous or glassy carbon particles to graphite as the source of extinction.

**Table 3.8.** Derived values for extinction $[A_V/E(B–V)]$ for declines of RCB stars.

| Star | Decline | $A_V/E(B–V)$ | Reference |
|---|---|---|---|
| RY Sgr | 1967 | 4.3 | Alexander *et al.* (1972) |
| R CrB | 1977<br>1981<br>1983 | 3.2 | Pugach (1988)<br>(mean of 3 declines) |
| R CrB | 1985 | 5.3 | Yefimov (1986) |
| UW Cen | 1986 | 7.0 | Section 3.1.5.1 |
| V CrA | 1988 | 9.7 | Section 3.2.3.2 |
| S Aps | 1986 | 5.7 | Marang *et al.* (1989) |
| S Aps | 1989 | 10.3 | Section 3.2.3.1 |

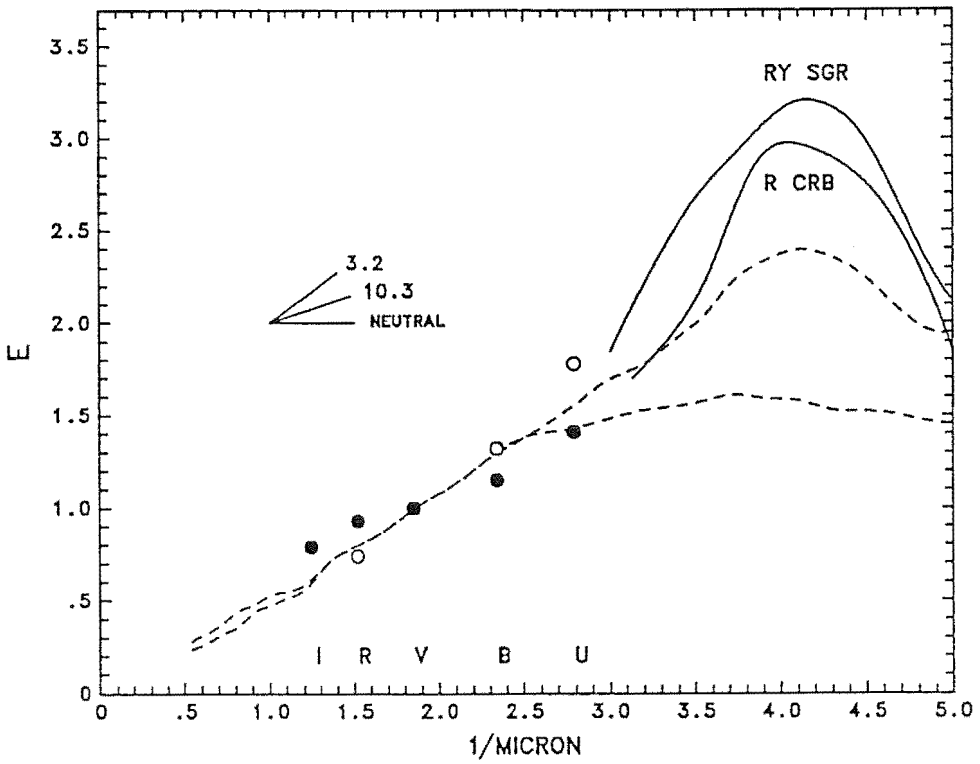


**Figure 3.23.** Extinction (E) for declines of RCB stars versus inverse wavelength ($\mu m^{-1}$) normalised to E($V$) = 1. The points are *UBVRI* photometry for the declines of Table 3.8 with values for $A_V/E(B\text{-}V)$ of 3.2 (○) and 10.3 (●). The filters are indicated at the bottom of the figure. The key in the upper left part of the figure indicates the slope for various values for $A_V/E(B\text{-}V)$. Note that the extinction is neutral when $A_V/E(B\text{-}V) = \infty$. The dashed lines are the extinction curves of Borghesi, Bussoletti & Colangeli (1985) where the upper line is for the 40Å particles and the lower line is for the 150Å particles. The solid curves are *IUE* data for RY Sgr and R CrB (and so labelled; see text).

Note that the 1983 decline of R CrB is one of the declines in Table 3.8 with a low (and essentially interstellar) value for $A_V/E(B\text{-}V)$ and this may be consistent with the extinction hump for this decline. [We have no $BV$ photometry for the decline of RY Sgr observed by Holm *et al.* (1984) with *IUE*.] A greater value for $A_V/E(B\text{-}V)$ implies a more neutral extinction for these declines, which indicates a larger particle size. [This is also consistent with the laboratory work of Borghesi, Bussoletti & Colangeli (1985).] The results of Borghesi, Bussoletti & Colangeli, in conjunction with *IUE*–based extinction measurements, indicate that near–visual photometry is a poor indicator of particle size and that this information can only be obtained at ultraviolet wavelengths. (Note that during the rising branch of the decline, the obscuring dust cloud is optically thin and obscures the photosphere and chromosphere of the star. Thus the observed extinction is not affected by changes in the relative flux contributions of the photosphere and chromosphere, as may occur during the initial decline.)

### 3.2.5 CONCLUSIONS

Observations of declines of RCB stars have indicated that there is some diversity in the photometric behaviour of these events.

Photometric data obtained during the initial decline, without the benefit of simultaneous spectroscopic data, can be interpreted within the framework of declines for which photometric and spectroscopic data *are* available. The 1989 decline of S Aps has been interpreted as a 'red' type decline on account of the trend towards redder colours at the decline onset. The 1988 decline of V CrA is either a 'blue' type or possibly an intermediate type in that the $(U–B)$ and $(B–V)$ colours remained at values near those at maximum for $\sim$ 35 d after the decline onset.

During the rise from the decline minima, the extinction $A_V/E(B–V)$ due to the obscuring shell has been observed, for a number of declines, to vary between limits of 3.2 and 10.3. The higher values imply a more neutral extinction for these declines, which indicates a larger particle size. This result is consistent with laboratory measurements of extinction. Laboratory, and *IUE* data, indicate an extinction hump near 2400Å which is highly dependent upon particle size. This result indicates that near–visual photometry is a poor indicator of particle sizes and that this information can only be obtained at ultraviolet wavelengths with, e.g., *IUE*. The best time to obtain observations that measure the extinction properties of the obscuring dust cloud is during the rising branch of the decline. During this time, the dust is optically thin and spectroscopy indicates that the spectrum of the star is similar to that at maximum light (see Section 3.1.4.3). This latter point indicates that the flux of the star is being altered only by the obscuring dust.

Rao, Vasundhara & Ashoka (1986) showed extinction curves obtained during the 1972 and 1974 declines of R CrB that indicated that there is a decrease in mean particle size as the star rises from a decline minimum. (We discussed these results in Section 3.1.5.7 as support for the idea that the cloud may be relatively close to the star and that heating of the dust could cause the grains to dissociate and so decrease in size.) A decrease in mean particle size may explain the bluer $(U–B)$ colours during the rising branch of the decline of S Aps (Section 3.2.3.1). Smaller particles cause additional extinction, as indicated by the laboratory curves in Fig. 3.23. The $U$ band is the most sensitive indicator of changes in the extinction properties of the dust that we have available for this decline.

The suggestion for future work in this area is that ultraviolet measurements obtained throughout a decline, and particularly during the rise from minimum, would be a sensitive indicator of the extinction of the obscuring dust, and its evolution with time. A point in favour of such observations is that they need not be obtained at critical phases of the decline, which would ease the scheduling requirements of such Target of Opportunity observations.

# Chapter 4

# The R Coronae Borealis star NSV 6708

## 4.1 INTRODUCTION

NSV 6708 (= V854 Cen) has attracted a great deal of interest since the star was noted to be a variable with an amplitude of $\sim$ 8 mag by McNaught & Dawes (*IAU* Circ. 4233). Much of the work in determining the type of variability of the star was done by McNaught who suggested that the star was probably an RCB star on the basis of a light curve derived from photographic records and several years of visual estimates. One of the most attractive features of this star is its magnitude at maximum of $V \approx 7$, making NSV 6708 the third brightest member of this class of 25 or so known objects (Drilling & Hill 1986).

Most RCB stars spend a majority of their time near maximum light with major declines in light due to carbon dust obscuration occurring at intervals of a few, to ten or more, years (see the visual light curves in Lawson, Cottrell & Bateson 1988, 1989). In comparison, NSV 6708 appears to have been an extremely active RCB star. McNaught (*IAU* Circ. 4245) found that the star was fainter than $B = 10$ in Harvard patrol plates obtained between 1913–37, suggesting a light curve composed of many superimposed decline light curves. This extended period at faint magnitudes, without having been observed at maximum light, is probably a major reason why the star has been observationally neglected in the past.

In this Chapter, photometric and spectroscopic observations of NSV 6708 obtained during 1988 and 1989 are discussed. The 1988 observations were obtained from about 40 d prior to the 1988 decline of this object until soon after the star reached a minimum magnitude of $V \approx 14$. The 1989 observations were obtained after the star had risen to maximum light and were continued until after the onset of the 1989 decline (McNaught; *IAU* Circ. 4936). Our observations were supplemented by SAAO observations obtained mainly during the 1988 decline (Kilkenny & Marang 1989), and by visual estimates.

## 4.2 OBSERVATIONS

Photometric (*UBVRI*) observations of NSV 6708 commenced at MJUO during 1988 May (JD 2447336) after we were informed by McNaught (personal communication to A.C. Gilmore and P.M. Kilmartin at MJUO) that the star was a suspected RCB variable star. The photometric observations were obtained with the two 0.6–m reflectors at MJUO using Bessell (1976) filters and either EMI 9558B or RCA C31034A photomultiplier tubes. The measurements were obtained differentially with respect to the comparison star HR 5449, defined during 1988 as $V = 5.740$, $(U\text{–}B) = -0.397$, $(B\text{–}V) = -0.090$, $(V\text{–}R) = -0.028$, $(V\text{–}I) = -0.064$. The observations of NSV 6708, and of a check star HR 5446, were then transformed to the standard system using mean coefficients determined from observations

of E–region standards (Cousins 1983).

During 1989, the photometry of the comparison star indicated that it was a variable star. The $V$ mag, and colours, of HR 5449 during 1989 were approximately $V = 5.60$, $(U–B) = -0.25$, $(B–V) = -0.20$, $(V–R) = -0.13$, $(V–I) = -0.34$. The 1989 observations of NSV 6708 were offset by the difference between the 1988 and 1989 $V$ mag and colours of the check star, HR 5446, so that they would remain consistent with the 1988 observations. The uncertainty in this offset should be less than 0.02 mag. Future observations of NSV 6708 should use HR 5446 as the comparison star which is currently defined as $V = 6.15$, $(U–B) = 0.87$, $(B–V) = 1.04$, $(V–R) = 0.57$, $(V–I) = 1.08$.

In addition to the uncertainty in this offset as a source of error in the photometry, the scatter in the observations of NSV 6708, and of the check star, indicated an additional uncertainty of 1–2 per cent near maximum light, increasing to 2–3 per cent near the decline minimum. The $V$, $(U–B)$, $(B–V)$, $(V–R)$ and $(V–I)$ observations of NSV 6708 are listed in Table 4.1.

A series of spectra were also obtained: at MJUO, with the 1.0–m telescope, échelle spectrograph and the Linear Diode Array (MacQueen 1986), and at Mount Stromlo Observatory (MSO) with the 1.9–m telescope, at both the Cassegrain and coudé foci, and the Photon Counting Array (Stapinski, Rodgers & Ellis 1981). Spectra were obtained in a number of key regions including the H$\alpha$, H$\beta$, Na D/5876Å He I and 6707Å Li I regions. The spectroscopic observations are listed in Table 4.2.

**Table 4.1.** MJUO *UBVRI* photometry of NSV 6708.

| JD–2440000 | $V$ | $(U–B)$ | $(B–V)$ | $(V–R)$ | $(V–I)$ | JD–2440000 | $V$ | $(U–B)$ | $(B–V)$ | $(V–R)$ | $(V–I)$ |
|---|---|---|---|---|---|---|---|---|---|---|---|
| 7336.984 | 7.212 | | 0.485 | 0.364 | 0.669 | 7379.881 | 7.101 | | 0.501 | 0.318 | 0.644 |
| 7343.922 | 7.264 | 0.193 | 0.510 | 0.386 | 0.696 | 7394.841 | 7.112 | 0.164 | 0.498 | 0.344 | 0.631 |
| 7352.948 | 7.260 | 0.190 | 0.530 | 0.397 | 0.712 | 7396.988 | 7.132 | 0.106 | 0.496 | 0.356 | 0.647 |
| 7354.898 | 7.240 | 0.191 | 0.529 | 0.402 | 0.696 | 7400.857 | 7.166 | 0.176 | 0.505 | 0.372 | 0.653 |
| 7360.949 | 7.208 | | 0.537 | 0.378 | 0.696 | 7406.902 | 7.460 | | 0.514 | 0.395 | 0.683 |
| 7362.933 | 7.222 | 0.187 | 0.536 | 0.389 | 0.704 | 7411.993 | 7.975 | 0.183 | 0.556 | 0.465 | 0.758 |
| 7367.839 | 7.193 | 0.189 | 0.538 | 0.382 | 0.681 | 7413.832 | 8.309 | 0.186 | 0.547 | 0.482 | 0.818 |
| 7370.833 | 7.168 | 0.180 | 0.528 | 0.372 | 0.665 | 7417.903 | 9.602 | 0.271 | 0.670 | 0.565 | 0.983 |
| 7372.851 | 7.155 | 0.187 | 0.518 | 0.366 | 0.662 | 7419.868 | 11.269 | | 0.791 | 0.615 | |
| 7375.880 | 7.109 | 0.172 | 0.512 | 0.345 | 0.627 | 7420.966 | 12.137 | | 0.756 | 0.591 | 1.088 |
| 7423.889 | 13.628 | | 0.824 | 0.691 | 1.343 | 7616.162 | 7.408 | 0.227 | 0.541 | 0.355 | 0.719 |
| 7427.869 | 13.868 | | 0.782 | 0.650 | 1.608 | 7620.053 | 7.412 | 0.229 | 0.543 | 0.361 | 0.697 |
| 7435.849 | 13.837 | | | | | 7621.050 | 7.420 | 0.231 | 0.537 | 0.366 | 0.734 |
| 7439.858 | 14.034 | | | | | 7623.040 | 7.449 | 0.235 | 0.544 | 0.367 | 0.698 |
| 7570.054 | 7.672 | | 0.552 | 0.396 | 0.777 | 7628.042 | 7.533 | | 0.521 | 0.376 | 0.745 |
| 7571.119 | 7.670 | | 0.567 | 0.404 | 0.785 | 7636.023 | 7.649 | 0.241 | 0.572 | 0.459 | 0.850 |
| 7573.035 | 7.757 | 0.306 | 0.608 | 0.471 | 0.882 | 7644.115 | 7.622 | 0.216 | 0.561 | 0.451 | 0.864 |
| 7588.184 | 7.951 | 0.326 | 0.649 | 0.504 | 0.965 | 7655.089 | 7.517 | 0.211 | 0.550 | 0.418 | 0.793 |
| 7592.090 | 7.914 | 0.329 | 0.634 | 0.474 | 0.912 | 7664.053 | 7.351 | 0.215 | 0.504 | 0.374 | 0.716 |
| 7611.020 | 7.390 | | 0.507 | 0.297 | 0.665 | 7674.048 | 7.426 | | 0.481 | 0.355 | 0.706 |
| 7683.005 | 7.473 | | 0.526 | 0.375 | 0.751 | 7731.856 | 8.190 | 0.266 | 0.673 | 0.460 | 0.892 |
| 7694.938 | 7.513 | 0.242 | 0.546 | 0.399 | 0.727 | 7734.880 | 8.001 | 0.278 | 0.618 | 0.446 | 0.860 |
| 7700.019 | 7.407 | | 0.497 | 0.337 | 0.696 | 7735.959 | 7.891 | 0.284 | 0.587 | 0.429 | 0.832 |
| 7704.978 | 7.405 | | 0.520 | 0.333 | 0.689 | 7736.964 | 7.806 | 0.258 | 0.601 | 0.403 | 0.802 |
| 7722.028 | 8.014 | 0.264 | 0.593 | 0.398 | 0.805 | 7746.983 | 7.377 | 0.211 | 0.541 | 0.381 | 0.725 |
| 7724.810 | 8.150 | 0.271 | 0.632 | 0.428 | 0.834 | 7755.901 | 7.379 | 0.202 | 0.550 | 0.406 | 0.752 |
| 7726.926 | 8.239 | 0.284 | 0.647 | 0.450 | 0.879 | 7759.876 | 7.399 | 0.216 | 0.539 | 0.419 | 0.765 |
| 7728.908 | 8.284 | 0.267 | 0.682 | 0.481 | 0.906 | 7765.944 | 7.366 | 0.154 | 0.503 | 0.398 | 0.738 |
| 7729.912 | 8.279 | 0.278 | 0.674 | 0.476 | 0.921 | 7770.893 | 7.301 | 0.183 | 0.516 | 0.362 | 0.683 |
| 7730.988 | 8.233 | 0.271 | 0.657 | 0.460 | 0.897 | 7772.943 | 7.286 | 0.195 | 0.479 | 0.330 | 0.664 |
| 7774.869 | 7.296 | 0.178 | 0.505 | 0.351 | 0.675 | 7798.875 | 9.238 | 0.179 | 0.694 | 0.452 | 0.869 |
| 7778.928 | 7.271 | 0.149 | 0.471 | 0.365 | 0.687 | 7799.852 | 9.552 | 0.160 | 0.785 | 0.430 | 0.903 |
| 7780.878 | 7.206 | 0.160 | 0.510 | 0.295 | 0.618 | 7860.114 | 8.632 | 0.253 | 0.677 | 0.436 | 0.851 |
| 7791.872 | 7.956 | 0.229 | 0.542 | 0.420 | 0.758 | | | | | | |

**Table 4.2.** Log of NSV 6708 spectra and radial velocity measurements.

| Year | JD–2440000 | $\lambda_{centre}$ (Å) | $v_{radial}$ (kms$^{-1}$) | $\phi$ | Comments |
|---|---|---|---|---|---|
| 1988 | 7329.09 | 6360 | -26.1 ± 1.8 | 0.45 | MJUO (6363Å [O I] region) |
| | 7329.85 | 6360 | | | MJUO (6363Å [O I] region) |
| | 7329.94 | 6580 | | | MJUO (Hα region) |
| | 7333.81 | 6580 | -25.5 ± 3.3 | 0.49 | MJUO (Hα region) |
| | 7333.87 | 6700 | | | MJUO (6707Å Li I region) |
| | 7333.91 | 5880 | | | MJUO (Na D region) |
| | 7336.05 | 6600 | | | MSO (Hα region) |
| | 7349.03 | 6580 | -24.8 ± 1.3 | 0.63 | MJUO (Hα region) |
| | 7352.92 | 6560 | | | MSO (Hα region) |
| | 7353.88 | 6560 | | | MSO (Hα region) |
| | 7353.90 | 6700 | | | MSO (6707Å Li I region) |
| | 7354.82 | 6580 | -24.2 ± 2.1 | 0.68 | MJUO (Hα region) |
| | 7357.98 | 6580 | -26.0 ± 3.2 | 0.71 | MJUO (Hα region) |
| | 7360.92 | 6560 | | | MSO (Hα region) |
| | 7360.93 | 5880 | | | MSO (Na D region) |
| | 7365.84 | 5880 | | | MSO (Na D region) |
| | 7367.82 | 6580 | -24.3 ± 2.5 | 0.79 | MJUO (Hα region) |
| | 7369.98 | 5880 | | | MSO (Na D region) |
| | 7370.87 | 6580 | -24.3 ± 3.6 | 0.83 | MJUO (Hα region) |
| | 7370.88 | 6560 | | | MSO (Hα region) |
| | 7371.90 | 6580 | | | MSO (Hα region) |
| | 7387.90 | 4700 | | | MSO (λλ 3700–5700Å) |
| | 7407.88 | 6580 | -26.0 ± 2.2 | 0.16 | MJUO (Hα region) |
| | 7412.89 | 6580 | -25.0 ± 3.8 | 0.21 | MJUO (Hα region) |
| 1989 | 7721.98 | 6560 | -23.8 ± 0.9 | | MJUO (Hα region) |
| | 7732.87 | 6560 | | | MJUO (Hα region) |
| | 7735.87 | 6560 | -26.2 ± 2.0 | | MJUO (Hα region) |
| | 7736.96 | 6560 | -27.1 ± 0.9 | | MJUO (Hα region) |

In addition to our own observations, SAAO *JHKL* photometry and spectra have been published by Kilkenny & Marang (1989). The SAAO photometry were obtained concurrently with our 1988 photometry, whereas the SAAO spectra were obtained during the 1988 decline at fainter magnitudes than were our spectra. Visual estimates of NSV 6708 have been published in *IAU* Circ. 4679, 4729, 4814, 4821, 4879 and 4936. These estimates often complete the light curve of the star in the absence of photoelectric photometry.

## 4.3 ANALYSIS AND DISCUSSION

### 4.3.1 Photometry at maximum light during 1988

Although the *UBVRI* photometry obtained during 1988 cover little more than half a cycle of NSV 6708 (Fig. 4.1a and 4.1b), SAAO *JHKL* photometry complete the light curve for about 1.5 cycles before the decline onset (Fig. 4.2). A period of $\sim$ 110 d is indicated in the light curves of NSV 6708 with maxima near JD 2447280 in the SAAO data, and

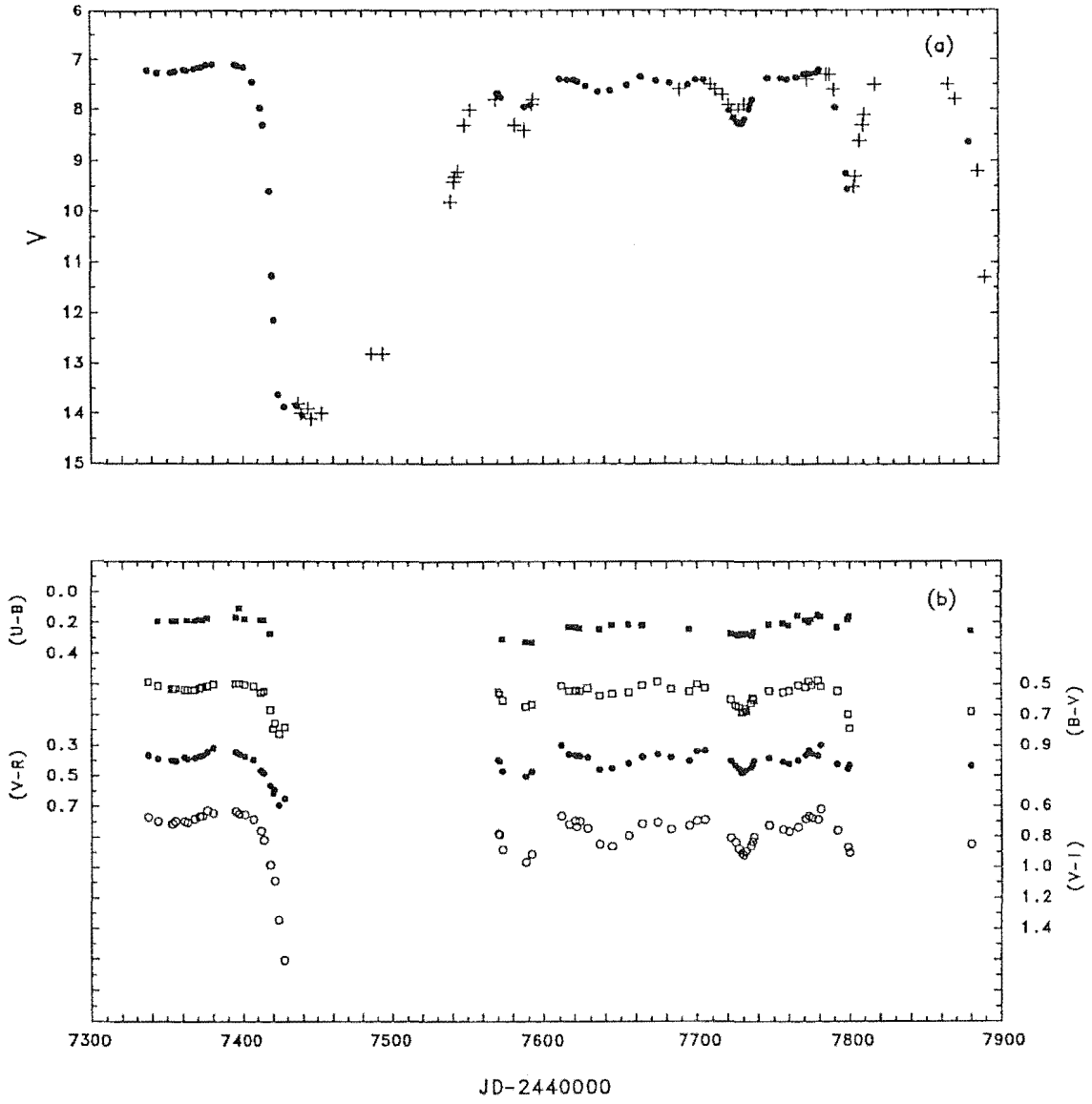


**Figure 4.1.** (a) $V$ light and (b) colour curves for NSV 6708 during 1988–1989 plotted against Julian Date.

near JD 2447390 in the combined dataset. [The infrared data provide an estimate of the time of maxima as the star still dominates the flux distribution of an RCB star/dust shell system at $J$ and $H$ wavelengths (see Section 4.3.3).]

The amplitude behaviour of the *UBVRI* photometry in NSV 6708 is different from the behaviour noted in the light curves of other RCB stars. In NSV 6708 the amplitude of the pulsations decrease with increasing wavelength (see Fig. 4.2), the exception being

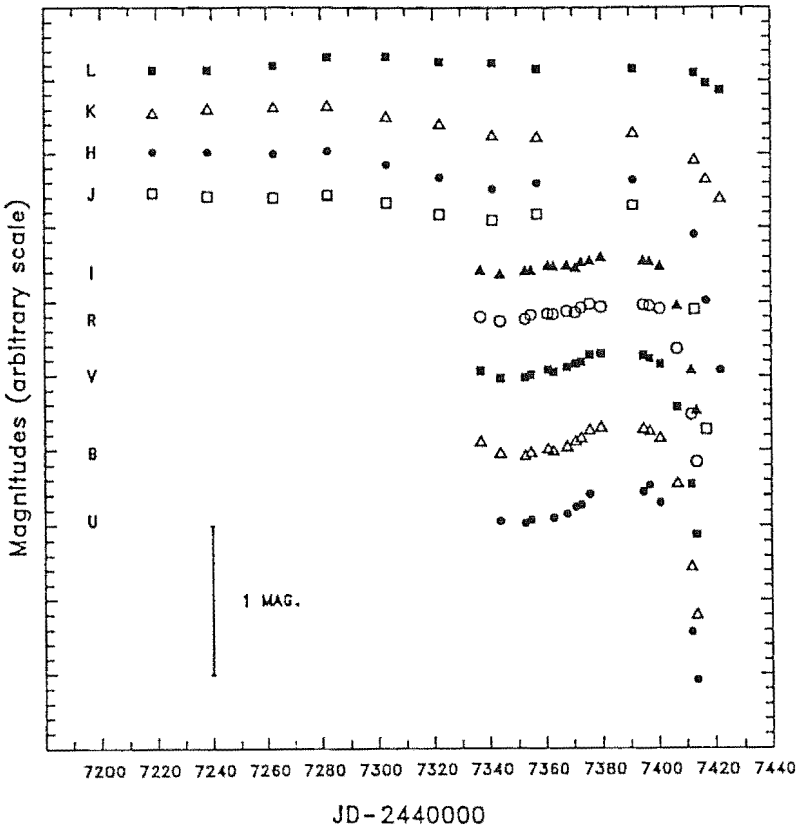


**Figure 4.2.** MJUO (*UBVRI*) and SAAO (*JHKL*) individual magnitudes versus Julian Date for NSV 6708 during 1988.

that the $U$ and $B$ amplitudes are almost identical. This is also indicated (Fig. 4.1b) by the nearly featureless ($U$–$B$) colour curve and the increasing amplitude towards the redder, i.e. longer wavelength, colour indices prior to the decline onset near JD 2447402. [For the other RCB stars observed at MJUO (Section 2.4.1), there is a general decrease in amplitude with increasing wavelength.]

### 4.3.2 Photometry through the 1988 decline onset

The decline of NSV 6708 began near JD 2447402 (see Fig. 4.1a and 4.1b), $\approx$ 12 d after the maxima in the light curves near JD 2447390. If we assume that the $\sim$ 110 d period was the dominant periodicity in the light curve of NSV 6708 during 1988, then the decline onset occurred at a phase of $\phi \approx 0.1$, assuming that $V_{\max}$ defines $\phi = 0.0$. The $V$ curve (Fig. 4.1a) was characterised by a rapid decrease in magnitude with a timescale, $t_{1/2} \approx 9$ d, where $t_{1/2}$ defines the time for the star to fade to half its brightness prior to the decline onset. The star faded from $V \approx 7.1$ to a minimum of $V \approx 14$ in 25 d. Visual estimates obtained after our photometry (*IAU* Circ. 4679) indicated that the star remained near $V \approx 14$ for about a month before beginning to brighten slowly.

The colour curves redden from the onset of the decline (see Fig. 4.1b), and therefore we classify the decline as a 'red' type following the description of decline types given in Section 3.1.5.1. In the $(V\text{-}R)/(B\text{-}V)$ and $(V\text{-}I)/(B\text{-}V)$ colour–colour planes (see Fig. 4.3), NSV 6708 reddened in a manner similar to the interstellar reddening relationships given by Schultz & Wiemer (1975). The last two $(V\text{-}I)$ observations showed some deviation away from the expected trend, which may indicate a small ($\sim$ 0.3 mag) contribution to the $I$ magnitude from the intervening dust, when the star is faint (see Section 4.3.3). The behaviour of this decline is similar to the 1985 decline of R CrB (Fernie, Percy & Richer 1986) which also reddened from the decline onset. The 1985 decline reddened along the interstellar reddening line in the $(U\text{-}B)/(B\text{-}V)$ plane. These observations indicate that, for some declines, the obscuring dust has extinction properties similar to that of interstellar dust.

The distribution of decline types in NSV 6708 is uncertain. Other than this event, the only other well observed decline of NSV 6708 was the 1987 decline (McNaught 1988) which was only observed visually. Without multicolour photometry, or spectroscopy, of the early stages of this decline, it is impossible to identify the type of decline. [Note, however, that the limited photometry of the two decline events during 1989 (Section 4.3.5) probably indicates 'red' type declines.]

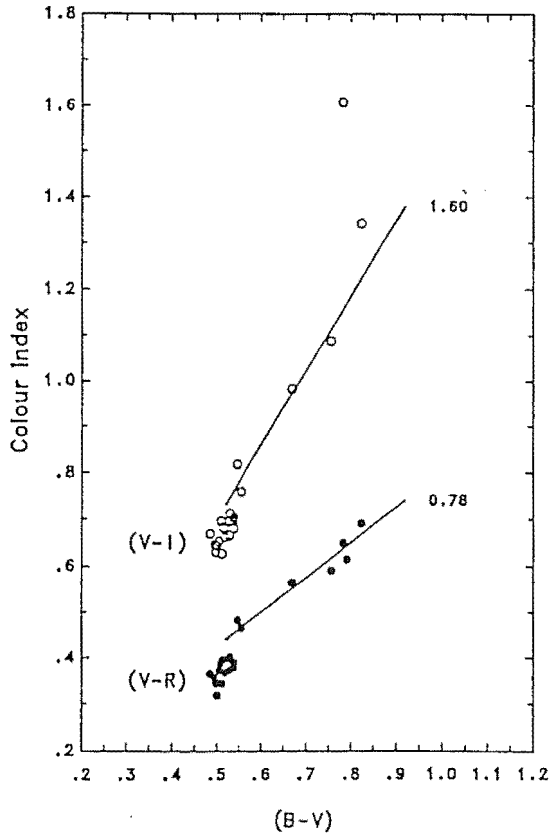


**Figure 4.3.** $(V\text{-}I)/(B\text{-}V)$ and $(V\text{-}R)/(B\text{-}V)$ colour–colour diagrams for the 1988 decline of NSV 6708. The solid lines (with slopes given on the right side of the figure) are the interstellar reddening lines of Schultz & Weimer (1975) for these colour–colour planes.

In Fig. 4.2 we showed the effects of the decline on the *UBVRIJHKL* magnitudes. (Only the two brightest magnitudes for each filter are shown.) Both the decline amplitude and decline rate decrease at wavelengths longer than *J* (1.25$\mu$m). This corresponds to the increasing contribution, to the flux at these wavelengths, made by the permanent dust shell surrounding NSV 6708 (see Section 4.3.3). We note that Menzies (1986) has found, in RY Sgr, that the permanent shell flux varies over timescales of hundreds of days. Such timescales are much longer than the duration of an initial decline.

### 4.3.3 Flux distribution

In Fig. 4.4 we plot the flux distribution of NSV 6708 and its surrounding dust shell, for several Julian Dates, throughout the decline. The *UBVRI* and *JHKL* data are MJUO and SAAO photometry respectively, with 12, 25 and 60$\mu$m fluxes from the *IRAS Point Source Catalog* (*IRAS* PSC). The *UBVRIJHKL* data were converted into fluxes using the transformations of Bessell (1979) and Wilson *et al.* (1972). The flux distribution of NSV 6708 at maximum light shows the characteristic RCB star feature of a cool shell dominating the flux at wavelengths longer than $\sim$ 2$\mu$m. At *JHKL* wavelengths the dust shell contributes approximately 3, 40, 70 and 95 per cent of the flux respectively. Photometry obtained at maximum (designated 'max' in Fig. 4.4) were averaged to give a mean flux for NSV 6708. We have shown the MJUO and SAAO data as connected points whenever these data were obtained 1–2 d apart. This avoids any major discrepancy in the flux distribution due to the rapidly changing photospheric contribution during the decline. The respective Julian Dates, when the MJUO and SAAO data were obtained, are shown rounded and abbreviated to the nearest day. The flux distribution of the star reddened appreciably throughout the decline (also see Section 4.3.2). The *I* magnitude may be influenced by flux from either the permanent dust shell, or possibly the ejected dust, when the star is faint.

We find that a blackbody temperature of 6250±250 K satisfies the *BVRIJ* data at maximum light. (We have ignored the *U* magnitude because of the increasing effects of line blanketing in this wavelength range). This value is in close agreement with the temperature of 6500±500 K derived by Kilkenny & Marang (1989). These estimates for the temperature of NSV 6708 should only be taken as a guide. Previous attempts to estimate the temperature of RCB stars by the fitting of blackbody curves (e.g. Kilkenny & Whittet 1984) gave values that were $\approx$ 1000 K cooler than spectroscopically derived temperatures (see e.g. Cottrell & Lambert 1982a, Schönberner 1975, Giridhar & Rao 1986). An adjusted temperature estimate of 7000–7500 K gives NSV 6708 a similar effective temperature to, or possibly slightly higher than, R CrB (7000 K; Cottrell & Lambert; Schönberner), RY Sgr (7000 K; Schönberner) and UW Cen (6800 K; Giridhar & Rao).

The blackbody fit to the dust shell fluxes is not as straightforward. While Kilkenny & Marang (1989) found that the *JHKL* data, when the star was faint, appeared best fitted by a blackbody of temperature 1000–1100 K, such a distribution does not satisfy the *IRAS* PSC data. Instead, we adopt a mean shell temperature of 900±50 K which offers a reasonable fit to the *JHKL* and *IRAS* data, although the *L* data is not fitted very well during the decline. The various fits to the infrared data may indicate a small range of dust temperatures ($\sim$ 100–200 K) in the shell, or that spectral features of the dust in the wavelength interval $\lambda\lambda$1–5$\mu$m cause deviations from the blackbody distribution. The

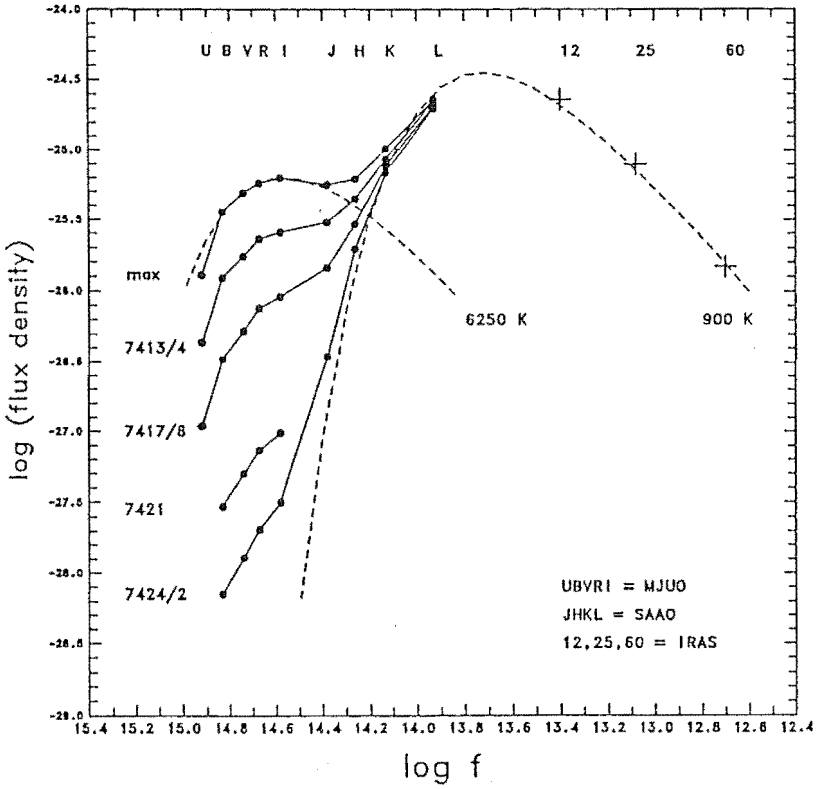


**Figure 4.4.** Flux density ($Wm^{-2}hz^{-1}$) versus frequency for the 1988 decline of NSV 6708. The numbers next to each curve are the Julian Dates of the MJUO (UBVRI) and SAAO (JHKL) observations, respectively. Fitted blackbody distributions to the star at maximum, and to the dust shell, are shown as dashed lines. The temperatures of these two distributions are given. The filters are indicated at the top of the figure.

estimate of 900 K is comparable to the dust temperature around RY Sgr and WX CrA (Walker 1986). The flux contribution made by the shell, compared to the flux contribution made by the star, usually defined as the $V$–[12] colour (see Waters, Cote & Aumann 1987), has a value at maximum of $V$–[12] = 7.4. This value is within the range for RCB stars of $V$–[12] = 6 to 9 (see Section 2.5.2, Fig. 2.32).

### 4.3.4 The spectrum during the decline

Spectra were obtained at MJUO during the early stages of the decline until the magnitude of the star was $V \approx 8.4$. The spectra obtained after the decline onset show only slight filling–in of some absorption lines due, presumably, to some chromospheric contribution to the observed line profiles. Kilkenny & Marang (1989) describe spectra obtained at SAAO when the magnitude of the star was $V \approx 10$–14. Their spectra indicate that the transition phase from the normal photospheric absorption line spectrum to an emission line dominated spectrum occurred when the star's magnitude was $V \approx 11$–12. This transition is due to the flux from the star's chromosphere masking the photospheric flux. In this

decline it occurred when NSV 6708 was 4–5 mag below maximum light. This may also explain the deviation from the reddening relationship of the initial decline noted in the $V/(B-V)$ plane (Fig. 4.5) when $V \approx 11$. If this interpretation is correct, there was an excess in $B$ of $\sim 0.2$ mag when $V \sim 14$, probably caused by the chromospheric emission.

The transition occurs 2–3 magnitudes further below maximum light in NSV 6708 than in the 1988 decline of R CrB which was a 'blue' decline (Chapter 3.1.5.1). In the R CrB decline, the transition occurred when the star was $V \approx 8.4$, or $\sim 2.5$ mag below maximum light. In Section 3.1.6, we concluded that only part of the photosphere was obscured initially in a 'blue' decline and that the transition to an emission spectrum occurred at about the time the photosphere was totally obscured. In a 'red' decline, the entire photosphere, and probably much of the inner chromosphere, is obscured at the decline onset and the transition may occur when the unobscured outer chromospheric flux dominates the obscured photospheric (and inner chromospheric) flux.

### 4.3.5 Photometry during 1989

A more extensive photometric coverage of NSV 6708 was achieved during 1989 than was possible during 1988. Note that the $V$ mag has a maximum value of $\sim 7.3$ during 1989 compared to $V \sim 7.1$ during 1988. This difference was probably due to the star continuing to recover from the 1988 decline. The $V$ light curve (Fig. 4.1a) shows several cycles of $\sim 45$ d duration, but with a highly variable amplitude. The cycle near JD 2447730 was initially announced to be a decline (Lawson, Kilmartin & Gilmore; *IAU* Circ. 4814) but

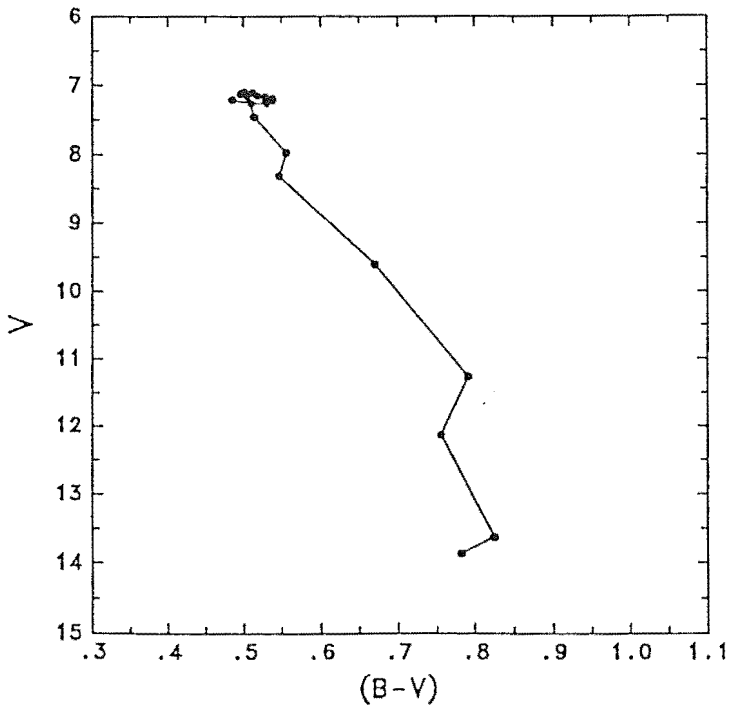


**Figure 4.5.** $V/(B-V)$ mag–colour diagram for the 1988 decline of NSV 6708. Note the deviation from the reddening line of the initial decline for $V > 11$.

this announcement was subsequently retracted (Lawson; *IAU* Circ. 4821). If this cycle was purely a pulsation–related event (i.e., with no short–term dust formation contributing to the larger amplitude) then its amplitude rivalled that of the photometric variations of RY Sgr. The event near JD 2447800 was probably a decline of short duration, as the amplitude ($\Delta V \approx 2.3$ mag) was greater than that normally associated with the pulsations of RCB stars (see Section 2.4.1). However, the width of this event (40–45 d) is comparable in duration to the $\sim$ 45 d cycle noted above. The final feature of the photometry of NSV 6708 during 1989 was a decline near JD 2447860. Visual estimates show that the star had faded to $V \approx 11.3$ by JD 2447891 (*IAU* Circ. 4879). Limited photometry near the decline onset of both these decline events show redder colours (Fig. 4.1b) than the normal colours of the star at maximum light, which probably indicates 'red' type declines.

### 4.3.6 Fourier analysis of the 1988 and 1989 photometry

In Section 2.3 we discussed the Lomb–Scargle Fourier method for non–equally spaced data. This method, if undertaken in an iterative manner, permits the identification of periodicities in the dataset and a determination of the significance of these periods. A synthetic light curve can be constructed from these periods and compared to the photometry.

An iterative Fourier analysis of the $V$ photometry obtained between JD 2447570–2447781 (the 1989 data) extracted 6 periodicities (see Table 4.3) with frequencies $f$ and periods $P$ at; $f_1 = 0.0136$ d$^{-1}$ ($P_1 = 73.5$ d), $f_2 = 0.0101$ d$^{-1}$ ($P_2 = 99.0$ d), $f_3 = 0.0242$ d$^{-1}$ ($P_3 = 41.3$ d), $f_4 = 0.0148$ d$^{-1}$ ($P_4 = 67.6$ d), $f_5 = 0.0275$ d$^{-1}$ ($P_5 = 36.4$ d) and $f_6 = 0.0043$ d$^{-1}$ ($P_6 = 232.6$ d) respectively. Note that $P_2$ is similar in value to the $\sim$ 110 d cycle observed during 1988. The period $P_6$ accounts for the gradual change in the mean $V$ mag throughout 1989, as it is similar in value to the width of the dataset. Note also the similarity of two pairs of periods ($P_1 \approx P_4$ and $P_3 \approx P_5$) which probably indicates that the Fourier analysis was hampered by the limited number of observations.

A power spectrum of the 1989 $V$ data is shown in Fig. 4.6 and a synthetic curve generated from these 6 periodicities is compared to the photometry in Fig. 4.7.

Although the general features of the $V$ photometry are preserved by the synthetic light curve, if this 6 period fit is extended outside the Julian Date limits of the selected photometry, then the behaviour of the synthetic curve becomes less than convincing (Fig. 4.8).

Including the 1988 photometry obtained prior to JD 2447401, without offsetting this dataset for the different mean mags in 1988 and 1989, the Fourier analysis gives 2 significant periodicities at $f = 0.0071$ d$^{-1}$ ($P = 140.9$ d) and $f = 0.0221$ d$^{-1}$ ($P = 45.3$ d). After offsetting the 1989 $V$ photometry by –0.2 mag so that the 1989 data had a similar maximum $V$ mag as that during 1988, a Fourier analysis finds 3 periodicities at $f = 0.0072$ d$^{-1}$ ($P = 138.9$ d), $f = 0.0141$ d$^{-1}$ ($P = 70.9$ d) and $f = 0.0215$ d$^{-1}$ ($P = 46.5$ d). All of these frequencies are summarised in Table 4.3.

In both cases where the 1988 $V$ data were included in the Fourier analysis, a poor fit to the light curve was obtained. The Fourier analyses were hampered by both the limited number of observations obtained during 1988 and by the dominating effect of the larger amplitude cycles near JD 2447590 and JD 2447730. The latter gave rise to the $\sim$ 140 d period in both solutions. A more final solution to the range of periods in the photometry

**Table 4.3.** Fourier components of NSV 6708 $V$ photometry.

| Data | | $f$ ($d^{-1}$) | $P$ (d) | $A$ (mag) | $\phi$ (rad) | $F$ |
|---|---|---|---|---|---|---|
| 1989 | $f_1$ | 0.0136 | 73.5 | 0.4177 | 5.27788 | 1.0 E-4 |
| | $f_2$ | 0.0101 | 99.0 | 0.1857 | 3.58142 | 1.3 E-2 |
| | $f_3$ | 0.0242 | 41.3 | 0.1113 | 1.82212 | 1.4 E-1 |
| | $f_4$ | 0.0148 | 67.6 | 0.1257 | 1.44513 | 9.8 E-3 |
| | $f_5$ | 0.0275 | 36.4 | 0.0824 | 3.83274 | 7.9 E-2 |
| | $f_6$ | 0.0043 | 232.6 | 0.0787 | 0.81681 | 9.0 E-3 |
| 1988 + 1989 | | 0.0071 | 140.9 | 0.4096 | 1.50796 | 1.5 E-6 |
| | | 0.0221 | 45.3 | 0.1920 | 2.19911 | 1.6 E-3 |
| 1988 + 1989 | | 0.0072 | 138.9 | 0.3415 | 1.31947 | 7.2 E-6 |
| (1989 $V$ − 0.2) | | 0.0141 | 70.9 | 0.2007 | 3.20442 | 1.7 E-4 |
| | | 0.0215 | 46.5 | 0.1181 | 4.08407 | 7.7 E-3 |

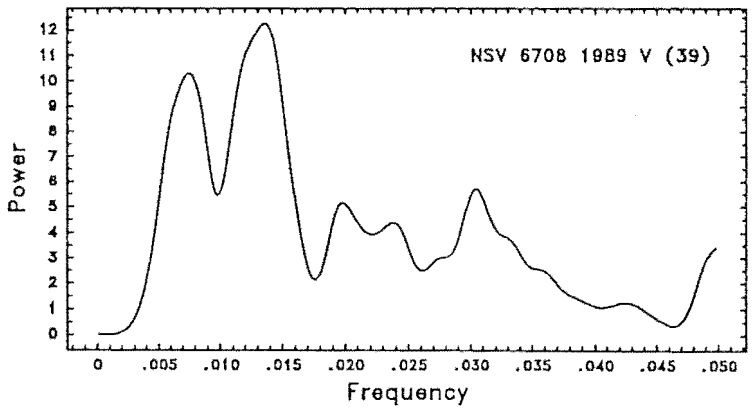


**Figure 4.6.** Power spectrum for the 1989 $V$ photometry of NSV 6708 between JD 2447570–2447781. The number of data points is indicated within the figure.

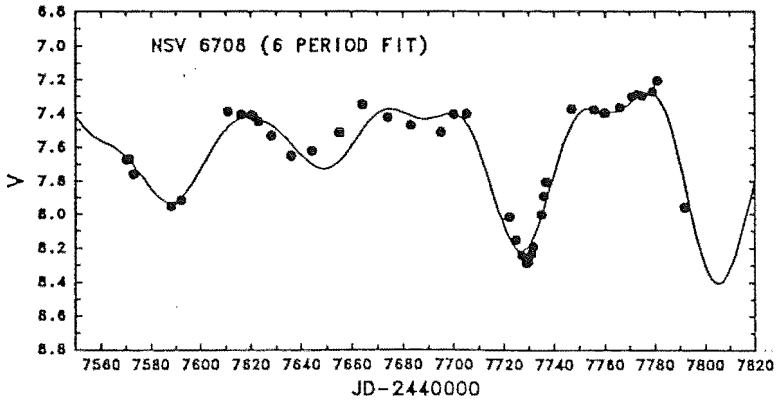


**Figure 4.7.** A 6 period synthetic fit (solid line) to the 1989 $V$ photometry of NSV 6708 between JD 2447570–2447781. The periodicities are summarised in Table 4.3.

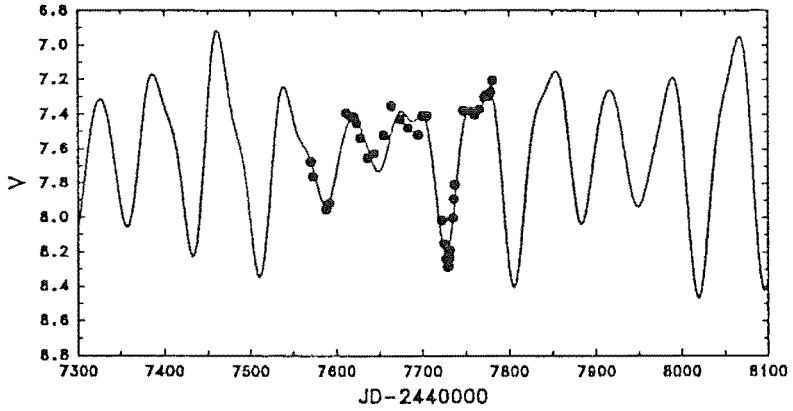


**Figure 4.8.** An example of why caution should be exercised when a Fourier analysis is applied to a short dataset. While the 1989 $V$ photometry is apparently well fitted, the 6 period synthetic curve is less believable outside the Julian Date range of the photometry.

of NSV 6708 must await the availability of additional observations. A Fourier analysis of the colour data yielded almost identical results to the analysis of the $V$ photometry.

### 4.3.7 Radial velocity variations during 1988 and 1989

The MJUO spectra of NSV 6708 were wavelength calibrated to an uncertainty of 2–4 mÅ using spectra of a thorium–argon source taken immediately following the exposure of the star. Radial velocities were determined from the measured wavelengths of the dominant absorption lines in the spectra, with the identifications and rest wavelengths being obtained from the line list of Cottrell & Lambert (1982a).

The phase coverage of the 1988 spectra was less than ideal due to the intervening weather. In particular, no spectra were obtained near the maximum in the photometry near JD 2447390. The averaged radial velocity measurements, and the phase ($\phi$) of these measurements, assuming a period $P$ = 110 d, are listed in Table 4.2. These data are compared to the 1988 $V$ photometry in Fig. 4.9a. There was little indication of variability above the 2–4 kms$^{-1}$ uncertainty in the radial velocities measurements. The mean radial velocity of NSV 6708 during 1988 was –25.1 kms$^{-1}$.

Spectra obtained prior to the decline onset showed no indication of line profile changes. This is due to the low, or non-existent, radial velocity variations. We note that no line profile changes have been detected in spectra of R CrB, which has a radial velocity amplitude of 4–8 kms$^{-1}$ (Fernie, Sherwood & DuPuy 1972; Raveendran, Ashoka & Rao 1986), as a consequence of the pulsations of this star.

During 1989 only 4 spectra of NSV 6708 were obtained and of these, only 3 had accompaning thorium–argon arcs. The mean radial velocities for these 3 spectra are given in Table 4.2 and these data are compared to the 1989 $V$ photometry in Fig. 4.9b. Note the larger difference between the radial velocity measurements, when compared to the 1988 data, which may indicate the presence of a low radial velocity amplitude ($< 4$ kms$^{-1}$).

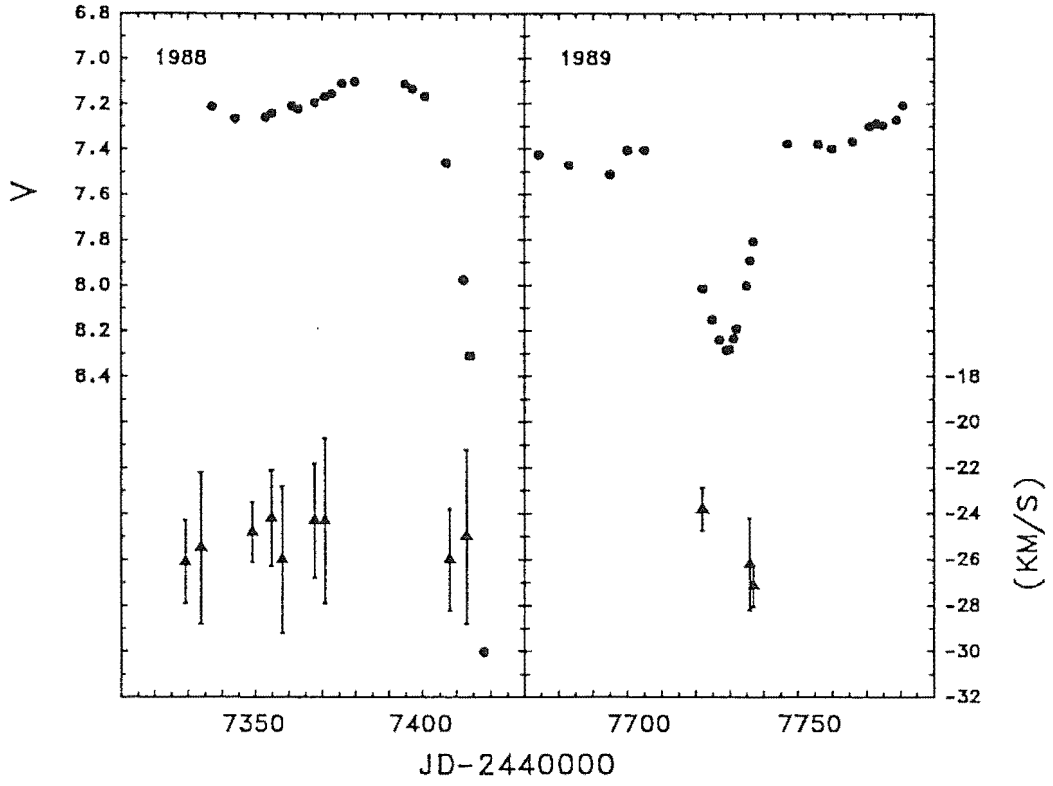


**Figure 4.9.** Radial velocity measurements of NSV 6708 compared to $V$ photometry for 1988 and 1989.

More data, obtained simultaneously with photometry, are required to test this possibility.

The duration and amplitude of the photometric variations during this cycle in 1989 rivalled the typical photometric variations of RY Sgr (Section 2.4.1.4). RY Sgr has a radial velocity amplitude of 30–40 $\text{kms}^{-1}$ with a shock wave near $V_{\max}$ (Section 5.2). The radial velocity behaviour of NSV 6708 is clearly very different from that of RY Sgr.

### 4.3.8 Hydrogen lines

In Fig. 4.10 we show MJUO spectra of NSV 6708, R CrB and the F8 Ia standard star $\delta$ CMa (for comparison) in the region about H$\alpha$. These spectra show the much stronger H$\alpha$ line in NSV 6708 compared to R CrB. The hydrogen abundance for R CrB has been given, by Cottrell & Lambert (1982a), as log (H/Fe) = 0.2. [Even this value may be an upper limit due to possible blending with a Ti I line at 6562.1Å (Hunger, Schönberner & Steenbock 1982).] Kilkenny & Marang (1989) also reported lines of H$\beta$ and H$\gamma$ in NSV 6708.

The strong hydrogen lines observed in NSV 6708 are not unique amongst this type of star. If we consider the RCB stars to be a subset of a larger group of hydrogen deficient

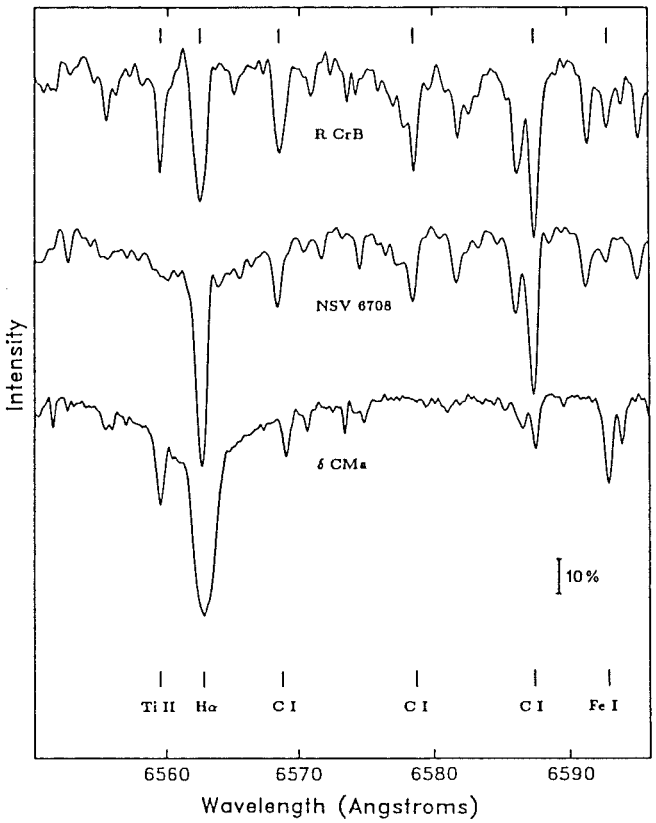


**Figure 4.10.** Comparative MJUO spectra of R CrB, NSV 6708 and the F8 Ia standard star $\delta$ CMa in the region about H$\alpha$. Important spectral features are indicated.

carbon stars, which include the HdC stars (Warner 1967), there are at least two other stars with relatively strong hydrogen lines. An analysis of the spectral characteristics of a large sample of RCB and HdC stars is currently being undertaken (Cottrell *et al.*, in preparation). Of the stars surveyed, the HdC star HD 148839 is already known to have strong hydrogen lines (Warner 1967) and a strong H$\alpha$ line was found in the little studied suspected RCB star LR Sco. LR Sco has an infrared excess of $V$–[12] = 8.7 and Walker (1986) has derived a shell temperature of 400 K from *IRAS* PSC data. These values are comparable to the RCB stars. [We note that LR Sco is currently classified in the *General Catalogue of Variable Stars* (Kholopov *et al.* 1985) as a semi–regular, SRd, variable.]

## 4.4 CONCLUSIONS

We noted in Section 2.5.1 that NSV 6708 was one of several cool hydrogen deficient carbon stars that show a periodicity longer than the predicted radial fundamental mode of Weiss (1987a). We suggested that the longer than fundamental period ($\sim$ 110 d for NSV 6708) may be evidence for non–radial pulsations and that this may be the reason for the non–detection of radial velocity variations during 1988. The suggestion of a radial velocity

amplitude of $< 4$ kms$^{-1}$ in 1989, possibly commensurate with a $\sim 45$ d mode, is clearly much lower (by a factor of 10) than the radial velocity amplitude of RY Sgr (Section 5.2). However, such a low amplitude may not be inconsistent with the radial velocity amplitude of R CrB (4–8 kms$^{-1}$; see Raveendran, Ashoka & Rao 1986). The detection of radial velocity variations in other RCB, and HdC, stars will be difficult, if such low amplitudes are typical.

More photometry is necessary in order to examine the range of periodicities present in NSV 6708. To further study the presence of radial velocity variations in NSV 6708, additional spectra, obtained simultaneously with photometry, are required. The obtaining, and analysis of such data, will be hampered by the high frequency of declines of this star (which permits only datasets of short duration to be obtained) and by the possibility of several periodicities being present (as indicated in the 1989 data). The latter may cause some uncertainty in the phasing of any observed radial velocity variations.

Kilkenny & Marang (1989) suggested that the apparently high incidence of deep minima for NSV 6708 might indicate a period shorter than is typically observed in other RCB stars. This suggestion is not supported by the current observations which indicate a range of periods that are similar to other RCB stars (Section 2.4.3). This, and the low radial velocity amplitude of NSV 6708, may be further evidence for the dissociating of the pulsations of RCB stars as the direct cause of the decline events (see also the arguments on decline onset phases in Section 3.1.5.3). Why NSV 6708 should be more active than other RCB stars is uncertain. We suggest that the high rate of declines of this star makes NSV 6708 an ideal target for the studies of these events. Such studies are facilitated by the brightness of this star ($V \approx 7$ at maximum; $V = 10$–$14$ at minimum), which permits the declines to be observed throughout their duration.

# Chapter 5

# The R Coronae Borealis star RY Sgr

## 5.1 Pulsation period variations

### 5.1.1 INTRODUCTION

Two recent papers have examined the possibility of period shortening in the pulsations of RY Sgr. Kilkenny (1982) and Marraco & Milesi (1982) have shown that observations of RY Sgr can be satisfied by a quadratic solution with a negative quadratic coefficient $k$. The quadratic solutions give a linearly decreasing rate of change for the pulsation period $dP/dn = 2k$ d cycle$^{-1}$. Kilkenny found, from 231 minima identified between 1926–1978, $dP/dn = (-1.02 \pm 0.04)$ d cycle$^{-1}$. Marraco & Milesi found, from 460 maxima and and equal number of minima identified between 1897–1977, $dP/dn = (-1.54 \pm 0.02)$ d cycle$^{-1}$. Both investigations were prompted by Pugach (1977) who noted, from a study of visual estimates obtained between 1926–1974, that RY Sgr appeared to have a variable period.

We extend the analyses of Kilkenny and Marraco & Milesi by including more recent observations of RY Sgr and find that their quadratic solutions are unable to account for observed changes in the pulsation period. We analyse these observations using quadratic, cubic and linear piecewise solutions and then discuss each of these in terms of their evolutionary consequences. We then discuss the likely mass of the RCB stars. The luminosity of these objects is determined from observations of RCB stars in the LMC. The $T_{eff}$ and surface gravity used are those derived in recent model atmosphere analyses (Schönberner 1975; Cottrell & Lambert 1982a).

This work was originally undertaken in two parts. The first (Lawson & Cottrell 1988; hereafter Paper I within this Chapter) considered observations of RY Sgr up to 1986 October. The second (Lawson & Cottrell 1990; hereafter Paper II within this Chapter), which included observations up to 1989 April, was undertaken after a change was noted in the pulsation period of RY Sgr. This Section extends this dataset to 1989 December.

### 5.1.2 OBSERVATIONS

We analysed a majority of the observations considered by Kilkenny (1982) and Marraco & Milesi (1982). Specifically, these data and light curves are those published by Innes (1903) and Jacchia (1933), in the circulars of the Variable Star Section of the Royal Astronomical Society of New Zealand (VSSRASNZ) between 1940–1973 (see Marraco & Milesi for detailed references), in the publications of the VSSRASNZ (Bateson 1973, 1975, 1978), and the photoelectric data of Alexander *et al.* (1972).

More recently Lawson, Cottrell & Bateson (1988) have extended the series of VSS-RASNZ observations of RY Sgr from 1977–1986. These data were presented as light curves and tabulated in 5 d means. Photoelectric observations from 1984–1986 were published by Lawson *et al.* (1987). Additional photometry obtained from 1986–1989 September are listed in Section 2.4.1.4 and data from 1989 September–December are unpublished MJUO photometry.

Observations published as either 5 or 10 d means were used without correction. Individual visual estimates were combined in either 5 or 10 d means depending upon the number of observations. The times of maxima were obtained directly from the light curve derived from the mean observations, or if these were not available, from the published light curve. The times of maxima are listed in Table 5.1.

**Table 5.1.** Times of maxima for cycle numbers $n = -483$ to $n = 369$.

| $n$ | JD–2400000 | $n$ | JD–2400000 | $n$ | JD–2400000 | $n$ | JD–2400000 | $n$ | JD–2400000 |
|---|---|---|---|---|---|---|---|---|---|
| -483 | 14830 | -466 | 15497 | -287 | 22540 | -259 | 23623 | -241 | 24323 |
| -482 | 14876 | -465 | 15535 | -286 | 22579 | -258 | 23661 | -240 | 24355 |
| -481 | 14915 | -464 | 15580 | -284 | 22642 | -257 | 23689 | -239 | 24396 |
| -480 | 14951 | -463 | 15621 | -281 | 22770 | -253 | 23844 | -238 | 24443 |
| -479 | 14994 | -462 | 15658 | -280 | 22815 | -252 | 23889 | -233 | 24629 |
| -474 | 15181 | -461 | 15688 | -279 | 22847 | -251 | 23927 | -232 | 24674 |
| -473 | 15216 | -455 | 15938 | -278 | 22890 | -250 | 23975 | -231 | 24713 |
| -472 | 15260 | -454 | 15975 | -277 | 22922 | -244 | 24201 | -230 | 24751 |
| -471 | 15299 | -289 | 22459 | -269 | 23231 | -243 | 24245 | -229 | 24787 |
| -470 | 15344 | -288 | 22504 | -267 | 23306 | -242 | 24283 | -228 | 24821 |
| -225 | 24953 | -213 | 25411 | -201 | 25889 | -188 | 26399 | -139 | 28300 |
| -224 | 24978 | -212 | 25447 | -200 | 25927 | -186 | 26478 | -138 | 28339 |
| -223 | 25022 | -211 | 25492 | -197 | 26041 | -185 | 26518 | -137 | 28374 |
| -222 | 25071 | -210 | 25523 | -196 | 26079 | -184 | 26560 | -136 | 28407 |
| -221 | 25102 | -209 | 25560 | -195 | 26114 | -183 | 26595 | -135 | 28447 |
| -220 | 25142 | -206 | 25697 | -194 | 26153 | -182 | 26633 | -134 | 28482 |
| -219 | 25177 | -205 | 25731 | -193 | 26193 | -147 | 27990 | -130 | 28645 |
| -218 | 25216 | -204 | 25762 | -192 | 26238 | -146 | 28032 | -128 | 28725 |
| -215 | 25340 | -203 | 25804 | -191 | 26277 | -145 | 28073 | -127 | 28755 |
| -214 | 25378 | -202 | 25845 | -189 | 26362 | -144 | 28098 | -126 | 28795 |
| -125 | 28835 | -35 | 32332 | -14 | 33135 | -2 | 33594 | 22 | 34515 |
| -59 | 31401 | -33 | 32395 | -13 | 33173 | 1 | 33707 | 23 | 34548 |
| -45 | 31924 | -28 | 32595 | -12 | 33203 | 3 | 33780 | 24 | 34589 |
| -44 | 31973 | -27 | 32638 | -11 | 33247 | 4 | 33818 | 25 | 34635 |
| -43 | 32008 | -26 | 32680 | -8 | 33360 | 5 | 33858 | 26 | 34670 |
| -42 | 32039 | -24 | 32744 | -7 | 33396 | 6 | 33890 | 27 | 34701 |
| -41 | 32091 | -22 | 32832 | -6 | 33437 | 14 | 34202 | 29 | 34786 |
| -40 | 32120 | -21 | 32865 | -5 | 33476 | 15 | 34240 | 30 | 34825 |
| -39 | 32155 | -17 | 33015 | -4 | 33514 | 16 | 34282 | 31 | 34857 |
| -36 | 32286 | -16 | 33060 | -3 | 33557 | 17 | 34316 | 32 | 34895 |
| 34 | 34977 | 46 | 35423 | 61 | 36010 | 75 | 36547 | 100 | 37514 |
| 35 | 35010 | 48 | 35503 | 62 | 36052 | 77 | 36620 | 101 | 37558 |
| 36 | 35043 | 51 | 35618 | 63 | 36090 | 88 | 37051 | 102 | 37595 |
| 39 | 35168 | 52 | 35660 | 64 | 36124 | 89 | 37092 | 103 | 37635 |
| 40 | 35207 | 53 | 35698 | 65 | 36165 | 90 | 37124 | 105 | 37710 |
| 41 | 35235 | 54 | 35744 | 67 | 36245 | 91 | 37160 | 106 | 37756 |
| 42 | 35271 | 55 | 35792 | 68 | 36278 | 92 | 37198 | 107 | 37793 |
| 43 | 35302 | 58 | 35895 | 72 | 36432 | 93 | 37247 | 108 | 37825 |
| 44 | 35345 | 59 | 35937 | 73 | 36470 | 98 | 37435 | 109 | 37867 |
| 45 | 35386 | 60 | 35968 | 74 | 36512 | 99 | 37470 | 112 | 37976 |

**Table 5.1** – *continued*

| $n$ | JD–2400000 | $n$ | JD–2400000 | $n$ | JD–2400000 | $n$ | JD–2400000 | $n$ | JD–2400000 |
|---|---|---|---|---|---|---|---|---|---|
| 118 | 38210 | 137 | 38932 | 154 | 39587 | 168 | 40138 | 185 | 40790 |
| 119 | 38250 | 138 | 38976 | 155 | 39634 | 169 | 40175 | 186 | 40832 |
| 120 | 38296 | 139 | 39020 | 156 | 39668 | 173 | 40328 | 187 | 40861 |
| 121 | 38332 | 140 | 39056 | 157 | 39715 | 174 | 40370 | 192 | 41070 |
| 122 | 38362 | 141 | 39091 | 159 | 39780 | 175 | 40405 | 193 | 41109 |
| 127 | 38555 | 144 | 39208 | 163 | 39945 | 176 | 40448 | 194 | 41140 |
| 128 | 38600 | 145 | 39248 | 164 | 39984 | 177 | 40480 | 195 | 41179 |
| 134 | 38823 | 146 | 39290 | 165 | 40020 | 178 | 40522 | 196 | 41219 |
| 135 | 38861 | 149 | 39401 | 166 | 40059 | 183 | 40719 | 197 | 41252 |
| 136 | 38902 | 150 | 39442 | 167 | 40096 | 184 | 40752 | 202 | 41452 |
| 203 | 41489 | 215 | 41941 | 227 | 42394 | 241 | 42946 | 252 | 43357 |
| 204 | 41524 | 216 | 41971 | 229 | 42475 | 242 | 42977 | 254 | 43439 |
| 205 | 41566 | 219 | 42096 | 230 | 42526 | 243 | 43015 | 255 | 43478 |
| 206 | 41598 | 220 | 42136 | 231 | 42558 | 244 | 43053 | 258 | 43587 |
| 207 | 41638 | 221 | 42172 | 232 | 42591 | 245 | 43089 | 259 | 43625 |
| 210 | 41753 | 222 | 42204 | 233 | 42632 | 246 | 43123 | 260 | 43673 |
| 211 | 41785 | 223 | 42239 | 234 | 42666 | 248 | 43200 | 261 | 43702 |
| 212 | 41824 | 224 | 42282 | 235 | 42706 | 249 | 43234 | 262 | 43735 |
| 213 | 41864 | 225 | 42328 | 239 | 42857 | 250 | 43275 | 263 | 43778 |
| 214 | 41899 | 226 | 42361 | 240 | 42894 | 251 | 43323 | 264 | 43818 |
| 266 | 43906 | 278 | 44348 | 290 | 44816 | 302 | 45275 | 315 | 45778 |
| 267 | 43938 | 279 | 44388 | 291 | 44856 | 303 | 45308 | 316 | 45820 |
| 268 | 43972 | 280 | 44427 | 292 | 44892 | 305 | 45391 | 317 | 45857 |
| 269 | 44006 | 281 | 44470 | 293 | 44929 | 306 | 45431 | 318 | 45891 |
| 270 | 44046 | 282 | 44512 | 296 | 45058 | 307 | 45471 | 319 | 45934 |
| 271 | 44094 | 283 | 44548 | 297 | 45087 | 308 | 45508 | 320 | 45972 |
| 272 | 44126 | 284 | 44580 | 298 | 45134 | 309 | 45544 | 321 | 46007 |
| 273 | 44156 | 287 | 44702 | 299 | 45166 | 310 | 45582 | 324 | 46130 |
| 274 | 44197 | 288 | 44737 | 300 | 45204 | 311 | 45623 | 325 | 46164 |
| 277 | 44310 | 289 | 44771 | 301 | 45239 | 312 | 45656 | 326 | 46201 |
| 327 | 46243 | 336 | 46587 | 346 | 46961 | 356 | 47330 | 365 | 47677 |
| 328 | 46274 | 337 | 46625 | 347 | 46997 | 357 | 47368 | 366 | 47717 |
| 329 | 46319 | 338 | 46657 | 348 | 47036 | 358 | 47412 | 367 | 47755 |
| 330 | 46353 | 339 | 46696 | 349 | 47076 | 359 | 47453 | 368 | 47791 |
| 331 | 46392 | 340 | 46731 | 350 | 47107 | 360 | 47485 | 369 | 47830 |
| 334 | 46496 | 344 | 46878 | 354 | 47265 | 363 | 47599 | | |
| 335 | 46546 | 345 | 46925 | 355 | 47305 | 364 | 47642 | | |

### 5.1.3 ANALYSIS

As our main interest in RY Sgr is directed towards a study of the absorption line splitting near maximum visual light (Section 5.2) we compare our results with those of Marraco & Milesi (1982) because they published a solution for maxima. We have analysed maxima from cycle number $n = -483$ to $n = 369$ and have identified 383 maxima in 852 cycles. We have a continuous record of times of maxima, with seasonal gaps, from $n = -45$.

We have calculated the O–C residuals using Marraco & Milesi's linear and quadratic solution for maxima. The residuals are plotted in Fig. 5.1 and in Fig. 5.2a respectively. The quadratic solution is drawn as a dashed line through the linear residuals in Fig. 5.1 for comparison. Our residuals, for $n < 250$, show no significant difference from Marraco & Milesi's residuals (see their figs 2a and 3a). However, it is apparent, from the asymetry

in Fig. 5.1 and the positive residuals for $n > 250$ in Fig. 5.2a, that the more recent data deviate from Marraco & Milesi's quadratic solution. The discrepancy in the O–C residual is nearly 30 d at $n = 340$.

#### 5.1.3.1 The results of Paper I for cycle numbers to $n = 340$

Three possible improvements over Marraco & Milesi's quadratic solution were investigated: (i) a revised quadratic, (ii) a cubic and (iii) a series of linear piecewise solutions.

(i) All alternative quadratic solutions had O–C residuals of a similar form to the quadratic residuals in Fig. 5.2a. A quadratic equation of the form $JD_n = JD_o + P_o n + kn^2$ where

$JD_o = 2433667$ d,

$P_o = 38.6225$ d,

$k = -707 \times 10^{-6}$ d,

reduced the amplitude of the discrepant positive residuals for $n > 250$ at the expense of increasing the amplitude of the residuals near $n = -490$ and $n = 250$.

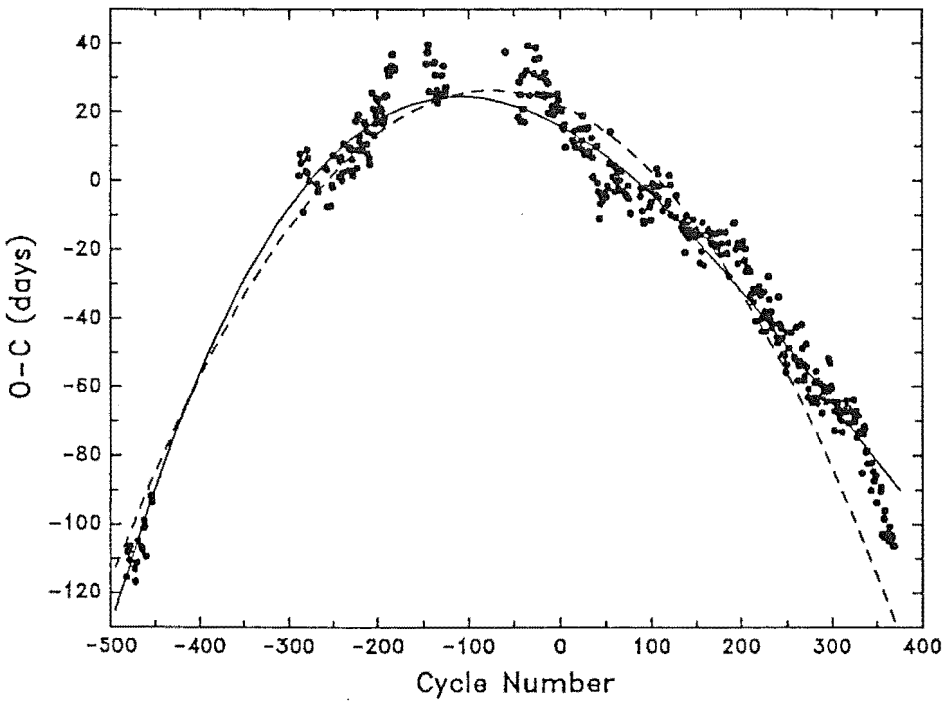


**Figure 5.1.** O–C residuals for the linear solution of Marraco & Milesi (1982): $JD_n = 2433648 + 38.7216n$. The dashed line is quadratic solution of Marraco & Milesi: $JD_n = 2433670 + 38.6056n - 784 \times 10^{-6} n^2$. The solid line is the cubic solution determined in Section 5.1.3.1 (ii) for pulsation cycles $n < 340$. The quadratic and cubic solutions are extended to $n = 475$.

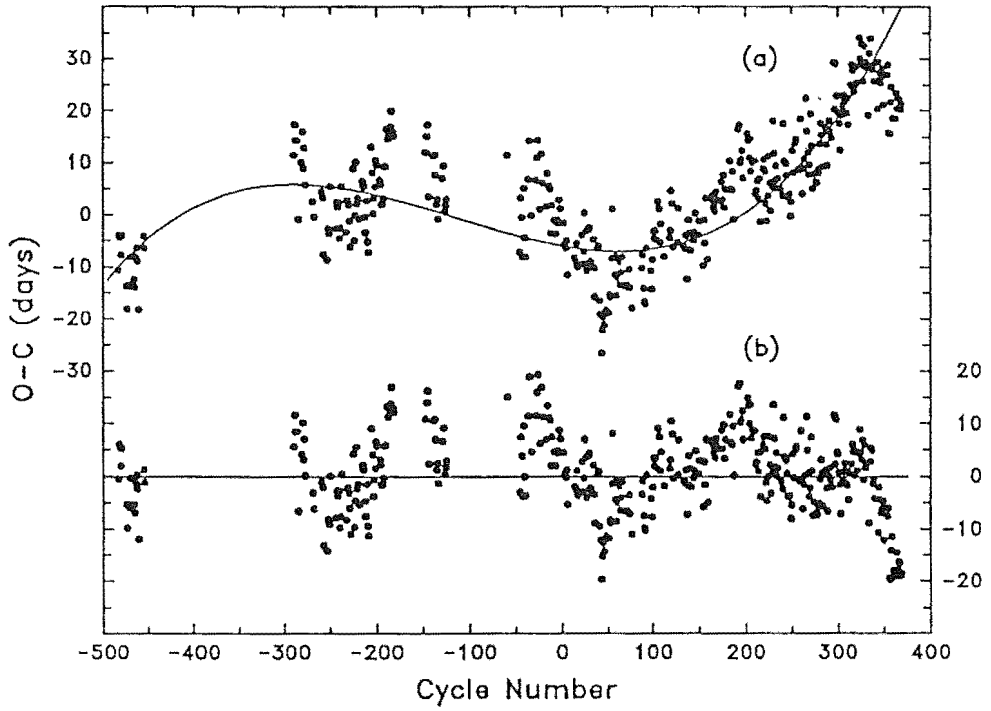


Figure 5.2. (a) O–C residuals for the quadratic solution of Marraco & Milesi (1982). (b) O–C residuals for the cubic solution. The solid line in both graphs is the cubic solution, determined in Section 5.1.3.1 (ii), extended to $n = 475$.

(ii) Noting the trend of the residuals in Fig. 5.2a we solved a cubic equation of the form $JD_n = JD_o + P_o n + k_1 n^2 + k_2 n^3$, obtaining:

$JD_o = 2433664$ d,

$P_o = 38.5736$ d,

$k_1 = (-581 \pm 11) \times 10^{-6}$ d,

$k_2 = (-594 \pm 50) \times 10^{-9}$ d.

The cubic O–C residuals are plotted in Fig. 5.2b. The cubic solution is drawn as a solid line through the quadratic residuals in Fig. 5.2a and through the linear residuals in Fig. 5.1 for comparison.

(iii) A polynomial solution cannot account for the modulation of the residuals on a timescale of 100–200 cycles which was noted by Kilkenny (1982) and Marraco & Milesi (1982). Marraco & Milesi listed the features near $n = -280$, $-170$, $-60$ and 200 as real deviations in the O–C residuals. We also list the distinct minimum in the residuals near $n = 40$ as significant. This minimum is due to three consecutive short periods of approximately 28, 36 and 31 d duration respectively. If, instead of a polynomial solution, we consider a series of linear piecewise solutions between these features their dominating effect on the O–C residuals is removed.

We analysed only the maxima for $n > -28$ and fitted three least squares regressions (hereafter LP1, LP2 and LP3 respectively) of the form $JD_n = JD_o + P_o n$, obtaining:

$JD_o = 2433668.9 \pm 0.6$ d, $P_o = 38.34 \pm 0.03$ d (between $n = -28$ and $n = 40$),

$JD_o = 2433658.0 \pm 1.6$ d, $P_o = 38.56 \pm 0.01$ d (between $n = 58$ and $n = 195$),

$JD_o = 2433686.3 \pm 3.3$ d, $P_o = 38.38 \pm 0.01$ d (between $n = 210$ and $n = 340$).

These three linear solutions are drawn as bold lines in Fig. 5.3, where the residuals are plotted with respect to the LP2 solution, and are labelled LP1, LP2 and LP3 respectively. These solutions suggest that the pulsation period readjusts on a timescale of 15–20 cycles. The changes of period are centred on the features near $n = 40$ and $n = 200$. We did not interpret the maxima prior to $n = -28$ as the residuals appeared to be more erratic and the dataset was less complete. We note that Pugach (1977) considered linear piecewise solutions but was hindered by a lack of data. Also note that these solutions differ slightly from those of Paper I. The solutions, and uncertainties, given here are calculated using a standard least squares regression. In Paper I, the solutions were calculated using a 'mini-max' technique.

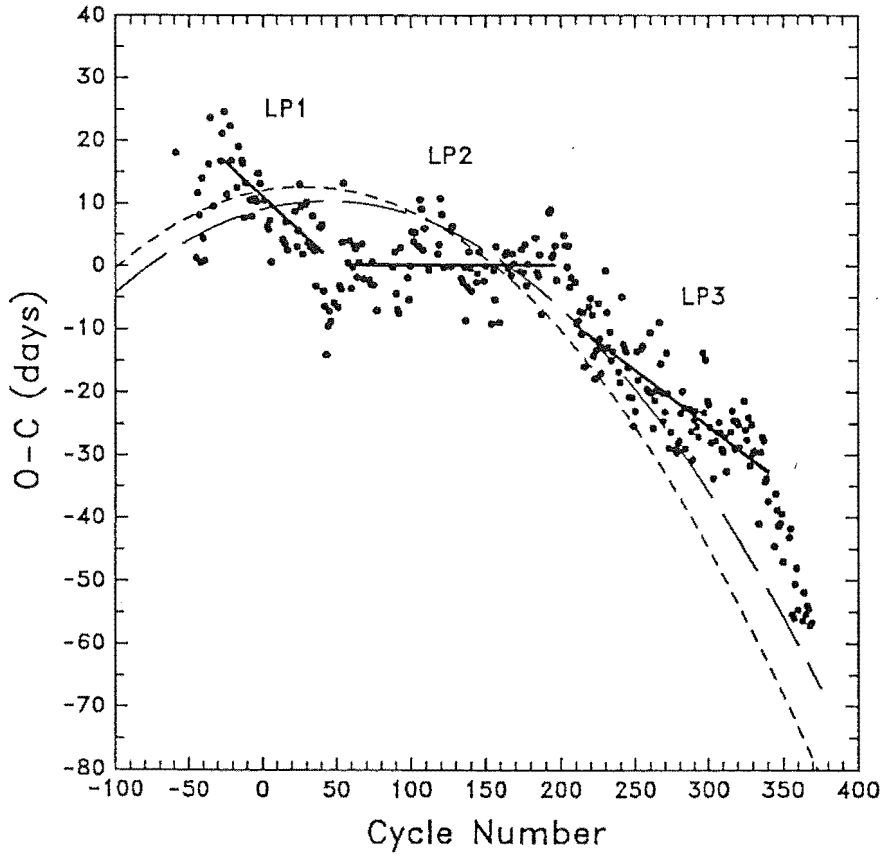


**Figure 5.3.** O–C residuals for the LP2 solution of Section 5.1.3.1 (iii). The dashed lines are the quadratic solutions of Section 5.1.3.1 (i) (long dashes) and Marraco & Milesi (1982) (short dashes). The solid lines are the LP1, LP2 and LP3 solutions determined in Sections 5.1.3.1 (iii).

#### 5.1.3.2 The results of Paper II (to $n = 364$) and beyond (to $n = 369$)

The O–C residuals for $n = 340$ to $n = 369$ indicated that a new period was already in effect towards the end of the observations considered in Section 5.1.3.1. This is indicated by the strong negative trend away from the cubic solution for cycle numbers $n > 324$ in Fig. 5.1 and 5.2, and from the LP3 solution in Fig. 5.3. We fitted a least squares regression of the form $JD_n = JD_o + P_o n$ to these data, obtaining (for a new LP4 solution):

$JD_o = 2433878.6 \pm 15.0$ d, $P_o = 37.81 \pm 0.04$ d (between $n = 324$ and $n = 369$).

Although expressing the solution in this form conveniently retains the Marraco & Milesi numbering system, the uncertainties in the $JD_o$ become more meaningful if we redefine the cycle numbers for this particular solution. Expressing the linear solution in the form $JD_m = JD_o + P_o m$, where cycle number $m = 0$ is equivalent to $n = 324$, gives:

$JD_o = 2446127.5 \pm 1.1$ d, $P_o = 37.81 \pm 0.04$ d (between $m = 0$ and $m = 40$).

Note that this LP4 solution differs slightly from that of Paper II due to the greater number of cycles used in this analysis.

We also fitted higher order polynomials to these data. However, the higher order terms contributed less than 0.3 per cent of the contribution made by the linear term in the predicted times of maxima. This contribution is comparable to the effect of the uncertainty in the linear term.

There is a possibility that the LP3 solution is not the most appropriate solution for cycle numbers $n = 210$ to $n = 324$. The positive trend in the O–C residuals between $n = 303$ and $n = 324$ may represent the time taken for the star to adjust to the new period. This time (21 cycles) is similar to the time taken for the period of the star to adjust between the LP1 and LP2 (18 cycles), and LP2 and LP3 (15 cycles), linear solutions. If this interpretation is correct, the LP3 period ($P_o = 38.38$ d) needs to be revised downwards to account for the slightly negative slope of the O–C residuals between $n = 210$ and $n = 303$. A linear solution of the form above, using the Marraco & Milesi numbering system gives:

$JD_0 = 2433693.3 \pm 5.2$ d, $P_0 = 38.35 \pm 0.02$ d (between $n = 210$ and $n = 303$).

Redefining the numbering system within the limits of this solution, say where cycle number $\ell = 0$ is equivalent to $n = 210$, gives:

$JD_0 = 2441747.4 \pm 1.1$ d, $P_0 = 38.35 \pm 0.02$ d (between $\ell = 0$ and $\ell = 93$).

The revised LP3 solution and the LP4 solution are shown as solid lines in Fig. 5.4.

### 5.1.4 DISCUSSION

#### 5.1.4.1 Analysis of the four linear solutions

The O–C residuals for those cycle numbers used to calculate the individual solutions have, for the LP1 solution, a scatter with standard deviation $\sigma \sim 4.0$ d. The corresponding

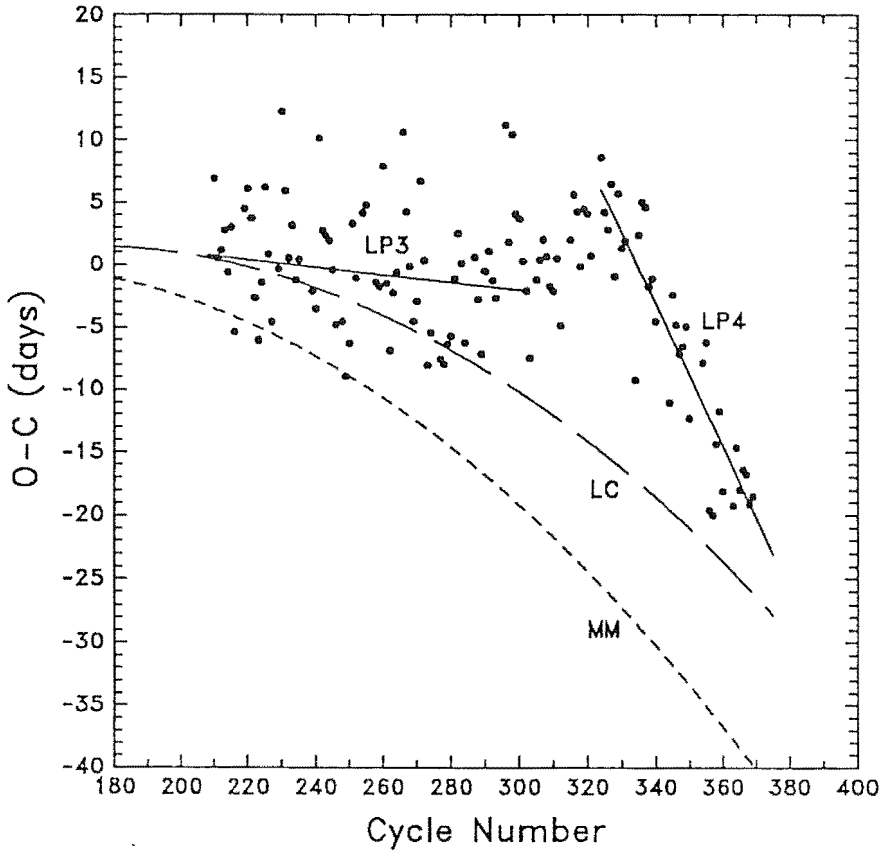


**Figure 5.4.** O–C residuals for the LP3 solution of Section 5.1.3.1 (iii). The solid lines are the revised LP3 solution and the LP4 solution determined in Section 5.1.3.2. The dashed lines are the quadratic solutions of Section 5.1.3.1 (i) (labelled LC) and Marraco & Milesi (1982) (labelled MM).

values of $\sigma$ for the LP2, revised LP3 and LP4 solutions are 4.3, 4.9 and 3.6 d respectively. Note that the scatter in the LP4 residuals is lower than those of the earlier solutions. This may be due to the earlier data being derived from visual estimates, whereas the LP4 data are derived largely from MJUO $V$ photometry. The times of maxima can be determined to $\pm 3$ to 5 d from visual curves. This uncertainty is reduced to $\pm 1$ to 2 d from photoelectric $V$ curves. However, the intrinsic variability in the pulsation period can exceed 10–20 per cent of the mean pulsation period of the star, i.e. 4–8 d for a period of $\sim$40 d. This range of variability is thus comparable to, or greater than, the uncertainties associated with determining the times of maxima. This also indicates that, for RY Sgr, the O–C analysis is largely independent of the source of data. [This may not be true for most other RCB stars since the amplitude of the pulsations is much smaller (see Section 2.4.1).]

The four linear solutions identified since 1951 indicate that either positive or negative changes to the pulsation period are possible, but that the overall trend would appear to be towards shorter periods. The lifetimes of the previous three linear solutions ($\approx$ 70, 130 and 90 cycles respectively) may indicate that the pulsation period of the star changes on

a timescale of ~100 cycles (equivalent to ~10 yrs).

The times of transition between the various solutions do not appear to be associated with the large amplitude declines of RY Sgr. A 6 mag decline occurred near JD 2445000 (Lawson, Cottrell & Bateson 1988; figs 2a, 2b and 2c; reproduced here as Fig. 5.5). However, the transition between the revised LP3 and LP4 solution occurred between $n\approx303$ (JD~2445300) and $n\approx324$ (JD~2446100). Consequently, these cycles occurred from during the rise to maximum light until after the star had fully recovered from the decline.

### 5.1.4.2 Evolutionary implications

Schönberner (1977) published time–dependent evolutionary tracks in the log $T_{eff}$–log $g$ plane for 0.7 and 1.0 $M_{\odot}$ stars with C/O cores and helium envelopes. These models were evolved through the regions occupied by the RCB stars and the hot helium

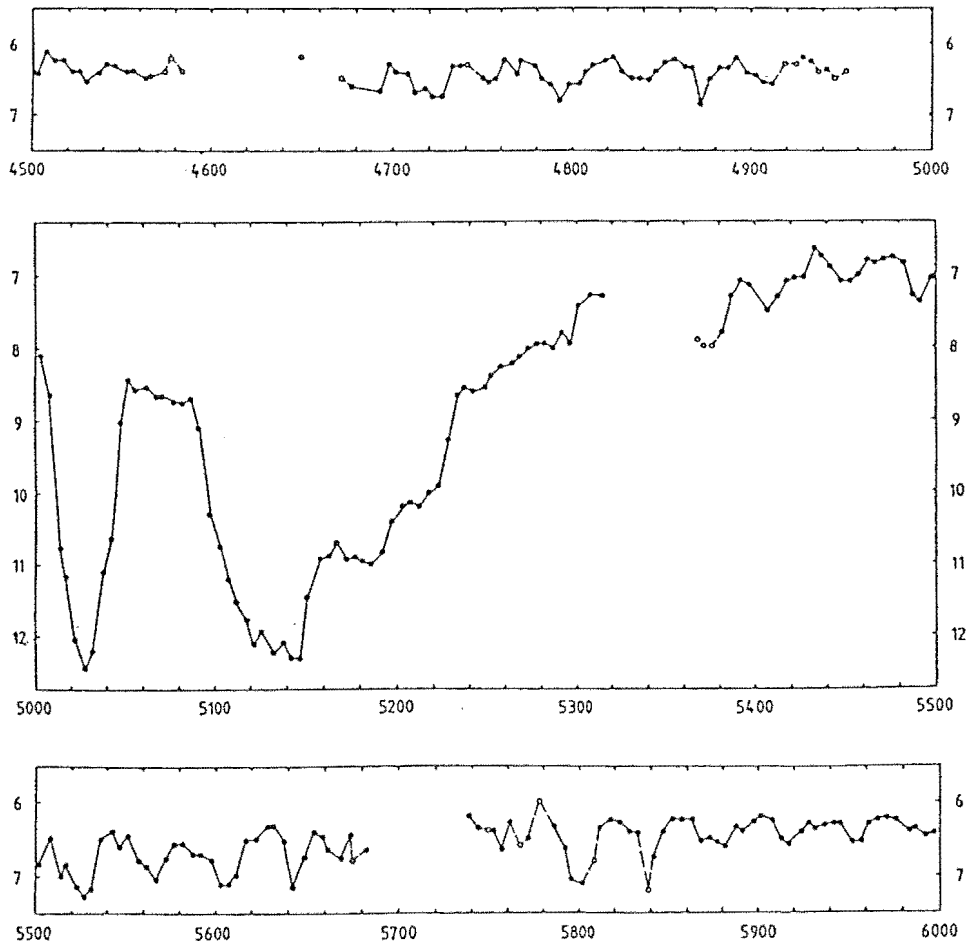


**Figure 5.5.** Visual light curve of RY Sgr from JD 2444500–2446000. The light curve is reproduced from Lawson, Cottrell & Bateson (1988) figs 2a, 2b and 2c.

stars. Schönberner (1975) re–analysed spectroscopic data of the F–type RCB stars R CrB, RY Sgr and XX Cam (now classified as an HdC star; see Section 2.4.3) using a model atmosphere grid to obtain values of log $T_{eff}$ and log $g$. Values of log $T_{eff} \approx 3.84$ ($T_{eff} \approx$ 7000 K) and log $g$ = 0.45–0.65 were obtained after the inclusion of line blanketing effects. Cottrell & Lambert (1982a) obtained, using higher resolution and higher signal–to–noise spectra of R CrB and XX Cam and Schönberner's model atmosphere grid, very similar values of log $T_{eff}$ and log $g$. When the log $T_{eff}$–log $g$ values derived by Schönberner (1975) and Cottrell & Lambert (1982a) are plotted in the log $T_{eff}$–log $g$ plane, they are centred around the 0.7 $M_{\odot}$ track of Schönberner (1977).

The time dependent tracks of Schönberner (1977) can be used to derive a period rate of change. Following Kilkenny & Lynas–Gray (1982), the pulsation period $P$ is proportional to $g^{-3/4}$. The period rate of change can be estimated from the gradient between successive log $g$ points on the 0.7 $M_{\odot}$ track and by normalising the pulsation period to 38.6 d when log $g$ = 0.65. [This value for log $g$ was determined for RY Sgr by Schönberner (1975).] The analysis of this evolutionary track (see Paper I) gave values for $dP/dn$ of $-1.2 \times 10^{-3}$ d cycle$^{-1}$ to $-2.5 \times 10^{-3}$ d cycle$^{-1}$ for log $T_{eff}$ = 3.83–3.93 ($T_{eff}$ = 6800–8500 K).

Recently, Weiss (1987a) calculated model period decrease rates for hydrogen deficient carbon stars evolving through the region of the H–R diagram occupied by the RCB stars. His preferred model for RY Sgr ($M = 0.825\ M_{\odot}$, $T_{eff}$=7218 K) (Weiss, personal communication) gives a decrease rate of $-1.4 \times 10^{-3}$ d cycle$^{-1}$ (see Weiss 1987a table 7).

The second derivative of the quadratic solution of Marraco & Milesi (1982), and that of Section 5.1.3.1 (i), gives the the pulsation period rate of change $dP/dn = 2k$. Using the value for $k$ of Marraco & Milesi, and that of Section 5.1.3.1 (i), $dP/dn = -1.6 \times 10^{-3}$ d cycle$^{-1}$ and $-1.4 \times 10^{-1}$ d cycle$^{-1}$ respectively.

For the cubic solution of Section 5.1.3.1 (ii), the second derivative gives the period rate of change $dP/dn = 2k_1 + 6nk_2$. Using the values of $k_1$ and $k_2$ determined in Section 5.1.3.1 (ii), $dP/dn = 0$ when $n = 326$. When $n < 326$, $dP/dn < 0$ and the pulsation period decreases. Conversely, the pulsation period increases when $n > 326$ and $dP/dn > 0$. The value of $dP/dn$ varies between $-2.9 \times 10^{-3}$ d cycle$^{-1}$ when $n = -483$ and $5.0 \times 10^{-5}$ d cycle$^{-1}$ when $n = 369$, averaging $-1.4 \times 10^{-3}$ d cycle$^{-1}$.

The observationally determined values for $dP/dn$ are in general agreement with the model values of Weiss (1987a) and those determined from the models of Schönberner (1977).[1]

The masses of the galactic RCB stars cannot be determined directly due to uncertainties in the distances to these objects. However, it is possible to derive masses for the RCB stars in the LMC. Photometry of the two F–type RCB stars in the LMC, W Men and HV 12842 (see Section 2.4.2), showed that the average magnitude of these stars was $V \sim 13.8$ and 13.7 respectively. Assuming a distance modulus of 18.6 (see Wood, Bessell & Paltoglou 1985) and a small ($\sim 0.2$) bolometric correction for F–type supergiants (see Allen 1976), we derive $M_{bol} = -5$ which gives log $L/L_{\odot} \sim 4$. If the log $T_{eff}$–log $g$ values for the LMC stars are similar to the values derived by Schönberner (1975) and Cottrell &

[1] Kilkenny (1982) analysed the evolutionary tracks of Schönberner (1977) and found agreement between the model and observed values of the quadratic coefficient $k$ at the $T_{eff}$ = 6900 K point on the 1.0 $M_{\odot}$ track, in contrast to our calculations. We note that Kilkenny incorrectly assigned $dP/dn = k$ rather than $2k$, which may account for the discrepancy. In addition, the models of Weiss (1987a) and the luminosity of the LMC RCB stars would seem to preclude stars with masses as great as 1.0 $M_{\odot}$.

Lambert (1982a) for the galactic RCB stars then the possible mass range becomes $M$ = 0.5–0.75 $M_{\odot}$.

The various mass estimates for these stars point towards a typical mass of the RCB stars of 0.7–0.8 $M_{\odot}$.

Although the LP4 solution suggests that the O–C residuals are showing a tendency to re–approach the quadratic solutions of Marraco & Milesi (1982) and that of Section 5.1.3.1 (i), we indicated in Section 5.1.3.1 (iii) that a polynomial solution cannot account for the observed modulations of the residuals. However, the polynomial solutions derived in Sections 5.1.3.1 (i) and (ii) could be considered as describing the mean period rate of change observed during the last 90 yrs.

The cubic solution derived in Section 5.1.3.1 (ii) implies that the star's evolution in the log $T_{eff}$–log $g$ plane reaches a stationary point when $dP/dn = 0$ and reverses as the pulsation period increases. As the models of Weiss (1987a) and Schönberner (1977) indicate that the long–term evolution is towards shorter pulsation periods, the cubic solution probably reflects the general change in the pulsation period of the star over the past 90 yrs rather than the long–term evolution of the star.

### 5.1.5 CONCLUSIONS

A series of discrete changes in the pulsation period of RY Sgr appear to offer the most satisfactory explanation for the behaviour of the O–C residuals of this star. A series of linear solutions to the times of maxima overcome the major detraction of a polynomial solution, i.e. the modulation of the O–C residuals on a timescale of 70–130 cycles. This evidence for rapid, and possibly semi-periodic, changes in the pulsation period of RY Sgr justifies the continued monitoring of this interesting star.

The polynomial solutions can be considered as describing the mean period rate of change of RY Sgr. The mean observed period rate of change is in agreement with the theoretical rate of evolution of recent models. These models, and observational evidence, indicate that the likely mass of the RCB stars is 0.7–0.8 $M_{\odot}$.

## 5.2 Radial velocity variations

### 5.2.1 INTRODUCTION

The periodic variations of RY Sgr were first noted by Jacchia (1933). Jacchia found a $\sim$ 39 d period with an amplitude of $\sim$ 0.5 mag in his own observations of RY Sgr, obtained between 1920–1932, and concluded that the star was pulsating. Such variations could have been discovered over 3 decades earlier if they had been noticed in a photographic light curve of the star obtained at the Cape between 1897–1901 (Innes 1903). During the 1967–1971 decline of RY Sgr, Alexander *et al.* (1972) obtained photometric and spectroscopic observations, mainly at SAAO, which confirmed that the star was pulsating, with a radial velocity amplitude of 30–40 $\mathrm{kms}^{-1}$.

A series of high resolution ($\Delta\lambda = 0.15$Å), high signal–to–noise (>100:1), échelle spectra were obtained by Cottrell & Lambert (1982b) at McDonald Observatory with a Reticon detector system, which revealed line–splitting of most absorption lines in some spectra. The time duration between the spectra with line–splitting suggested some correlation with the $\sim$ 39 d period of the star, but this could not be investigated further due to a lack of spectra. Line–splitting in some ionised species had also been noticed by Danziger (1963), in some of the spectra obtained for his analysis of RY Sgr, but he did not investigate this aspect further.

Lawson (1986) obtained photometry and échelle photographic spectra of RY Sgr, at MJUO, throughout a pulsation cycle during 1985. The line–splitting was found to occur near $V_{\mathrm{max}}$ and have a duration of $<$ 10 d ($\sim$ 0.25 of a cycle). The event was interpreted as a shock wave occurring about the time of minimum radius. In later MJUO observations (Cottrell, Lawson & Smith 1988), the line–splitting phase had a duration of $\sim$ 6 d, commencing near the time of $(B\text{–}V)_{\mathrm{max}}$, in one well–observed cycle of the star during 1986. In addition to the doubling of absorption lines during the line–splitting phase, there were significant variations in the line profiles, due presumably to changes in photospheric conditions, e.g. temperature, throughout the pulsation cycle.

The analysis of the MJUO observations was limited by the photographic plate/image tube system used at that time. These spectra were generally of low signal–to–noise ($<$ 20:1), and distortion in the photographic image introduced by the image tube prevented accurate radial velocities from being obtained, other than for lines in the central échelle order. For most of these spectra, échelle order 36 (Latham & Sternberg 1977) was used for the radial velocity measurements as the two Si II lines in this order ($\lambda$6347Å and 6371Å respectively) were relatively unaffected by blending and the line–splitting was particularly evident in these lines.

To overcome the limitations of the photographic spectra, and to take advantage of the opportunities offered by the 1.0–m reflector and the 1872–element Reticon–based Linear Diode Array (LDA; MacQueen 1986), an extensive series of observations of RY Sgr were obtained during 1988.

In this Section, we report a preliminary analysis of these spectra. These spectra will eventually be used for more detailed analysis of the shock wave and an abundance analysis of RY Sgr. [The line profile variations prevented Cottrell & Lambert (1982a), who obtained abundances for R CrB and XX Cam, from such an analysis because of a lack of

phase information for their spectra.]

### 5.2.2 OBSERVATIONS

The spectra were obtained at MJUO between 1988 March–October with the 1.0–m reflector and 1872–element LDA (MacQueen 1986). Spectra of échelle orders 35 (H$\alpha$ region, either centred on $\lambda$6560Å or 6580Å) and 36 (Si II region, usually centred on $\lambda$6360Å) were obtained for radial velocity measurements, with a wavelength interval of $\sim$ 60 Å being recorded for each spectrum. Spectra of the $\lambda$6360Å region, obtained from JD 2447302–2447334, are shown in Fig. 5.6. This figure shows the spectral evolution of RY Sgr throughout the line–splitting event near JD 2447330.

Additional regions, obtained mainly for future analysis, included orders 39 (He I and Na I *D* region) and 43 (6707Å Li I region). These spectra are summarised in Table 5.2.

### 5.2.3 REDUCTION OF THE SPECTRA

A flat–field spectrum and thorium–argon arc comparison spectrum were recorded after the acquisition of each spectrum of RY Sgr. Following the subtraction of the array fixed pattern from the raw data frames, the flat–field frame was divided into the stellar spectrum and comparison frames. The stellar spectrum was then de–glitched to remove cosmic ray strikes on the diode array. The de–glitched stellar spectrum and the comparison spectrum were Fourier transformed, the frequency at which noise became the dominant contribution identified, and then the spectra were reconstructed after the removal of these noise dominated frequencies.

The stellar spectra were wavelength calibrated to an uncertainty of 2–4 mÅ using the dispersion solutions derived for the companion comparison spectra. Radial velocities were determined from the measured wavelengths of dominant absorption lines in the spectra of RY Sgr. The line identifications and rest wavelengths were mainly sourced from the line list of Cottrell & Lambert (1982a). Mean radial velocities were calculated for lines with excitation potentials ($\chi$) < 3 eV (low $\chi$) and >8 eV (high $\chi$), there being few lines of intermediate excitation suitable for measuring for velocities [see Section 5.2.4 (ii)]. The low excitation lines consisted mainly of ionised species, including Fe II and Ti II lines. The high excitation lines were the two Si II lines ($\chi$ = 8.12 eV) and C I lines ($\chi \approx 9$ eV). Whenever two or more spectra were obtained on a given night, the radial velocity estimates were combined. The mean radial velocity, which was obtained in the geocentric rest frame, was adjusted to a heliocentric velocity. The heliocentric radial velocity ($v_{\rm radial}$), an uncertainty $\sigma_{\rm n-1}$, and the number of measurements for each group of lines, are listed in Table 5.2. (Most of the software to support these operations are integrated as menu–driven options within the LDA–controller program.)

### 5.2.4 DISCUSSION OF THE RADIAL VELOCITIES

The mean heliocentric radial velocities, for low and high excitation lines, are compared to the 1988 *V* light curve and (*B*–*V*) colour curve in Fig. 5.7. The photometry of RY Sgr was

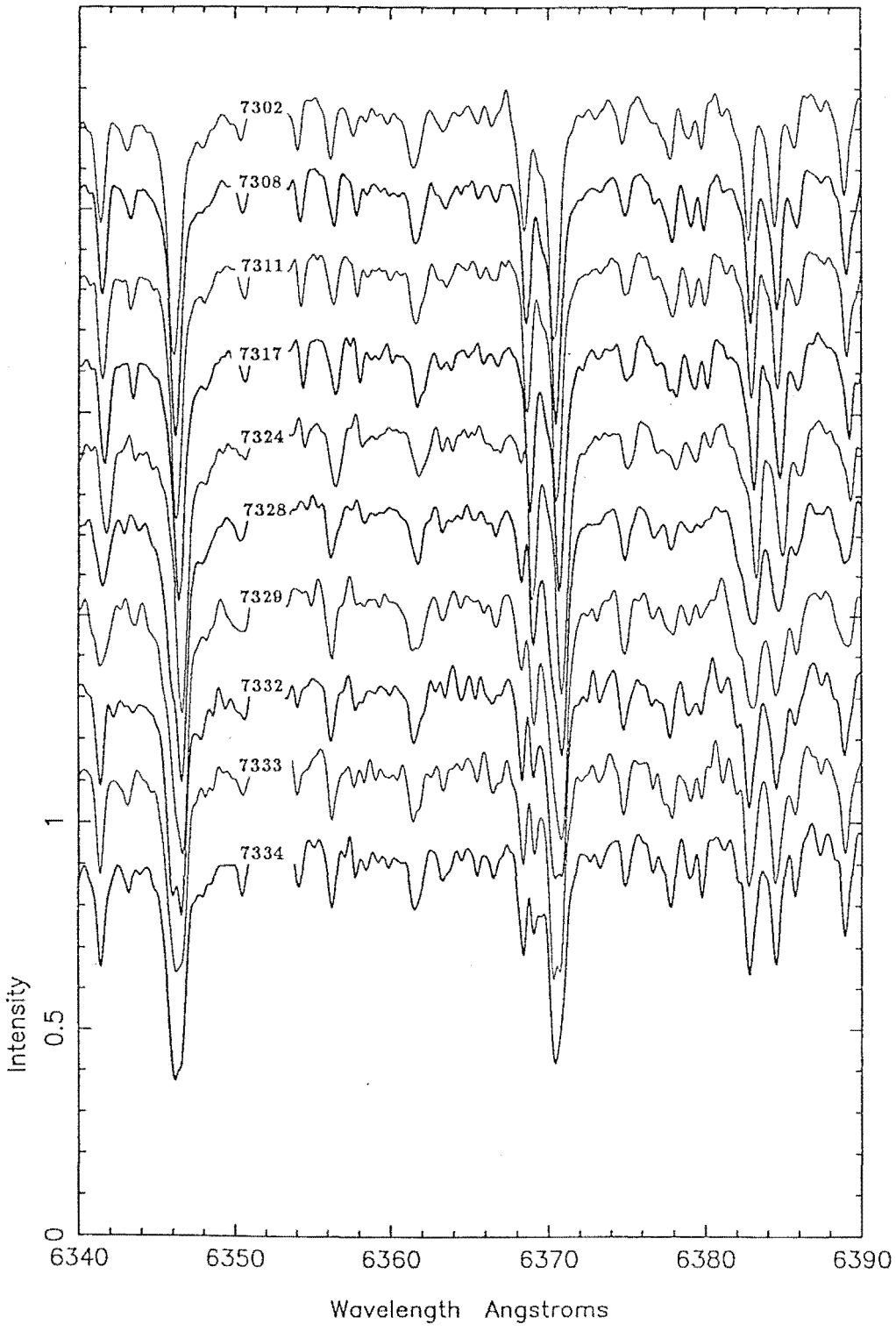


**Figure 5.6.** Time series of the spectral evolution of RY Sgr between JD 2447302–2447334 in the region λλ6340–6390Å. The Julian Date, less 2440000 and rounded to the nearest day, is given for each spectrum. The spectra are on an arbitrary flux scale, with each spectrum offset by 0.2 in intensity. Details of these spectra are listed in Table 5.2 and discussed in the text.

**Table 5.2.** Log of MJUO spectra of RY Sgr during 1988.

| MJUO ♯* | UT Date | JD–2440000 | order | $\lambda_c$ (Å) | $v_{radial}$ ($\chi$ >8 eV) | $\sigma$ | $n$ | $v_{radial}$ ($\chi$ <3 eV) | $\sigma$ | $n$ |
|---|---|---|---|---|---|---|---|---|---|---|
| PLC0089 | Mar 20.72 | 7241.22 | 35 | 6560 | -14.4 | 2.3 | 3 | -17.2 | 2.5 | 2 |
| MC87 | Apr 02.69 | 7254.19 | 35 | 6560 | -19.5 | 4.7 | 3 | -14.9 | 6.3 | 2 |
| WAL0017 | Apr 19.58 | 7271.08 | 35 | 6580 | -21.0 | 1.1 | 3 | -22.9 | 0.9 | 3 |
| WAL0018 | Apr 19.67 | 7271.17 | 35 | 6580 | | | | | | |
| WAL0021 | Apr 20.63 | 7272.13 | 34 | 6700 | | | | | | |
| WAL0023 | Apr 22.55 | 7274.05 | 34 | 6700 | | | | | | |
| WAL0028 | Apr 22.77 | 7274.27 | 35 | 6580 | -18.4 | 0.9 | 3 | -19.5 | 0.8 | 3 |
| WAL0049 | Apr 24.63 | 7276.13 | 35 | 6560 | -17.9 | 1.4 | 3 | -16.7 | 2.2 | 2 |
| MC116 | Apr 29.65 | 7281.15 | 35 | 6560 | | | | | | |
| WAL0052 | May 14.51 | 7296.01 | 36 | 6360 | | | | | | |
| WAL0053 | May 14.60 | 7296.10 | 35 | 6580 | -16.9 | 1.9 | 2 | -12.3 | 0.7 | 3 |
| WAL0054 | May 14.64 | 7296.14 | 34 | 6700 | -26.2 | 3.6 | 2 | -30.2 | 7.4 | 3 |
| MC131 | May 15.54 | 7297.04 | | | | | | -16.1 | | 1 |
| | | 7297.04 | | | -25.8 | 7.3 | 2 | -33.4 | 4.9 | 2 |
| WAL0055 | May 17.60 | 7299.10 | 36 | 6360 | -29.2 | 1.6 | 2 | -29.6 | 0.5 | 2 |
| MC135 | May 20.54 | 7302.04 | 36 | 6360 | | | | | | |
| MC136 | May 20.63 | 7302.13 | 35 | 6560 | -26.4 | 1.1 | 5 | -28.5 | 1.1 | 5 |
| MC137 | May 20.71 | 7302.21 | 34 | 6700 | | | | | | |
| MC140 | May 21.57 | 7303.07 | 35 | 6580 | -26.4 | 2.0 | 3 | -30.7 | 2.7 | 3 |
| MC141 | May 22.49 | 7303.99 | 35 | 6580 | -25.0 | 1.3 | 3 | -26.4 | 2.1 | 3 |
| MC147 | May 23.62 | 7305.12 | 35 | 6580 | -25.0 | 1.5 | 3 | -25.4 | 1.3 | 3 |
| MC150 | May 24.52 | 7306.02 | 35 | 6580 | -24.2 | 0.7 | 3 | -26.3 | 1.1 | 2 |
| MC155 | May 25.47 | 7306.97 | 35 | 6580 | -24.1 | 1.7 | 3 | -25.6 | 1.7 | 3 |
| MC161 | May 26.63 | 7308.13 | 36 | 6360 | -23.5 | 1.4 | 2 | -22.9 | 0.7 | 2 |
| MC166 | May 27.45 | 7308.95 | 36 | 6360 | -24.0 | 1.3 | 2 | -22.4 | 1.4 | 2 |
| MC172 | May 29.53 | 7311.03 | 35 | 6580 | | | | | | |
| MC173 | May 29.59 | 7311.09 | 36 | 6360 | -21.6 | 1.6 | 4 | -22.2 | 1.2 | 5 |
| MC179 | May 30.53 | 7312.03 | 35 | 6580 | -19.1 | 2.7 | 3 | -19.8 | 0.7 | 3 |
| MC182 | May 31.45 | 7312.95 | 35 | 6580 | -19.1 | 1.5 | 5 | -18.4 | 0.9 | 5 |
| MC189 | Jun 01.55 | 7314.05 | 35 | 6580 | -18.8 | 1.8 | 3 | -17.6 | 0.9 | 3 |
| MC192 | Jun 04.45 | 7316.95 | 35 | 6580 | | | | | | |
| MC193 | Jun 04.52 | 7317.02 | 36 | 6360 | -16.4 | 1.2 | 5 | -14.8 | 0.5 | 5 |
| MC200 | Jun 05.63 | 7318.13 | 35 | 6580 | -12.7 | 2.1 | 3 | -13.3 | 1.1 | 3 |
| MC205 | Jun 11.55 | 7324.05 | 35 | 6580 | | | | | | |
| MC206 | Jun 11.60 | 7324.10 | 36 | 6360 | -11.4 | 0.9 | 4 | -10.4 | 0.9 | 5 |
| MC213 | Jun 13.48 | 7325.98 | 35 | 6580 | -13.1 | | 1 | -11.2 | 0.6 | 3 |
| WAL0056 | Jun 14.44 | 7326.94 | 35 | 6580 | -12.4 | | 1 | -9.9 | 2.9 | 3 |
| WAL0060 | Jun 15.48 | 7327.98 | 35 | 6580 | -13.8 | 0.4 | 3 | -9.8 | 1.2 | 4 |
| WAL0061 | Jun 15.57 | 7328.07 | 36 | 6360 | | | | -45.7 | 0.1 | 2 |
| WAL0062 | Jun 16.51 | 7329.01 | 36 | 6360 | -14.1 | 3.0 | 2 | -9.0 | 2.0 | 2 |
| | | 7329.01 | | | | | | -47.4 | 2.2 | 2 |
| WAL0066 | Jun 19.46 | 7331.96 | 36 | 6360 | -17.1 | 1.5 | 3 | -11.9 | 1.2 | 4 |
| WAL0067 | Jun 19.52 | 7332.02 | 35 | 6580 | -38.6 | 3.5 | 3 | -43.7 | 1.7 | 5 |
| WAL0068 | Jun 19.66 | 7332.16 | 39 | 5880 | | | | | | |
| WAL0069 | Jun 20.55 | 7333.05 | 36 | 6360 | -19.2 | 1.8 | 2 | -9.4 | 1.3 | 2 |
| WAL0070 | Jun 20.59 | 7333.09 | 35 | 6580 | -36.4 | 4.2 | 2 | -41.7 | 1.6 | 2 |
| WAL0076 | Jun 21.55 | 7334.05 | 35 | 6580 | -20.0 | 1.0 | 2 | -11.5 | 1.0 | 3 |
| WAL0077 | Jun 21.60 | 7334.10 | 36 | 6360 | -35.9 | 1.1 | 5 | -40.3 | 1.4 | 5 |
| MC217 | Jul 01.53 | 7344.03 | 35 | 6580 | -27.3 | 1.2 | 3 | -29.9 | 0.4 | 2 |
| MC222 | Jul 04.57 | 7347.07 | 35 | 6580 | -21.9 | 1.0 | 3 | -24.6 | 1.4 | 3 |

**Table 5.2.** *continued*

| MJUO code | UT Date | JD–2440000 | order | $\lambda_c$ (Å) | $v_{radial}$ ($\chi$ >8 eV) | $\sigma$ | $n$ | $v_{radial}$ ($\chi$ <3 eV) | $\sigma$ | $n$ |
|---|---|---|---|---|---|---|---|---|---|---|
| MC232 | Jul 12.45 | 7354.95 | 35 | 6580 | -13.7 | 1.3 | 3 | -15.4 | 2.1 | 3 |
| MC236 | Jul 15.54 | 7358.04 | 35 | 6580 | -8.9 | 0.9 | 3 | -11.5 | 1.8 | 3 |
| MC241 | Jul 16.49 | 7358.99 | 35 | 6580 | | | | | | |
| WAL0081 | Jul 25.40 | 7367.90 | 35 | 6580 | | | | | | |
| WAL0082 | Jul 25.45 | 7367.95 | 35 | 6500 | | | | | | |
| WAL0083 | Jul 25.50 | 7368.00 | 36 | 6360 | -7.3 | 1.0 | 3 | -4.7 | 1.1 | 5 |
| WAL0084 | Jul 25.56 | 7368.06 | 36 | 6430 | -39.9 | 3.3 | 3 | -45.4 | 1.3 | 5 |
| WAL0086 | Jul 26.46 | 7368.96 | 35 | 6580 | -6.1 | | 1 | -5.6 | 0.6 | 2 |
| | | 7368.96 | | | -47.2 | 2.5 | 3 | -46.4 | 1.1 | 3 |
| MC244 | Jul 28.49 | 7370.99 | 35 | 6580 | | | | -5.0 | 0.1 | 2 |
| | | 7370.99 | | | -42.1 | 1.8 | 2 | -45.9 | 0.8 | 3 |
| MC247 | Aug 30.37 | 7403.87 | 35 | 6580 | | | | | | |
| | | 7404.88 | | | -6.1 | 2.1 | 2 | -9.3 | 0.9 | 3 |
| WAL0087 | Sep 02.41 | 7406.91 | 35 | 6580 | -7.5 | 0.5 | 3 | -9.3 | 1.8 | 3 |
| WAL0092 | Sep 05.32 | 7409.82 | 35 | 6580 | | | | | | |
| WAL0094 | Sep 05.43 | 7409.93 | 35 | 6500 | -9.0 | 0.8 | 3 | -6.8 | 2.5 | 5 |
| WAL0095 | Sep 05.50 | 7410.00 | 36 | 6360 | -33.4 | 4.1 | 2 | -29.6 | 4.0 | 2 |
| WAL0096 | Sep 05.55 | 7410.05 | 36 | 6430 | | | | | | |
| WAL0098 | Sep 07.46 | 7411.96 | 35 | 6580 | -7.7 | | 1 | -9.1 | 1.5 | 2 |
| WAL0099 | Sep 07.51 | 7412.01 | 35 | 6500 | | | | -33.0 | 0.8 | 2 |
| WAL0101 | Sep 08.46 | 7412.96 | 35 | 6580 | -7.1 | | 1 | -5.1 | 5.9 | 3 |
| | | 7412.96 | | | -32.0 | 0.9 | 2 | -31.9 | 2.6 | 2 |
| MC254 | Sep 13.42 | 7417.92 | 35 | 6580 | | | | | | |
| MC256 | Sep 13.50 | 7418.00 | 35 | 6500 | -13.6 | | 1 | -7.7 | 3.1 | 2 |
| MC257 | Sep 13.59 | 7418.09 | 35 | 6560 | -32.4 | 1.3 | 3 | -33.7 | 1.9 | 3 |
| MC259 | Sep 14.47 | 7418.97 | 35 | 6580 | -6.4 | | 1 | -8.8 | 0.2 | 2 |
| MC260 | Sep 14.52 | 7419.02 | 35 | 6500 | -30.1 | 1.8 | 3 | -30.7 | 3.9 | 3 |
| MC261 | Sep 15.39 | 7419.89 | 35 | 6500 | | | | -8.1 | 1.8 | 2 |
| MC262 | Sep 15.44 | 7419.94 | 35 | 6580 | -30.2 | 1.2 | 3 | -32.9 | 3.3 | 3 |
| MC264 | Sep 16.39 | 7420.89 | 35 | 6580 | -7.9 | | 1 | -14.4 | 3.7 | 2 |
| | | 7420.89 | | | -31.1 | 1.4 | 3 | -36.2 | 6.4 | 2 |
| MC288 | Oct 25.40 | 7459.90 | 35 | 6580 | -28.6 | 1.1 | 3 | -29.9 | 2.9 | 3 |
| MC289 | Oct 30.37 | 7464.87 | 35 | 6580 | | | | | | |

*Observer code: PLC = P. Cottrell, MC = M. Clark, WAL = W. Lawson

discussed in Section 2.4.1.5. There are several aspects, and implications, of the pulsations of RY Sgr that are worthy of discussion.

(i) The spectra shown in Fig. 5.6 indicate that, during the line–splitting event, the two line components had a similar depth near JD 2447332. This Julian Date corresponds to about the time of $V_{max}$, and occurs 4–5 d after the maximum recessional velocity. This Julian Date is also 8–10 d after the lines were first noted to be asymmetric. Although we have no spectra of this particular event after JD 2447334, the time duration where two line components are visible may be 16–20 d, which corresponds to 0.4–0.5 of a pulsation cycle. This duration is greater than that noted in Section 5.2.1 (6–10 d) and demonstrates the advantage of digital spectra for studies of line profile changes.

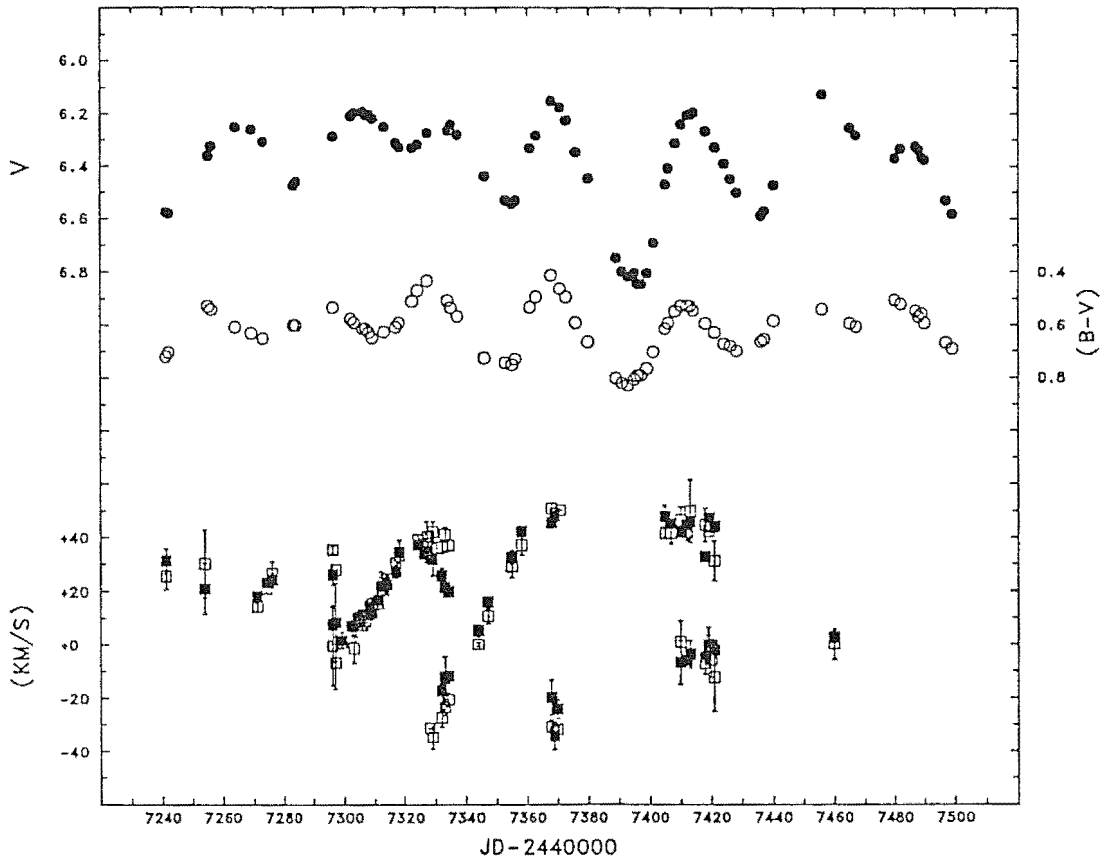


Figure 5.7. Light, $(B-V)$ colour and radial velocity curves for RY Sgr during 1988. For the radial velocity data, □ denotes the radial velocity for high excitation lines ($\chi > 8$ eV), whereas □ denotes that for low excitation lines ($\chi < 3$ eV).

The line asymmetries are less visible for the high excitation lines ($\chi > 8$ eV) due to the lower shock amplitude for these lines ($\sim 20$ kms$^{-1}$ near JD 2447332). [The low excitation lines (e.g. the 2.89 eV $\lambda$6369Å Fe II line) have a shock amplitude of $\sim 35$ kms$^{-1}$ near JD 2447332.] However, there appears to be little, or no, difference in the behaviour of lines as a function of excitation potential. This may indicate that there is no phase difference between the radial motions of the respective line formation regions.

(ii) There is some modulation of the radial velocity amplitude, but the period of the radial velocity curve appears almost constant from cycle to cycle. A mean cycle length of $\sim 40$ d can be estimated from points on the radial velocity curve at similar phases, e.g. at the centre of the line-splitting event or near the mean radial velocity ($\sim 5$ kms$^{-1}$). We Fourier analysed the radial velocity data following the method outlined in Section 2.3, and a periodicity of 41.0 d was identified. The Fourier analysis returned a high value for the 'false alarm' probability (Section 2.3), which indicates that the periodicity is *not* particularly significant. The analysis is hampered by the majority of the data being obtained near the shock events, thus limiting the phase coverage throughout the cycles,

and the analysis must interpolate between the two radial velocity measurements for each Julian Date.

In addition, unless the data is weighted in some arbitrary way, the analysis will favour fitting parts of the radial velocity curve where there are larger numbers of observations, e.g. near JD 2447320. (An indication of the poor fit to these data can be had from the amplitude of the 41.0 d periodicity of 9.6 $kms^{-1}$, whereas the amplitude of the variations range from 15–40 $kms^{-1}$.) There was some indication of shorter periods of $\sim$ 20 d duration from the Fourier analysis, which would be consistent with the presence of harmonics of the $\sim$ 40 d period. (Such harmonics are by–products of the analysis attempting to fit the asymmetry in the radial velocity curve with sine waves, but these are not necessarily physical parameters of the star.) There was little indication of longer periods.

A Fourier analysis of the MJUO $V$ photometry of RY Sgr, obtained between 1986–1989, indicated a most significant period of $\sim$ 39 d, and a next most significant period of $\sim$ 52 d. However, an analysis of the photometry obtained during the individual years suggested that the $\sim$ 52 d period had a larger amplitude than that of the $\sim$ 39 d period during 1988. (The presence of two dominant periods in these data explains the irregular appearance of the light curve during that year.) There is no clear evidence of the $\sim$ 52 d period, identified in the photometry, contributing to the period of the radial velocity data. However, note that the amplitude of the radial velocity data appears to change in sympathy with changes in the amplitude of the light amplitude. This may indicate that the $\sim$ 52 d period is making some contribution to the radial velocity variations, but that the $\sim$ 40 d period is the dominant pulsation mode. Possibly, the $\sim$ 52 d mode is not a radial mode. We suggested, in Section 2.5.1 that such modes in RCB stars, which are generally longer in period than the expected radial mode, may be indicative of non–radial pulsations.

(iii) In most of the line–splitting events, and in particularly near JD 2447325, there is a clear separation between the mean radial velocities for low and high excitation lines. We interpret this division as being due to the low excitation lines being formed in the higher (outer) regions of the highly extended photospheres of these stars, and are thus subject to pulsations of larger amplitude than are the higher excitation lines, which are generally formed at deeper (inner) layers. The effect is more apparent near JD 24474325, than for other cycles, due to these measurements being dominated by the velocities of the two Si II lines in order 36 (Section 5.2.1), which give particularly consistent radial velocity measurements, whereas the later spectra where mainly obtained in order 35 (H$\alpha$ region). The H$\alpha$ region contains more lines than does order 36, but there is a decrease in the accuracy of measurements for lines in this region due to the effects of greater line blending.

(iv) The photometric variations of RY Sgr are greater in amplitude than for any other known RCB (or HdC) star, and they appear to be driven by radial pulsations. Radial velocity variations have been searched for in a systematic way in only two other RCB stars. Raveendran, Ashoka & Rao (1986) found that the radial velocity amplitude of R CrB was 4–8 $kms^{-1}$ from published radial velocities obtained since 1972, and phased these data to a period of 47.18 d. [Note that the value for the period determined by Raveendran, Ashoka & Rao is similar to the value of $\sim$ 45 d, determined by Fernie (1989), from a Fourier analysis of photometry obtained since 1972.] In Section 4.3.7 we discussed radial

velocities of NSV 6708 obtained at MJUO during 1988 and 1989. Only an upper limit of $\sim$ 4 $kms^{-1}$ could be estimated from these data, which gave little indication of an amplitude above the 2–4 $kms^{-1}$ uncertainty in these measurements.

The results of Chapter 2 and 4, and published photometry of R CrB (Fernie 1989), indicate that the light and colour amplitudes of most RCB and HdC stars are typically 0.1–0.2 mag. Of these stars, few have amplitudes that approach those of RY Sgr. U Aqr and NSV 6708 are examples, and yet we found that NSV 6708 must have a very low radial velocity amplitude. It is possible that such low ($< 10$ $kms^{-1}$) radial velocities variations are typical in these stars, and that the amplitude of the pulsations in RY Sgr are unique amongst known RCB and HdC stars.

(v) The formation of dust in RCB stars, which leads to the declines of these stars (Chapter 3), is usually linked to radial pulsations. Frequently, the large amplitude pulsations of RY Sgr are cited in support of this claim, yet the pulsation amplitude of RY Sgr is not typical. Pugach (1977) claimed that declines of RY Sgr commenced near maximum light on visual light curves of this star. It is not surprising that this claim has been taken in support of the linking of the pulsations of this star and the dust formation mechanism (Lawson 1986; Hill 1987). However, we consider it uncertain whether visual light curves offer sufficient accuracy to determine the onset phase. The 0.3–0.7 mag $V$ amplitude of RY Sgr will dominate the early light curve of the decline, as the timescale of the photometric variations at maximum is similar to that of the initial stages of a decline. Thus the light curve may give the appearance of the decline starting near a $V$ maximum, irrespective of the onset phase.

We note that while there has been no extensive survey of the occurence of declines in RCB stars, the decline rate of RY Sgr appears to be typical. Such data are, in general, only available from visual light curves. The occurence of declines in RY Sgr (see Mayall 1972) appears similar to that of R CrB (see Hoffmeister, Richter & Wenzel 1985), and both stars appear less active than NSV 6708 (Section 4.1). Thus, within the limited sample of RCB stars for which radial velocity information exists, there is no obvious correlation between pulsation amplitude and the decline rate.

(vi) Saio (1986) reviewed attempts to model the pulsations of cool hydrogen deficient carbon stars. For most early attempts (Trimble 1972; Wood 1976; King *et al.* 1980), great difficulty was had in attaining stable limit cycles. The non–linear pulsations of 1 $M_{\odot}$ models with $T_{eff} \sim 6000$ K and $L/L_{\odot} \sim 10^4$ were so violent the the amplitude grew until the expansion velocity attained the escape velocity of the star (Trimble 1972). King *et al.* (1980) showed that models with $M > 1.6$ $M_{\odot}$, $T_{eff} = 6300$ K and $L/L_{\odot} = 1.13 \times 10^4$ had pulsations that had stable amplitudes, and they suggested that the masses of the RCB stars should be greater than $\sim 1.4$ $M_{\odot}$. This mass was in conflict with the result of Schönberner (1977) who had obtained a value of $\sim 0.7$ $M_{\odot}$ by using spectroscopically determined surface gravities and evolutionary models with a CO core and a thin helium envelope. In addition to the mass problem for these stars, the analyses of Schönberner (1975) and Cottrell & Lambert (1982a) had shown the effective temperatures of R CrB, XX Cam and RY Sgr to be about 7000 K.

Saio & Wheeler (1985) showed that the pulsations remained within bound limits for

**Table 5.3.** Comparison between RY Sgr and Model 7 of Saio & Wheeler.

| | RY Sgr | Model 7 |
|---|---|---|
| Mass ($M_\odot$) | $\sim 0.7$ | 0.9 |
| $T_{eff}$ (K) | $\sim 7000$ | 7200 |
| log ($L/L_\odot$) | $\sim 4$ | 4.23 |
| $\Delta$V (mag) | 0.2–0.7 | 0.8–1.0 |
| $\Delta v_{radial}$ (kms$^{-1}$) | 15–50 | 30–40 |
| phase of shock | $\sim V_{max}$ | $\sim V_{min}$ |

$T_{eff} \sim 7000$ K and $M < 1.0\ M_\odot$. The pulsations of the low mass models were irregular and the growth in the pulsation model was restrained by a shock wave which dissipated the kinetic energy of the pulsations. Thus, the models of Saio & Wheeler would seem to have some characteristics similar to those observed in RY Sgr. A comparison is made between the characteristics of RY Sgr and those Model 7 of Saio & Wheeler, which most closely resemble RY Sgr, in Table 5.3. Although the radial velocity amplitude of the model is similar to that of the star, the light amplitude is somwhat larger and the phase relationship between the light and radial velocity variations of the model does not agree with the observed one. Despite a partial agreement between the characteristics of RY Sgr and Model 7, it is difficult to reconcile the lower radial velocity amplitudes observed in R CrB and NSV 6708 with these models.

### 5.2.5 CONCLUSIONS

The large amplitude (15–50 kms$^{-1}$) radial velocity amplitude of RY Sgr may be unique amongst currently known RCB stars. The only other RCB stars which have been surveyed for radial velocity variations, R CrB and NSV 6708, have pulsation amplitudes of 4–8 kms$^{-1}$ and $<4$ kms$^{-1}$ respectively. If the low radial velocity amplitudes observed in R CrB and NSV 6708 are typical for RCB and HdC stars, then observing such low amplitudes in other RCB stars will be a difficult task. An attempt should be made, however, to detect radial velocity variations in the stars with larger amplitude photometric variations, e.g. U Aqr. With some knowledge of the photometric characteristics of the star, observations to obtain radial velocities could be made at extreme phases (e.g., $V_{max}$ and $V_{min}$), to enhance to detection of radial velocity variations.

The declines of RCB stars have generally been associated with the pulsations of the star. The suggestion is that the radial pulsations cause the ejection of gas which condenses into the obscuring dust. The low pulsation amplitude observed in R CrB and NSV 6708 leads us to question this association, as the occurence of declines in RY Sgr is not enhanced by the larger amplitude pulsations of this star. The onset of a decline of RY Sgr has yet to be observed photoelectrically or spectroscopically. The acquisition of such data may hold important keys about the role of the pulsations, if any, with the declines.

The most successful models of the pulsations of RCB stars (Saio & Wheeler 1985) reproduce the typical radial velocity amplitude observed in RY Sgr, but not the light

amplitude or the phase relationship between the light and velocity variations. However, these models do not explain the lower light or radial velocity amplitudes observed in most other RCB stars. The reduction in both light and radial velocity amplitude, and explaining the differences between these stars, must be the main ambitions of future attempts to model the pulsations of these stars.

# Chapter 6

# Summary and future work

## 6.1 SUMMARY

Observations of many R Coronae Borealis (RCB) stars and Hydrogen deficient Carbon (HdC) stars have been obtained to more fully understand the characteristics of these types of stars.

The properties of the low amplitude light variations observed in all of these stars were discussed and analysed using Fourier techniques. Photometry was obtained over intervals of 700–1100 d for many of these stars, which permitted a more accurate analysis of the light and colour curves of these objects than was possible with previously published data. Prior to the MJUO survey of these objects, these types of observations had only been obtained over short durations and at highly irregular intervals. The Fourier analysis of the photometry indicated the presence of several periodicities in the light curves of most stars, and period switching in others.

Preliminary results of a spectroscopic survey of these stars were also discussed. Temperatures were estimated for these stars by a comparison with the spectra of RCB and HdC stars with known temperatures. By combining the observed periods and estimated temperatures, a period–temperature relationship was produced. The positions of most RCB and HdC stars in this plane, and those of the hotter extreme Helium (eHe) stars, can be satisfied by a single relationship for model hydrogen deficient carbon stars pulsating in the fundamental radial mode. Some stars have periods that can be attributed to either first, or second, harmonic radial modes. Several stars have periods longer than the fundamental radial mode. These longer periods may be due to non–radial pulsations.

The onsets of declines for several RCB stars have been observed. The analyses of these observations have extended our understanding of these events, and have indicated a diversity of characteristics.

Significantly, the observations of the 1988 decline of R CrB represent the first occasion where both photometric *and* spectroscopic observations were obtained throughout a decline onset. The spectra showed a rapid transition from the photospheric absorption spectrum observed at maximum light, to one dominated by chromospheric emission. In addition, a broad emission of unconfirmed origin, was observed at about this time, which caused the $(U–B)$ and $(B–V)$ colours to become bluer than at maximum light. Photometrically, this event was similar to the decline onset of several other RCB stars. We have called these declines 'blue' type declines. The model of these 'blue' type declines is the standard eclipse model, namely where a obscuring cloud, smaller in size than the photosphere and initially optically thick, expands (either radially or laterally or both) and progressively obscures the photosphere, and then the chromosphere.

For other declines, the photometric colours became redder in phase with the fade in

the $V$ magnitude. These declines we have termed 'red' declines. About half of all declines, for which the decline onset has been observed photoelectrically, are of this type. The most likely explanation for the colour behaviour of this type of event is that the dust cloud obscures the entire photosphere, and possibly much of the inner chromosphere, at the decline onset.

Photometry obtained during the rising branch of declines show a range of extinction, due to the obscuring material, with observed values for $A_V/E(B-V)$ between 3.2 and 10.3. By applying the results of recent laboratory values of extinction due to amorphous carbon and graphite particles, this range of extinction may be due to different particle sizes being present during different declines.

Extensive observations of the recently identified RCB star NSV 6708 were obtained at MJUO and sourced from the literature. Spectra of NSV 6708 show significant hydrogen, in contrast to most other RCB stars. SAAO *JHKL* and *IRAS* PSC infrared photometry indicate a dust shell temperature of 900±50 K. Photometry obtained during 1988 and 1989 indicated a range of periodicities between $\sim$ 45 d and $\sim$ 110 d. Radial velocity measurements indicate an upper limit to the the pulsation amplitude of $\sim$ 4 kms$^{-1}$. This low amplitude causes some difficulty for the standard decline model, which assumes that the dust formation is linked to radial pulsations.

Two aspects of the RCB star RY Sgr were investigated in detail. (i) Existing O–C analyses, that determined the rate of change of the pulsation period of the star, were extended using more recent MJUO photometry and visual estimates. The times of maxima on the light curve were interpreted with quadratic, cubic and linear piecewise solutions. Only a series of linear piecewise solutions satisfied the O–C residuals to within the observational uncertainty. Four such solutions were identified since 1948. These solutions had lifetimes of $\sim$ 100 cycles (equivalent to $\sim$ 10 yrs), which suggests that the period changes may be semi–periodic. The polynomial solutions can be considered as describing the mean period rate of change. These gave a value of $-1.4 \times 10^{-3}$ d cycle$^{-1}$. This rate is consistent with model hydrogen deficient carbon stars evolving through the region of the H–R diagram occupied by the RCB stars towards higher temperatures. (ii) MJUO échelle spectra were obtained during several pulsation cycles of RY Sgr during 1988. These spectra were obtained to study the line–splitting event near $V_{\max}$, which is due to a shock wave near minimum radius, and for a future abundance analysis. The radial velocity variations appear to be in phase with the $\sim$ 38 d period identified in the MJUO photometry of this star. Low excitation ($\chi < 3$ eV) lines showed a greater shock amplitude than did the high excitation ($\chi > 8$ eV) lines. This division was interpreted as being due to low excitation lines being formed in the upper regions of the highly extended photospheres of these stars.

## 6.2 FUTURE WORK

Many of the findings of this thesis would benefit from the acqusition of additional data to support, or improve, our current understanding of these stars.

In Chapter 2, significant harmonic contributions were identified in the photometry of several stars, e.g. U Aqr and RT Nor. In the case of U Aqr, the two identified periods (81.30 d and 40.16 d) are in the ratio 2.02:1 which indicates that the 40.16 d period is probably an harmonic of a 81.30 d fundamental mode (where a 2:1 ratio would be

expected), rather than a first harmonic radial mode [where the 'Case 1' of Weiss (1987a) predicts a ratio of $\sim$ 3:1 near $T_{eff}$ = 5500 K]. The Fourier analysis of the 1986–1987 $V$ photometry also indicated a period of $\sim$ 23.5 d, which may be the second harmonic of the 81 d period, or possibly the second harmonic radial mode. This period was considered to be insignificant, using the 'false alarm' probability discussed in Section 2.3, and it was not included in Table 2.21. Additional data may improve the values of these periods and confirm the reality of this third period.

For several stars, periods longer than the model fundamental radial mode of the 'Case 1' of Weiss (1987a) were found. We tentatively suggested that non–radial modes may be the cause of these longer periods. Discussions with others [Weiss (Max Planck), Wheeler (McDonald Observatory), Hill and Jeffery (St. Andrews)] have not yet produced an alternative explanation for these periods.

Many RCB and HdC stars remain poorly observed. Stars for which little, or no, photometry has been obtained at maximum light include UW Cen, WX CrA and VZ Sgr and, with the exception of R CrB (Fernie 1989), most of the northern members of these stars. The photometric programme at MJUO should be extended to observe neglected southern stars. Northern hemisphere RCB and HdC stars should be observed in a parallel programme.

In Section 5.2, we discussed the uniqueness of the radial velocity amplitude, and the shock event in RY Sgr. We mentioned the partial success of pulsation models in reproducing some of the aspects of the pulsations of RY Sgr. We also noted the failure of these models to predict the lower light amplitudes in most other RCB and HdC stars and the low radial velocity amplitudes observed in R CrB and NSV 6708.

We hope that the observed periods, and radial velocity amplitudes, for these stars will encourage new attempts to model the evolution and pulsations of the cool hydrogen deficient carbon stars. Such aspects as explaining the longer periods, and the low light and radial velocity amplitudes (which may be typical), should be the main ambitions of such attempts.

The evolution of these stars, and the direction of evolution, remains in dispute. We discussed in Section 2.5.2 that a single relationship in the period–temperature plane can satisfy the observed periods and temperatures of most RCB, HdC and eHe stars. The observed period rate of change of RY Sgr (Section 5.1) is consistent with the direction of evolution being towards higher temperatures, and presumably, towards the eHe stars. However, the lack of declines and circumstellar material surrounding most eHe (and HdC) stars, causes great difficulty for this evolutionary scheme.

The most favoured origin for these stars is the merger of a CO-He white dwarf binary (Webbink 1984). Recently, Iben & Tutukov (1989) have related the theoretical 'superhorizontal branch' formed by such mergers to the observed sequence of eHe, HdC and RCB stars. Iben & Tutukov suggest that the direction of evolution is from the eHe stars, via the HdC stars, to the RCB stars. Such a direction would explain the lack of declines and rarity of dust shells in eHe and HdC stars. Support for this scheme may come from the evolutionary models of Weiss (1987b), which suggested that less luminous hydrogen deficient stars (by inference the eHe and HdC stars) evolve towards lower temperatures while the more luminous stars (the RCB stars) evolve in the opposite direction.

While the periods and temperatures of RCB, HdC and eHe stars are mostly satisfied by a single period–temperature relationship, it is possible that the situation is more complex

in the period–luminosity or temperature–luminosity plane. We have shown such an evolutionary sequence, in schematic form, in Fig. 6.1. The direction of evolution is from a white dwarf binary (not shown), via the eHe, HdC and RCB stars to the hot RCB/PN–type stars (DY Cen, MV Sgr, V348 Sgr), and back to a degenerative system (not shown).

Such an evolutionary scheme remains to be confirmed. The analysis of spectroscopic data, for a large sample of the RCB, HdC and eHe stars, may confirm the suggestion of differing CNO abundances between these groups. Differences in the abundances of key elements, if confirmed, may act as a tracer of the evolution of these objects. Such information may also be had from a determination of the period rate of change for more of these stars and from estimates of their luminosities.

The photometry of the declines of RCB stars suggested that there are two extreme types of colour behaviour. We termed these decline types 'blue' and 'red', depending upon the behaviour of the ($U$–$B$) and ($B$–$V$) colours during the initial stages of the decline. We related these types to the size of the obscuring dust cloud with respect to the size of the photosphere of the star (Section 3.1.5.1). While spectroscopic data are available for the 1967–1971 decline of RY Sgr and the 1988-1989 of R CrB, which were both 'blue' type declines, there is little spectroscopic data for 'red' type declines. (The only spectra obtained during the initial stages of a 'red' type decline were for the 1988 decline of NSV 6708 (Chapter 4).] If our model of the 'red' type declines is correct, we anticipate two spectroscopic signatures. (i) We expect that only low excitation chromospheric lines would be present after the obscured (and combined) photospheric and inner chromospheric flux were sufficiently suppressed for these low excitation emission lines (from the outer chromosphere) to be visible. (ii) We predict that the transition from a photospheric– to a chromospheric–dominated spectrum would occur at a fainter magnitude, than during a 'blue' decline, as the chromosphere is already largely obscured by the dust cloud.

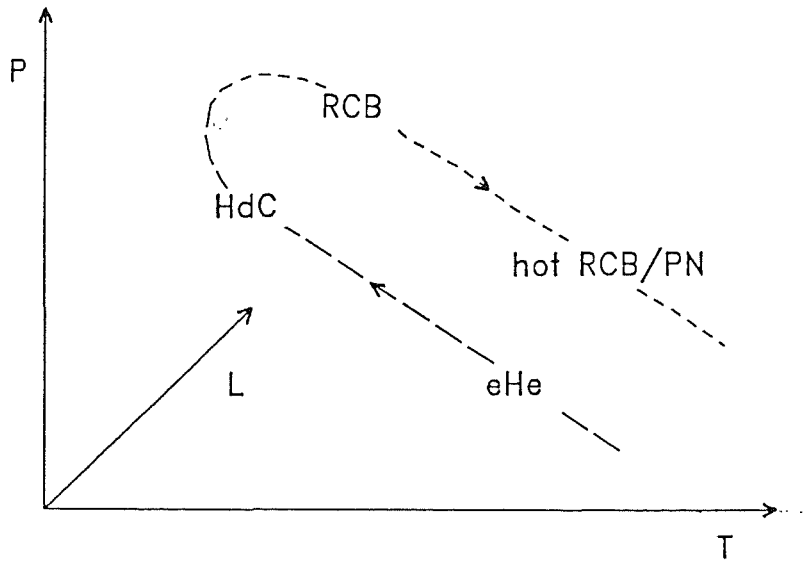


**Figure 6.1.** Schematic evolutionary sequence, in the period (P), temperature (T) and luminosity (L) planes, of Iben & Tutukov (1989).

SAAO spectra of the decline of NSV 6708 supported this second point (see Section 4.3.4). High–to–medium resolution ($\Delta\lambda$0.1–1.0Å) spectra need to be obtained during the transition between the photospheric– and chromospheric–dominated spectrum to confirm the first point.

We have questioned the possible relationship between the radial pulsations of these stars and the declines. The decline onsets appear to occur at different phases of the low amplitude variations of R CrB (Section 3.1.5.4) and there appears to be no relationship between the radial velocity amplitude, and the occurrence of declines, for these stars [Section 5.2.4 (iv)]. If these observations are supported by future data, then the dust formation mechanism remains uncertain. Little is known about the location of the dust, whether the growth of the dust cloud is mainly *lateral* or *radial*, or the eventual fate of the dust cloud. Spectroscopy (including the 1–5$\mu$m region), polarimetry and multi–colour photometry of the star and its circumstellar shell, obtained during the initial decline stage, may place constraints upon the location and early evolution of the obscuring cloud.

Photometry obtained during the rising branch of the decline indicated a range of extinction due to the obscuring material. We noted in Section 3.2.4 that near–visual or infrared photometry is a poor indicator of the evolution of particle size and that this information will only be obtained at ultraviolet wavelengths. In particular, the extinction peak near 2400Å is highly dependent upon particle size. We suggest that *IUE* spectrophotometry (or similar) obtained during the decline, and in particular during the rise, would be a sensitive indicator of the extinction of the obscuring dust, and its evolution with time.

# Acknowledgements

I would like to thank my supervisor, Dr Peter Cottrell, for suggesting this project. Much of the planning for this programme, and its execution, has been a collaborative effort between us. The RCB stars have always been rewarding to study, and there have been many occasions where established ideas about these stars have required much revision.

Alan Gilmore and Pam Kilmartin have obtained most of the photometric observations for this project and they have maintained this effort for over 3 years. Mike Clark obtained many of the échelle/LDA spectra of RY Sgr, R CrB and NSV 6708. I am indebted to Alan, Pam and Mike for obtaining these observations. This thesis would have been very different without their efforts. I would also like to thank Alan and Pam for the many meals that I was invited to, and Mike and June Clark for their hospitality, during my frequent visits to Mount John.

Mike Clark and John Baker did a lot of running repairs to the detectors, often at night, so that I could keep observing. In the Department, Graham Kershaw, Wayne Smith, Ross Ritchie and Stephen Beuzenberg, amongst others, have maintained and improved the telescopes and detectors.

William Tobin stood in as my advisor while Peter was on Study Leave at Mount Stromlo Observatory. Thanks William. I hope that I didn't cause too much trouble.

Bryan Lawrance gave me a VAX FORTRAN version of the Lomb–Scargle Fourier code that made the analysis of the photometry all the more interesting. Bryan, and the other graduate students in the Physics Department, have made my time in the Department very enjoyable.

My fellow Astronomy students during this time (Phil, Jason, Kaylene, Karen, Michael, Alan and Steve) have often been sources of good ideas. I hope that I have contributed as much in return to their own work.

Many other Astronomers have influenced my study of these stars. In no special order, they include those I met in India during 1985; Michael Feast, Phil Hill, Alexander Pugach, Hideyuki Saio, Yu Fadayev and David Lambert. At other times, either personally or through correspondence, Peter Wood, George Wallerstein, Craig Wheeler, Achim Weiss and Dave Kilkenny have commented on my work and have offered advice or support. I would also like to thank Frank Bateson for supplying visual estimates of these stars, and decline reports.

Throughout most of the duration of this thesis, I have held a Department of Physics Teaching Assistantship, for which I am grateful. I would also like to acknowledge financial support from: the Department of Physics and the Kingdon–Tomlinson fund of the Royal Astronomical Society of New Zealand, to observe in Australia during November 1988; the Kingdon–Tomlinson fund of the RASNZ, the Royal Society of New Zealand Canterbury Branch and the organising committee of the *6th Cambridge Workshop on Cool Stars, Stellar Systems and the Sun*, to attend this meeting in Seattle during September 1989; and the Astronomy Department of the University of Texas at Austin, which funded my visit to Austin during September 1989. David and Daphne Lambert deserve special thanks for their hospitality during my stay in Austin.

Lastly, a very special thank you Jennie, for your patience and support during my years as a graduate student.

# References


Alexander, J.B., Andrews, P.J., Catchpole, R.M., Feast, M.W., Lloyd Evans, T., Menzies, J.W., Wisse, P.N.J. & Wisse, M., 1972. *Mon. Not. R. astr. Soc.*, **158**, 305.

Allen, C.W., 1976. *Astrophysical Quantities*, 3rd edn, Athlone Press, London.

Allen, D.A., 1980. *Astrophys. Lett.*, **20**, 131.

Ashoka, B.N. & Pukalenthi, S., 1986. *Info. Bull. Var. Stars No. 2908.*

Bateson, F.M., 1958. *The observation of variable stars,* Var. Star Section, R. astr. Soc. New Zealand, Tauranga.

Bateson, F.M., 1973. *Publs var. Star Section, R. astr. Soc. New Zealand,* **1**, 33.

Bateson, F.M., 1975. *Publs var. Star Section, R. astr. Soc. New Zealand,* **3**, 1.

Bateson, F.M., 1978. *Publs var. Star Section, R. astr. Soc. New Zealand,* **6**, 39.

Bateson, F.M., 1989. *Publs var. Star Section, R. astr. Soc. New Zealand, Circ. No., M88/12, M89/1, M89/2, M89/3, M89/4.*

Bateson, F.M. & Jones, A.F., 1975. *Circ. var. Star Section, R. astr. Soc. New Zealand No. 193.*

Bateson, F.M. & Morel, M., 1988. *Charts for southern variables Series 20,* Astronomical Research Ltd., Tauranga.

Bateson, F.M., Morel, M. & Sumner, B., 1982. *Charts for southern variables Series 14,* Astronomical Research Ltd., Tauranga.

Bateson, F.M., Morel, M., Sumner, B. & Winnett, 1977. *Charts for southern variables Series 9,* Astronomical Research Ltd., Tauranga.

Bateson, F.M., Morel, M., Sumner, B. & Winnett, 1979a. *Charts for southern variables Series 11,* Astronomical Research Ltd., Tauranga.

Bateson, F.M., Morel, M., Sumner, B. & Winnett, 1981. *Charts for southern variables Series 13,* Astronomical Research Ltd., Tauranga.

Bateson, F.M., Morel, M. & Winnett, R., 1979b. *Charts for southern variables Series 10,* Astronomical Research Ltd., Tauranga.

Berman, L., 1935. *Astrophys. J.*, **81**, 369.

Bessell, M.S., 1976. *Publs astr. Soc. Pacif.*, **88**, 557.

Bessell, M.S., 1979. *Publs astr. Soc. Pacif.*, **91**, 589.

Bidelmann, W.P., 1953. *Astrophys. J.*, **117**, 25.

Bidelmann, W.P., 1986. In: *IAU Coll. 87,* p. 3, eds K. Hunger *et al.*, Reidel, Dordrecht.

Böhme, D., 1983. *Info. Bull. Var. Stars No. 2442.*

Böhme, D., 1985. *Info. Bull. Var. Stars No. 2835.*

Böhme, D., 1986. *Info. Bull. Var. Stars No. 2962.*

Böhme, D., 1987. *Info. Bull. Var. Stars No. 3115.*

Bond, H.E., Luck, R.E. & Newman, M.J., 1979. *Astrophys. J.*, **233**, 205.

Borghesi, A., Bussoletti, E., Colangeli, L., 1985. *Astr. Astrophys.*, **142**, 225.

Burnstein, D. & Heiles, C., 1982. *Astrophys. J.*, **87**, 1165.

Cottrell, P.L. & Lambert, D.L., 1982a. *Astrophys. J.*, **261**, 595.

Cottrell, P.L. & Lambert, D.L., 1982b. *Observatory*, **102**, 149.

Cottrell, P.L., Lawson, W.A. & Smith, S.M., 1988. In: *IAU Symp. 132*, p.205, eds G. Cayrel de Strobel & M. Spite., Reidel, Dordrecht.

Cousins, A.W.J., 1983. *Circ. South African Astr. Obs.*, **7**, 36.

Cox, J.P., 1980. *Theory of Stellar Pulsation*, Princeton University Press, Princeton, New Jersey.

Danziger, I.J., 1963. *PhD thesis*, Australian Nat. Univ.

Deeming, T.J., 1975. *Astrophys. Space Sci.*, **36**, 137.

Dunn, R.B., Evans, J.W., Jefferies, J.T., Orrall, F.Q., White, O.R. & Zirker, J.B., 1967. *Astrophys. J. Suppl.*, **15**, 275.

Drilling, J.S., 1986. In: *IAU Coll. 87*, p. 9, eds K. Hunger *et al.*, Reidel, Dordrecht.

Drilling, J.S. & Hill, P.W., 1986. In: *IAU Coll. 87*, p. 499, eds K. Hunger *et al.*, Reidel, Dordrecht.

Eggen, O.J., 1970. *Publs astr. Soc. Pacif.*, **82**, 851.

Fadeyev, Y.A., 1988. *Mon. Not. R. astr. Soc.*, **233**, 65.

Feast, M.W., 1972. *Mon. Not. R. astr. Soc.*, **158**, 11P.

Feast, M.W., 1979. In: *IAU Coll. 46*, p. 246. ed. F.M. Bateson, University of Waikato, New Zealand.

Feast, M.W., 1986. In: *IAU Coll. 87*, p. 151, eds K. Hunger *et al.*, Reidel, Dordrecht.

Fernie, J.D., 1982. *Publs astr. Soc. Pac.*, **94**, 172.

Fernie, J.D., 1989. *Publs astr. Soc. Pacif.*, **101**, 166.

Fernie, J.D., Percy, J.R. & Richter, M.G., 1986. *Publs astr. Soc. Pac.*, **98**, 605.

Fernie, J.D., Sherwood, V. & DuPuy, D.L., 1972. *Astrophys. J.*, **172**, 383.

Genet, R.M., Boyd, L.J. & Hall, D.S., 1986. In: IAU Symp. 118, p. 47, eds J.B. Hearnshaw & P.L. Cottrell, Reidel, Dordrecht.

Gillet, D., Duquennoy, A., Bouchet, P. & Gouiffes, C., 1989. *Astron. Astrophys.*, **215**, 316.

Gillett, F.C., Backman, D.E., Beichman, C. & Neugebauer, G., 1986. *Astrophys. J.*, **310**, 842.

Giridhar, S. & Rao, N.K., 1986. In: *IAU Coll. 87*, p.177, eds K. Hunger *et al.*, Reidel, Dordrecht.

Goldsmith, M.J. & Evans, A., 1985. *Irish Astron. J.*, **17**, 308.

Goncharova, R.I., Kovalchuk, G.U. & Pugach, A.F., 1983. *Astrophys.*, **19**, 161.

Gordon, M.A., 1976. In: *Methods in Experimental Physics*, **12C**, p. 277, ed. M.L. Meek, Academic Press, New York.

Gustad, J.E., Stein, W.,A., Forrest, W.J. & Pipher, J.L., 1988. *Publs astr. Soc. Pacif.*, **100**, 388.

Hecht, J., Holm, A.V., Donn, B. & Wu, C.C., 1984. *Astrophys. J.*, **280**, 228.

Herbig, G.H., 1949. *Astrophys. J.*, **110**, 143.

Hill, P.W., 1987. *Q. Jl. R. astr. Soc.*, **28**, 225.

Hodge, P.W. & Wright, F.W., 1969. Astrophys. J. Suppl., **17**, 467.

Hoffmeister, C., Richter, G. & Wenzel, W., 1985. *Variable Stars,* Springer–Verlag, Berlin.

Holm, A.V., Wu, C.C. & Doherty, L.R., 1982. *Publs astr. Soc. Pacif.*, **94**, 548.

Holm, A.V., Hecht, J., Wu, C.C. & Donn, B., 1987. *Publs astr. Soc. Pacif.*,**99**, 497.

Horne, J.H. & Baliunas, S.L., 1986. *Astrophys. J.*, **302**, 757.

Howarth, I.D., 1976. *Publs Var. Star Section, R. astr. Soc. New Zealand,* **4**, 4.

Howarth, I.D., 1977. *Acta Astr.*, **27**, 65.

Hunger, K, Schönberner, D. & Steenbock, W., 1982. *Astr. Astrophys.*, **107**, 93.

Iben, I. Jr. & Tutukov, A.V., 1985. *Astrophys. J. Suppl.*, **58**, 661.

Iben, I. Jr. & Tutukov, A.V., 1989. *Astrophys. J.*, **342**, 430.

Innes, R.T.A., 1903. *Ann. Cape Obs.*, **9**, 135B.

Jacchia, L., 1933. *Publs Oss. astr. U. Bol.*, **2**, 173.

Jeffery, C.S., Drilling, J.S. & Heber, U., 1987. *Mon. Not. R. astr. Soc.*, **226**, 317.

Jeffery, C.S., Hill, P.W. & Morrison, K., 1986. In: *IAU Coll. 87,* p. 95, eds K. Hunger *et al.*, Reidel, Dordrecht.

Jeffery, C.S., Skillen, I., Hill, P.W., Kilkenny, D., Malaney, R.A. & Morrison, K., 1985. *Mon. Not. R. astr. Soc.*, **217**, 701.

Joy, A.H. & Humason, M.L., 1923. *Publs astr. Soc. Pacif.*, **25**, 327.

Keenan, P.C. & Greenstein, J.L., 1963. *Contr. Perkins Obs. (Ohio)*, Series II, No. 13, p197.

Kilkenny, D., 1982. *Mon. Not. R. astr. Soc.*, **200**, 1019.

Kilkenny, D., 1983. *Mon. Not. R. astr. Soc.*, **205**, 907.

Kilkenny, D., 1989. *Observatory,* **109**, 88.

Kilkenny, D., Coulson, I.M., Laing, J.D., Spencer Jones, J.H. & Engelbrecht, C., 1985. *Circ. South African Astr. Observatory,* **9**, 87.

Kilkenny, D. & Flanagan, C., 1983. *Mon. Not. R. astr. Soc.*, **203**, 19.

Kilkenny, D., & Lloyd Evans, T., 1989. *Observatory,* **109**, 85.

Kilkenny. D. & Lynas–Gray, A.E., 1982. *Mon. Not. R. astr. Soc.*, **198**, 873.

Kilkenny, D. & Marang, F., 1989. *Mon. Not. R. astr. Soc.*, **238**, 1P.

Kilkenny, D., Marang, F. & Menzies, J.W., 1988. *Mon. Not. R. astr. Soc.*, **233**, 209. (KMM)

Kilkenny, D. & Whittet, D.C.B., 1984. *Mon. Not. R. astr. Soc.*, **208**, 25.

King, D.S., Wheeler, J.C., Cox, J.P., Cox, A.N. & Hodson, S.W., 1980. In: *'Nonradial and Nonlinear Stellar Pulsations,* eds H.A. Hill & W.A. Dziembowski, Springer–Verlag, Berlin.

Kholopov, P.N., Samus, N.N., Frolov, M.S., Goranskij, V.P., Gorynya, N.A., Kararovets, E.V., Kireeva, N.N., Kukarkina, N.P., Kurohkin, N.E., Medvedeva, G.I., Perova, N.B., Rastorguev, A.S. & Shugarov, S. Yu., 1985. *General Catalogue of Variable Stars,* 4th edn, Nauka Publishing House, Moscow.

Kurtz, D.W. & Marang, F., 1987. *Mon. Not. R. astr. Soc.*, **228**, 141.

Latham, D.W. & Sternberg, A., 1977. *Center for Astrophys. Preprint Series No. 827.*

Lambert, D.L., 1986. In: *IAU Coll. 87,* p. 127, eds K. Hunger *et al.,* Reidel, Dordrecht.

Lawson, W.A., 1986. In: *IAU Coll. 87,* p. 211, eds K. Hunger *et al.,* Reidel, Dordrecht.

Lawson, W.A. & Cottrell, P.L., 1988. *Mon. Not. R. astr. Soc.,* **231,** 609.

Lawson, W.A. & Cottrell, P.L., 1990. *Mon. Not. R. astr. Soc.,* **242,** 259.

Lawson, W.A., Cottrell, P.L. & Bateson, F.M., 1988. *Publs var. Star Section, R. astr. Soc. New Zealand,* **14,** 28.

Lawson, W.A., Cottrell, P.L. & Bateson, F.M., 1989. *Publs var. Star Section, R. astr. Soc. New Zealand,* **15,** 1.

Lawson, W.A., Kilmartin, P.M. & Gilmore, A.C., 1988a. *Info. Bull. Var. Stars No. 3214.*

Lawson, W.A., Kilmartin, P.M. & Gilmore, A.C., 1988b. *Info. Bull. Var. Stars No. 3178.*

Lawson, W.A., Kilmartin, P.M., Gilmore, A.C. & Clark, M., 1987. *Info. Bull. Var. Stars No. 3085.*

Lawson, W.A., Cottrell, P.L., Gilmore, A.C. & Kilmartin, P.M., 1989. *J. Astrophys. Astr.,* **10,** 151.

Lomb, N.R., 1976. *Astrophys. Space Sci.,* **39,** 447.

Loreta, E., 1934. *Astr. Nach.,* **254,** 151.

Ludendorff, H., 1906. *Astr. Nach.,* **173,** 3.

Luyten, W.J., 1927. *Bull. Harvard Observ.,* **846,** 33.

Lynas–Gray, A.E., Kilkenny, D., Skillen, I. & Jeffery, C.S., 1986. In: *IAU Coll. 87,* p. 87, eds K. Hunger *et al.,* Reidel, Dordrecht.

McNaught, R., 1988. *South. Astr.,* **1,** 40.

MacQueen, P.J., 1986. *PhD thesis,* University of Canterbury.

Marang, F., Kilkenny, D., Menzies, J.W. & Spencer Jones, J.H., 1989. preprint.

Marraco, H. G. & Milesi, G. E., 1982. *Astr. J.,* **87,** 1775.

Martinez, P., 1989. *Mon. Not. R. astr. Soc.,* **238,** 439.

Matthews, J.M., Kreidl, T.J. & Wehleu, W.H., 1988. *Publs astr. Soc. Pacif.,* **100,** 255.

Mayall, M.W., 1972. *J. R. astr. Soc. Canada,* **66,** 233.

Milone, L.A., 1975. *Info. Bull. Var. Stars No. 989.*

Menzies, J.W., 1986. In: *IAU Coll. 87,* p. 207, eds K. Hunger *et al.,* Reidel, Dordrecht.

Morgan, D.H., Nandy, K. & Rao, N.K., 1986. In: *IAU Coll. 87,* p. 225, eds K. Hunger *et al.,* Reidel, Dordrecht.

Noyes, R.W. & Avrett, E.H., 1987. *"The Solar Chromosphere"* in *"Spectroscopy of Astrophysical Plasmas"*, eds A. Dalgarno & D. Layzer, (Cambridge University Press), p125.

O'Keefe, J.A., 1939. *Astrophys. J.,* **90,** 294.

Payne–Gaposchkin, C., 1963. *Astrophys. J.,* **138,** 320.

Payne–Gaposchkin, C.E., 1971. *Smithsonian Cont., No. 13.*

Percy, J.R., Carriere, L.E.M. & Fabro, V.A., 1987. *Astron. J.,* **93,** 200.

Pickering, E.C., 1896. *Astr. Nach., No. 3362.*

Piggott, E., 1797. *Phil. Trans. R. Soc., Pt. I,* 133.

Poretti, E., 1989. *Astron. Astrophys.*, **220,** 144.

Press, W.H. & Teukolsky, S.A., 1988. *Computers in Physics,* Nov/Dec, p. 77. American Inst. of Phys., New York.

Pugach, A.F., 1977. *Info. Bull. Var. Stars No. 1277.*

Pugach, A.F., 1988. *Info. Bull. Var. Stars No. 3147.*

Rao, N.K., Ashok, N.M. & Kulkarni, P.V., 1980. *J. Astrophys. Astr.*, **1,** 71.

Rao, N.K., Vasundhara, R. & Ashoka, B.N., 1986. In: *Proc. IAU Coll. 87,* eds K. Hunger *et al.* (Dordrecht, Reidel), p185.

Raveendran, A.V., Ashoka, B.N. & Rao, N.K., 1986. In: *IAU Coll. 87,* p. 191, eds K. Hunger *et al.,* Reidel, Dordrecht.

Rufus, W.C., 1923. *Publs Obs. Michigan,* **3,** 260.

Saio, H., 1986. In: *IAU Coll. 87,* p. 425, eds K. Hunger *et al.,* Reidel, Dordrecht.

Saio, H. & Wheeler, J.C., 1985. *Astrophys. J.*, **295,** 38.

Scargle, J.D., 1982. *Astrophys. J.*, **263,** 835.

Schönberner, D., 1975. *Astr. Astrophys.*, **44,** 383.

Schönberner, D., 1977. *Astr. Astrophys.*, **57,** 437.

Schönberner, D., 1979. *Astr. Astrophys.*, **79,** 108.

Schönberner, D., 1986. In: *IAU Coll. 87,* p. 471, eds K. Hunger *et al.,* Reidel, Dordrecht.

Schultz, G.V. & Wiemer, W., 1975. *Astr. Astrophys.*, **43,** 133.

Shenavrin, V.I., Taranova, O.G., Moroz, V.I. & Grigorev, A.V., 1979. *Sov. Astron.*, **23,** 567.

Sherwood, V.E., 1975. In: *IAU Symp. 67,* p. 147, eds V.E. Sherwood & L. Plaut, Reidel, Dordrecht.

Stanford, S.A., Clayton, G.C., Meade, M.R., Nordsieck, K.H., Whitney, B.A., Murison, M.A., Nook, M.A. & Anderson, C.M., 1988. *Astrophys. J.*, **325,** L9.

Stapinski, T.E., Rodgers, A.W. & Ellis, M.J., 1981. *Publs astr. Soc. Pacif.*, 93, 242.

Stein, W.A., Gaustad, J.E., Gillett, F.C. & Knacke, R.F., 1969. *Astrophys. J. Letters,* **155,** L3.

Sterne, T.E., 1935. *Bull. Harvard Observatory,* **896,** 17.

Totochava, A.G., 1973. *Astron. Circ. U.S.S.R. No. 744.*

Trimble, V., 1972. *Mon. Not. R. astr. Soc.*, **156,** 411.

Walker, H.J., 1986. In: *IAU Coll. 87,* p. 407, eds K. Hunger *et al.,* Reidel, Dordrecht.

Warner, B., 1967. *Mon. Not. R. astr. Soc.*, **137,** 119.

Waters, B.H.J., 1966. *Circ. var. Star Section, R. astr. Soc. New Zealand No. 119.*

Waters, L.B.F.M., Cote, J. & Aumann, H.H., 1987. *Astr. Astrophys.*, **172,** 225.

Wilson, W.J., Schwartz, P.R., Neugebauer, G., Harvey, P.M. & Becklin, E.E., 1972. *Astrophys. J.*, **177,** 523.

Webbink, R.F., 1984. *Astrophys. J.*, **277**, 355.

Weiss, A., 1987a. *Astr. Astrophys.*, **185**, 178.

Weiss, A., 1987b. *Astr. Astrophys.*, **185**, 165.

Wheeler, J.C., 1978. *Astrophys. J.*, **225**, 212.

Wood, P.R., 1976. *Mon. Not. R. astr. Soc.*, **174**, 531.

Wood, P.R., Bessell, M.S. & Paltoglou, G., 1985. *Astrophys. J.*, **290**, 477.

Yefimov, Y.S., 1986. *Proc. 6th Soviet–Finnish Astr. Meeting*, eds U. Känni & I. Tuominen, Estonian Acad. Sci., Tallinn.

# Appendix

# Determining the signal–to–noise ratio and the significance of periodicities

Recently, some caution has been expressed against the over–interpretation of the 'false alarm' probability (Scargle 1982; Horne & Baliunas 1986) in determining whether an observed periodicity is significant. Martinez (1989) concluded, after a study of SAAO and published photometry of the Ap star HD 116763, that an earlier claim of two periodicities (Matthews, Kreidl & Wehlau 1988) was largely unfounded. Martinez concluded that the conservative application of the 'false alarm' probability to the data of Matthews, Kreidl & Wehlau suggested that their claimed periods were probably spurious.

Martinez showed that the correct application of the 'false alarm' probability relies on an appropriate assessment of the noise level to use when calculating the probability. For instance, in determining the rotation period of HD 6532, Kurtz & Marang (1987) showed that a crude estimate of the noise indicated that their peak signal was spurious, whereas a realistic assessment of the noise showed it to be highly significant.

The routine of Press & Teukolsky (1988), which forms the basis of the Fourier analysis routine used in Chapter 2, makes the assumption that the signal–to–noise ratio of the peak signal in the power spectrum is that of the power of that peak, i.e. the noise is deemed to equal one. Such an assumption may not be inappropriate where there is unambiguous evidence for a periodicity in the dataset (i.e., a very small value for the probability) and where an accurate assessment of the probability is not required (i.e., it is enough to know that the periodicity *is* highly significant). But where the significance level is marginal, or in cases where there is evidence for several periodicities in the dataset, a more realistic estimate of the signal–to–noise ratio may be required in order to determine the reality of such signals. We would anticipate that the probability of highly signficant signals might improve (decrease) after a realistic assessment of the noise, whereas a marginally significant peak may become less likely (probability increases).

The 'false alarm' probability of Scargle gives the probability $F$ of finding a peak at a signal–to–noise $z$ in a power spectrum of white noise as

$$F = 1-[1-e^{-z}]^N, \tag{1}$$

where $N$ is the number of independent frequencies searched. For a given Nyquist frequency $f_N$, the number of independent frequencies $N$ is roughly given by

$$N \approx f_N \Delta T \tag{2}$$

where $\Delta T$ is the total time–span of the dataset. For equally spaced data obtained at time intervals $\Delta t$, the Nyquist freqency is simply defined as $f_N = 1/2\Delta t$. For non–equally spaced data, we can establish a mean Nyquist frequency $\overline{f}_N = 1/2\overline{\Delta} t$, where $\overline{\Delta} t$ is the mean time interval. For astronomical data, the definition of $\overline{f}_N$ can be further relaxed as there are often large gaps in the dataset, e.g. seasonal gaps. A typical value for the

Nyquist frequency in equation (2) might be $2\overline{f}_N$.

Furthermore, if the probability $F$ is small, equation (1) can be series expanded to give

$$F \approx Ne^{-z}. \quad (3)$$

The code of Press & Teukolsky utilises equation (3) when $F < 0.01$, thus minimising computer roundoff errors in the calculation of $F$ for typical values of $z$ (4–25) and $N$ (100).

From equation (3), $F$ scales linearly with $N$. As practical significance levels are factors of 5 or 10 apart, $N$ need not be defined very accurately.

The signal–to–noise $z$ in the power spectrum is the square of the ratio (signal/noise) in the amplitude spectrum. The noise in the amplitude spectrum can be estimated by either; (i) assessing a noise level from the amplitude spectrum for frequencies near the peak signal frequency or (ii), examining the amplitude spectra for a series of randomised datasets of the photometry under investigation, i.e. retain the original data–spacing but randomise the magnitudes.

For two examples of these methods, we will re–examine the $V$ photometry of S Aps (Section 2.4.1.1) and the $(B–V)$ photometry of Y Mus (Section 2.4.1.4). In Section 2.4.1.1, we concluded that there were 3 significant periodicities in the $V$ photometry of S Aps and, in Section 2.4.1.4, that there was a marginally significant periodicity in the $(B–V)$ photometry of Y Mus (see Table 2.11).

In Table A.1, we show the results of the spectral analysis of the $V$ photometry of S Aps and the results of 20 random sorts of these data. The columns denote the frequency of the peak signal $f$, the corresponding period $P$, with amplitude $A$, onset phase $\phi$, root–mean–square residual scatter in the photometric data (res.) and probability $F$ from the code of Press & Teukolsky. The seed values for the random sorts are initialisation values for the VAX FORTRAN random number generator RAN. This number must be large and odd.

Note the low amplitude of the peak signal in the random sorts (typically 0.03 mag), compared to the residual scatter (typically 0.06 mag). In contrast, each identified period in the $V$ photometry results in a reduction of the residual scatter in these data. Note also the low values of $F$ for the random sorts. Below the table are details of the $V$ photometry dataset, and the mean and standard uncertainties for the probabilities of the 20 random sorts. A typical value of $F = 0.42$ is 2–4 orders of magnitude less significant that the probabilities derived for the $V$ photometry.

In panel (a) of Figure A.1, we plot the amplitude spectrum for the $V$ photometry of S Aps after the removal of the two low frequency periodicities discussed in Section 2.4.1.1. Panels (b), (c) and (d) show the amplitude spectra after the removal of the periods identified in Section 2.4.1.1 (and listed in Table A.1). Note the reduction in the amplitude of the successive peak signals. This is expected, as we have identified the most significant peak in turn. Also note the reduction in signal–to–noise for each panel, the value for which we determine below. We associate the broad peak near $f = 0.007$ d$^{-1}$ with the low frequency changes in the mean magnitude of the star, discussed in Section 2.4.1.1, and we do not include this feature in our estimate of the noise level.

In panel (e), we show the amplitude spectra for random sort 18, chosen as being typical because the probability of the peak signal ($F = 0.5$) was near the average value ($F = 0.42$) for the 20 sorts. In panel (e), we estimate the noise to be 0.012–0.015 mag. After examining panels (a)–(d), we conclude that 0.012 mag is a more realistic value as

**Table A.1.** Significance levels of S Aps $V$ photometry and of random sorts of these data.

| Star | Run | Seed | $f$ | $P$ | $A$ | $\phi$ | res. | $F$ |
|---|---|---|---|---|---|---|---|---|
| S Aps $V$ | | | 0.0125 | 80.00 | 0.0494 | 5.02655 | 0.0560 | 5.9 E–5 |
| | | | 0.0232 | 43.10 | 0.0401 | 2.63894 | 0.0493 | 5.2 E–4 |
| | | | 0.0257 | 38.91 | 0.0329 | 4.77522 | 0.0429 | 3.1 E–3 |
| Random Sort | 1 | 2257 | 0.0258 | 38.76 | 0.0265 | 5.08938 | 0.0630 | 7.9 E–1 |
| | 2 | 3113 | 0.0348 | 28.74 | 0.0290 | 6.22035 | 0.0621 | 3.3 E–1 |
| | 3 | 5747 | 0.0464 | 21.55 | 0.0229 | 3.45575 | 0.0635 | 9.7 E–1 |
| | 4 | 1235 | 0.0420 | 23.81 | 0.0282 | 0.37699 | 0.0624 | 4.6 E–1 |
| | 5 | 9999 | 0.0482 | 20.75 | 0.0271 | 3.70768 | 0.0623 | 3.9 E–1 |
| | 6 | 8778 | 0.0192 | 52.08 | 0.0331 | 2.82743 | 0.0615 | 1.4 E–1 |
| | 7 | 6663 | 0.0134 | 74.63 | 0.0255 | 1.82212 | 0.0628 | 6.7 E–1 |
| | 8 | 4471 | 0.0113 | 88.50 | 0.0350 | 5.15221 | 0.0609 | 6.5 E–2 |
| | 9 | 4975 | 0.0189 | 52.91 | 0.0295 | 4.52389 | 0.0614 | 9.8 E–2 |
| | 10 | 1357 | 0.0261 | 38.31 | 0.0300 | 4.39823 | 0.0620 | 2.7 E–1 |
| | 11 | 2733 | 0.0112 | 89.29 | 0.0317 | 5.08938 | 0.0613 | 1.0 E–1 |
| | 12 | 8223 | 0.0090 | 111.11 | 0.0281 | 4.02124 | 0.0625 | 5.3 E–1 |
| | 13 | 6881 | 0.0115 | 86.96 | 0.0289 | 2.45044 | 0.0623 | 4.0 E–1 |
| | 14 | 6227 | 0.0350 | 28.57 | 0.0302 | 5.15221 | 0.0619 | 2.4 E–1 |
| | 15 | 6229 | 0.0222 | 45.05 | 0.0322 | 4.58673 | 0.0616 | 1.7 E–1 |
| | 16 | 1665 | 0.0415 | 24.10 | 0.0285 | 3.58142 | 0.0629 | 6.8 E–1 |
| | 17 | 2467 | 0.0440 | 22.73 | 0.0264 | 1.57080 | 0.0625 | 5.2 E–1 |
| | 18 | 6463 | 0.0461 | 21.69 | 0.0281 | 5.34071 | 0.0625 | 5.0 E–1 |
| | 19 | 5511 | 0.0358 | 27.93 | 0.0232 | 2.63894 | 0.0633 | 9.0 E–1 |
| | 20 | 3883 | 0.0423 | 23.64 | 0.0313 | 1.00531 | 0.0618 | 2.1 E–1 |

S Aps

$V_{\text{mean}} = -0.003$
$\sigma^2 = 4.338$ E–3 mag$^2$
$\sigma = 0.066$ mag
mean data interval = 8.181 d
mean $f_N = 0.06112$ d$^{-1}$.

Random sorts

$n = 20$
$x_{\text{mean}} = 4.2$ E–1
$\sigma_{20} = 2.7$ E–1
$\sigma_{19} = 2.7$ E–1

it encompasses most of the noise peaks, whereas a noise level of 0.015 mag appears to be too high.

The mean Nyquist frequency $\overline{f}_N$ for the $V$ photometry of S Aps is 0.06112 d$^{-1}$, but we adopt $f_N = 0.1$ d$^{-1}$ as being a more realistic value. From equation (3), the number of independent frequencies $N \approx 0.1$ x 859 $\approx$ 86.

With the noise and $N$ determined, it is a simple task to calculate the signal–to–noise ratios of the three peaks in Table A.1. The signal–to–noise ratios, in amplitude [S/N (amp)] and power $z$, and the probability $F$ of these peaks, are tabulated in Table A.2. Compare the probabilities in this table with those from the code of Press & Teukolsky in

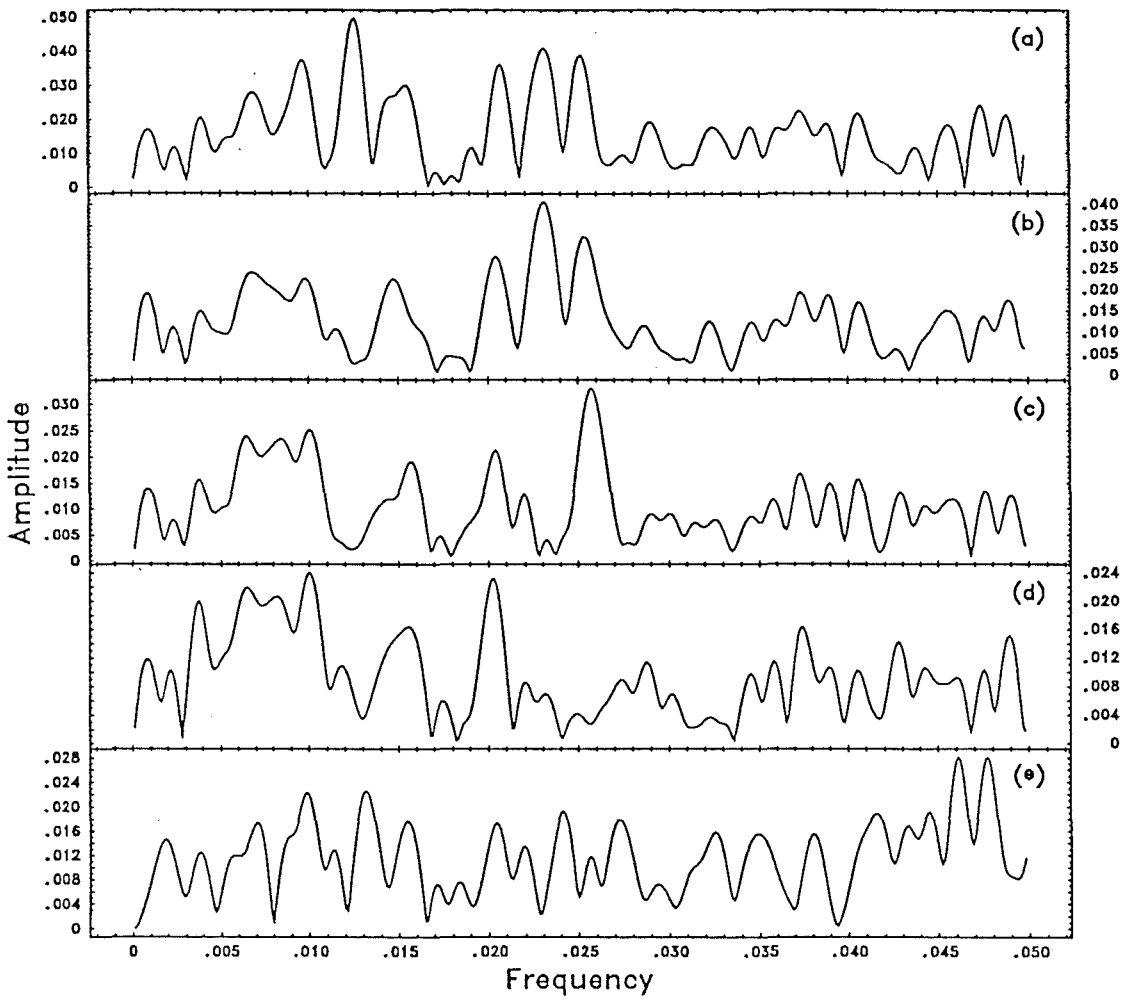


**Figure A.1.** Amplitude spectra from the Fourier analysis of $V$ photometry of S Aps. (a) is the amplitude spectrum after the removal of the two low frequency components discussed in Section 2.4.1.1. Panels (b)–(d) show the spectra after the removal of identified frequencies. Panel (e) is the spectrum of a random sort of the $V$ photometry (see text).

Table A.1. Note that the probabilities of the 80.00 d and 43.10 d periods have decreased by a factor of 13, and increased by a factor of 3, respectively. Such changes in the probabilities were anticipated in the discussion above. Both periods remain *highly* significant. The probability of the 38.91 d period ($F = 0.056$) is in the regime between being considered significant (S/N = 3; $z = 9$; $F = 0.01$) or insignificant (S/N = 2; $z = 4$; $F = 0.80$). We conclude that this period is most probably significant. A synthetic curve, based on these 3 periods, was compared to the $V$ photometry of S Aps in Fig. 2.3.

**Table A.2.** Signal–to–noise ratios and probabilities for periodicities in the S Aps $V$ photometry.

| $f$ | $P$ | S/N (amp) | $z$ | $F$ |
|---|---|---|---|---|
| 0.0125 | 80.00 | 4.1 | 16.8 | 4.3 E–6 |
| 0.0232 | 43.10 | 3.3 | 10.9 | 1.6 E–3 |
| 0.0257 | 38.91 | 2.7 | 7.3 | 5.6 E–2 |

In Fig. A.2, we show the amplitude spectrum for the $(B–V)$ photometry of Y Mus [panel (a)] and that for random sort 9 to these data (Table A.3). We consider that a noise level of 0.008 mag is a realistic value for (b), but that a noise level in the range of 0.008–0.010 mag may be more appropriate for (a). The mean Nyquist frequency $\overline{f}_N$ for the $(B–V)$ photometry of Y Mus is 0.04167 $d^{-1}$, but we adopt $f_N$ = 0.1 $d^{-1}$. Thus, from equation (3), the number of independent frequencies $N \approx 0.1 \times 1116 \approx 112$.

Using noise levels of 0.008 and 0.010 mag, and $N$ = 112, we calculate the signal–to–noise and significance of the peak at $f$ = 0.0092 $d^{-1}$ ($P$ = 108.70 d) in Fig. A.2(a). These values are summarised in Table A.4. The result is marginally significant for a noise of 0.008 mag, but insignificant for a noise level of 0.010 mag. We note, however, that a periodicity of $\sim$ 109 d is observed in the $V$, $(U–B)$ and $(B–V)$ photometry of Y Mus, and that a period of this value is the most likely period of the star (see Section 2.4.1.4).

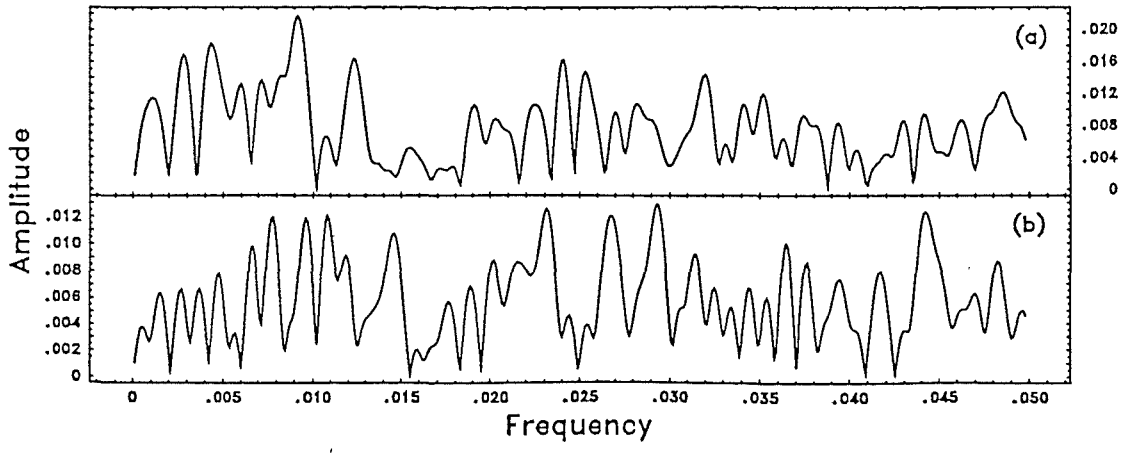


**Figure A.2.** Amplitude spectra from the Fourier analysis of $(B–V)$ photometry of Y Mus. (a) is the spectrum of the original dataset. (b) is the spectrum of a random sort to these data (see text).

**Table A.3.** Significance levels of Y Mus ($B$–$V$) photometry and of random sorts of these data.

| Star | Run | Seed | $f$ | $P$ | $A$ | $\phi$ | res. | $F$ |
|---|---|---|---|---|---|---|---|---|
| Y Mus ($B$–$V$) | | | 0.0092 | 108.70 | 0.0217 | 5.46637 | 0.0271 | 1.9 E–3 |
| Random Sort | 1 | 6633 | 0.0170 | 58.82 | 0.0158 | 0.50265 | 0.0287 | 1.2 E–1 |
| | 2 | 5881 | 0.0300 | 33.33 | 0.0123 | 4.27257 | 0.0298 | 9.4 E–1 |
| | 3 | 9227 | 0.0023 | 434.78 | 0.0115 | 5.08938 | 0.0299 | 9.8 E–1 |
| | 4 | 1995 | 0.0151 | 66.23 | 0.0137 | 5.96903 | 0.0296 | 8.4 E–1 |
| | 5 | 4449 | 0.0461 | 21.69 | 0.0122 | 3.01593 | 0.0297 | 9.1 E–1 |
| | 6 | 1111 | 0.0411 | 24.33 | 0.0136 | 5.34071 | 0.0296 | 8.4 E–1 |
| | 7 | 8603 | 0.0495 | 20.20 | 0.0146 | 0.31416 | 0.0293 | 5.6 E–1 |
| | 8 | 9077 | 0.0483 | 20.70 | 0.0145 | 4.27257 | 0.0292 | 4.2 E–1 |
| | 9 | 7841 | 0.0293 | 34.13 | 0.0129 | 1.69646 | 0.0296 | 8.3 E–1 |
| | 10 | 5135 | 0.0444 | 22.52 | 0.0133 | 1.69646 | 0.0296 | 1.9 E–1 |

Y Mus

$(B-V)_{\rm mean} = 0.926$
$\sigma^2 = 9.718$ E–4 mag$^2$
$\sigma = 0.031$ mag
mean data interval = 12.000 d
mean $f_N = 0.04167$ d$^{-1}$.

Random Sorts

$n = 10$
$x_{\rm mean} = 7.3$ E–1
$\sigma_{10} = 2.6$ E–1
$\sigma_9 = 2.8$ E–1

**Table A.4.** Signal–to–noise ratios and probabilities for periodicities in the Y Mus ($B$–$V$) photometry.

| noise | $f$ | $P$ | S/N (amp) | $z$ | $F$ |
|---|---|---|---|---|---|
| 0.008 | 0.0092 | 108.70 | 2.7 | 7.3 | 7.3 E–2 |
| 0.010 | 0.0092 | 108.70 | 2.2 | 4.8 | 6.0 E–1 |